The Potential Impact of Carbon Dioxide Injection on Freshwater Aquifers: The Surat and Eromanga Basins in Queensland

Jonathan Hodgkinson[1], Micaela Preda[1], Allison Hortle[2],
Mike McKillop[1], Owen Dixon[1] and Linda Foster[3]

Edited by John Draper[1]

[1]Queensland Carbon Geostorage Initiative, Geological Survey of Queensland
[2]CSIRO Petroleum, ARRC, Perth
[3]Queensland Department of the Environment and Resource Management

This report is a scientific review and does not include policy and regulatory issues

Table of Contents

List of tables

List of figures

Figure 18b. Major ion hydrochemical signatures for the Precipice Sandstone in the Eromanga Basin, shown using Stiff diagrams and total dissolved solids (TDS). The Precipice water is generally fresh and sodium-bicarbonate type (see table with descriptive statistics for 59 samples). The mineralogy is based on 17 samples analysed by X-ray diffraction by Carmichael (1989); chlorite and calcite occur as localised traces. Limitations: 1) the water samples represent the shallow Precipice Sandstone and the relevance of these chemical data for the deeper section of the unit remains unknown; 2) the mineralogy is based on samples collected from depths of 1200 to 2500 m.

Figure 18c. Major anion distribution for the Precipice Sandstone in the Surat Basin (exploded view). Labels display known mixing between Precipice and Evergreen (E), Hutton (H), Injune Creek (I) and Walloon (W) waters. The Precipice water is generally bicarbonate-rich, but it can become Cl-rich when mixed with some Walloon waters.

Figure 18d. Major anion distribution for the Precipice Sandstone in the Eromanga Basin (exploded view). Labels display known mixing between Precipice and Hutton (H), waters. The Precipice water is generally bicarbonate-rich, but it can become Cl-rich locally.

Figure 18e. Major ion hydrochemical signatures for the Evergreen Formation in the Surat Basin, shown using Stiff diagrams and total dissolved solids (TDS). The Evergreen water is generally fresh to brackish and sodium-bicarbonate type (see table with descriptive statistics for 56 samples). Limitations: 1) the water samples represent the shallow Evergreen Formation and the relevance of these chemical data for the deeper section of the unit remains unknown; 2) no mineralogical data are available; 3) the number of water analyses is limited.

Figure 18f. Major anion distribution for the Evergreen Formation in the Surat Basin (exploded view). Labels display known mixing between Evergreen and Precipice (P), Hutton (H), Injune Creek (I) and Marburg (M) waters. The Evergreen water is generally bicarbonate-rich, but it can become Cl-rich when mixed with Injune Creek and locally with Hutton waters.

Figure 18g. Major ion hydrochemical signatures for the Hutton Sandstone in the Surat Basin, shown using Stiff diagrams and total dissolved solids (TDS). The Hutton water is mainly fresh and sodium-bicarbonate type (see table with descriptive statistics for 246 samples). The mineralogy is based on 60 samples analysed by X-ray diffraction by Carmichael (1989); chlorite, calcite and siderite occur as localised traces. Limitations: 1) the water samples represent the shallow Hutton Sandstone and the relevance of these chemical data for the deeper section of the unit remains unknown; 2) the mineralogy is based on samples collected from the Eromanga Basin, from depths of 500 to 1200 m.

Figure 18h. Major ion hydrochemical signatures for the Hutton Sandstone in the Eromanga Basin, shown using Stiff diagrams and total dissolved solids (TDS). The Hutton water is mainly fresh and sodium-bicarbonate type (see table with descriptive statistics for 935 samples). The mineralogy is based on 60 samples analysed by X-ray diffraction by Carmichael (1989); chlorite, calcite and siderite occur as localised traces.

Figure 18i. Major anion distribution for the Hutton Sandstone in the Surat Basin (exploded view). Labels display known mixing between Hutton and Precipice (P), Evergreen (E), Walloon (W), Injune Creek (I), Gubberamunda (G), Mooga (Mo), Bungil (B), Marburg (Ma) and Kumbarilla (K) waters. The Hutton water is generally bicarbonate-rich, but it can become Cl-rich when mixed with some Walloon and Injune Creek waters. The Cl signature appears to be more prominent in the northern and western sections of the basin.

Figure 18j. Major anion distribution for the Hutton Sandstone in the Eromanga Basin (exploded view). Labels display known mixing between Hutton and Precipice (P), Adori (A), Hooray (H), Wallumbilla (W) and Griman Creek (GR) waters. The Hutton water is generally bicarbonate-rich, but it can become Cl-rich locally.

Figure 18k. Major ion hydrochemical signatures for the Walloon Subgroup in the Surat Basin, shown using Stiff diagrams and total dissolved solids (TDS). The Walloon water is generally brackish and sodium-chloride type (see table with descriptive statistics for 300 samples). The mineralogy is based on 113 samples analysed by X-ray diffraction by Carmichael (1989); calcite, siderite, dolomite, pyrite and halite occur as localised traces. Limitations: the mineralogy is based on samples collected from the Eromanga Basin, from depths of 400 to 2200 m.

Figure 18l. Major ion hydrochemical signatures for waters assigned to the Injune Creek Group in the Eromanga Basin (equivalent Birkhead, Adori and Westbourne), shown using Stiff

diagrams and total dissolved solids (TDS). The Injune water is mainly fresh and sodium-bicarbonate type (see table with descriptive statistics for 77samples). No mineralogy is available.

Figure 18m. Major anion distribution for the Walloon Subgroup in the Surat Basin (exploded view). Labels display known mixing between Walloon and Eurombah (E), Precipice (P), Hutton (H), Springbok (S), Injune Creek (I), Westbourne (W), Gubberamunda (G), Marburg (M) and Kumbarilla (K) waters. The Walloon water is generally chloride-rich, but it can become bicarbonate-rich when mixed with some Kumbarilla waters. Overall, the water becomes richer in bicarbonate southwards.

Figure18n. Major anion distribution for the Injune Creek Group in the Eromanga Basin (exploded view). The Injune water is generally bicarbonate-rich, with localised Cl enrichments. No water mixtures are reported.

Figure 18o. Major ion hydrochemical signatures for the Springbok Sandstone in the Surat Basin, shown using Stiff diagrams and total dissolved solids (TDS). The Springbok water is generally fresh and sodium-bicarbonate type (see table with descriptive statistics for 33 samples) with some chloride input in the east and north-east. Limitations: 1) no mineralogical data are available; 2) the number of water analyses is limited.

Figure 18p. Major ion hydrochemical signatures for the Adori Sandstone in the Eromanga Basin, shown using Stiff diagrams and total dissolved solids (TDS). The Adori water is mainly fresh and sodium-bicarbonate type (see table with descriptive statistics for 190 samples). No mineralogy is available.

Figure 18q. Major anion distribution for the Springbok Sandstone in the Surat Basin (exploded view). Labels display known mixing between Springbok and Walloon (W), Gubberamunda (G), Mooga (Mo), Hooray (Ho), and Kumbarilla (K) waters. The Springbok water is generally bicarbonate-rich, but it can become Cl-rich when mixed with Walloon waters. The Cl signature appears to be more prominent in the north and east of the basin and caused by Walloon water.

Figure 18r. Major anion distribution for the Adori Sandstone in the Eromanga Basin (exploded view). Labels display known mixing between Adori and Hutton (Hu), Westbourne (We), Hooray (Ho), Wallumbilla (Wa) and Winton (Wi) waters. The Adori water is generally bicarbonate-rich, with localised Cl enrichments.

Figure 18s. Major ion hydrochemical signatures for the Westbourne Formation in the Surat Basin, shown using Stiff diagrams and total dissolved solids (TDS). The Westbourne water is highly variable in terms of salinity and type (see table with descriptive statistics for 14 samples). The mineralogy is based on 121 samples analysed by X-ray diffraction by Carmichael (1989); calcite, siderite, dolomite, pyrite and halite occur as localised traces. Limitations: 1) the number of water analyses is very limited and no mixtures are reported; 2) the mineralogy is based on samples collected from the Eromanga Basin, from depths of 200 to 2000 m.

Figure 18t. Major ion hydrochemical signatures for the Westbourne Formation in the Eromanga Basin, shown using Stiff diagrams and total dissolved solids (TDS). The Westbourne water is fresh and largely sodium-chloride type (see table with descriptive statistics for 9 samples). The mineralogy is based on 121 samples analysed by X-ray diffraction by Carmichael (1989); calcite, siderite, dolomite, pyrite and halite occur as localised traces.

Figure 18u. Major anion distribution for the Westbourne Formation in the Surat Basin (exploded view). The Westbourne water is highly variable, but largely chloride type. Due to the limited number of samples, no definitive conclusions can be drawn; no water mixtures are reported.

Figure 18v. Major anion distribution for the Westbourne Formation in the Eromanga Basin (exploded view). The Westbourne water is highly variable, but due to the limited number of samples, no definitive conclusions can be drawn; no water mixtures are reported.

Figure 18v. Major ion hydrochemical signatures for the Gubberamunda Sandstone in the Surat Basin, shown using Stiff diagrams and total dissolved solids (TDS). The Gubberamunda water is generally fresh and sodium-bicarbonate type (see table with descriptive statistics for 260 samples) with some chloride input in the east. Limitations: no mineralogical data are available.

Wallumbilla (Wa) and Kumbarilla (K) waters. The Bungil water can be both bicarbonate-rich or chloride-rich, with complex mixtures that do not match the known character of those waters. For example, Mooga is sodium-bicarbonate type but in this case it appears to change the character of Bungil waters towards chloride-dominated.

Figure 18kk. Major ion hydrochemical signatures for the Gilbert River Formation in the Eromanga Basin, shown using Stiff diagrams and total dissolved solids (TDS). The Gilbert water is mainly fresh and sodium-bicarbonate type (see table with descriptive statistics for 219 samples). No mineralogy is available.

Figure 18ll. Major anion distribution for the Gilbert River Formation in the Eromanga Basin (exploded view). Labels display known mixing between Gilbert River and Hutton (Hu), Adori (A) and Hooray (Ho) waters. The Gilbert water is generally bicarbonate-rich, with localised Cl input.

Figure 18mm. Major ion hydrochemical signatures for the Longsight Sandstone in the Eromanga Basin, shown using Stiff diagrams and total dissolved solids (TDS). The Longsight water is mainly fresh and sodium-bicarbonate type (see table with descriptive statistics for 224 samples). No mineralogy is available.

Figure 18nn. Major anion distribution for the Longsight Sandstone in the Eromanga Basin (exploded view). The water is generally bicarbonate-rich, with localised Cl input. No mixtures are reported.

Figure 18oo. Major ion hydrochemical signatures for the Wyandra Sandstone Member in the Eromanga Basin, shown using Stiff diagrams and total dissolved solids (TDS). The Wyandra water is mainly fresh and sodium-bicarbonate type (see table with descriptive statistics for 254 samples). No mineralogy is available.

Figure 18pp. Major anion distribution for the Wyandra Sandstone Member in the Eromanga Basin (exploded view). Labels display known mixing between Wyandra and Hutton (Hu), Hooray (Ho), Gilbert River (G), Wallumbilla (Wa) and Winton (Wi) waters. The water is generally bicarbonate-rich, with localised Cl input.

Figure 18qq. Major ion hydrochemical signatures for the Wallumbilla Formation in the Surat Basin, shown using Stiff diagrams and total dissolved solids (TDS). The Wallumbilla water is generally brackish and sodium-chloride type (see table with descriptive statistics for 255 samples). Limitations: no mineralogical data.

Figure 18rr. Major ion hydrochemical signatures for the Wallumbilla Formation in the Eromanga Basin, shown using Stiff diagrams and total dissolved solids (TDS). The Wallumbilla water is fresh to brackish and sodium-chloride type (see table with descriptive statistics for 298 samples). No mineralogy is available.

Figure 18ss. Major anion distribution for the Wallumbilla Formation in the Surat Basin (exploded view). Labels display known mixing between Wallumbilla and Hutton (H), Wyandra (Wy), Wallumbilla (Wa), and Kumbarilla (K) waters. . The Wallumbilla water is generally chloride-rich, with localised enrichments in bicarbonate.

Figure 18tt. Major anion distribution for the Wallumbilla Formation in the Eromanga Basin (exploded view). Labels display known mixing between Wallumbilla and Hooray (Ho), Longsight (L), Wyandra (Wy), and Winton (Wi) waters. The water is generally chloride-rich, with localised HCO_3 input from Wyandra.

Figure 18uu. Major ion hydrochemical signatures for the Surat Siltstone in the Surat Basin, shown using Stiff diagrams and total dissolved solids (TDS). The Surat water is generally brackish and sodium-chloride type (see table with descriptive statistics for 12 samples). Limitations: limited chemical data and no mineralogy.

Figure 18vv. Major anion distribution for the Surat Siltstone in the Surat Basin (exploded view). The Wallumbilla water is generally chloride-rich, with localised enrichments in bicarbonate.

Figure 18www. Major ion hydrochemical signatures for the Griman Creek Formation in the Surat Basin, shown using Stiff diagrams, total dissolved solids (TDS) and pie diagrams. The water is fresh and sodium-bicarbonate type (see table with descriptive statistics for 4 samples, collected from one bore). Limitations: very limited chemical data and no mineralogy.

Figure 19. Water type variation with depth – an example for the Gubberamunda waters in the Surat Basin. Deep waters are fresh Na-HCO_3 waters, while the shallower waters can become

chloride-rich and saltier. The very fresh waters that occur close to the recharge areas are mainly Na-Cl. The -800 m critical depth is shown for reference.

Figure 20. Water type variation with depth – an example for the Hooray waters in the Eromanga Basin. The Na-HCO_3 character does vary with the depth; the deeper waters from the central basin are saltier but preserve the Na-HCO_3 character. The -800 m critical depth is shown for reference.

Figure 21a. pH – alkalinity relationship for the main Jurassic groundwaters of the Surat Basin. The pH largely varies between 6 and 9, while the alkalinity can reach 1800 mg/L. The Precipice waters are generally circumneutral, with low alkalinities, while the Walloon waters include some high pH and alkalinity samples. Other groundwaters such as the Hutton and Gubberamunda are highly variable. Note: interpretation is based only on non-mixed water analyses.

Figure 21b. pH – alkalinity relationship for the main Jurassic groundwaters of the Eromanga Basin. The pH largely varies between 6.5 and 9, while the alkalinity can reach 1800 mg/L. The Precipice and Ronlow waters are generally circumneutral, with low alkalinities, while the Adori and some Hooray waters include high pH and alkalinity samples. Other groundwaters such as the Hutton and Injune are highly variable. Note: interpretation is based only on non-mixed water analyses.

Figure 21c. pH – alkalinity relationship for the main Cretaceous groundwaters of the Surat Basin. The pH varies largely between 6 and 9, while the alkalinity can reach 1200 mg/L. The Mooga waters have pHs around 8 and high alkalinities, while the Wallumbilla waters tend to have a similar pH, but lower alkalinity. Note: interpretation is based only on non-mixed water analyses.

Figure 21d. pH – alkalinity relationship for the main Cretaceous groundwaters of the Eromanga Basin. The pH varies largely between 6 and 9, while the alkalinity can reach 1200 mg/L. The Wyandra waters have pHs around 8 and high alkalinities, while the Wallumbilla waters tend to have a similar pH, but lower alkalinity. The Longsight water has pHs from 7 to 9, but constant alkalinity, around 400; Gilbert River water is similar in terms of pH values, but has lower than 400 alkalinities. Note: interpretation is based only on non-mixed water analyses.

Figure 22a. Bicarbonate – chloride relationship for the main Jurassic groundwaters in the Surat Basin. The HCO_3 can reach concentrations of thousands of mg/L, while chloride has concentrations of up to 10,000 mg/L. The Precipice waters are very fresh with both anions present in the order of hundreds of mg/L. The Hutton water is highly variable, with a significant proportion of waters that have a similar concentration of HCO_3 and Cl. The Walloon has the saltiest water, with about 10 times more Cl than HCO_3; in addition, the two parameters display an inverse relationship, although the overall trend is of direct proportionality. The Gubberamunda water has an intermediate character, similar to the Hutton, but with about 10 times more HCO_3 than Cl. Note: interpretation is based only on non-mixed water analyses.

Figure 22b. Bicarbonate – chloride relationship for the main Jurassic groundwaters in the Eromanga Basins. The HCO_3 can reach concentrations of thousands of mg/L, while chloride has concentrations of up to 30,000 mg/L. The elements are directly proportional. The Precipice waters are very fresh with both anions present in the order of hundreds of mg/L. The Hutton and Adori waters are highly variable, but largely HCO_3-dominated, with 5 - 10 times more HCO_3 than Cl. The Hooray and Ronlow contain well-defined populations of HCO_3-rich samples, but they also have numerous outliers of Cl-dominated waters. Note: interpretation is based only on non-mixed water analyses.

Figure 22c. Bicarbonate – chloride relationship for the main Cretaceous groundwaters in the Surat Basin. The HCO_3 can reach concentrations of up to 1000 mg/L, while chloride of up to 10,000 mg/L; the elements are inversely proportional. The Mooga waters have an intermediate character, similar to Gubberamunda, with about 10 times more HCO_3 than Cl. The Wallumbilla water is saltier, with about 10 times more Cl than HCO_3. The water assigned to the Hooray Sandstone consists of several populations: 1) bicarbonate-rich, similar in character to Mooga, but with less HCO_3; 2) salty, similar to Wallumbilla; and 3) very fresh. Note: interpretation is based only on non-mixed water analyses.

Figure 22d. Bicarbonate – chloride relationship for the main Cretaceous groundwaters in the Eromanga Basin. The HCO_3 can reach concentrations of up to 5000 mg/L, while chloride

Figure 26b. Major cations in the South Australian section of the Great Artesian Basin. Out of the 2600 bores, about 600 have chemical analyses. The water is generally sodium-rich.

Figure 27. Average mineral composition of Mesozoic formations based on Carmichael (1989). See also Fig. 11 for site locations and Fig. 18 for details.

Figure 28a. Equilibration of mean Precipice Sandstone groundwater with mean aquifer mineral composition. The reaction paths show the increase in the quantity of minerals precipitated during the reaction to the end point of equilibrium between the groundwater and the aquifer media. The overall change in mineral composition is minor: quartz content is unchanged; calcite is reduced by 12%; illite/mica is reduced by 40%; kaolinite is increased by 19%; dolomite, daphnite and saponite precipitate in small quantities and chlorite dissolves. Overall the aquifer media remains dominated by quartz arenites. Groundwater type remains as Na-HCO_3 but with a reduction of 41% in HCO_3, concomitant with reductions in dissolved silica and potassium and an increase in dissolved calcium due to carbonate dissolution.

Figure 28b. Changes in aquifer media mineral composition in the Precipice Sandstone after equilibration with 1 mole of CO_2 (this equates to the approximate maximum solubility of CO_2 in fresh water under the conditions of interest). The starting solution composition and the aquifer mineralogy are taken from the equilibrated mean groundwater composition and the equilibrated mean aquifer media mineral composition. Solution pH remains constant throughout the simulation, buffered by the dissolution of calcite. There is a substantial increase in dolomite at the expense of calcite and saponite. The silicate minerals show little change due to the buffered circum-neutral pH of the groundwater. Fluid composition remains largely unchanged.

Figure 28c. Mineral transformations resulting from flushing of Precipice Sandstone aquifer media with 100 kg of 1 molar CO_2 aqueous solution. Constant flushing of the rock mass with CO_2 saturated fluid induces a rapid drop in pH, rapidly consuming carbonates, daphnite and saponite. Dolomite precipitates as calcite and saponite are consumed and magnesite and siderite precipitate, but are re-dissolved early in the flushing event. Kaolinite precipitates at the expense of mica/illite and there is minor precipitation of quartz, some dolomite is consumed in the latter stages of flushing. There are significant mineralogical changes within the aquifer media but the overall framework composition remains highly quartzose. Fluid composition is radically changed with a very large increase in salinity and pH of less than 5. Dissolved potassium, magnesium and calcium concentrations are orders of magnitude greater than the initial solution and CO_2 fugacity is close to saturation.

Figure 29a. Equilibration of mean Hutton Sandstone groundwater with mean aquifer mineral composition. The reaction paths show the increase in the quantity of minerals precipitated during the reaction to the end point of equilibrium between the groundwater and the aquifer media. The change in aquifer media mineral composition is quite significant, suggesting that groundwater in the Hutton Sandstone is not in equilibrium with the aquifer media. There is a slight increase in groundwater salinity, pH is 0.2 higher, combined with the complete dissolution of albite, K-feldspar and chlorite. Additional quartz and kaolinite precipitate, along with some micaceous minerals and dolomite. The new fluid composition is enriched in dissolved aluminium and sodium from the dissolution of albite and severely depleted in magnesium and calcium, due to calcite and dolomite precipitation.

Figure 29b. Changes in aquifer media mineral composition in the Hutton Sandstone after equilibration with 1 mole of CO_2 (this equates to the approximate maximum solubility of CO_2 in fresh water under the conditions of interest). The starting solution composition and the aquifer mineralogy are taken from the equilibrated mean groundwater composition and the equilibrated mean aquifer media mineral composition. Solution pH remains generally constant throughout the simulation, buffered by the dissolution of calcite. There is a substantial increase in dolomite at the expense of calcite and saponite. Dawsonite also precipitates due to the release of aluminium and sodium from the dissolution of albite. The silicate minerals show little change due the buffered alkaline pH of the groundwater. There is an 87% increase in fluid salinity; however, the groundwater remains in the low brackish range (4120 mg/L). There is a substantial increase in bicarbonate concentration and a significant reduction in calcium.

Figure 29c. Mineral transformations resulting from flushing of Hutton Sandstone aquifer media with 100 kg of 1 molar CO_2 aqueous solution. Constant flushing of the rock mass with CO_2 saturated fluid induces a rapid drop in pH, rapidly consuming carbonates, daphnite,

saponite and paragonite. Dolomite precipitates as calcite and saponite are consumed and magnesite precipitates, but is re-dissolved early in the flushing event. Kaolinite precipitates at the expense of mica/illite and there is minor precipitation of quartz, some dolomite is consumed in the latter stages of flushing. There are significant mineralogical changes within the aquifer media and the framework composition becomes dominated by quartz arenite. Fluid composition is radically changed with a very large increase in salinity and pH of 5.1. Dissolved potassium, magnesium and calcium concentrations are orders of magnitude greater than the initial solution and CO_2 fugacity is greatly increased.

Figure 30a. Comparative simulation results for the target aquifers, the Precipice and Hutton sandstones. The results of the simulations are similar for both aquifer materials. The main difference relates to the salinity changes that can occur when the system is equilibrated with 1 molar CO_2. The mineralogical composition of the Hutton Sandstone is more prone to dissolution than the Precipice and, under acidic conditions, the dissolution of minerals can produce saltier water that can lead to carbonate precipitation (mainly dolomite). Flushing with 1 molar CO_2 produces similar results with most minerals being initially removed; dolomite may precipitate but it would be redissolved under the persistent acidic conditions.

Figure 30b. Mineral stability diagrams for dolomite at different temperatures, in the presence of Precipice average major ions. Temperature affects the domains of brucite and magnesite, but it does not affect the stability of dolomite, which persists even at low pH, providing that there is enough Ca in the system.

Figure 31. Stability diagrams for K-feldspar under various conditions of temperature and CO_2 fugacity. Pressure is 100 bars in all cases. The domain of kaolinite stability shifts towards higher silica activity, with increased temperature, while CO_2 fugacity has little effect.

Figure 32. Stability diagrams for albite under various conditions of temperature and CO_2 fugacity. Pressure is 100 bars in all cases. The domain of kaolinite stability shifts towards higher silica activity, with increased temperature, while CO_2 fugacity controls the stability of dawsonite.

Figure 33. Locations of formation pressure data points from petroleum wells, that have been assessed using the CSIRO PressureQC™ methodology.

Figure 34a. Pressure/depth relationship between the Precipice Sandstone and the Hutton Sandstone in the eastern Surat Basin, north of the Moonie oil field. The pressure measurements show good reliability and the separation between values is much greater than the accepted 30 psia error margin. The pressure values in this well show that the Precipice Sandstone is slightly underpressured relative to the Hutton Sandstone. The relationship implies that the Evergreen Formation may be acting as a seal between the two sandstone dominated units.

Figure 34b. Pressure/depth relationship between the Precipice Sandstone and the Hutton Sandstone on the Kumbarilla Ridge, southwest of Dalby. The pressure measurements in both the formations of interest show good reliability and the separation between values is much greater than the accepted 30 psia error margin. The relationship is similar to that in Arlington 1, northwest of Moonie.

Figure 34c. Pressure/depth relationship between the Precipice Sandstone and the Hutton Sandstone near the eastern margin of the Surat Basin, east of Moonie. The relationship between the two units is similar to that in the wells Arlington 1 and Tipton 1, whereby the Precipice Sandstone is slightly underpressured relative to the Hutton Sandstone. A drill stem test in the Evergreen Formation shows the low permeability characteristic of this unit in many areas. Although the Evergreen Formation test is less reliable that those in the more permeable formations, it provides further evidence for the potential sealing properties of this unit.

Figure 34d. Drill stem tests in PPC Yarrala 1 also show the Precipice Sandstone as underpressured, but relative to both the Evergreen Formation and Hutton Sandstone. This also implies the presence of a seal between the upper Precipice Sandstone and the Evergreen Formation. Formation 'tightness' exhibited in PPC Waggaba 1 is not evident in PPC Yarrala 1 and formation pressure in the Evergreen Formation is on-gradient with the overlying Hutton Sandstone. The drill stem test in the deeper section of the Precipice Sandstone shows slight underpressure compared to the shallower test; however, the test has a low reliability

the DERM GWDB and yellow dots are hydraulic heads calculated from formation pressure measurements in petroleum wells. This is a provisional interpretation based on currently assessed data and will be subject to change as more data become available. It should also be noted that the pressure gauge error margin of 30 psia equates to an equivalent freshwater head error of +-21 m. Groundwater flow vectors in the Eromanga are based on similar data to the model of Habermehl (1980) and, therefore, show agreement with the earlier hypothesis. The flow regime in the northern Surat Basin was largely excluded from the earlier model and shows a strong northward flow component similar to that in the Evergreen Formation. There is also some evidence for the presence of a groundwater divide in the central region of the basin, which concurs with Hitchon and Hays (1971) interpretation.

Figure 39b. 3D flow vector plot for the Hutton Sandstone incorporating the results of early/pre-production formation pressure tests (1960-65) and groundwater potentiometric heads prior to 1960. Unlike the models for the Evergreen Formation and the Precipice Sandstone, the modelled flow vectors of the Hutton Sandstone in the northern Surat Basin do not agree with the manual interpretation. This is due to limitations in the interpolation algorithm.

Figure 39c. 3D flow vector plot for the Hutton Sandstone incorporating groundwater potentiometric heads only post 1960. The post 1960 model shows greater similarity to the manual interpretation of the pre 1960 data.

Figure 40a. 3D flow vector plot for the Gubberamunda Sandstone incorporating the results of early/pre-production formation pressure tests (1960-65) and groundwater potentiometric heads prior to 1960.

Figure 40b. 3D flow vector plot for the Gubberamunda Sandstone incorporating groundwater potentiometric heads only post 1960.

Figure 41a. 3D flow vector plot for the Hooray Sandstone incorporating the results of early/pre-production formation pressure tests (1960-65) and groundwater potentiometric heads prior to 1960.

Figure 41b. 3D flow vector plot for the Hooray Sandstone incorporating groundwater potentiometric heads only post 1960. The implied northward regional flow is based on limited data and should be considered with caution.

Figure 42. Conceptual model of a multi-reservoir – conventional/unconventional seal system, similar to the Precipice-Evergreen (conventional regional seal) / Hutton-Walloon (unconventional regional seal) reservoir/seal pairs. The recharge water is slightly acidic and of Na-Cl type, while the deeper groundwater is alkaline and of Na-HCO_3 type. The reservoirs/aquifers are largely quartz-rich ± feldspar ± mica, while the seals/aquitards are clay-rich. Opposite flow patterns due to topographic highs can create localised flow cells. Injection of CO_2 will dissolve most mineral phases and lower the pH; the mineral matrix will be dominated by quartz and kaolinite, with short-lived carbonate phases (e.g. dolomite). Favourable hydrodynamics assist in limiting vertical and horizontal migration of the CO_2 plume; however, injection pressure-induced reversal of the hydraulic gradient could reduce the effectiveness of the retardation mechanism.

Executive Summary

The carbon reduction challenges facing Australia have become increasingly more evident, with the results of continuing efforts by research agencies and government groups to identify large volume storage sites. The National Carbon Storage Task Force through the federal Department of Resources, Energy and Tourism commissioned this report to gain an understanding of the issues associated with CO_2 sequestration in freshwater aquifers. The Surat and Eromanga basins form the larger part of the Great Artesian Basin in Queensland, South Australia, New South Wales and the Northern Territory. These two basins host vast quantities of fresh groundwater and significant hydrocarbon wealth, and are also potentially prime targets for high volume carbon geostorage.

An up to date literature review is included to show examples of recent research into the implications of CO_2 storage in aquifers nationally and internationally. Open-file datasets have been sourced from the Geological Survey of Queensland, the Department of the Environment and Natural Resources, the Geological Survey of South Australian, CSIRO, Geoscience Australia and collaborative projects between various agencies, consultants and government groups. The gap analysis presented in a previous report by the Queensland Carbon Geostorage Initiative is used as the basis for the more specialised data review and analysis presented in this study. This work is primarily focused on: the distribution of groundwater types spatially and with depth, the mineralogy of reservoir/seal and aquifer/aquitard pairs, and the hydrochemical and geochemical reactions associated with the injection of CO_2 into the freshwater aquifers of the Surat and Eromanga basins.

At the regional scale, a number of simplifying assumptions can be made with regard to the expected behaviour of the groundwater system in response to stress induced by the injection of CO_2. Major ion hydrochemical signatures are predominantly of uniform Na-HCO_3 type throughout the basin, with the exception of the shallow regions proximal to the basin margins. Groundwater in the Walloon Subgroup, Westbourne Formation, Bungil Formation and Wallumbilla Formation is of Na-Cl type and vertical mixing between the overlying and underlying units appears nominal. The preliminary results of equilibrium speciation modelling and geochemical reaction path modelling indicate that the acid buffering capacity of the groundwater is large. This concurs with the mainly high pH and alkalinity measurements collected across the Great Artesian Basin (GAB). Simulation results also suggest that the groundwater systems have the capacity to naturally remediate the induced low pH conditions resulting from CO_2 injection.

Extrapolation of mineralogical data across the basins shows favourable mineral stability characteristics in the sandstones of the principle storage targets. Mineral stability modelling and water-rock reaction simulations suggest that the compositions of the Precipice Sandstone and the Lower Poolowanna Formation would be the least affected by carbon geostorage activities. The Hutton Sandstone and some of the shallower prospective geostorage units in the Eromanga Basin have a less stable mineral composition. The aquifer media in these units is predicted to evolve to a mineralogical composition similar that of the Precipice Sandstone in close proximity to the injection wells.

The interpretations of hydrodynamic data show that the aquifers of the Precipice Sandstone in the Surat Basin operate independently of the underlying and overlying groundwater systems over a large area. Combination of formation pressure data from petroleum wells with potentiometric head data from groundwater bores suggests that a number of groundwater divides and subsurface confluence areas exist within the Precipice Sandstone. Further data assessment is required prior to the construction of a similar model for the Eromanga Basin. The preliminary results of this study show that the continuum model of Hitchon and Hays is not likely to be appropriate for the assessment of carbon geostorage in the Surat Basin. The resolution of published regional flow models for the GAB is too coarse for carbon geostorage assessment purposes and also assumes a high level of vertical connectivity between aquifers. In addition, only the Hooray Sandstone and equivalent aquifers are explicitly modelled in these groundwater flow studies. Additional data and further interpretations are required to put tighter constraints on the interrelationships between the stacked aquifers and aquitards in both basins.

The location of carbon geostorage injection well fields relative to existing resource and environmentally sensitive areas is critical to the mitigation of detrimental contamination effects. In the short-term, the seal capacity of aquitards overlying the target aquifers needs to be great enough to inhibit the vertical migration of free-phase CO_2. The long-term effects of injection-induced pressure wave propagation need to be modelled to predict the potential changes in the hydrodynamic regime and the consequent effects on CO_2 plume migration. The prevailing hydrodynamic regime will dictate

the volume of CO_2 that can be safely stored in the long-term, without negative impacts on groundwater resources, hydrocarbon production, mining operations and groundwater-dependent ecosystems.

The cost of remediation strategies for damage to existing infrastructure resulting from CO_2 contamination could be prohibitive. Environmental impacts could be severe but remain speculative and cannot be quantified with currently available information. Estimates of the approximate costs for drilling new groundwater bores and completions with inert casing are provided for guidance. In most cases, it is considered uneconomical to remediate existing groundwater bores completed with standard steel casing. Oil and gas infrastructure remediation strategies can be more complex and their implementation is governed by the perceived economics of a producing hydrocarbon field. The high cost of drilling new production wells favours the remediation of existing infrastructure; however, this can also be prohibitively expensive. It should be considered, however, that the severe near-well changes to the groundwater system are most likely to be restricted to a limited radius from the injection well. A combination of high acid buffering capacity, low fluid flow velocities and high groundwater residence times would contribute to a high level of confidence in an adequate safety margin, if injection well fields are sited correctly.

Future work is planned for the Surat and Eromanga basins, which includes the collection of new data as part of a deep well drilling program and re-sampling of existing groundwater bores. Core collected from previous stratigraphic drilling projects will also be sampled for analysis by X-ray diffraction, X-ray fluorescence and scanning electron microscopy. Newly acquired core samples will be tested for permeability and porosity and will also be subjected to core-flood analysis. Seal capacity will be tested using standard techniques such as mercury injection capillary pressure analysis. Nested peizometer configurations are proposed for the new drilling sites to provide detailed field observations and focused sampling programs to establish the vertical relationships between the aquifers/reservoirs and aquitards/seals. This is of particular importance in estimating the effectiveness of unconventional sealing units.

Introduction

The federal Department of Resources, Energy and Tourism on behalf of the National Carbon Storage Taskforce commissioned this report, to investigate the potential impacts of injecting carbon dioxide into onshore freshwater aquifers in Australia. This request resulted principally because of the lack of extensive onshore saline aquifers and the potentially very large storage capacity of the freshwater aquifers in the Great Artesian Basin. The Jurassic/Cretaceous Surat and Eromanga basins are the focus of this study (Fig. 1).

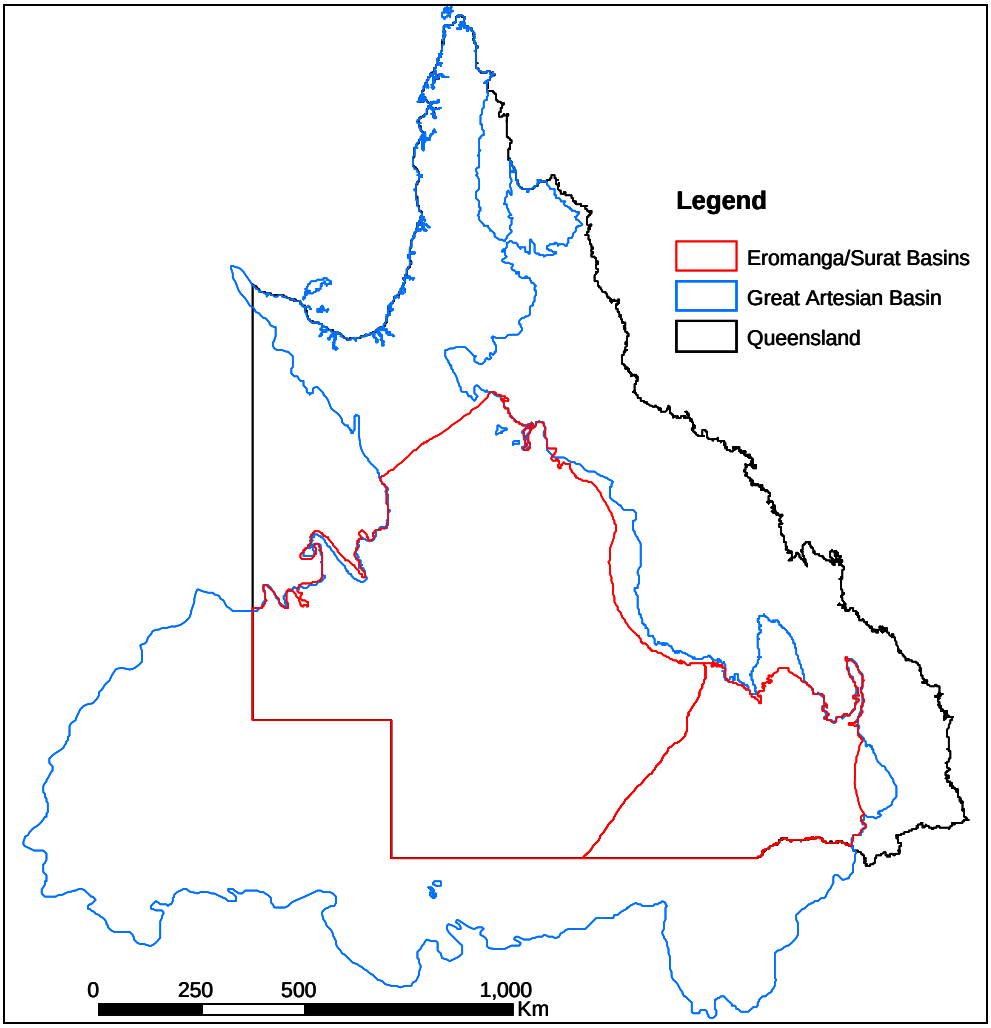

Figure 1. Extent of the Great Artesian Basin in relation to Queensland and the Eromanga and Surat basins.

The report has been compiled by the Geological Survey of Queensland (GSQ) Carbon Geostorage Initiative (QCGI) in collaboration with CSIRO Petroleum and the Queensland Department of the Environment and Resource Management (DERM). The GSQ hold most of the geological data pertaining to both basins; additional information has been sourced from the Geological Survey of South Australia. The Eromanga Basin is the most important onshore oil producing basin in Australia and both basins form the larger part of the Great Artesian Basin, which is one of the most significant fresh groundwater resources in the world.

The main storage options for CO_2 are depleted oil and gas fields and aquifers. There are many issues associated with both; there are huge hydrocarbon bearing basins across the globe, but many are far from being depleted and even if they were available now, they do not have the requisite storage volumes for long term sequestration (e.g. Bachu and Bennion, 2008). Aquifers have much larger storage capacities and until now the focus has been on saline groundwater systems. This has primarily been driven by the U.S. Department of the Environment, which has ruled out the possibility of injection into freshwater aquifers. Both the United States and Canada have extensive onshore saline

(or more correctly, brackish) aquifers, whereas Australia does not. In the United States, water with more than 10,000 mg/L total dissolved solids (TDS) is considered saline, although such water is commonly used to water cattle and sheep, without any detrimental effects. In this study, the following TDS-based water classification has been adopted:

- Fresh: < 1500 mg/L
- Brackish: 1500 – 35,000 mg/L (low brackish < 20,000 mg/L; high brackish > 20,000 mg/L)
- Saline: 36,000 mg/L
- Hypersaline/brine: > 36,000 mg/L

Despite the acknowledgement that aquifers are likely to be the only storage option large enough to accommodate the perceived volumes of waste CO_2 (Bachu and Bennion, 2008), limited research into capacity estimation and the possible ramifications of injection has been carried out. The core studies of the U.S. Department of Energy (DOE, 2006), the Carbon Storage Leadership Forum (CSLF, 2007) and the CO2CRC (Ainsworth et al., 2008) provide the underlying methodologies, however, CO_2 storage estimation for aquifers is highly complex and most prospective sites suffer from a lack of data (Bachu et al., 2007). Much of the initial work on aquifer storage was conducted by Bachu and co-workers (e.g. Bachu, 1995a; Bachu, 1995b; Bachu, 2000; Bachu, 2002; Bachu and Adams, 2003) and Gunter and co-workers (e.g. Gunter et al., 1996; Gunter et al., 2000) and was focused on Canadian sedimentary basins. Studies looking at the potential environmental consequences of injecting CO_2 into saline aquifers are now starting to emerge (e.g. Birkholzer et al., 2009; Nicot, 2008) and informative research derived from the offshore Sleipner oilfield has been published (e.g. Gaus et al., 2005a; Portier and Rochelle, 2005). However, no studies looking at the impact of direct injection into currently exploited freshwater aquifers appear to have been conducted.

This report provides a comprehensive gap analysis for the Surat and Eromanga basins, derived from preliminary work carried out by the Queensland Carbon Geostorage Initiative (QCGI, 2009). The limitations of the current datasets are discussed and a review of the recent research carried out relevant to aquifer storage, together with background on the Great Artesian Basin (GAB) is included. Hypotheses based on the interpretation of available data are provided to illustrate the possible impacts, both beneficial and detrimental associated with CO_2 storage in these two basins. The principle targets for CO_2 injection are the Precipice Sandstone in the Surat Basin and the Precipice Sandstone, Lower Poolowanna Formation and the Hutton Sandstone in the Eromanga Basin. These units were identified in a previous QCGI study (QCGI, 2009) and are the main focus of this work.

Potential Issues

The following list of points summarises the main issues associated with the large volume injection of CO_2 into freshwater aquifers. Addressing these issues is a fundamental aspect of carbon geostorage site characterisation, which incorporates risk analysis and hazard mitigation:

- Primary fresh groundwater supply contamination – the injection of both gaseous and supercritical CO_2 causes significant pH reductions in the vicinity of the injection well (Gunter et al., 2000) and also causes desiccation of the host groundwater (Kaszuba et al., 2003). The size of the area affected by the increased hydrogen ion activity and consequent acidification is dependent on the groundwater and CO_2 flow velocities/vectors, the pH buffering capability of the aquifer media (due to chemical reaction) and the host groundwater and the CO_2 injection rate.
- Secondary fresh groundwater supply contamination – aquifer media commonly contain reactive mineral assemblages and variable amounts of organic material. Trace element mineral impurities are common in many minerals and harmful organic compounds can be liberated from organic materials (e.g. BTEX compounds, furans and PCBs). The impact of these contaminants ranges from benign to toxic, dependent on concentration and the resultant aqueous species. Detailed analyses of aquifer media mineralogy and geochemistry are required to quantify any potential detrimental effects.
- Infrastructure risk – existing infrastructure that is not designed to cope with low pH fluids (e.g. petroleum and groundwater wells) is at risk of degradation if mitigation steps are not taken. This has implications for groundwater and hydrocarbon exploitation practices currently in force.
- Injection induced pressure gradients – pressure effects can extend tens of km from the injection point, causing significant changes to regional groundwater flow regimes. Excessive injection rates may reverse hydraulic gradients and induce up-dip groundwater flow.
- Environmental consequences – there are potentially positive and negative ramifications for in-aquifer and groundwater dependent ecosystems and other natural environments. Changes in the

regional water table could assist in restoring artesian conditions in depleted areas. Increased base flow could rejuvenate dry streams and lakes. Conversely, evapotranspiration can be unfavourably augmented by raised water tables and acidic CO_2-charged groundwater can have detrimental effects on delicately balanced ecosystems.

- Sterilisation of undiscovered resources – this is a factor of resource management and stewardship. Available pore-space for geostorage is a resource in itself and will generate resource conflicts similar to those already apparent (e.g. coal seam gas, oil and conventional gas and underground coal gasification). Decisions to inject CO_2 need to be made on the basis of existing information regarding other potential resources and the respective economic benefit of each.
- Mitigation measures – although technology from the oil and gas industry is mature and can be applied to certain aspects of CO_2 sequestration, the practice of carbon geostorage is in its infancy. Proposed mitigation strategies can only be based on the small amount of data available from demonstration projects and model output. Anecdotal evidence suggests that plume migration is severely retarded subsequent to cessation of injection but many modelling studies suggest otherwise (e.g. White et al., 2005). An assessment of the effectiveness of pressure-release wells and other proposed mitigation techniques is needed to verify their effectiveness. A basin-wide pH reduction of significance is unlikely but should not be ruled out. This could potentially be mitigated by adapting contaminated land remediation techniques such as 'liming' to increase the acid neutralising capacity of the groundwater. An adapted subsurface barrier method would have to be used, or deep slurry injection techniques employed to deliver the neutralising agents to the affected area. The removal of mobilised salts and heavy metals in solution would necessitate the use of techniques such as reverse osmosis, as used in the coal seam gas industry to purify groundwater abstracted during gas production. Membrane filtration systems are commonly used to remove organic compounds from water. It should be noted that there are currently large areas of the GAB in the northern regions which have naturally high dissolved CO_2 concentrations.

Previous Work and Background

Hydrodynamics

The study of petroleum system hydrodynamics and hydrogeology related to groundwater resources and environmental management has been prolific in the last few decades. Until the concept of large scale underground CO_2 sequestration emerged, these two branches of hydroscience have developed in relative isolation. Petroleum hydrogeology focuses predominantly on the behaviour of immiscible multi-phase fluid flow and the interaction of non-reactive fluids in deep basin systems. Conversely, resource and environmental hydrogeology typically deals with miscible fluids and reactive transport associated with water-rock interactions at shallower depths. Environmental hydrogeologists also solve multi-phase fluid flow problems when dealing with non-aqueous phase liquid contamination. The practice of CO_2 geostorage necessitates a union between the two sub-disciplines.

The petroleum systems approach to flow analysis is based primarily on pressure data obtained from hydrocarbon exploration and production wells (e.g. Hennig et al., 2006; Hitchon, 1969a; Hitchon, 1969b; Hitchon et al., 1990; Michael and Bachu, 2001; Otto et al., 2001; Underschultz et al., 2003) and by conversion to hydraulic heads (Hennig, 2007; Hennig et al., 2003; Hitchon and Hays, 1971). Groundwater resource and environmental studies most commonly use direct measurements of piezometric head from water supply and monitoring wells (Ezzy et al., 2006; Habermehl, 1980; Habermehl, 1986; Hodgkinson et al., 2007; Quarantotto, 1989). Formation pressure data from petroleum wells can be used to construct steady state models of fluid flow and petroleum production data can be used to formulate dynamic models using history matching techniques. Models derived from piezometric head measurements have the added advantage that they can be calibrated with field data. If adequate water level time series data are available, transient models can also be constructed and calibrated. Regional groundwater models commonly suffer from a lack of data for deep aquifers and the accuracy of models formulated with petroleum well data is limited by the errors inherent in pressure measurements. Union of the two data types into a hybrid model is not a trivial process, but can provide constraints on the interaction between shallow and deep aquifers on a regional scale if correctly formulated.

There is a significant body of work associated with the injection of CO_2 into saline aquifers (e.g. Bachu and Bennion, 2008; Bachu et al., 1994; Birkholzer et al., 2009; Doughty, 2008; Doughty et al., 2003; Doughty et al., 2008; Gaus et al., 2005a; Ghomian et al., 2008; Gunter et al., 1996; Gunter et al., 2000; Gunter et al., 1993; Gunter et al., 1997; Michael et al., 2008a; Michael et al., 2008b; Nordbotten et al., 2005; Qi et al., 2009). There are many concepts and analytical techniques which can be applied

to both saline and freshwater aquifers, and there is much to be gained from the available body of literature. There are, however, some important differences which must be considered and there has been no published research to date on the possible impacts of CO_2 injection directly into freshwater aquifers.

Recent studies have examined the potential impact on freshwater aquifers of injecting CO_2 into adjacent saline groundwater bodies (Birkholzer et al., 2009; Nicot, 2008). These studies examine the effects of the CO_2 injection-induced pressure wave and their results show that very large basin volumes are influenced relative to the size of the actual CO_2 plume. Birkholzer et al.'s model (2009) indicates that significant pressure buildups may occur more than 100 km from the injection site. Their model domain consists of a hypothetical stacked, horizontal aquifer/aquitard system that would serve as an appropriate analogue for the Surat and Eromanga basins. The TOUGH2/ECO2N multiphase simulator (Pruess, 2005; Pruess et al., 1999) is used to model the behaviour of the injected CO_2 and the associated induced pressure regime. Nicot's (2008) study used the single fluid phase MODFLOW96 groundwater modelling code (Harbaugh and McDonald, 1996) to compare two injection rate scenarios. This code was chosen to model the regional effects of pressure buildup and not the local near-well effects of dual phase fluid flow (Nicot, 2008). The results of the model simulations illustrate that balancing the CO_2 injection rate relative to the expected changes in the regional water table is of great importance.

A detailed baseline understanding of the groundwater system is required prior to modelling injection scenarios. The potential impacts of injection-derived fluid displacement can consist of: increased potentiometric heads, increased baseflow to streams, increased evapotranspiration and, in the case of brine displacement, degradation in water quality (Nicot, 2008). One of the most important findings of Nicot's (2008) research is that gradient reversal may take place if injection rates are excessive. This could lead to up-dip groundwater flow as opposed to down-dip flow, which would accelerate the migration of the CO_2 plume and eliminate the positive effects of antagonistic hydrodynamic flow trapping. This hypothesis is, however, based on model simulations where the injection rates are excessively high (5 Mtpa per well) and there are currently no field data to confirm or refute the results. The permeability of the overlying seal also has an important influence on pressure buildup. Seals that have relatively high permeability significantly reduce the buildup pressure, but also allow considerable vertical leakage into overlying units (Birkholzer et al., 2009). Where brackish and saline aquifers are chosen for injection, there is potential to contaminate an overlying freshwater aquifer. In the case of injection into a freshwater aquifer, leakage would result in CO_2 contamination only. In both cases, the rate of leakage would need to be quantified to asses whether the degree of contamination could be naturally absorbed into the overlying groundwater system, without any detrimental effects to water quality.

There are other factors that need to be considered when modelling a freshwater/CO_2 system as opposed to a brine/CO_2 system. Petroleum system analogues still apply, whereby supercritical CO_2 behaves as the non-wetting phase and water as the wetting phase (Doughty, 2008). Factors such as capillary pressure and relative permeability hysteresis exert important controls in such systems (Doughty et al., 2008; Ghomian et al., 2008; Spiteri and Juanes, 2006). Input values for freshwater models will be different to those for brackish/saline/hypersaline models. Both capillary pressure and relative permeability are partially dependent on the interfacial tension (IFT) between CO_2 and water (Bachu and Bennion, 2008). Interfacial tension is dependent on pressure, temperature and salinity and as the surface tension of aqueous liquids increases with increasing salinity (Bachu and Bennion, 2008) IFT and hence, capillary pressure and relative permeability vary between freshwater and saline systems. Relative permeability hysteresis and capillary trapping are also dependent on fluid/rock wettability characteristics (Qi et al., 2009; Spiteri and Juanes, 2006). This controls the dominant mechanism by which the non-wetting phase is transported and trapped in the reservoir media (Spiteri and Juanes, 2006). Water/CO_2 systems have been found to be only weakly water-wet, which is the opposite for many minerals in hydrocarbon systems (Chiquet et al., 2007; Qi et al., 2009). A consequence of this difference in wettability character is that the sealing capacity of caprocks may be substantially reduced if CO_2 becomes the wetting phase. A hydrocarbon system close to capillary leakage can only sustain a much lower CO_2 storage pressure than the initial reservoir pressure (Chiquet et al., 2007).

A common problem associated with high salinity groundwater systems is solving flow dynamics for variable density fluids. This situation takes two forms: variable density groundwater which is miscible, and water of constant density and non-aqueous immiscible fluids. Variable density flow is problematic in steeply dipping aquifers, where the effects of buoyancy become significant (Bachu, 1995a; Bachu and Michael, 2002). Davies (1987) developed a relationship referred to as the driving force ratio

(DFR), to assess the level of error apparent in a variable density flow field constructed using equivalent freshwater or environment hydraulic heads (Lusczynski, 1961). Hydrodynamic characterisation commonly includes DFR analysis when interpreting the potentiometric flow field (Bachu, 1995a; Bachu and Michael, 2002; Hennig et al., 2003; Otto et al., 2001). In flat-lying freshwater aquifers with little variation in groundwater density, DFRs are low and the errors that may be apparent in flow vectors are acceptable (Bachu, 1995a). Geothermal gradients also have to be considered, because temperature variations exert a greater influence on water density than salinity. The potentiometric flow field in an aquifer must be adequately constrained prior to CO_2 injection, to accurately estimate and predict plume migration and dispersal behaviour. The freshwater aquifers in the Surat and Eromanga basins can be successfully modelled as constant fluid density systems, showing only minor variations in salinity and temperature.

CO_2 solubility, hydrochemistry and geochemistry

Solubility and mineral trapping mechanisms are considered to be the long-term mechanisms by which CO_2 is immobilised in the subsurface (Gaus et al., 2008). Extensive investigations into CO_2 solubility in water at the pressure and temperature conditions applicable to carbon geostorage have been carried out (Bermejo et al., 2005; Diamond and Akinfiev, 2003; Johnson et al., 1992; Koschel et al., 2006; Portier and Rochelle, 2005; Spycher and Pruess, 2005; Spycher et al., 2003). This work ranges from generic experimental studies on freshwater solubility (e.g. Dhima et al., 1998; Diamond and Akinfiev, 2003; Takenouchi and Kennedy, 1964), to that on brackish/saline/hypersaline systems (e.g. Spycher and Pruess, 2005; Takenouchi and Kennedy, 1965; Yasanushi and Yoshida, 1979). Although most work has been focused on freshwater and Na-Cl solutions, other electrolyte compositions have been studied (e.g. Bermejo et al., 2005; Rumpf and Maurer, 1993; Yasanushi and Yoshida, 1979). There is a lack of research into CO_2 solubility in Na-HCO_3 solution compositions, which can present problems when modelling injection into groundwater of this type. The bias towards experimental work on Na-Cl solutions is due to the fact that many brines are of this type in deep sedimentary basins. In addition, natural evolution of groundwater from fresh Na-HCO_3 to saline NaCl character is predicted by the Chebotarev sequence (Chebotarev, 1955).

The solubility of CO_2 in aqueous electrolytes is low regardless of composition and, at fixed temperature and pressure, solubility decreases with increasing salinity (Gaus et al., 2008). At 50^{o}C and 8 MPa the solubility of CO_2 in freshwater is ~1.4 mol/kg water (Gaus et al., 2008), at the same temperature and pressure in a solution of seawater salinity (36,000 mg/L TDS), solubility is reduced to ~0.9 mol/kg water (Gaus et al., 2008; Portier and Rochelle, 2005). Despite this low solubility, recent research in naturally occurring CO_2 rich gas fields has shown that solution trapping is the dominant mechanism by which CO_2 is sequestered (Gilfillan et al., 2009).

The principle speciation reactions of concern during carbon geostorage into aqueous environments are the hydrolysis of CO_2 which produces carbonic acid and the subsequent dissociation to form bicarbonate:

Carbonic acid production:

$$CO_2 + H_2O \rightarrow H_2CO_3 \quad (1)$$

Dissociation to bicarbonate and acid production:

$$H_2CO_3 \leftrightarrow HCO_3^- + H^+ \quad (2)$$

This is only a very simplistic view and does not take account of the possible suite of reactions that may take place by changing the hydrochemistry of the host groundwater. In addition to speciation reactions within the fluid, water-rock reactions will also take place further changing the solution composition of the groundwater (e.g. Beaucaire et al., 2008; Ennis-King and Paterson, 2007; Ennis-King et al., 2003; Gaus et al., 2005a; Gaus et al., 2005b; Pauwels et al., 2007; Rosenbauer et al., 2005; Wigand et al., 2008).

Example buffering reaction from calcite dissolution:

$$CaCO_3 + H^+ \rightarrow HCO_3^- + Ca^{2+} \quad (3)$$
(calcite)

Weathering of albite to kaolinite:

$$2NaAlSi_3O_8 + 2CO_2 + 11H_2O \rightarrow Al_2Si_2O_5(OH)_4 + 2HCO_3^- + 2Na^+ + 4H_4SiO_4 \quad (4)$$
(albite) (kaolinite)

Modelling of these processes is complex and there are still significant limitations in the use of modern approaches (Gaus et al., 2008). The modelling of speciation and reactive transport related to solutions of high ionic strength present particular problems. High salinity speciation requires the use of approaches such as the extended Debye-Hückel or B-dot equation or virial techniques such as the Pitzer formulation (Anderson, 2005; Naresh and Singh, 2009; Pitzer, 1973; Pitzer, 1991). The latter produces the most accurate results but there are very few thermodynamic values available for the technique, which is largely restricted to modelling major ion chemistry only. This is significant, as shown by the work of Gunter et al. (2000), where the precipitation of siderite exerted strong control on the buffering capacity of the groundwater. It is, therefore, much easier to model the behaviour of dilute freshwater systems and the associated water-rock reactions using the standard Debye-Hückel theory (Debye, 1954).

The production and dissociation of carbonic acid (H_2CO_3) reduces the pH (equation 2) of circum-neutral groundwater significantly in the region of the injection well (Gunter et al., 2000). This results in the concomitant dissolution of minerals in the aquifer and subsequent precipitation of secondary minerals, the composition of which varies with distance from the well and over time (Gaus et al., 2005a; Xu et al., 2005; Xu et al., 2007; Zhang et al., 2009). Modelling approaches vary in complexity depending on the required outcomes and commonly begin with a thermodynamic equilibrium approach (Gaus et al., 2008). Time is an important factor when considering the effectiveness of mineral trapping mechanisms for carbon geostorage and the need for kinetic rate modelling is, therefore, introduced. Reaction rate coefficients for this type of modelling are less readily available than thermodynamic data (Bénézeth et al., 2007). Assumptions often have to be made that similar minerals have similar reaction rates, and precipitation and dissolution rates are commonly considered to be equivalent (Gaus et al., 2008; Gaus et al., 2005a; Gunter et al., 2000). Kinetic rate laws and their corresponding rate coefficients are generally more readily available for freshwater, than those for solutions of higher ionic strength.

Reactive transport models attempt to forecast the change in the primary mineral assemblage and the resulting secondary minerals that form due to the change in solution composition (Gaus et al., 2008). It is of great importance that appropriate primary and secondary mineral assemblages are selected for a given model (Gaus et al., 2005a). Accurate mineral analysis of aquifer media provides a first order constraint, but geochemical data are also required to accurately assess the composition of particular mineral groups, such as feldspars. Feldspar minerals in siliciclastic aquifers/reservoirs make the most significant contribution to ions in solution due to dissolution reactions and weathering to clay minerals (equation 4). Research into the effects of CO_2 injection on the caprock at the Sleipner project has shown that plagioclase feldspar dissolution rates are dependent on feldspar composition (Gaus et al., 2005a). Isomorphic solid solution is ubiquitous in the plagioclase feldspars, whereby mineral stability decreases with increasing calcium/sodium ratios from albite (Na end-member) to anorthite (Ca end-member).

Mineral trapping is the permanent form of CO_2 immobilisation and is thought to operate over the longest time-scales (Gaus et al., 2008). Experimental studies show that inorganic mineral reactions are similar for both sub- and supercritical CO_2 systems (Kaszuba et al., 2003; Kaszuba et al., 2005). The carbonate minerals: calcite, dolomite, magnesite, siderite and dawsonite are often cited as possible sinks for CO_2 (Bénézeth et al., 2007; Gunter et al., 2000; Kaszuba et al., 2005; Moore et al., 2003; Worden, 2006). Dawsonite, although a rare mineral, is frequently suggested as a CO_2 sink (Gaus et al., 2005a; Knauss et al., 2005; Moore et al., 2003; White et al., 2005), due to its natural occurrence in certain sedimentary basins (Baker et al., 1995; Moore et al., 2003; Worden, 2006). Recent research on dawsonite dissolution rates (Bénézeth et al., 2007; Hellevang et al., 2005) and paragenesis (Worden, 2006) indicate that the conditions under which the mineral forms are still poorly understood. Modelling the potential impact of mineral trapping involving dawsonite should be conducted with extreme care and the results interpreted with caution. Experimental results looking at the effects of CO_2 fugacity on dawsonite stability show that rapid dissolution takes place once CO_2 hydrolysis becomes advanced and the effective partial pressure of CO_2 is reduced (Hellevang et al., 2005). This raises the question as to why the mineral persists over geological time and suggests a strong kinetic influence on stability. There are currently no data to assess the rate constants for dawsonite precipitation (Bénézeth et al., 2007; Gaus et al., 2005a), which equates to an unsettling level of subjectivity in modelling results.

Great Artesian Basin

There are a vast number of publications related to the Great Artesian Basin (GAB), predominantly focused on water balance assessments and regional flow regimes (e.g. GABCC, 1998; Habermehl, 1980; Hennig, 2005; Quarantotto, 1989; Radke et al., 2000). Great effort has been made to constrain the system based on fragmented datasets of variable quality and limited time-series information. There are still significant knowledge gaps in the understanding of the basin hydrogeology, particularly the flow regimes and chemical character in the deeper regions of the known aquifers (GABCC, 2008).

The GAB is characterised as a hydraulic basin with boundaries that do not necessarily correspond with those of the constituent sedimentary basins. The limits of the GAB have been defined on the basis of accessibility to usable artesian groundwater supplies. On this basis, the Triassic units of the Bowen and Galilee basins are included. Most of the abstracted groundwater is, however, sourced from the Jurassic and Cretaceous sequences of the Surat and Eromanga Basins. The stratigraphic architecture of the Surat and Eromanga Basins formalised by (Exon, 1976) provided the basis for much of the hydrostratigraphy summarised by Habermehl (1980) and Quarantotto (1989). Both basins consist of relatively undeformed, flat-lying sedimentary units, which constitute a vertically stacked series of aquifers and aquitards. Many of the aquifer-aquitard systems also form hydrocarbon reservoir-seal pairs, particularly in the Eromanga Basin (Draper et al., 2002; Green et al., 1997).

One of the early landmark groundwater modelling achievements was the application of the GABHYD finite difference approach (Seidel, 1980), which provided more solid constraints on regional groundwater flow interpretations (Habermehl, 1980; Habermehl, 1986). The GABHYD model was superseded by the steady state GABFLOW model (Welsh, 2000) utilising the MODFLOW (U.S.G.S., 2005) groundwater modelling code and more recent data. A transient MODFLOW model has also been formulated (Welsh, 2006) but the paucity of time-series data limits effective calibration. Extensive groundwater age dating studies were carried out in the GAB, to assess residence times and increase understanding of recharge/discharge relationships (Habermehl, 1986; Radke et al., 2000). Implied hydrodynamic models derived from hydrochemical data have also been constructed for the aquifers in the Surat Basin (Quarantotto, 1989) and the Cadna-owie-Hooray aquifers across both the Surat and Eromanga basins (Radke et al., 2000). Groundwater flow vectors (Fig. 2) derived from shallow aquifer information show a regional flow path from major recharge areas in the north and northeast in Queensland to a major discharge centre at Lake Eyre in South Australia (Habermehl, 1980). Work on the Cadna-owie - Hooray aquifer system shows a more complex pattern (Fig. 3) with radial flow from the central GAB and some northward flow from the south of the Surat Basin (Radke et al., 2000).

A major shortcoming in many GAB modelling studies is the lack of information available for deep aquifers. Hitchon and Hays (1971) used the results of drill stem pressure tests from petroleum wells to construct a 2D flow model for the Surat Basin. This approach was employed to provide information on the flow regime prevalent in the deeper, unexploited regions of the aquifer systems. The steady state model provides a view of the flow system prior to extensive petroleum production from the Surat Basin. The flow regime postulated from this model contains two regional systems divided by the Thomby Ranges. Centripetal flow vectors indicate discharge or quasi-stagnation points in the central region of each flow domain, with some similarity to the shallow groundwater flow regimes suggested by Habermehl (1980) and Radke (2000). Hitchon and Hays' (1971) approach demonstrates that petroleum data can be effective in developing steady state hydrodynamic models. Similar methods have been used in more recent onshore and offshore studies (e.g. Hennig et al., 2006; Hitchon et al., 1990; Hortle (Hennig) et al., 2008).

The above is a short synopsis of some of the more prominent GAB studies, including recent work on flow modelling and implied hydrodynamics. Extensive bibliographies detailing the long history of hydrogeological research conducted in the GAB are given by Habermehl (1980), GABCC (1998) and Radke et al. (2000).

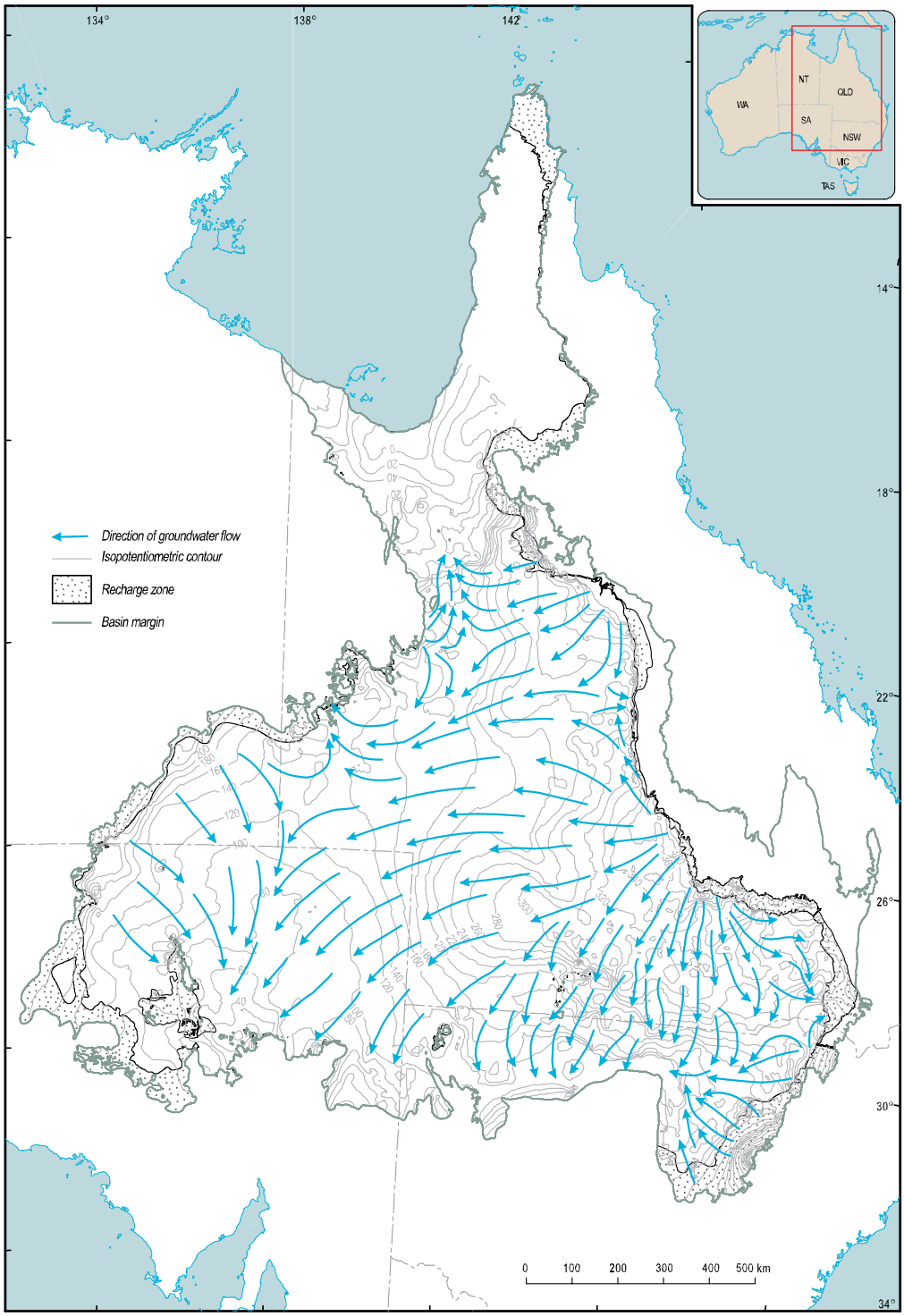

Figure 2. Regional flow vectors for the Great Artesian Basin groundwater system (after Habermehl, 1980).

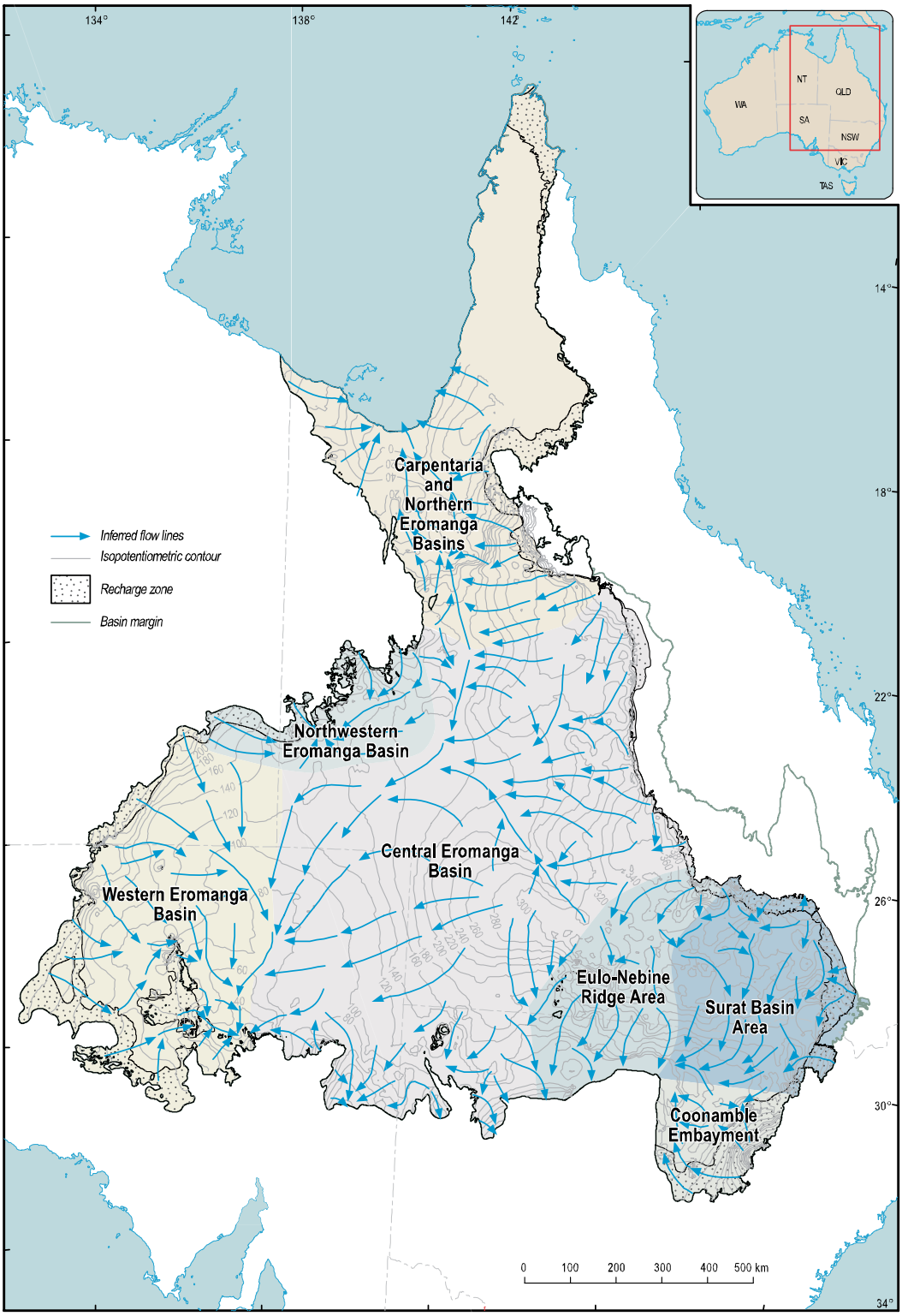

Figure 3. Implied hydrodynamic flow vectors for the Canda-owie - Hooray Sandstone aquifers in the Great Artesian Basin (after Radke et al., 2000).

CO2CRC projects related to aquifer/reservoir characterisation and hydrodynamics

Hydrogeological characterisation projects carried out by the CO2CRC have built on initial conceptual studies conducted as part of the GEODISC program (e.g. Sayers et al., 2005). Storage evaluation and geological modelling studies have been carried out for the Galilee Basin (Marsh et al., 2008; Rawsthorn et al., 2009) and the Bowen and Surat basins (Daniel, 2008; Kalinowski, 2006; Marsh and Scott, 2005; Patchett, 2006; Sayers et al., 2005). The CO2CRC has also conducted a number of specific aquifer characterisation and hydrodynamic studies in Queensland (Cinar, 2006; Hennig, 2005; Hennig et al., 2006; Patchett, 2006). The hydrodynamic characterisation projects are based on petroleum systems hydrogeology techniques also employed in the APCRC GEODISC Program (e.g. Hennig et al., 2003; Underschultz et al., 2003). These concepts have formed the basis of petroleum hydrodynamics for many years (Bachu, 1995a; Bachu, 1995b; Dahlberg, 1995; Davies, 1987; Hitchon, 1969a; Hitchon, 1969b; Hitchon et al., 1990; Hitchon and Hays, 1971; Michael and Bachu, 2001; Otto et al., 2001).

The objectives of hydrodynamic studies related to CO_2 geostorage are to establish the potential for hydraulic communication between adjacent formational units (in both the vertical and horizontal planes), including faults and to put first order constraints on groundwater flow vectors (e.g. Hennig et al., 2006). Conventional pressure/depth plots combined with hydraulic heads derived from pressure and water salinity measurements, have been employed to investigate the vertical connectivity between the Showgrounds Sandstone and the Rewan Formation, and the Showgrounds Sandstone and the Precipice Sandstone in the Surat Basin (Hennig et al., 2006). This work also examined the relationships between the pre- and post-production flow fields in the Wunger Ridge area by comparing hydraulic head gradients to spud dates. Input data were assessed and validated using the CSIRO PressureQC™ methodology (Hortle (Hennig) et al., 2002). The same techniques were applied to the Waarre Formation in the Otway Basin as part of the CO2CRC Otway CO_2 injection project (Hennig, 2007; Hortle (Hennig) et al., 2008). Vertical hydraulic connectivity relationships in the eastern Surat Basin were also interpreted using a similar but less rigorous approach (Patchett, 2006). This study postulated hydraulic communication between the Showgrounds Sandstone and the Precipice Sandstone and also between the Precipice Sandstone and the Evergreen Formation.

The CO2CRC conducted collaborative work with the Australian School of Petroleum, which examined the seal capacity of the Snake Creek Mudstone in the Wunger Ridge area of the Surat Basin (Daniel, 2008). This study complimented previous work on hydrodynamics and reservoir characterisation (Cinar, 2006; Hennig et al., 2006; Sayers et al., 2005). Research into CO_2 related diagenesis as part of the Otway injection project, has provided an indication of the effects of fluid-rock interactions resulting from carbon geostorage (Schacht, 2008).

Study Area

Geology of the Surat and Eromanga Basins

The Jurassic to Cretaceous Surat and Eromanga basins (Fig. 1), along with the Carpentaria Basin in the north of Queensland form the larger part of the Great Artesian Basin (Radke et al., 2000). The Surat Basin is contiguous with the Clarence-Moreton Basin (CMB) in the east, separated by the Kumbarilla Ridge (Green et al., 1997). The CMB is considered part of the GAB in Queensland up to the border with New South Wales. The compilation and integration study of the Surat Basin by Exon (1976) endeavoured to provide a synthesis of previous geological investigations, carried out over a period of approximately 100 years. This work was expanded with new data and reinterpretation of the basin evolution as part of the Sedimentary Basins of Eastern Australia (SBEA) project (Green et al., 1997). The report by Draper et al. (2002) on the geology of the Cooper and Eromanga basins provides a similar compilation and reinterpretation for the Eromanga Basin. Further research, resulting from the SBEA project regarding the Surat Basin, was published in a special edition of the Australian Journal of Earth Sciences (Vol. 56 issue 3) early in 2009. The reports by Green et al. (1997) and Draper et al. (2002) provide extensive bibliographies detailing prior work carried out in the Surat and Eromanga basins, respectively.

The Surat and Eromanga basins formed during a widespread sag phase, subsequent to an extensive period of uplift and erosion during the Middle-Late Triassic (Green et al., 1997). There has been some debate with regard to the driving mechanism behind the major phase of Jurassic basin initiation. Korsch et al. (1989) consider thermal sag to be the principle driver whereas Exon and Senior (1976) and Veevers et al. (1982) believe the basins to be pericratonic. Other models have been proposed

that include deep crustal metamorphism combined with thermal contraction (Middleton, 1980) and igneous underplating with coeval compression (Zhou, 1993). Modelling work suggests that dynamic platform tilting controlled subsidence in the Surat and Eromanga basins, similar to the mechanism postulated for the Bowen and Gunnedah Basins in the Late Permian (Korsch and Totterdell, 2009; Waschbusch et al., 2009). Subsidence in the western region of the Eromanga Basin is not consistent with this model (Waschbusch et al., 2009) and a thermal decay model seems more appropriate (Gallagher, 1990). The Surat Basin unconformably overlies basement rocks of the New England Fold Belt and the Triassic succession of the Bowen Basin (Hoffmann et al., 2009). The Eromanga Basin unconformably overlies the Permo-Triassic Cooper and Galilee basins and the Devono-Carboniferous Adavale Basin (Draper et al., 2002), the northern regions of the basin also overlie parts of the Devono-Carboniferous Drummond Basin and the Cambro-Ordovician Georgina Basin (Senior et al., 1978).

The sedimentary fill in both basins consists of a series of fining upward sedimentary cycles, beginning with braided stream deposits, followed by meandering stream and paludal coal-bearing sediments in the Jurassic section and a shift to coastal marine deposits in the Cretaceous (Gray et al., 2002; Green et al., 1997; Hoffmann et al., 2009). The continuity of stratigraphic units between the Surat Basin and the CMB across the Kumbarilla Ridge has been the subject of debate. The general consensus is that the formational units cannot be distinguished across the basement high and are grouped into the Kumbarilla beds. Stratigraphic continuity is, however, clearly evident between the Surat and Eromanga basins across the Nebine Ridge (Figs. 4 and 5). The older Precipice Sandstone and Evergreen Formation appear to pinch-out across the basement high, but the Hutton Sandstone, Walloon Subgroup/Birkhead Formation and the Lower Cretaceous units can be correlated successfully. The Surat Basin succession is up to 2500 m thick in the axis of the Mimosa Syncline (Fig. 4), which is the primary tectonic element in the basin (Hoffmann et al., 2009). The Eromanga Basin succession is 2500-2600 m thick in the deepest regions, which overlie tectonic elements in the underlying Cooper Basin (e.g. Windorah Trough and Yamma Yamma Depression) (Draper et al., 2002).

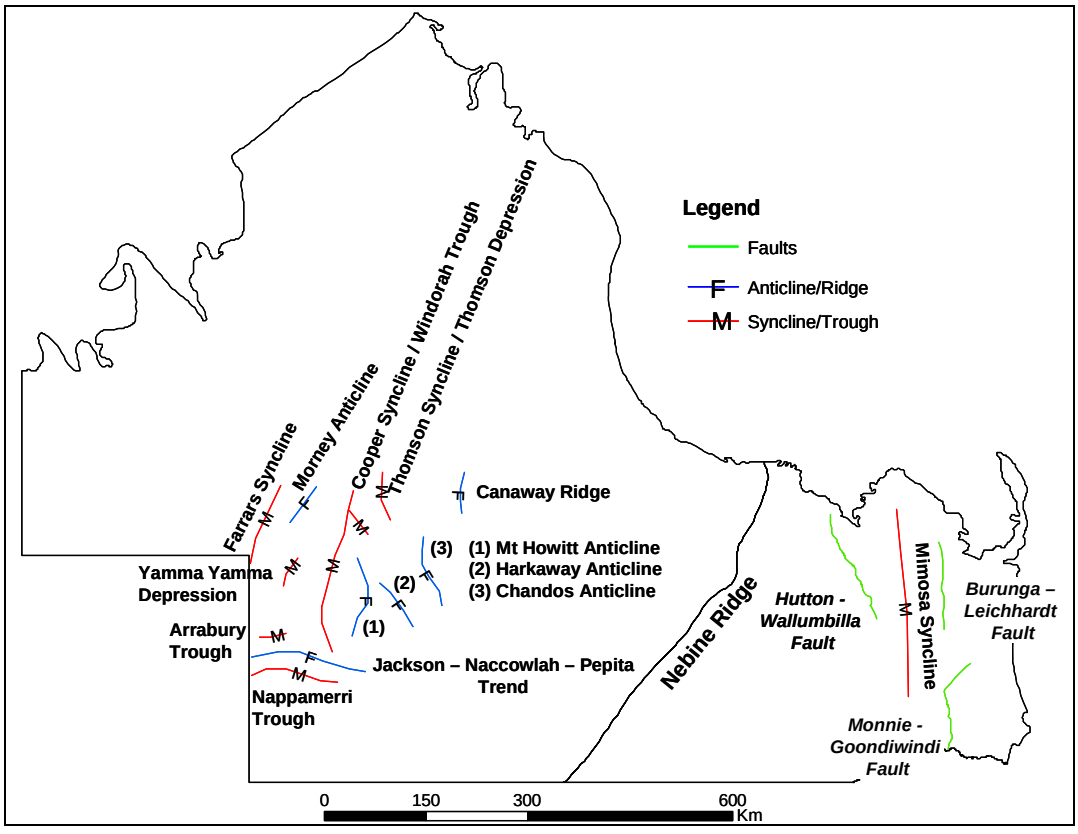

Figure 4a. Principle structural elements of the Surat and Eromanga basins.

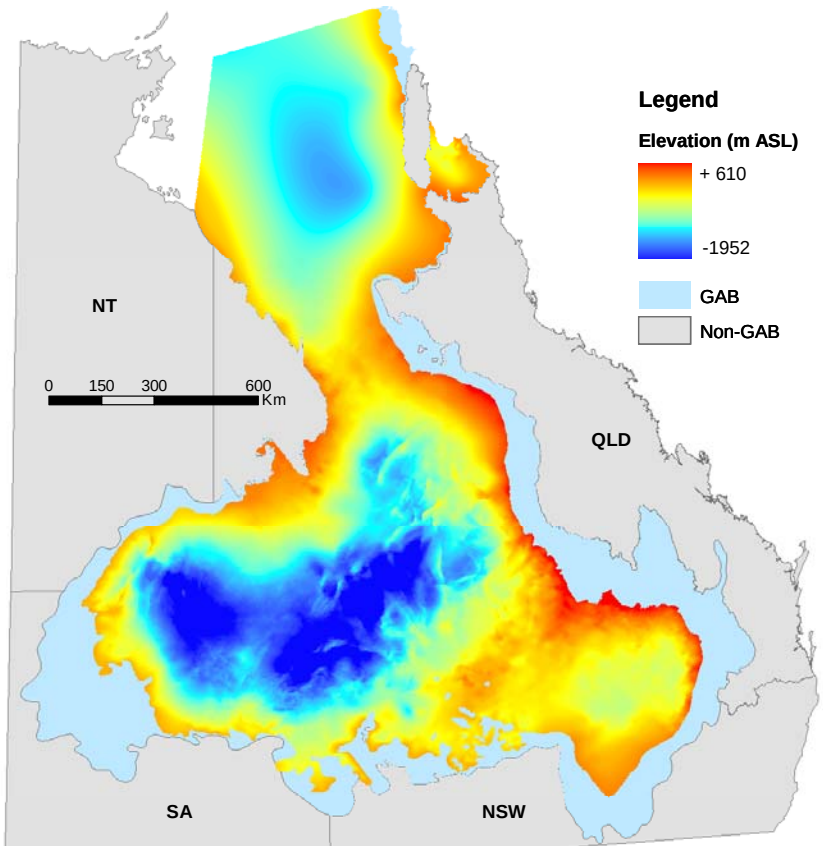

Figure 4b. Seismic C-horizon, which represents base Wallumbilla Formation (major seal for the GAB), in relation to GAB and state boundaries. Data from seismic interpretation constrained with petroleum wells and water bores.

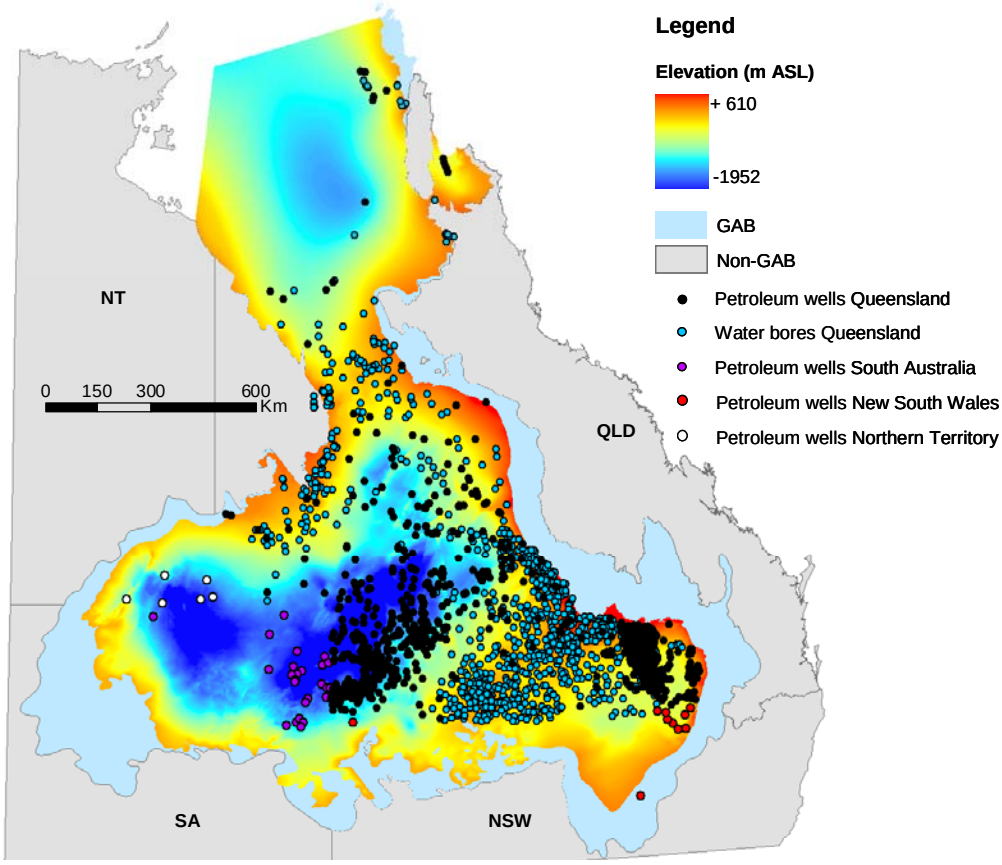

Figure 4c. Distribution of wells and bores used to constrain the seismic interpretation.

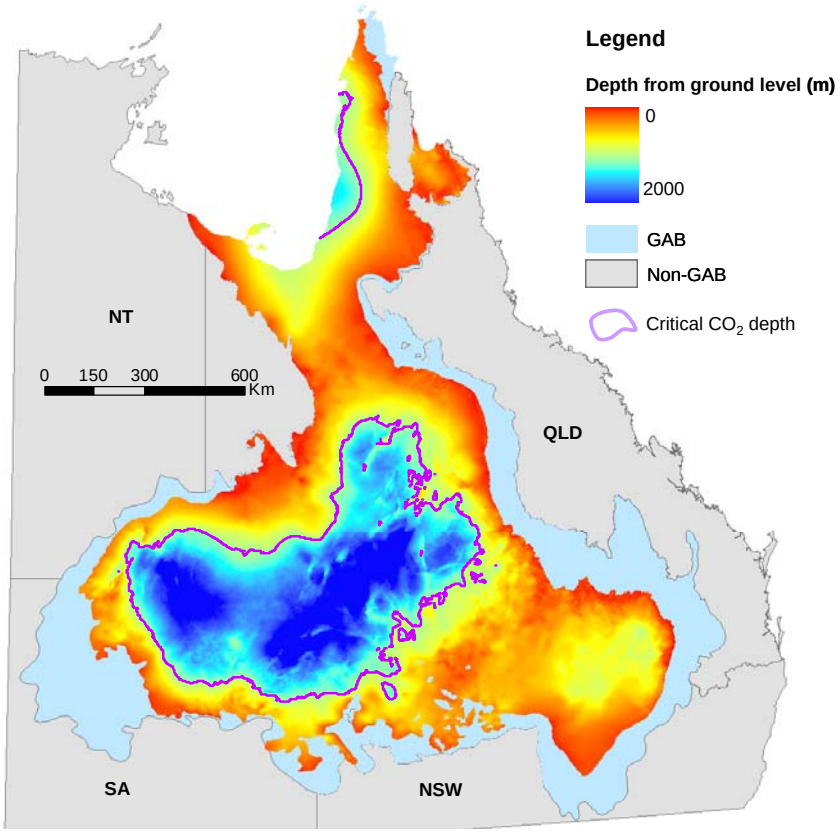

Figure 4d. Depth of base Wallumbilla Formation from surface. The outlined contour is the 800 m depth from ground level – approximate supercritical CO_2 depth.

The cyclic nature of the Jurassic/Cretaceous stratigraphy in the Surat and Eromanga basins forms a stacked sequence of reservoir/seal pairs and alternating aquifers and aquitards (Draper et al., 2002; Habermehl, 1980) (Fig. 6). Most groundwater bores are screened in the Jurassic/Cretaceous Hooray Sandstone aquifers in the Eromanga Basin and in the Gubberamunda Sandstone and the Mooga Sandstone in the Surat Basin. The Jurassic Hutton Sandstone is also a prolific source of groundwater in the north and northeast of both basins (QCGI, 2009). The vertically stacked aquifers and aquitards are 'leaky' in nature and groundwater migrates upward through the sequence (Habermehl, 1986). Oil is produced from both basins but predominantly from the Eromanga. All the reservoir sandstone units in the Eromanga Basin, from the Poolowanna Formation to the Cadna-owie Formation currently produce oil, with main production from the Birkhead Formation and the Hutton Sandstone (see Annual production and reserves figures produced by the Department of Employment, Economic Development and Innovation, 2008). Limited oil production comes from the Precipice Sandstone, Evergreen Formation and Hutton Sandstone in the Surat Basin. Vertical pooling of trapped hydrocarbons is common in many fields, testifying to the heterogeneous 'leaky' nature of the seals (Draper et al., 2002).

Structural deformation in both basins is minor. The major thrust faults and associated deformation in the underlying Permo-Triassic basins and basement rocks exert varying levels of influence on the younger strata. The principle structural element in the Surat Basin is the Mimosa Syncline which forms the axis of the basin above the Taroom Trough (Hoffmann et al., 2009). The east and west flanks of the Surat Basin are the most complex; reactivation of the Moonie-Goondiwindi and Burunga-Leichhardt thrust faults have influenced the overlying Jurassic units (QCGI, 2009). It is uncertain if the reactivation caused propagation of the faults through the younger units. The Hutton-Wallumbilla fault on the western flank displaces all the units, the magnitude of which decreases as the strata become younger (Fig. 4). The Jurassic units of the Surat Basin host a number of small faults with low displacements and limited strike lengths (Figs. 7a-e). The Eromanga Basin is similarly undeformed, with influence from the underlying Cooper Basin structures still evident in the Cadna-owie Formation (Fig. 7f). Late stage deformation is evident in the shaley intervals above the Cadna-owie Formation, and a widespread contractional event deformed the basin subsequent to deposition of the Winton Formation (Draper et al., 2002).

This page is intentionally left blank

Fig 5

Fig 5

Fig 6a

Fig 6a

Fig 6b

Fig 6b

Fig 6c

Fig 6c

Fig 6d

Fig 6d

Fig 6e

Fig 6e

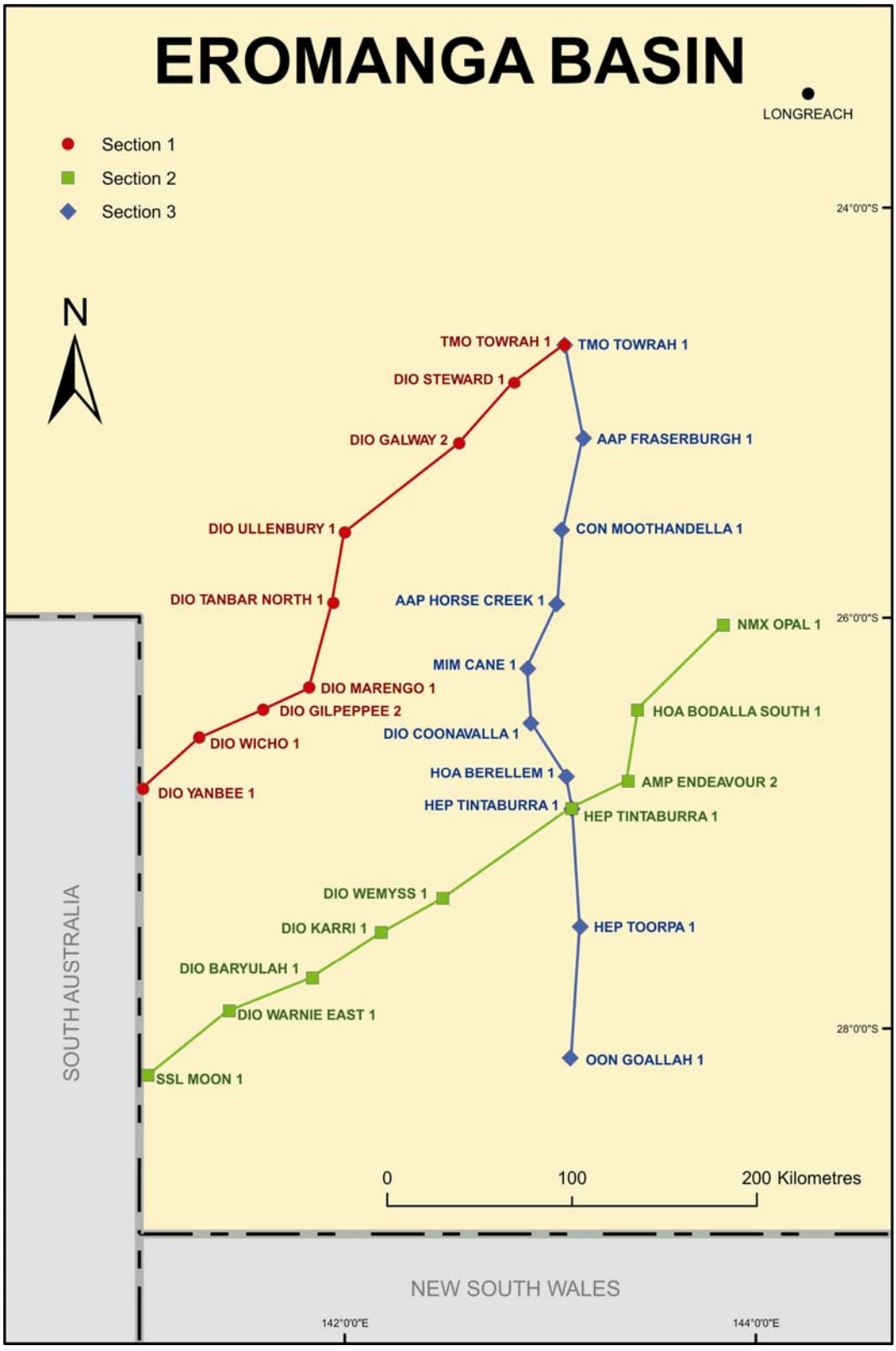

Figure 6f – Section locations in the Eromanga Basin.

This page is intentionally left blank

Fig 6g

Fig 6g

Fig 6h

Fig 6h

Fig 6i

Fig 6i

This page is intentionally left blank

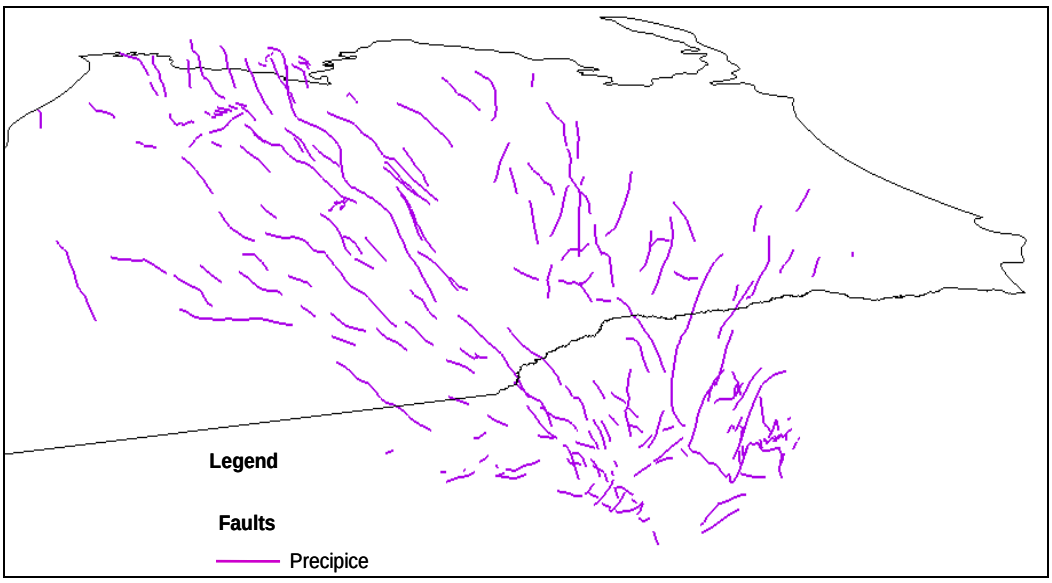

Figure 7a. Major faults mapped in the Precipice Sandstone, Surat Basin

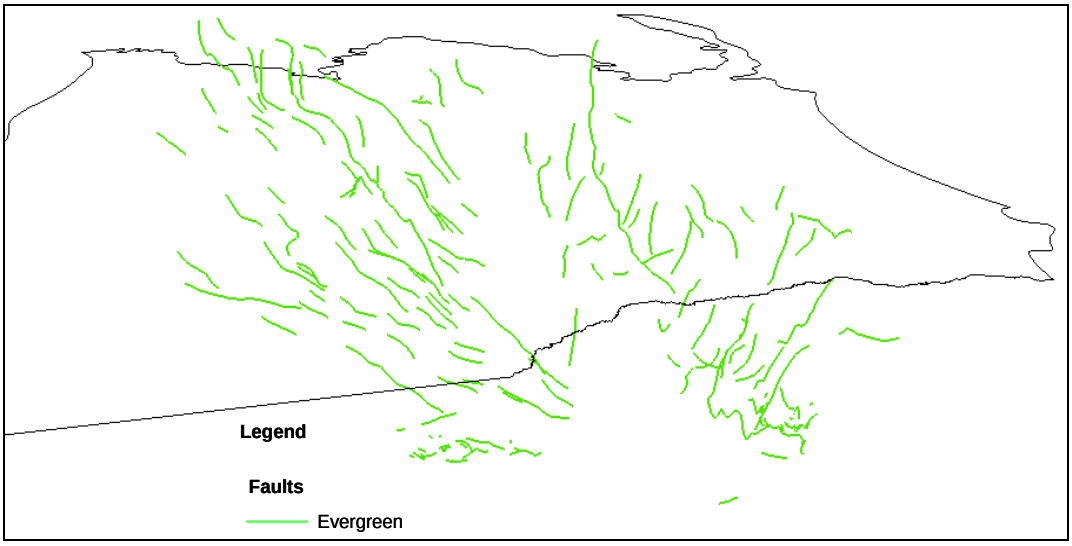

Figure 7b. Major faults mapped in the Evergreen Formation, Surat Basin

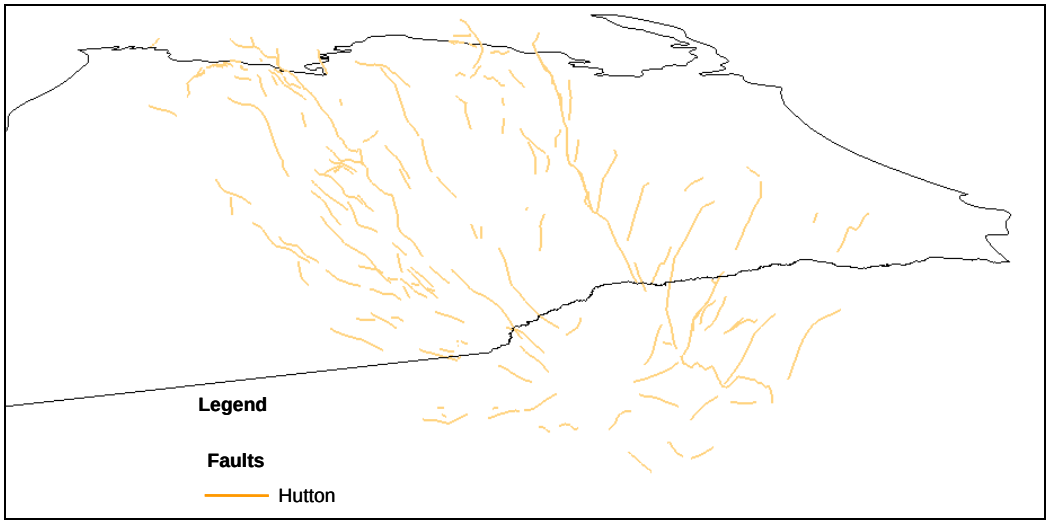

Figure 7c. Major faults mapped in the Hutton Sandstone, Surat Basin

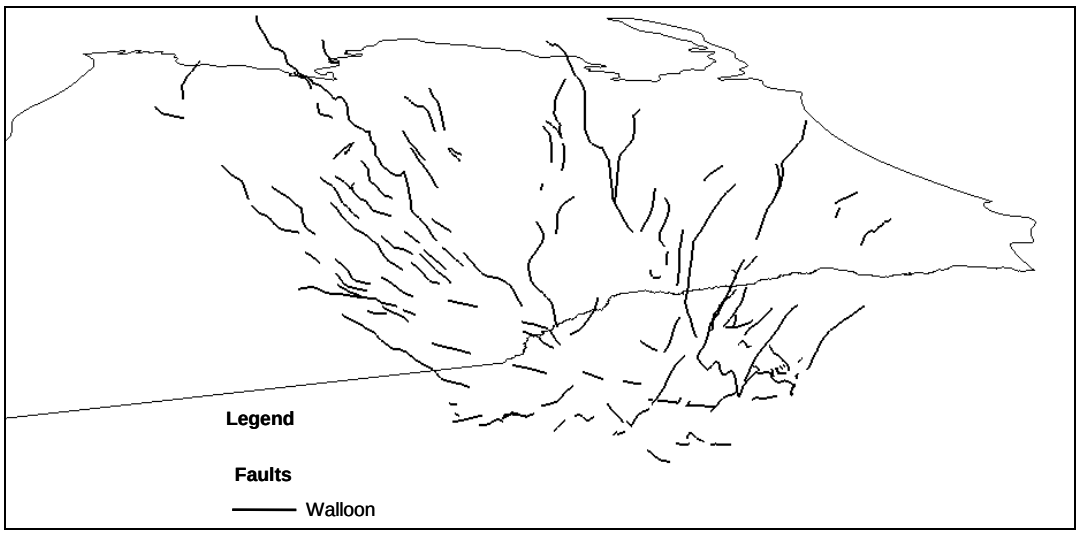

Figure 7d. Major faults mapped in the Walloon Subgroup, Surat Basin

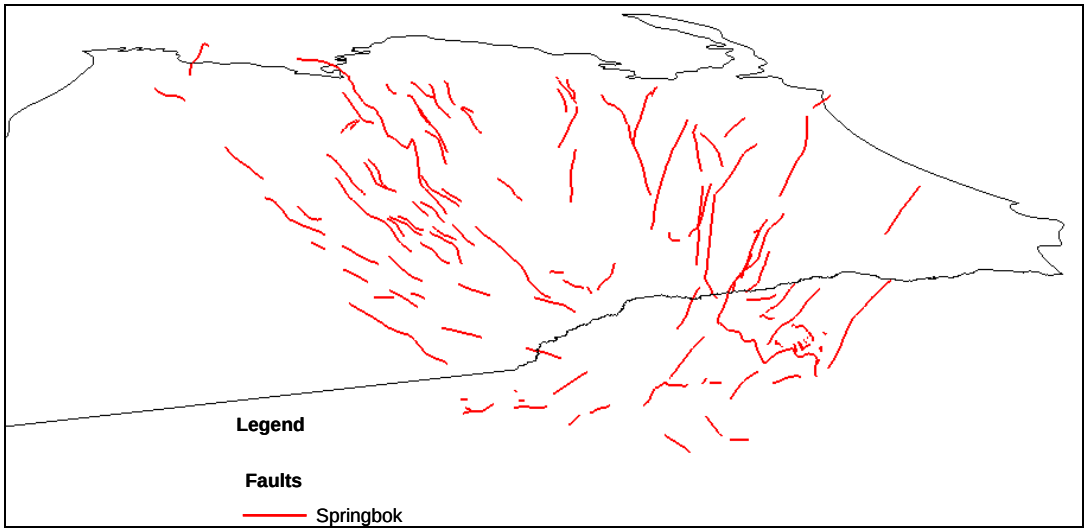

Figure 7e. Major faults mapped in the Springbok Sandstone, Surat Basin

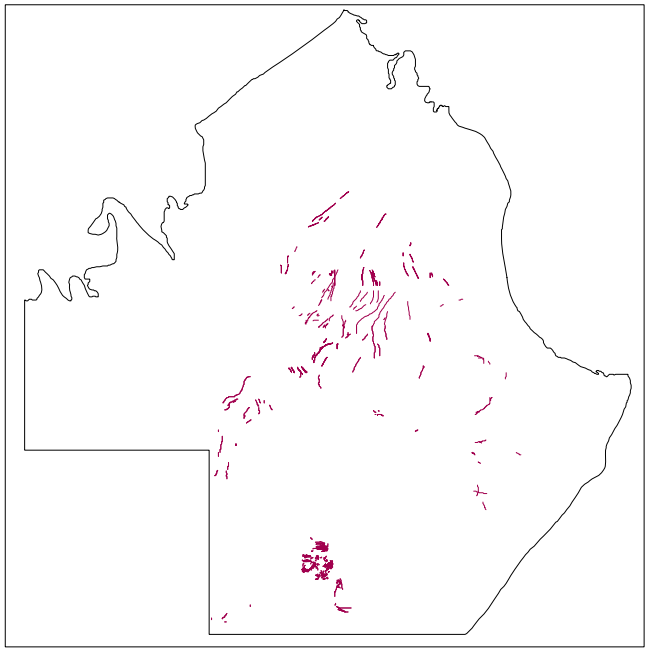

Figure 7f. Major faults mapped in the C-Horizon, Eromanga Basin.

Materials Methods and Data Limitations

The Department of the Environment and Resource Management Groundwater Database (DERM GWDB), the Queensland Petroleum Exploration Database (QPED), well completion reports (WCR) and mineralogical data from Carmichael (1989) are used as datasources for this study. Full details of the structure of the DERM GWDB and QPED and the rationale behind the use of the data can be found in "Potential for carbon geostorage in the Taroom Trough, Roma Shelf and the Surat, Eromanga and Galilee Basins - Preliminary Report" (QCGI, 2009). The gap analysis performed in the aforementioned report is used as the basis for this study. Data for the portion of the basins located in South Australia and New South Wales has been reviewed, but has not been subject to the same level of analysis as the Queensland datasets. This is due to the limited time available, and further more rigorous treatment of the data is warranted for future studies. Previous GAB studies have incorporated these datasets (GABCC, 1998; Habermehl, 1980; Radke et al., 2000) and their findings have been included in this work.

Modelling of geochemical interactions is restricted to inorganic phases; this is primarily due to the lack of data and the highly specialised topics of organic geochemistry which are beyond the scope of this work. References to interactions with organic material are included but restricted to a general qualitative context. A similar qualitative approach has been used to comment on the potential effects of reactive fluids on existing and future infrastructure. Discussions with the relevant personnel from government departments and industry consultants have provided estimates for the cost of remedial action, however, any estimates are provided strictly for guidance only. Detailed analysis of corrosion rates, material resistance and fluid leakage rates are required for quantitative economic modelling, which is also beyond the scope of this study.

Groundwater

The DERM GWDB is the principle source of groundwater hydrochemical and hydraulic head (water level) data. Both data subsets (hydrochemistry and water levels) cover a collection period spanning several decades and have been subdivided into appropriate collection time 'zones' (before and after 1960) to provide suitable comparative analysis. Long groundwater residence times in the Great Artesian Basin aquifers (up to 2 Ma (Radke et al., 2000)) and relatively low flow velocities (1-5 m y^{-1} (Habermehl, 1980; Habermehl, 1986)) permit the use of hydrochemical data spanning several decades (Fig. 8). This is in contrast to hydraulic head data which are subject to significant fluctuation over short timescales, due to intensive groundwater exploitation in the GAB. A subset of 9,751 groundwater bores is selected from a total of 22,567 in the Queensland sections of the Surat and Eromanga basins (Figs. 9 and 10). The selection is based on a data quality control exercise conducted by DERM. Hydrochemical analyses have been selected from the sub-set where the bores are considered to be abstracting groundwater from one formational unit only. This is to avoid the misinterpretation of mixing trends induced by the artefacts of water bore construction. The formations investigated are presented in Table 1.

Hydrochemical analyses from the DERM GWDB provide major ion compositions for the majority of the samples. Some analyses also include minor ion chemistry for dissolved species such as Al^{3+} and $SiO_2(aq)$. In many cases comprehensive analysis of minor and trace ions in solution was not carried out or the data are no longer available. Most of these analyses permit aqueous speciation calculations for major ion hydrochemistry only. Saturation indices provide an indication of the potential for minerals to precipitate from or dissolve into a solution. Using major ion hydrochemistry saturation indices can be calculated for minerals such as halite, sylvite, calcite, dolomite and magnesite. Analyses that include Al^{3+} and $SiO_2(aq)$ provide much greater scope and allow the generation of saturation indices for most clay minerals, feldspars and some rare minerals such as dawsonite. Comprehensive minor and trace ion analyses are required to calculate the saturation states for transition metal-bearing clay minerals and primary ferromagnesian minerals, which include the amphibole, pyroxene and olivine groups.

The GWDB also contains pH and alkalinity data which are important for establishing groundwater physico-chemical baselines. These data are used to provide starting solution acidity/alkalinity states for CO_2 injection simulations. The pH state and acid neutralising capacity of groundwater are important variables controlling mineral stability and are used to provide a conceptual understanding of the significance of hydrolysis, acidolysis and alkanolysis reactions.

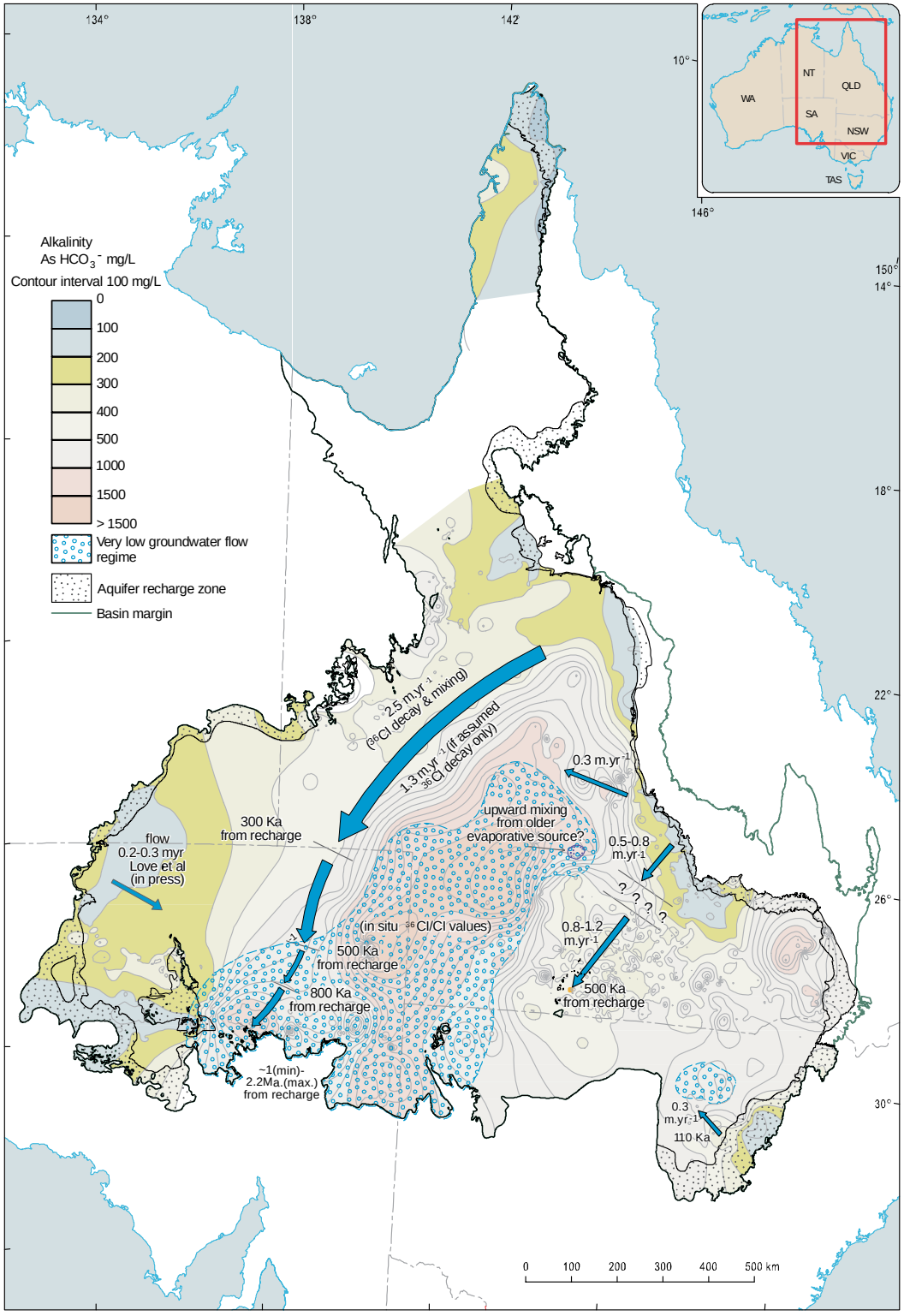

Figure 8. Mixing relationships and groundwater residence times in the Great Artesian Basin, after Radke et al. (2000).

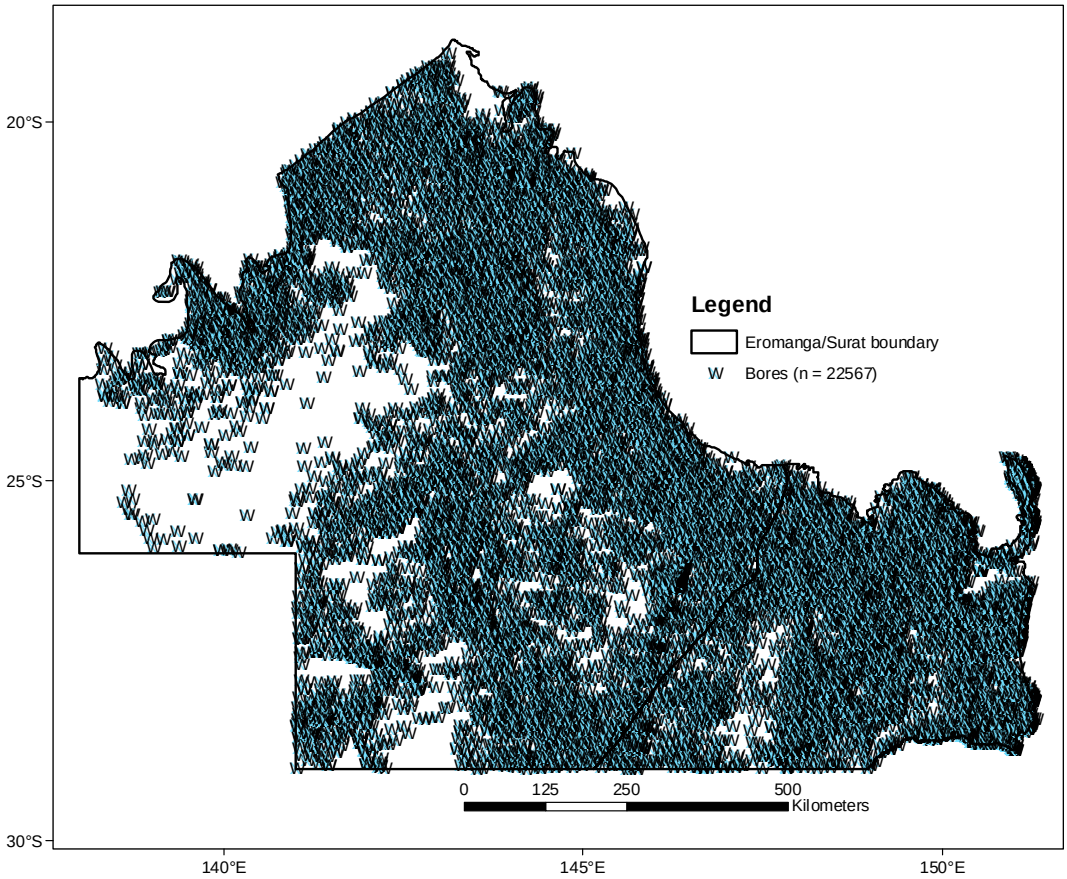

Figure 9. Distribution of all the groundwater bores recorded in the DERM GWDB.

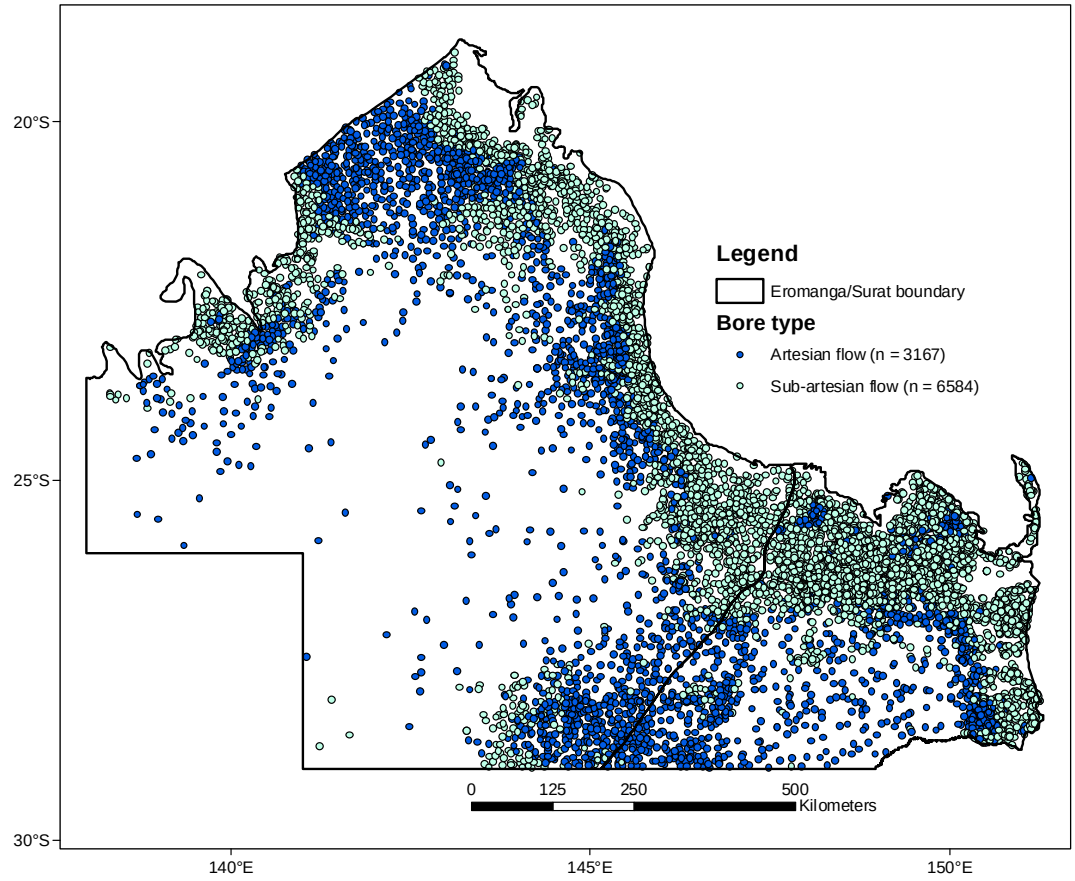

Figure 10. Distribution of groundwater bores with reliable information in regards to aquifer material, water chemistry and/or water levels (DERM GWDB).

Table 1. Equivalent stratigraphy between the Eromanga and the Surat basins

<table>
<tr><th>Era/Basin</th><th colspan="4">Eromanga</th><th colspan="3">Surat</th></tr>
<tr><td rowspan="8">Cretaceous</td><td colspan="4">Winton Formation
Mackunda Formation</td><td colspan="3">Griman Creek Formation</td></tr>
<tr><td colspan="4">Allaru Mudstone
Toolebuc Formation</td><td colspan="3" rowspan="2">Surat Siltstone</td></tr>
<tr><td rowspan="2">Wallumbilla Formation</td><td colspan="3">Coreena Member</td></tr>
<tr><td colspan="3">Doncaster Member</td><td rowspan="2">Wallumbilla Formation</td><td>Coreena Member</td></tr>
<tr><td colspan="3">Wyandra Sandstone Member
Cadna-owie Formation</td><td>Doncaster Member</td></tr>
<tr><td colspan="4">Bungil Formation</td></tr>
<tr><td rowspan="2">Hooray Sandstone</td><td rowspan="2">Longsight Sandstone</td><td rowspan="2">Gilbert River Formation</td><td colspan="3" rowspan="2">Mooga Sandstone
Orallo Formation
Gubberamunda Sandstone</td></tr>
<tr><td rowspan="4">Jurassic</td></tr>
<tr><td colspan="4">Ronlow beds
Westbourne Formation</td><td colspan="2">Westbourne Formation</td><td rowspan="3">Injune Creek Group</td></tr>
<tr><td colspan="4">Adori Sandstone</td><td colspan="2">Springbok Sandstone</td></tr>
<tr><td colspan="4">Birkhead Formation</td><td colspan="2">Walloon Subgroup</td></tr>
<tr><td colspan="4">Hutton Sandstone</td><td colspan="3">Hutton Sandstone</td></tr>
<tr><td colspan="4" rowspan="2">Poolowanna Formation</td><td colspan="3">Evergreen Formation</td></tr>
<tr><td colspan="3">Precipice Sandstone</td></tr>
</table>

yellow – reservoir/aquifer; green – seal/aquitard; grey – unconventional seal[1]/aquifer and/or aquitard

[1]Unconventional seals are defined as having extensively heterogeneous high and low permeability lithology, but dominated by fine-grained low permeability facies and of adequate thickness (>200 m) to inhibit the vertical migration of CO_2 under buoyancy forces.

Major ion hydrochemical compositions are used to plot regional trends in groundwater composition across the study area. In the trend plots, the groundwater sourced from a particular formation will be hereon termed 'water', i.e. 'Precipice Sandstone-sourced groundwater' will be termed 'Precipice water'. Analysis of the compositional distributions provides the basis for estimating potential mixing lines and hydraulic connectivity between aquifers. Basic equilibrium speciation simulations have been run using the major ion analyses from the GWDB. Initial simulations are run to estimate the possible state of equilibrium between the groundwater and the aquifer media. Subsequent simulations are run with the addition of CO_2 to the system. The fugacity of added CO_2 is systematically increased to examine the impact on solution pH. The Geochemist's Workbench (GWB) software package (Bethke and Yeakel, 2007) is used to perform the hydrochemical simulations. The generally low ionic strengths of the groundwater samples permit the use of the Debye-Hückel equation, for which the most extensive thermochemical data are available.

Mineralogical Data

The work of Carmichael (1989) in the Eromanga Basin is used in this study to provide basic mineral compositions for the rock types in the Surat and Eromanga Basins. Mineral identification of 347 samples from the succession in the Eromanga Basin was conducted using standard X-ray diffraction analytical techniques of whole rock powder samples and clay extracts. The spatial distribution of sample sites and the number of analyses in the Eromanga Basin are shown in Fig. 11.

The XRD mineral database provides basic whole rock and clay mineralogy for each sample, but does not distinguish solid solution series compositions (e.g. feldspars), and polymorphic differentiation is limited. This database provides the only source of mineral information for the deeper regions of the Jurassic/Cretaceous succession in the Eromanga Basin. There is currently no equivalent data for the Surat Basin. Fieldwork on formation outcrops and examination of hand specimen examples does, however, show that the framework compositions in both basins are equivalent. This is supported by optical microscopy studies and justifies applying the Eromanga Basin XRD results to the equivalent Surat Basin units.

Simple statistics have been applied to the dataset to provide a generalised representative mineralogy for each formational unit. These data are presented as a series of composite diagrams which contain summary tables and compositional pie charts normalised to 100 %. The distinction between detrital

and authigenic clay has not been made in the dataset, which introduces a degree of subjectivity into the interpretation of rock types. In the absence of petrographic analyses, lithic content cannot be distinguished. The rock types are, therefore, classified basis the relative abundance of quartz and feldspar. It is likely that a proportion of the kaolinite and smectite detected in the samples is of detrital origin, which would contribute to the lithic character in a given formation. Similarly the proportion of mineral content derived from diagenetic alteration cannot be ascertained from XRD analysis; a proportion of the quartz content is likely to be in the form of overgrowths resulting from dissolution precipitation reactions at depth (Carmichael, 1989; Green et al., 1989). The distinction between mineral origin and form is not of concern for the purposes of this study, because the existing mineralogy, regardless of origin and in combination with porosity and permeability distributions, will govern the water-rock reactions resulting from CO_2 injection.

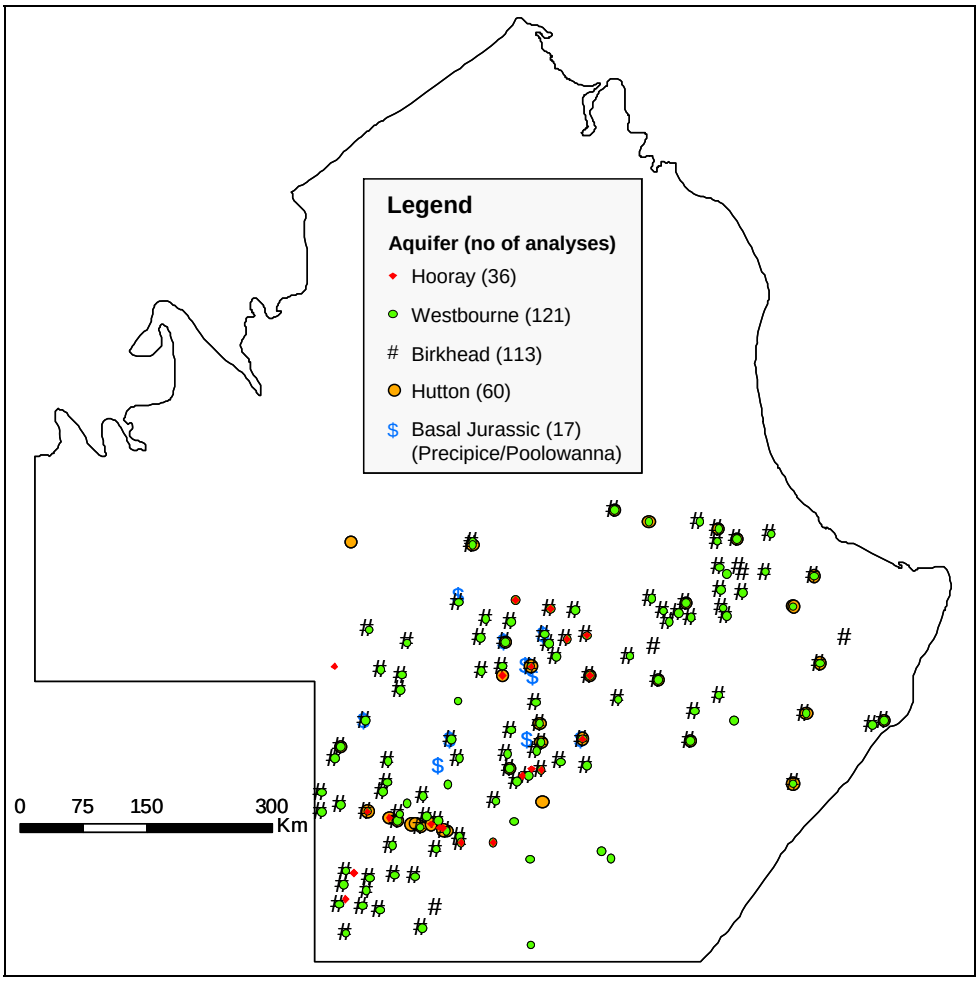

Figure 11. Distribution of quantitative X-ray mineralogical analyses undertaken in the Eromanga Basin (after Carmichael, 1989). Some wells were sampled in several units (hence superimposing symbols); heterogeneous units were sampled in both sandy and muddy sequences. The mineral character of the sampled formations was extrapolated to their equivalents in the Surat Basin.

The rock compositions are used in conjunction with groundwater hydrochemical and hydrological data to estimate the equilibrium state between the aquifer media and the hosted fluids. Basic geochemical simulations have been conducted, using the GWB software package to examine the possible water-rock reactions that may take place subsequent to CO_2 injection. Mineral and aqueous phase stability diagrams are used to illustrate the equilibrium conditions under which precipitation and dissolution reactions are likely to occur.

Hydrodynamic Analysis

The hydrodynamic analyses carried out by Habermehl (1980) and Radke et al. (2000) for the shallow regions of the GAB have been used as a regional baseline for this study (Figs. 2 and 3). It should be noted that the combined basin flow model provides only a very generalised indication of the regional

flow pattern and does not take account of localised deviations (Habermehl, 1980). Hitchon and Hays' (1971) hydrodynamic model of the Surat Basin provides the basis for an understanding of groundwater flow in the deeper regions of the basin but does not include the Eromanga Basin.

For this study formation pressure tests conducted in petroleum wells (drill stem tests: DSTs and wireline formation tests: WFTs) drilled in the eastern Surat Basin and the Eromanga Basin have been subjected to the CSIRO PressureQC™ quality control methodology (Hortle (Hennig) et al., 2002). A selection of these wells has been used to construct pressure/depth plots in order to establish the degree of vertical hydraulic connectivity between aquifer/reservoir units. In addition, the pressure data have been converted to equivalent freshwater hydraulic heads to investigate lateral hydraulic communication and the impact of faults and hydrocarbon extraction. Water level data from the DERM GWDB has been extracted for the time period corresponding to the pre-production petroleum well data. The two datasets have been integrated and compared in initial hybrid models for selected areas in the two basins. The 2D models are constructed manually and compared with 3D interpolations performed using the Surfer© software package.

The accuracy of the model is limited by the errors inherent in pressure measurements and subsequent extrapolation techniques used to estimate virgin formation pressures. The PressureQC™ methodology endeavours to provide confidence levels in the data used, but the spatial and vertical data distributions necessitate the use of measurements which have lower confidence levels than desired. The potential impact of groundwater production effects on deeper regions of the GAB aquifers is difficult to ascertain. The selection of water level recordings is also somewhat subjective but provides the best estimate of data comparable to the petroleum well measurements. Formation water samples collected during drill stem tests (DST) have also been subjected to quality control and used to provide an indication of groundwater chemistry at depth. These data provide similar information to analyses stored in the DERM GWDB, consisting predominantly of major ion concentrations, pH and alkalinity measurements.

Hypotheses formulated from the above analyses are compared with the models of Habermehl (1980), Radke et al. (2000) and Hitchon and Hays (1971) to produce a first order hydrodynamic characterisation of the Surat and Eromanga basins. This initial combined model is intended to provide a crude hydrogeological framework in order to comment on the possible effects of CO_2 injection on the existing hydrodynamic regime. Detailed hydrodynamic modelling will be needed to verify the initial hypotheses and is beyond the scope of the current study.

Modelling Strategies

Accurate geochemical/hydrochemical modelling requires that both rock and groundwater samples are sourced from the same location. The currently available datasets do not provide this information, in which case the geochemical simulation results are qualitative. The adopted approach does, however, provide important information on the possible changes in groundwater and aquifer media compositions and provides the basis for more detailed studies with new data.

Geochemical simulations are conducted for the primary injection targets in the basins (Precipice Sandstone and Hutton Sandstone) that were identified in a previous Carbon Geostorage Initiative study (QCGI, 2009). Aqueous speciation simulations, mineral stability models and reaction path models are formulated using the Geochemist's Workbench® software package. No mineralogical data are available for the deep sections of the Evergreen Formation/Upper Poolowanna Formation (regional seal rocks). Mineralogical data for the Precipice Sandstone is used as a proxy for the Lower Poolowanna Formation. Previous studies have confirmed the equivalence of these units (Draper et al., 2002; Green et al., 1997). Simulations are run using selected groundwater and mineralogical analyses to confirm the validity of using the average compositions. Given that the hydrochemical data are from different locations to the mineralogical data, the use of the average values is considered appropriate for initial investigations.

Aqueous equilibrium speciation simulations are run initially to establish the saturation state of any minerals of interest. A positive saturation index denotes a state of saturation that can lead to mineral precipitation. Conversely, a negative saturation index is indicative of undersaturation, in which case mineral dissolution should occur. A null saturation index indicates equilibrium.

The second group of simulations are run to equilibrate the groundwater composition with the aquifer media compositions, to represent the long groundwater residence times and low flow rates.

Subsequent simulations include static equilibration with CO_2 and displacement flushing of the aquifer with a CO_2 charged fluid.

The equilibrium approach adopted in this study provides an indication of the possible induced diagenetic changes and also produces a foundation framework for more detailed work. The inclusion of kinetic rate laws and multiphase reactive transport modelling is required to provide more quantitative analysis. Without new data (groundwater and rock mass sourced from the same location under controlled conditions), these advanced modelling techniques would still include a degree of subjectivity.

The hydrodynamic characterisation is limited to validating/disputing existing groundwater flow models. Interpretations are of the pre-petroleum and gas production flow regime, which is the equilibrium state that the system will strive to attain post-production. Subsequent to cessation of oil and gas production any unstressed system will change to achieve the prestressed state of equilibrium. These are the conditions under which CO_2 is most likely to be stored in the long term.

Formation pressure measurements from DSTs and WFTs in wells that have tested stacked formations are used to identify possible vertical hydraulic connectivity. Conventional pressure/depth plots are used in conjunction with converted hydraulic head/depth plots to illustrate the relationships. Formation pressures have been converted to equivalent hydraulic heads using the relationship:

$$H = Z + P/\text{Grad } P \quad (5)$$

Where:

H– Hydraulic head
Z – Elevation relative to mean sea surface (mSS)
P – Formation pressure in psia (psi atmospheric)
Grad P – hydrostatic gradient basis fresh water (1.42 psia/m)

The freshwater hydrostatic gradient can be used because the formations of interest host groundwater with a narrow salinity range between fresh and low brackish. The spatial distribution of converted hydraulic heads obtained for the Precipice Sandstone, Evergreen Formation and Hutton Sandstone are used in conjunction with groundwater levels to estimate horizontal and vertical flow vectors.

The quality of the available data is generally good, but the spatial distribution is unsystematic, being focused around structural highs and other areas thought to have good petroleum prospectivity. Clusters of wells are used where the separation distance is considered to be insignificant for regional studies. The predominantly flat-lying and largely undeformed sedimentary units permit this approach. Wells that did not encounter hydrocarbons or only minor oil and gas shows, with fluid recoveries dominated by water are preferable for this type of analysis.

Results

Groundwater Compositions

The distribution of groundwater bores screened in the Jurassic and Cretaceous units across both basins is shown in Fig. 12. Of the 4,490 available analyses in the Surat Basins, 3,686 are sourced from the formations of interest (Fig. 13a); in the Eromanga Basin 3,850 analyses are relevant out of a total of 5,742 (Fig. 13b). A relatively small number of groundwater bores are deep (up to 2 km) and the large majority draw water from much shallower depths. As a consequence, groundwater abstraction from the main CO_2 injection target formations is most commonly from shallow wells (200-500 m depth) located around the basin margins (Fig. 10). Bores located in the more central regions of both basins typically exploit groundwater from the Upper Jurassic and Cretaceous units (e.g. Springbok Sandstone, Gubberamunda Sandstone, Mooga Sandstone and Hooray Sandstone).

Trends in pH and alkalinity reflect the dominance of the Na-HCO_3 groundwater compositions (Figs. 14 and 15). Groundwater is mainly alkaline with a pH range of 8-9 in both basins (Fig. 14); in some regions pH is circum-neutral and acidic at shallow depths, in the Eromanga Basin (Fig. 14b). The distribution of alkalinity shows a reasonable correlation with groundwater type, with lower alkalinity values associated with Na-Cl compositions (Fig. 15). Both pH and alkalinity generally increase with depth but show only a weak positive correlation (Figs. 16 and 17).

The major ion hydrochemical groundwater trend dominating all but the Walloon Subgroup aquifers is Na-Cl compositions at shallow depths around recharge zones, evolving to Na-HCO_3 with increasing depth (Table 2, Figs. 18). Formation water samples from DSTs in the Precipice Sandstone and Hutton Sandstone concur with the compositions at shallower depths (Fig. 19). Groundwater salinity is mainly 300-1500 mg/L total dissolved solids (TDS) in the sandstone dominated units (Figs. 18). The Walloon Subgroup aquifers have a predominantly brackish salinity range of 1500-20000 mg/L TDS, although there are some areas producing fresh water (Fig. 18k,l).

The most saline groundwater corresponds with Na-Cl type compositions mainly located in recharge zones along the periphery of the basins (Figs. 18 and 20a). Salinity also increases with depth in the Precipice Sandstone and the Hutton Sandstone, but is generally less than 3500 mg/L TDS. Similar trends are also exhibited in shallower aquifers (Figs. 19 and 20).

Despite the high level of scatter in the hydrochemical data, important trends can be defined. The pH – alkalinity relationship exhibits an exponential trend, with large variations in pH for limited changes in alkalinity (Fig. 21). Groundwater hosted by the Jurassic aquifers in the Surat Basin show a negative correlation between Cl and HCO_3 (Fig. 22a,c), whereas the same units in the Eromanga show a positive correlation (Fig. 22b,d). Cretaceous aquifers in both basins show greater parity, although the signatures are mixed. The Wallumbilla Formation aquifers show a relatively strong negative correlation between Cl and HCO_3, the Gilbert River aquifers show a positive correlation, and a weak negative correlation is evident in the Gubberamunda Sandstone and the Longsight Formation (Fig. 22c,d). Scatter in data from the other formations obscures any definitive patterns. Plots of Na vs Ca show high scatter with some weak correlation evident in the Jurassic aquifers of both basins (Fig. 23a,c). Clear trends are shown in some of the Cretaceous aquifers, which generally show a positive correlation between the two ions (Fig. 23b,d); the Gilbert River Formation aquifers are an exception, showing a quite clear negative correlation (Fig. 23d). Plots of major ion ratios exhibit too much scatter to define any meaningful bivariate trends (Figs. 23 and 24). These diagrams do, however, provide useful information on relative ion concentration ranges which assist in distinguishing groundwater types in the different aquifers.

Groundwater Compositions – South Australia

The distribution of groundwater bores in the South Australian GAB is shown in Fig. 25. Only 23% of these bores have chemical analyses and no information on aquifer formation is available. Of note is the Na-Cl character of the water, which is in contrast with the dominant HCO_3 signature of Queensland groundwaters (Fig. 26).

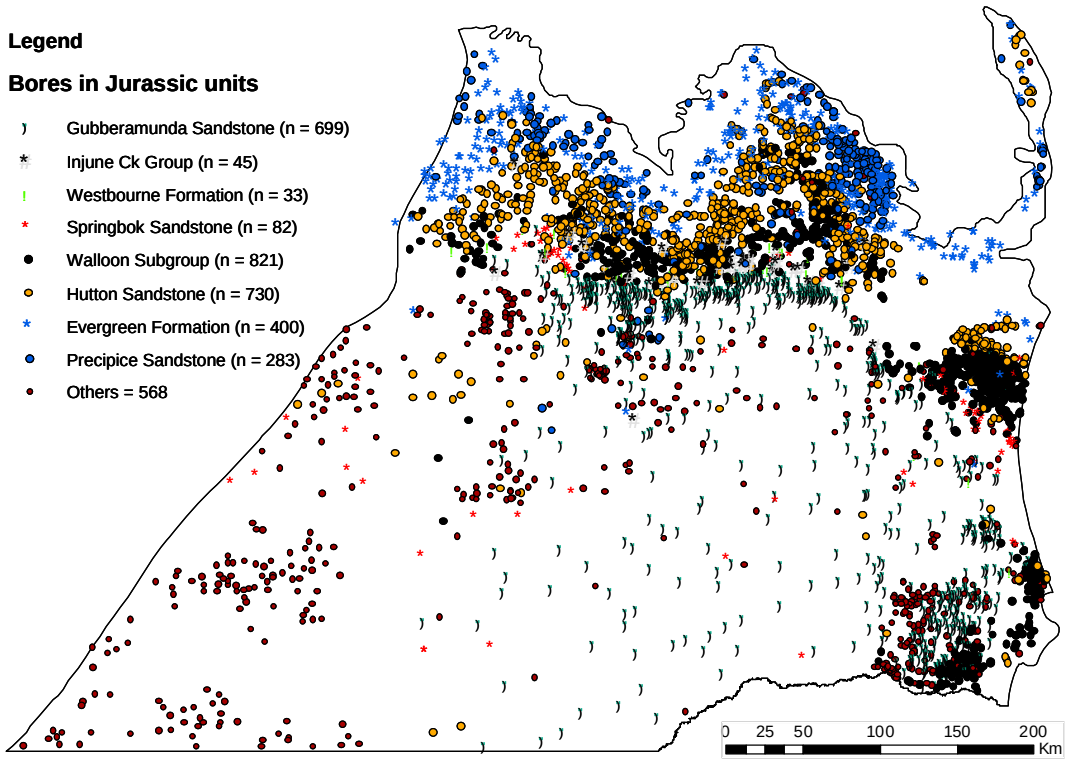

Figure 12a. Distribution of groundwater bores in Jurassic units, Surat Basin. 'Others' refers to bores extracting water from older (Bowen Basin formations) or younger units (alluvium and basalt).

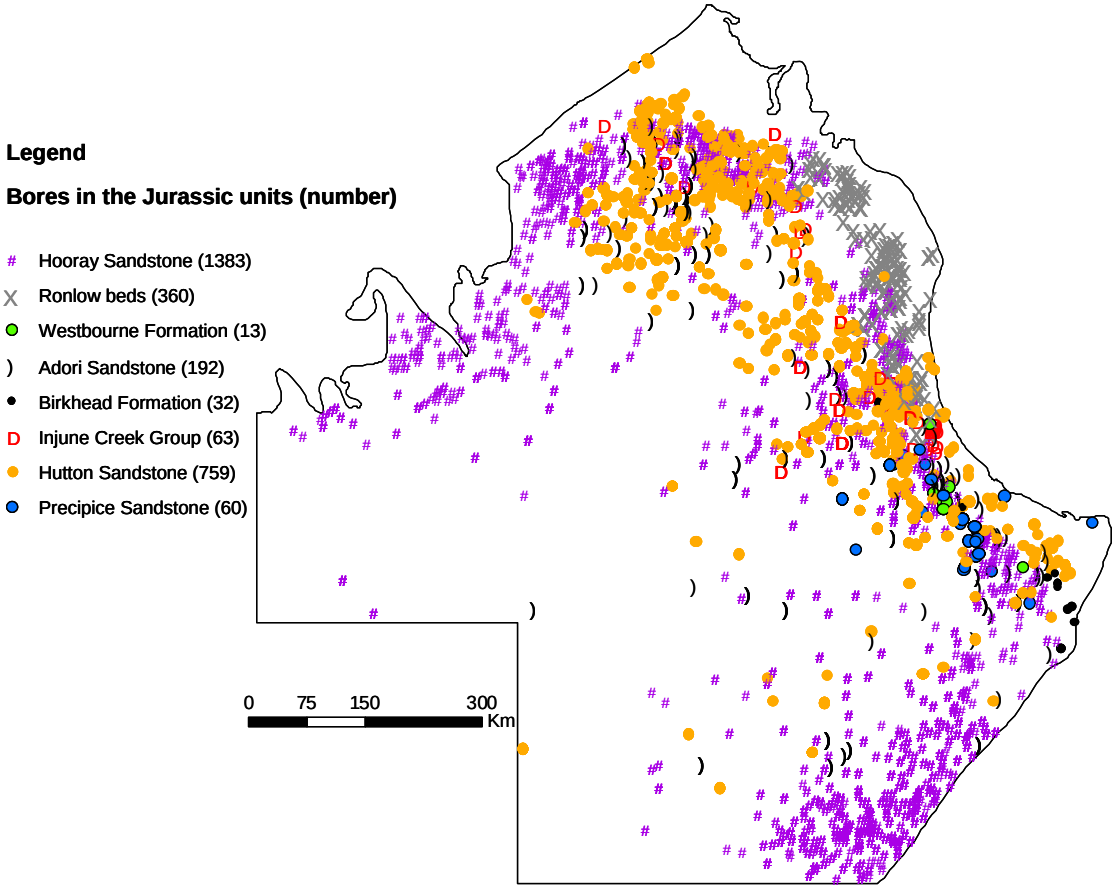

Figure 12b. Distribution of groundwater bores in Jurassic units, Eromanga Basin.

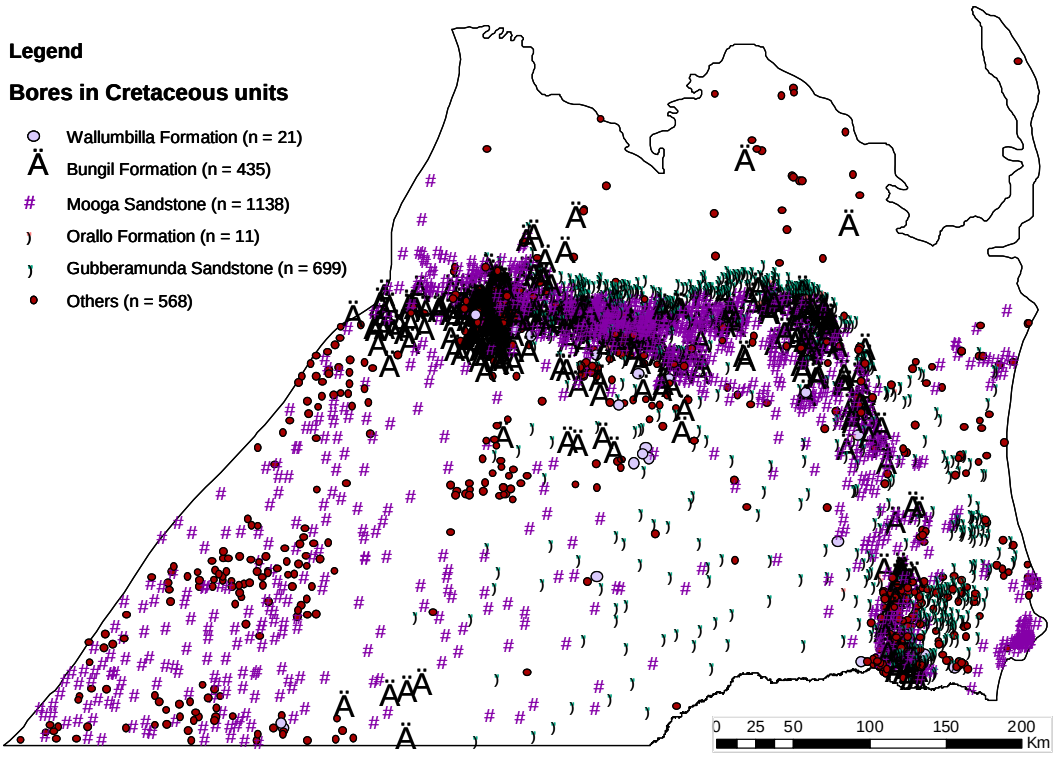

Figure 12c. Distribution of groundwater bores in Cretaceous units, Surat Basin. 'Others' refers to bores extracting water from older (Bowen Basin formations) or younger units (alluvium and basalt).

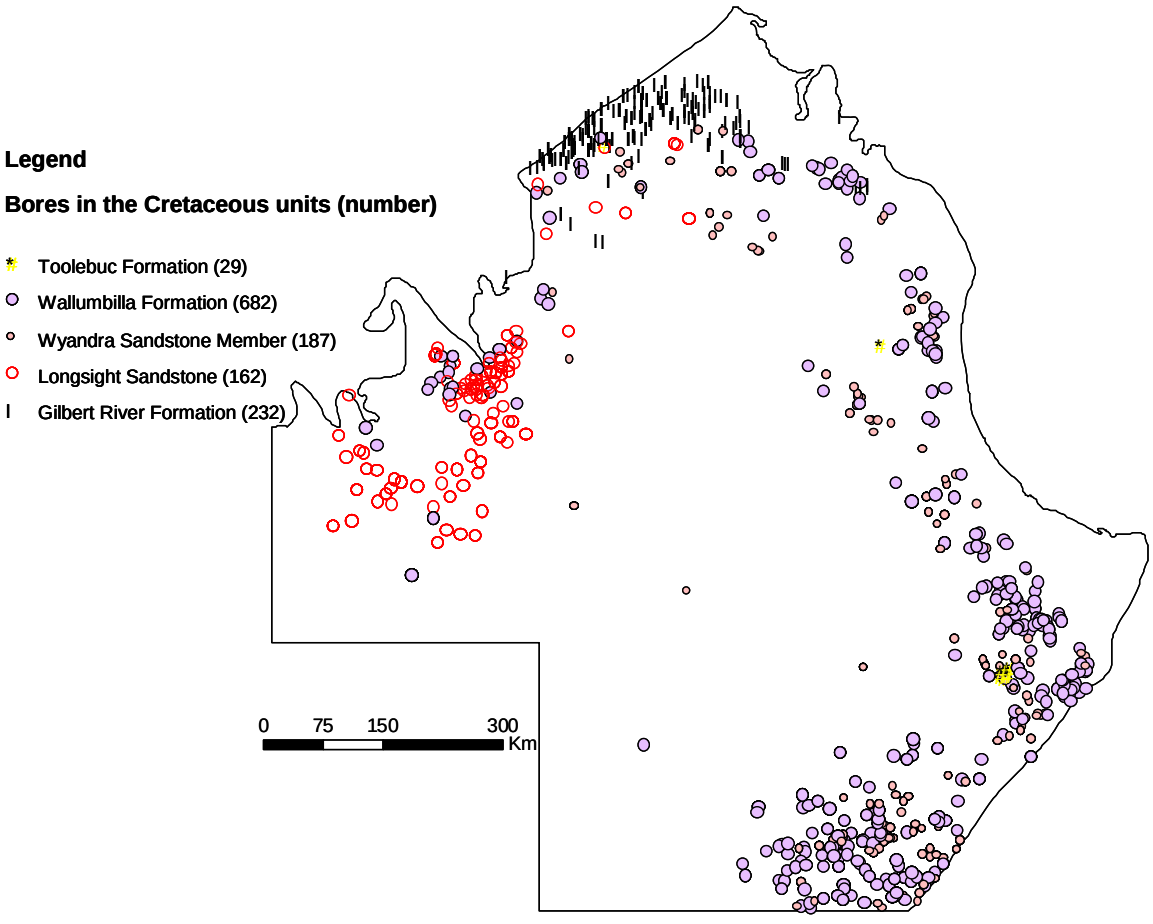

Figure 12d. Distribution of groundwater bores in Cretaceous units, Eromanga Basin.

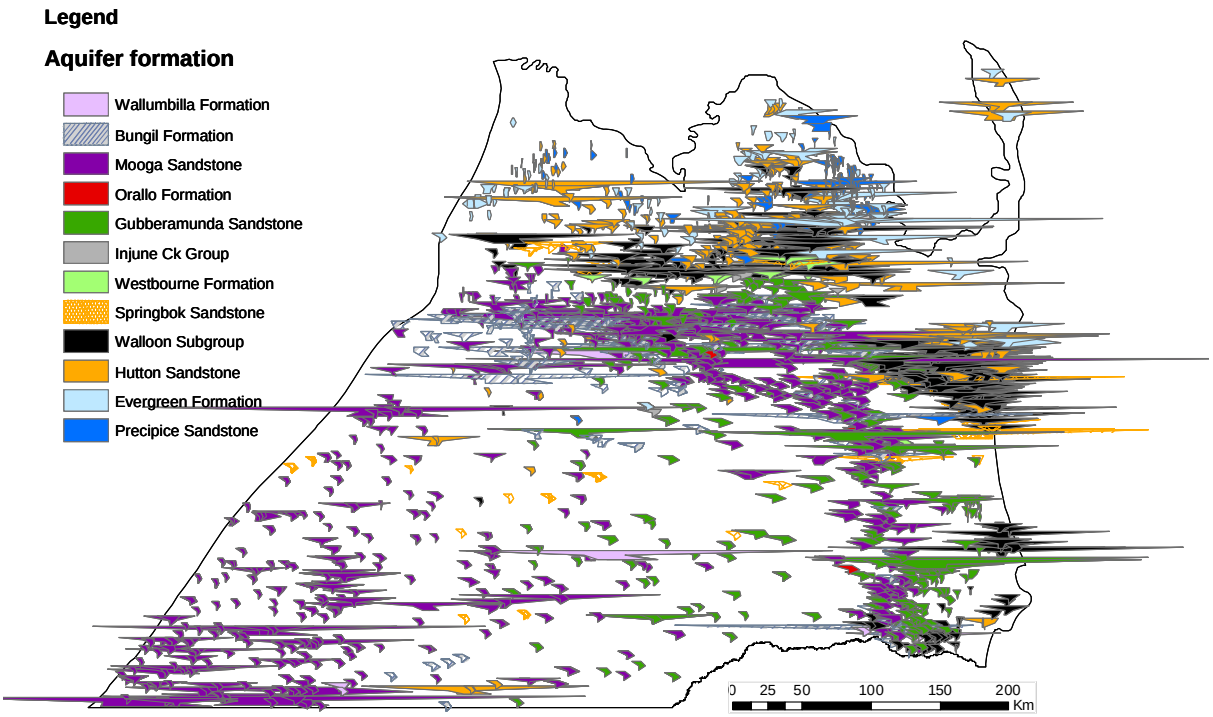

Figure 13a. Distribution of water chemical data with their aquifer formation, shown as Stiff diagrams. Out of the 4490 available water analyses, only 3686 sample the units of interest. The best represented is the Mooga Sandstone with almost 1500 analyses. Gubberamunda Sandstone and the Walloon Subgroup are characterised by approximately 500 analyses each, followed by the Precipice Sandstone (n = 300) and Bungil Formation (n = 230). The other formations have around 100 analyses or less, with Orallo being characterised by only 6 analyses.

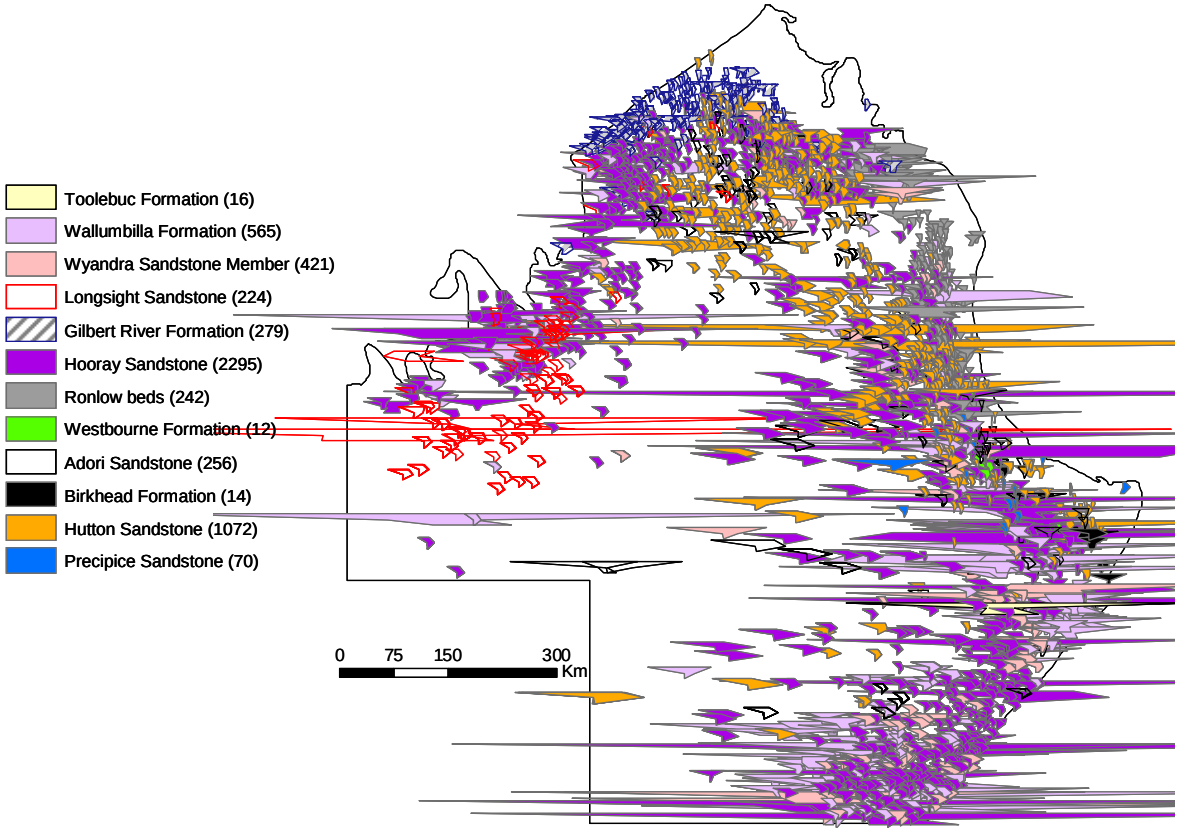

Figure 13b. Distribution of water chemical data with their aquifer formation. Out of the 5742 available water analyses, only 3850 (67%) sample the units of interest. The best represented are the Hooray and Hutton Sandstones with thousands of analyses.

Table 2. Groundwater type and character

Formation	Type	Basin	Number of analyses	Water type	pH	Alkalinity	Major cations	Major anions
Winton Formation	Af	Eromanga	5	Na-HCO_3 / Na-Cl	7.0-8.4	700-800	Na>>Ca>Mg>>K	HCO_3>Cl>SO_4
Mackunda Formation	Af	Eromanga	0					
Griman Creek Formation	Af	Surat	4	Na-HCO_3	8.1-8.8	900-920	Na>>Ca>Mg>>K	HCO_3>>Cl>SO_4
Allaru Mudstone	At	Eromanga	0					
Toolebuc Formation	At	Eromanga	16	Na-HCO_3 / Na-Cl	7.2-8.7	90-130	Na>>Ca~Mg>K	HCO_3>Cl>SO_4
Surat Siltstone	At	Surat	12	Na-HCO_3 / Na-Cl	7.5-8.4	200-800	Na>>Ca>Mg>>K	HCO_3>Cl>SO_4
Wallumbilla Formation	Af	both	552	Na-Cl	6.0-9.0	50-1200	Na>>Ca>Mg>>K	Cl>HCO_3>SO_4
Wyandra Member	Af	Eromanga	421	Na-HCO_3 / Na-Cl	7.0-9.0	100-1200	Na>>Ca>Mg>K	HCO_3>Cl>SO_4
Bungil Formation	Af	Surat	100	Na-Cl / Na-HCO_3	6.5-8.8	50-1000	Na>>Ca>Mg>K	Cl>HCO_3>SO_4
Longsight Sandstone	Af	Eromanga	224	Na-HCO_3 / Na-Cl	7.0-9.0	100-600	Na>>Ca>Mg>K	HCO_3>Cl>SO_4
Gilbert Creek Formation	Af	Eromanga	279	Na-HCO_3	6.0-9.0	100-600	Na>>Ca>Mg>K	HCO_3>>Cl>SO_4
Hooray Sandstone	Af	Eromanga	3094	Na-HCO_3 / Na-Cl	5.8-9.5	100-1600	Na>>Ca>Mg>K	HCO_3>Cl>SO_4
Mooga Sandstone	Af	Surat	486	Na-HCO_3	7.0-9.0	50-1200	Na>>Ca>Mg>K	HCO_3>>Cl>SO_4
Orallo Sandstone	Af	Surat	6	Na-HCO_3	8.0-9.0	600-1100	Na>>Ca>Mg>K	HCO_3>>Cl>SO_4
Gubberamunda Sandstone	Af	Surat	260	Na-HCO_3	6.5-9.0	50-1100	Na>>Ca>Mg>K	HCO_3>>Cl>SO_4
Ronlow beds	Af	Eromanga	242	Na-HCO_3 / Na-Cl	6.8-9.0	50-400	Na>Ca>Mg>K	HCO_3>Cl>SO_4
Injune Creek Formation	Af/At	Surat	88	Na-HCO_3 / Na-Cl	7.2-8.8	20-800	Na>>Ca>Mg>K	HCO_3>Cl>SO_4
Westbourne Formation	Af/At	both	26	Na-Cl / Na-HCO_3	7.6-8.6	70-320	Na>>Ca>Mg>K	Cl>HCO_3>SO_4
Adori Sandstone	Af	Eromanga	256	Na-HCO_3	6.8-9.0	20-1000	Na>>Ca>Mg>K	HCO_3>Cl>SO_4
Springbok Sandstone	Af	Surat	33	Na-HCO_3	7.0-9.0	100-600	Na>>Ca>Mg>K	HCO_3>Cl>SO_4
Birkhead Formation	At	Eromanga	14	Na-HCO_3	7.8-8.2	180-200	Na>Ca>Mg>K	HCO_3>Cl>SO_4
Walloon Subgroup	Af/At	Surat	300	Na-Cl	6.5-9.0	50-1800	Na>Ca~Mg>>K	Cl>HCO_3>SO_4
Hutton Sandstone	Af	both	1317	Na-HCO_3 / Na-Cl	6.0-9.5	50-1300	Na>Ca>Mg>K	HCO_3>Cl>SO_4
Evergreen Formation	At	Surat	56	Na-HCO_3 / Na-Cl	7.0-9.0	50-400	Na>Ca>Mg>K	HCO_3>Cl>SO_4
Poolowanna Formation	Af/At	Eromanga	0					
Precipice Sandstone	Af	both	318	Na-HCO_3	6.0-9.0	50-800	Na>Ca>Mg>K	HCO_3>>Cl>SO_4

Af – aquifer; At – aquitard

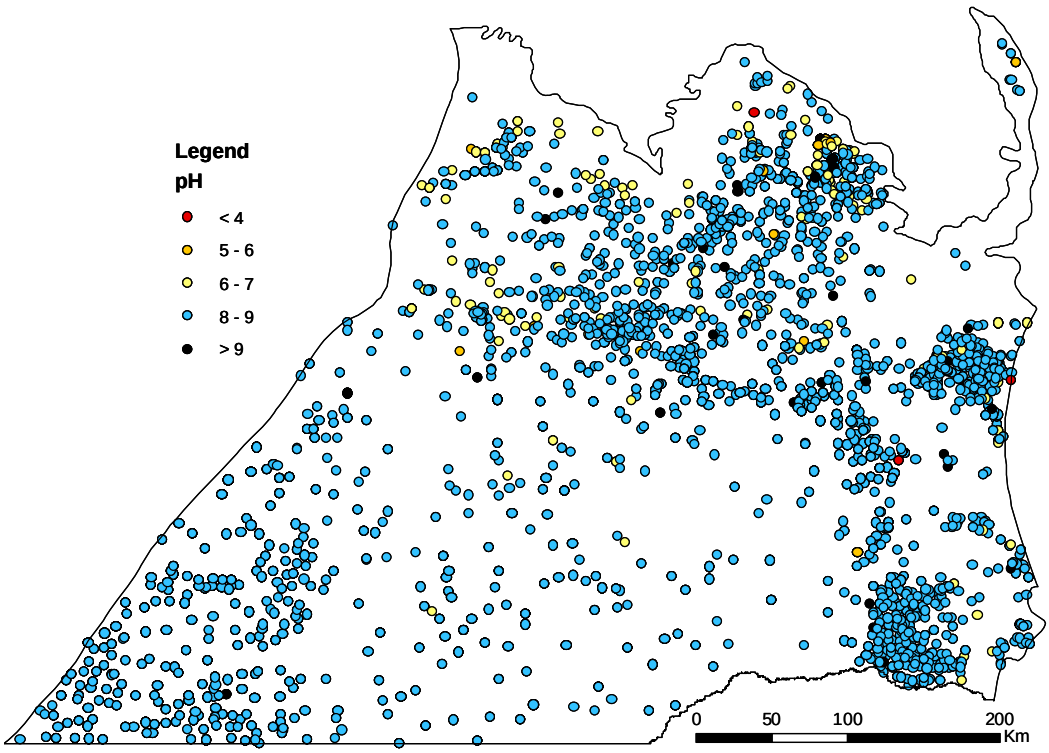

Figure 14a. Groundwater pH, Surat Basin. Most waters (62%) have a pH ranging between 8 and 8.6. Circumneutral waters occur in the north, close to recharge areas. A small proportion is either very acid or very alkaline waters. Note: only water analyses of non-mixed waters have been considered.

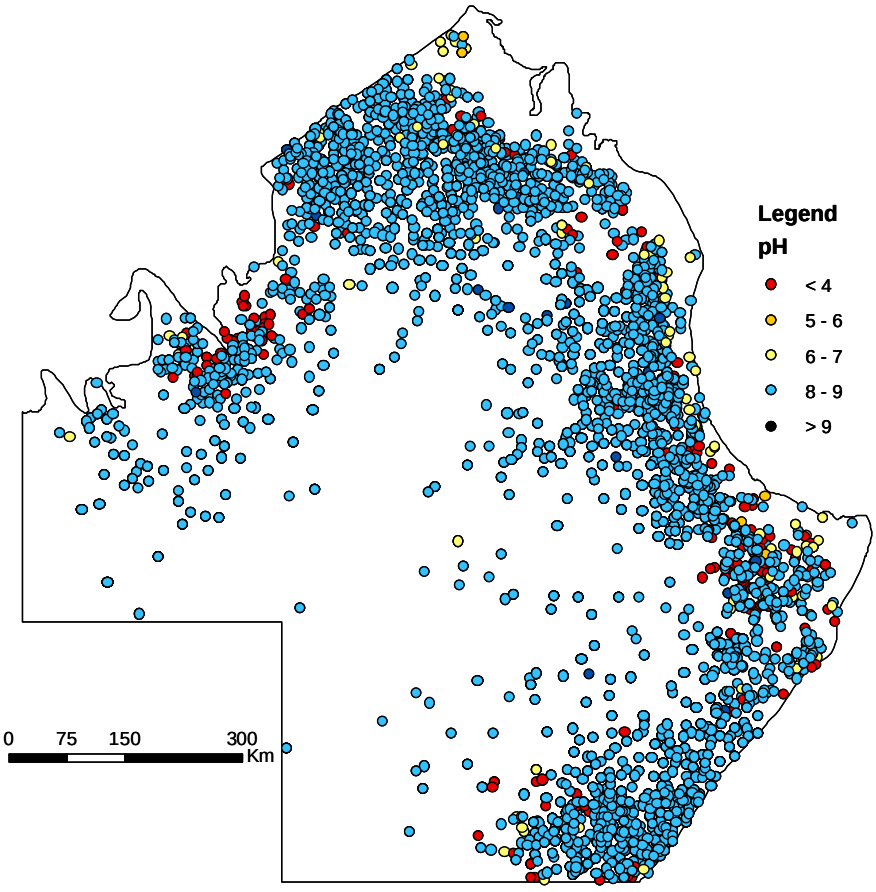

Figure 14b. Groundwater pH, Eromanga Basin. Most waters (66%) have a pH ranging between 8 and 8.6. Circumneutral waters occur in the north, close to recharge areas. A small proportion is either very acid or very alkaline waters. Note: only water analyses of non-mixed waters have been considered.

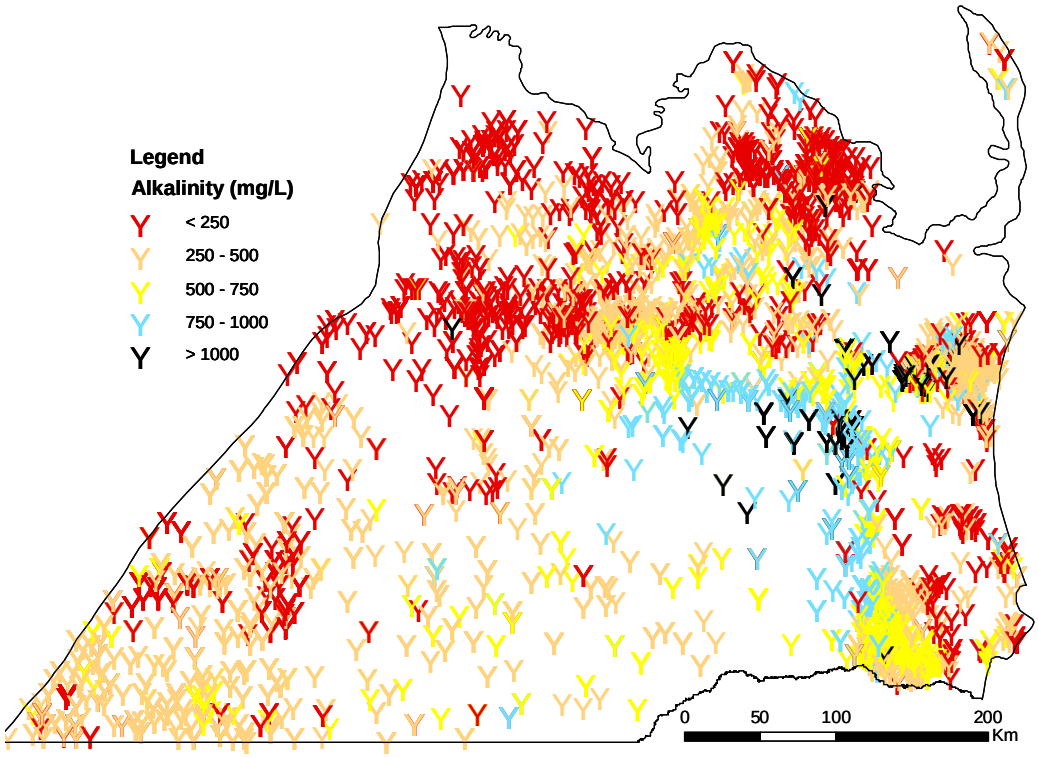

Figure 15a. Groundwater alkalinity, Surat Basin. A significant proportion (44%) has alkalinity of around 500 mg/L. A small number has high alkalinity, in the order of thousands of mg/L. Note: only water analyses of non-mixed waters have been considered.

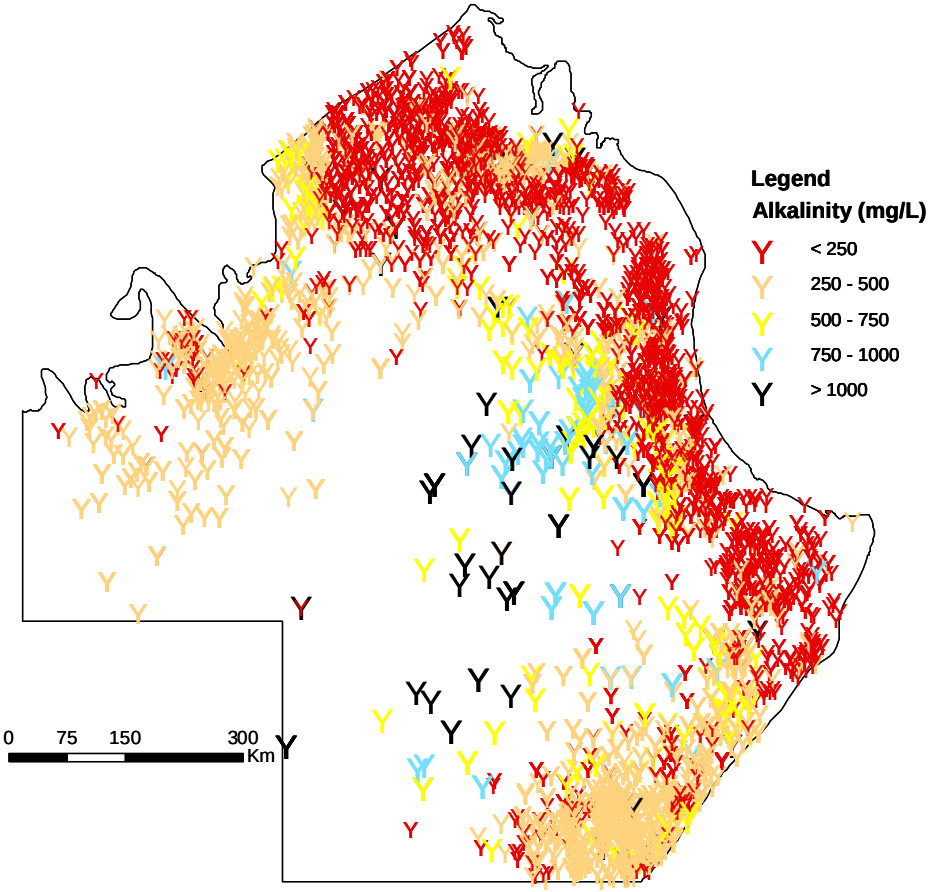

Figure 15b. Groundwater alkalinity, Surat Basin. A significant proportion (64%) has alkalinity of around 500 mg/L. A small number has high alkalinity, in the order of thousands of mg/L. Note: only water analyses of non-mixed waters have been considered.

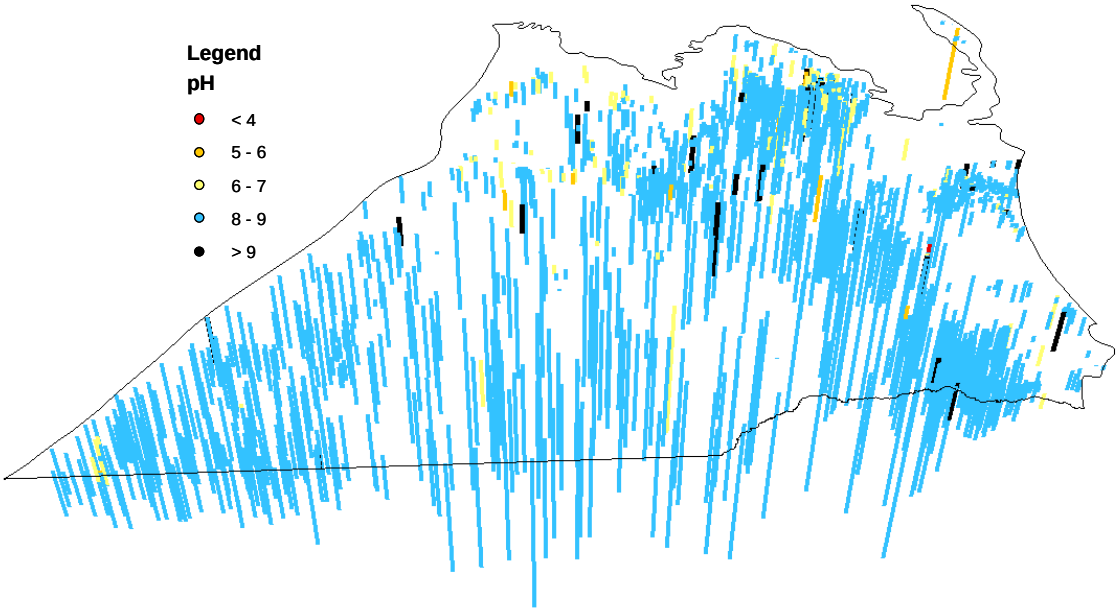

Figure 16a. Groundwater pH in relation to the depth of the aquifer. Deeper waters have a pH ranging between 8 and 9.

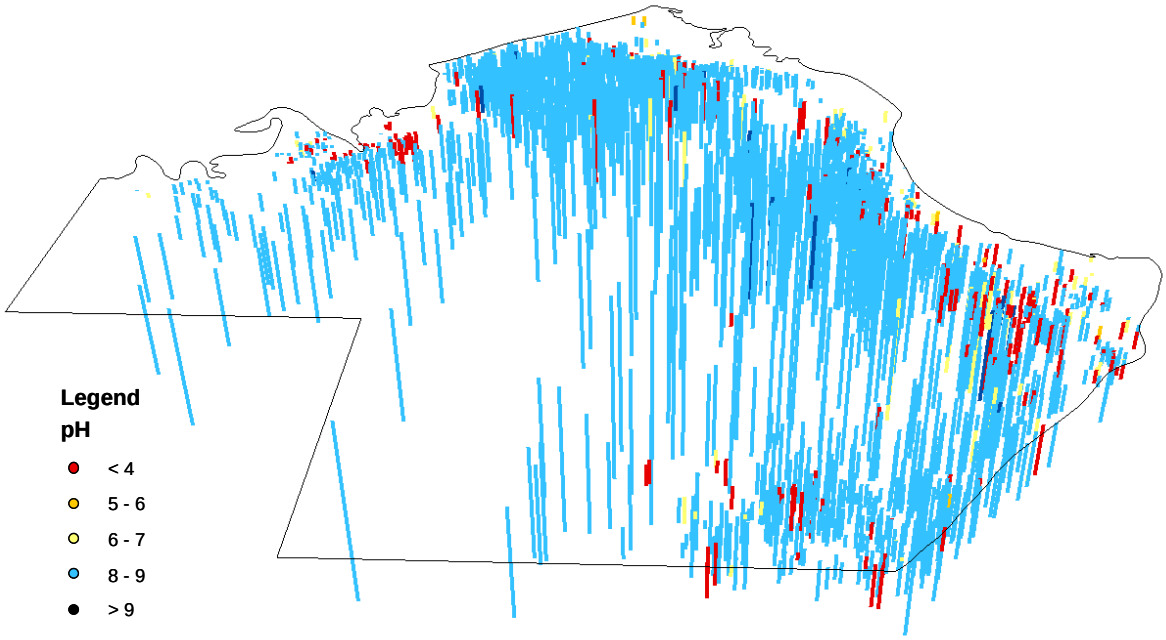

Figure 16b. Groundwater pH in relation to the depth of the aquifer. Deeper waters have a pH ranging between 8 and 9.

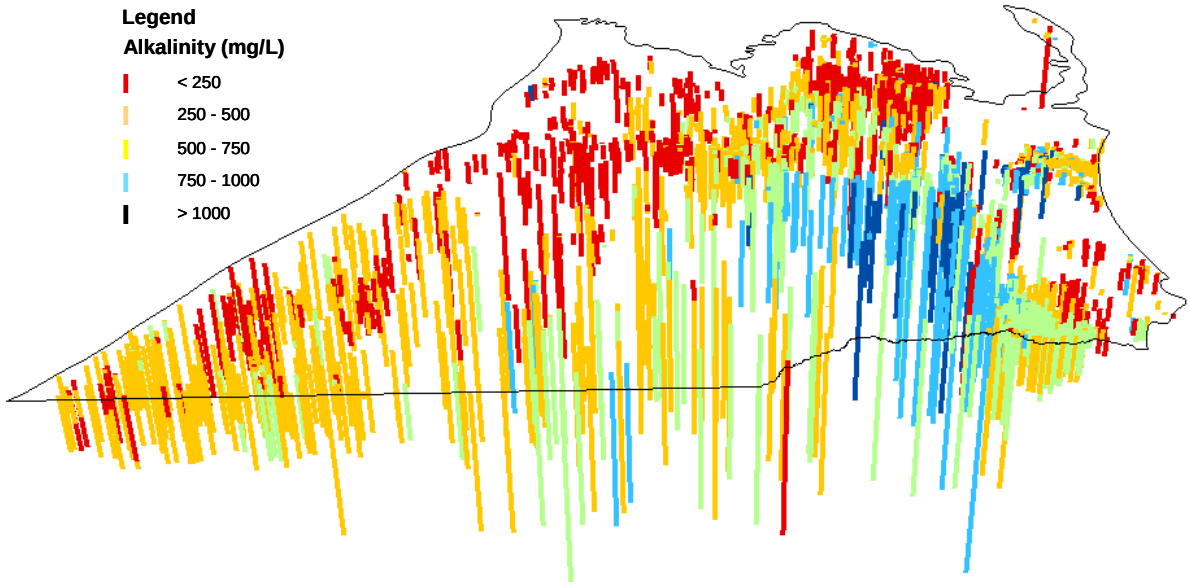

Figure 17a. Groundwater alkalinity in relation to the depth of the aquifer. Deeper waters have a higher neutralising capacity.

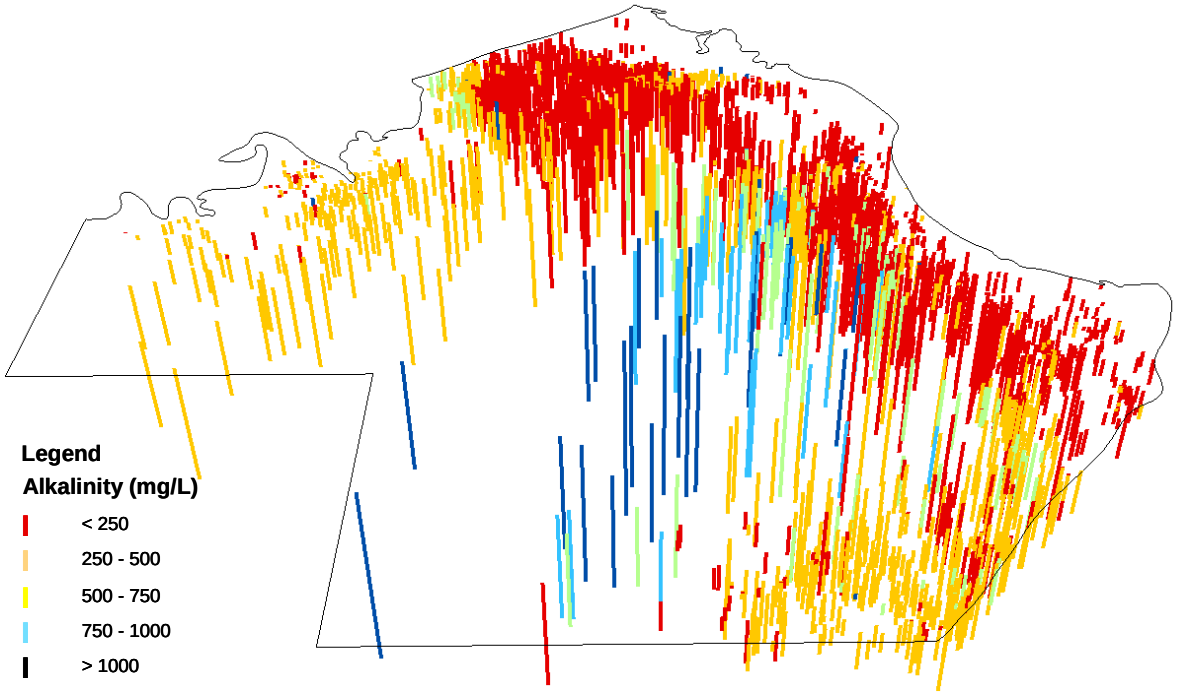

Figure 17b. Groundwater alkalinity in relation to the depth of the aquifer. Deeper waters have a higher neutralising capacity.

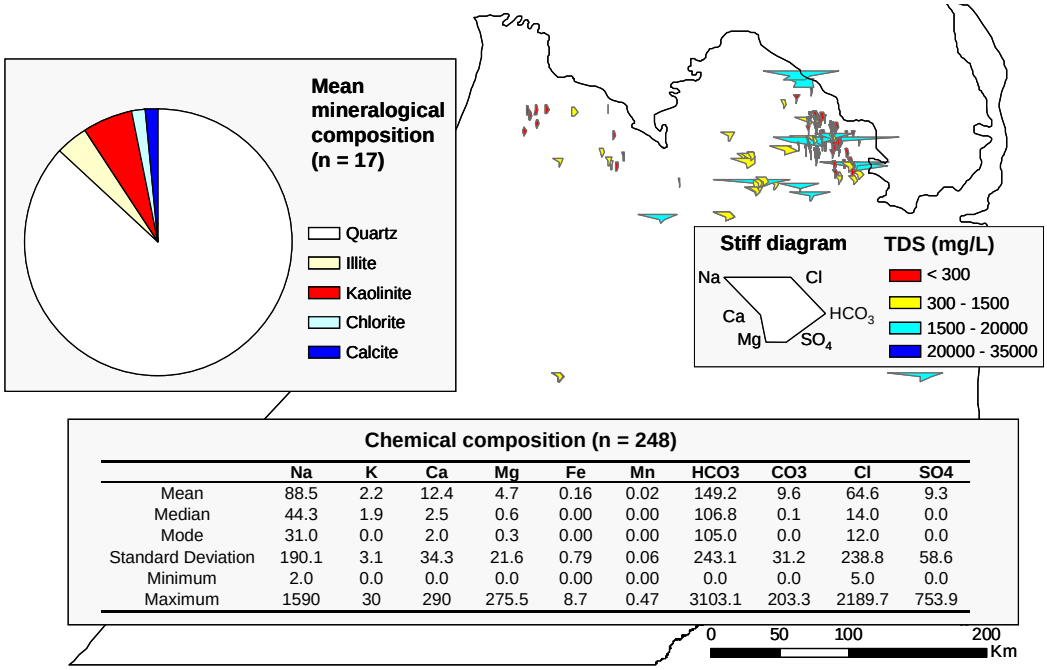

	Na	K	Ca	Mg	Fe	Mn	HCO3	CO3	Cl	SO4
Mean	88.5	2.2	12.4	4.7	0.16	0.02	149.2	9.6	64.6	9.3
Median	44.3	1.9	2.5	0.6	0.00	0.00	106.8	0.1	14.0	0.0
Mode	31.0	0.0	2.0	0.3	0.00	0.00	105.0	0.0	12.0	0.0
Standard Deviation	190.1	3.1	34.3	21.6	0.79	0.06	243.1	31.2	238.8	58.6
Minimum	2.0	0.0	0.0	0.0	0.00	0.00	0.0	0.0	5.0	0.0
Maximum	1590	30	290	275.5	8.7	0.47	3103.1	203.3	2189.7	753.9

Figure 18a. Major ion hydrochemical signatures for the Precipice Sandstone in the Surat Basin, shown using Stiff diagrams and total dissolved solids (TDS). The Precipice water is generally fresh and sodium-bicarbonate type (see table with descriptive statistics for 248 samples). The mineralogy is based on 17 samples analysed by X-ray diffraction by Carmichael (1989); chlorite and calcite occur as localised traces. Limitations: 1) the water samples represent the shallow Precipice Sandstone and the relevance of these chemical data for the deeper section of the unit remains unknown; 2) the mineralogy is based on samples collected from the Eromanga Basin, from depths of 1200 to 2500 m.

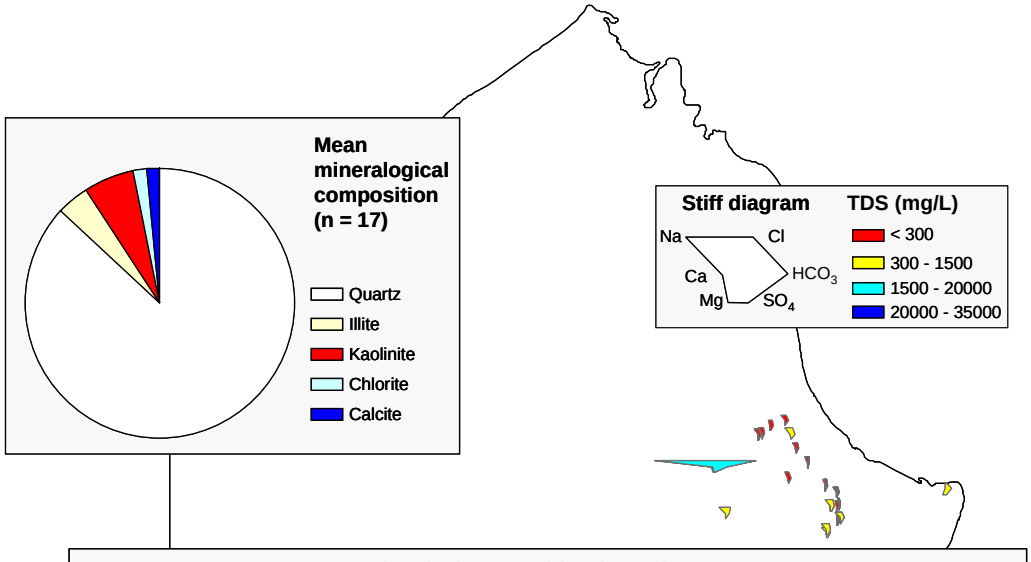

	Na	K	Ca	Mg	Fe	Mn	HCO3	CO3	Cl	SO4
Mean	122.8	5.5	8.3	3.1	0.03	0.02	139.3	10.2	112.7	13.8
Median	42.0	5.0	6.0	1.9	0.00	0.00	104.0	0.2	28.0	6.4
Mode	36.0	0.0	5.0	5.0	0.00	0.00	0.0	0.0	30.0	7.0
Standard Deviation	265.2	4.5	6.7	5.6	0.07	0.03	147.0	29.3	309.4	23.5
Minimum	22.0	0.0	1.7	0.0	0.00	0.00	0.0	0.0	13.0	0.0
Maximum	1260.0	18.0	34.0	43.0	0.47	0.13	755.0	144.4	1420.0	107.3

Figure 18b. Major ion hydrochemical signatures for the Precipice Sandstone in the Eromanga Basin, shown using Stiff diagrams and total dissolved solids (TDS). The Precipice water is generally fresh and sodium-bicarbonate type (see table with descriptive statistics for 59 samples). The mineralogy is based on 17 samples analysed by X-ray diffraction by Carmichael (1989); chlorite and calcite occur as localised traces. Limitations: 1) the water samples represent the shallow Precipice Sandstone and the relevance of these chemical data for the deeper section of the unit remains unknown; 2) the mineralogy is based on samples collected from depths of 1200 to 2500 m.

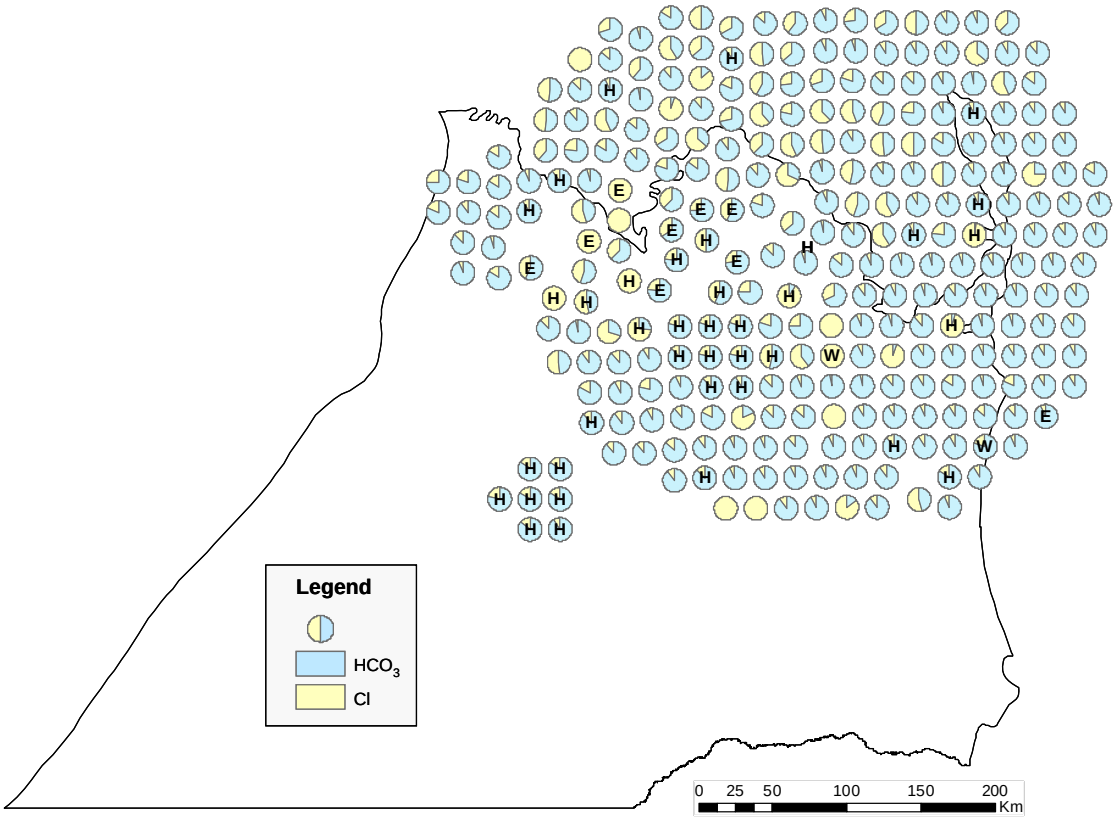

Figure 18c. Major anion distribution for the Precipice Sandstone in the Surat Basin (exploded view). Labels display known mixing between Precipice and Evergreen (E), Hutton (H), Injune Creek (I) and Walloon (W) waters. The Precipice water is generally bicarbonate-rich, but it can become Cl-rich when mixed with some Walloon waters.

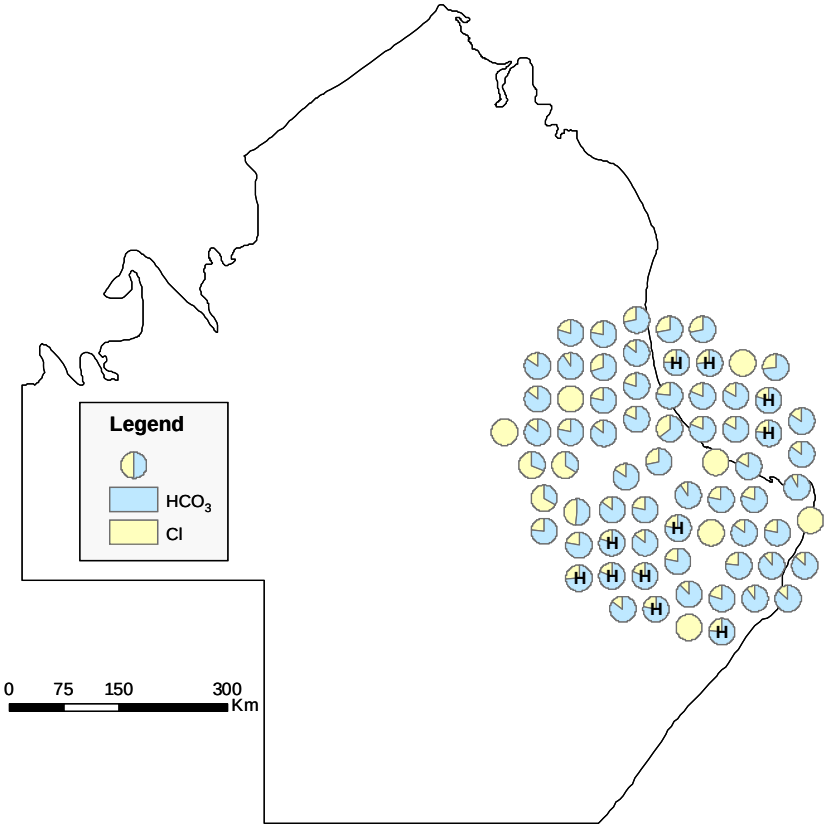

Figure 18d. Major anion distribution for the Precipice Sandstone in the Eromanga Basin (exploded view). Labels display known mixing between Precipice and Hutton (H), waters. The Precipice water is generally bicarbonate-rich, but it can become Cl-rich locally.

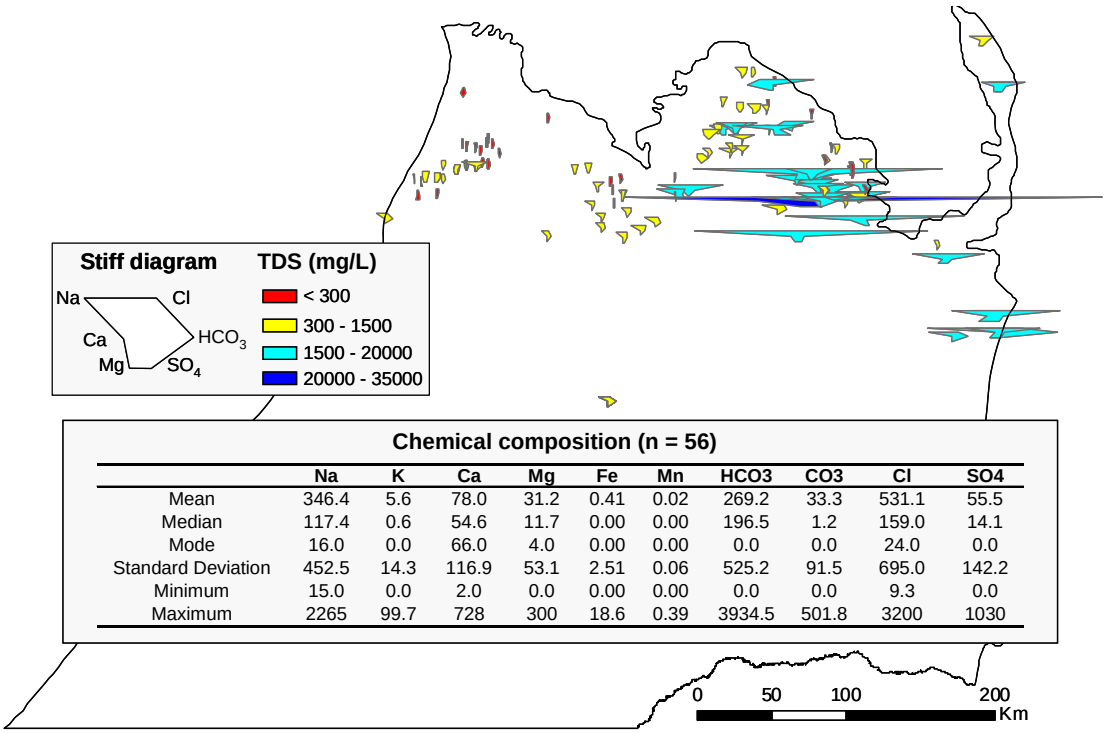

Chemical composition (n = 56)

	Na	K	Ca	Mg	Fe	Mn	HCO3	CO3	Cl	SO4
Mean	346.4	5.6	78.0	31.2	0.41	0.02	269.2	33.3	531.1	55.5
Median	117.4	0.6	54.6	11.7	0.00	0.00	196.5	1.2	159.0	14.1
Mode	16.0	0.0	66.0	4.0	0.00	0.00	0.0	0.0	24.0	0.0
Standard Deviation	452.5	14.3	116.9	53.1	2.51	0.06	525.2	91.5	695.0	142.2
Minimum	15.0	0.0	2.0	0.0	0.00	0.00	0.0	0.0	9.3	0.0
Maximum	2265	99.7	728	300	18.6	0.39	3934.5	501.8	3200	1030

Figure 18e. Major ion hydrochemical signatures for the Evergreen Formation in the Surat Basin, shown using Stiff diagrams and total dissolved solids (TDS). The Evergreen water is generally fresh to brackish and sodium-bicarbonate type (see table with descriptive statistics for 56 samples). Limitations: 1) the water samples represent the shallow Evergreen Formation and the relevance of these chemical data for the deeper section of the unit remains unknown; 2) no mineralogical data are available; 3) the number of water analyses is limited.

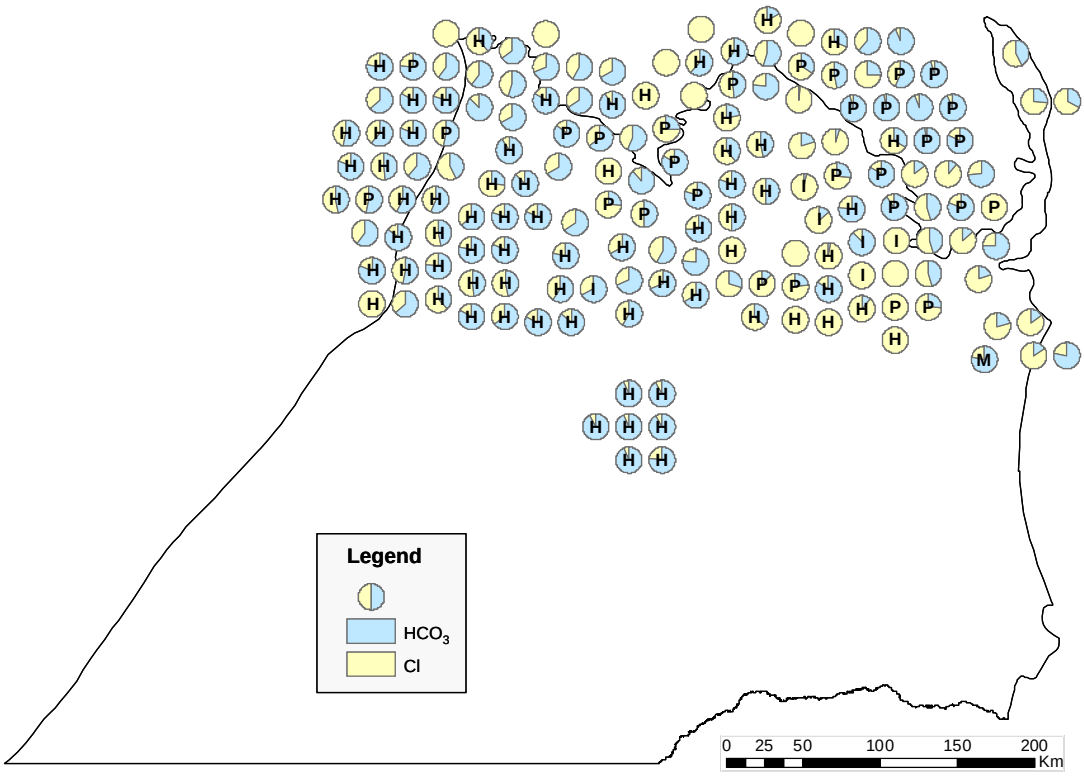

Figure 18f. Major anion distribution for the Evergreen Formation in the Surat Basin (exploded view). Labels display known mixing between Evergreen and Precipice (P), Hutton (H), Injune Creek (I) and Marburg (M) waters. The Evergreen water is generally bicarbonate-rich, but it can become Cl-rich when mixed with Injune Creek and locally with Hutton waters.

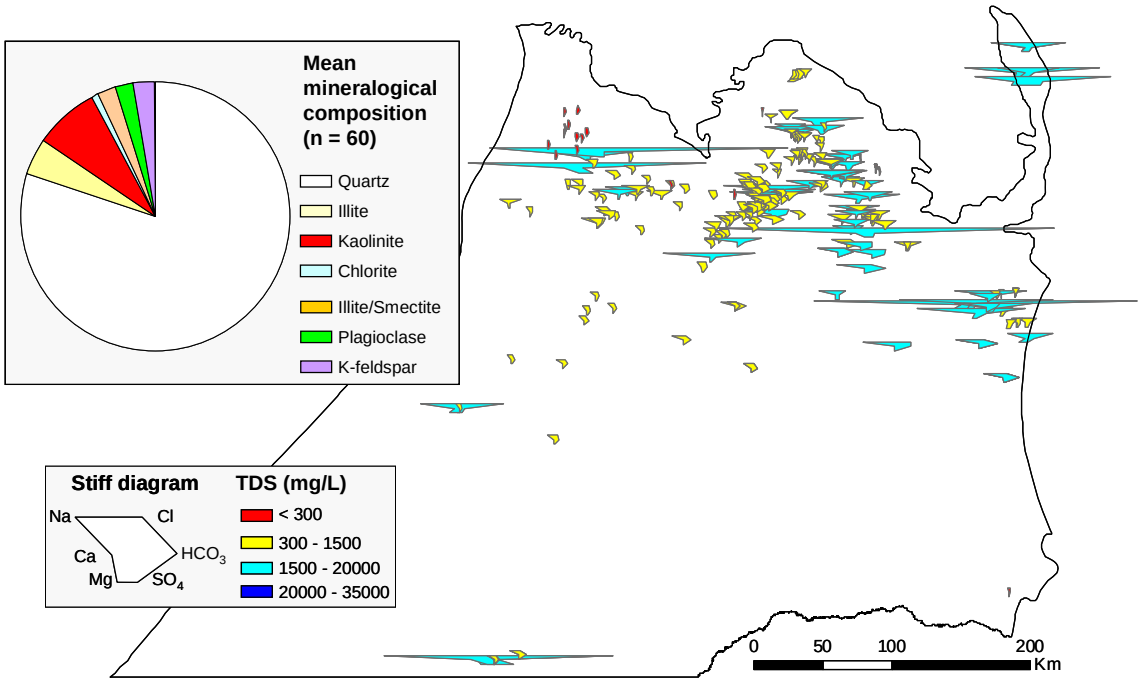

Chemical composition (n = 246)

	Na	K	Ca	Mg	Fe	Mn	HCO3	CO3	Cl	SO4
Mean	487.2	2.0	33.5	16.2	0.37	0.13	364.8	27.4	602.7	24.7
Median	272.2	0.9	5.1	1.0	0.00	0.00	260.8	3.6	170.0	4.6
Mode	1250.0	0.0	2.0	0.0	0.00	0.00	0.0	0.0	130.0	0.0
Standard Deviation	713.3	3.9	146.5	51.1	2.26	1.61	332.2	63.1	1319.8	72.5
Minimum	15.8	0.0	0.0	0.0	0.00	0.00	0.0	0.0	8.0	0.0
Maximum	5440	36	2060	490.5	26.3	25	1720	546.3	9940	805.1

Figure 18g. Major ion hydrochemical signatures for the Hutton Sandstone in the Surat Basin, shown using Stiff diagrams and total dissolved solids (TDS). The Hutton water is mainly fresh and sodium-bicarbonate type (see table with descriptive statistics for 246 samples). The mineralogy is based on 60 samples analysed by X-ray diffraction by Carmichael (1989); chlorite, calcite and siderite occur as localised traces. Limitations: 1) the water samples represent the shallow Hutton Sandstone and the relevance of these chemical data for the deeper section of the unit remains unknown; 2) the mineralogy is based on samples collected from the Eromanga Basin, from depths of 500 to 1200 m.

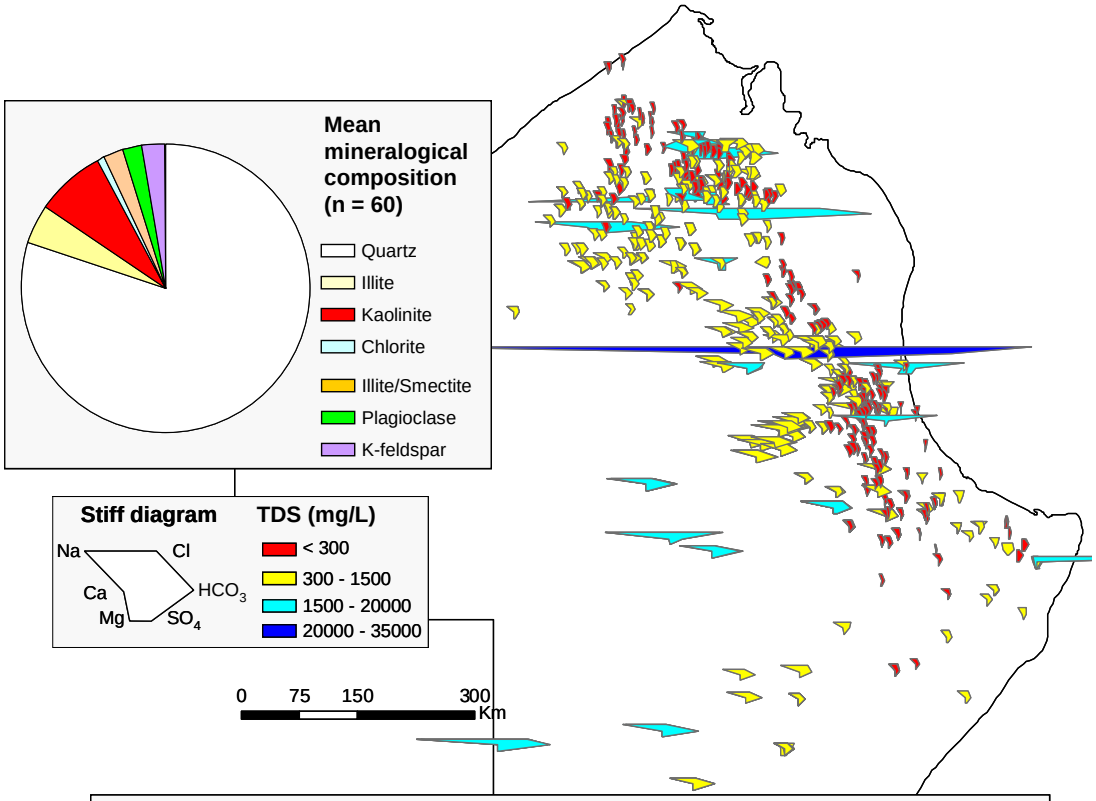

Chemical composition (n = 935)

	Na	K	Ca	Mg	Fe	Mn	HCO3	CO3	Cl	SO4
Mean	182.7	5.9	24.2	10.2	0.09	0.22	302.7	16.0	163.2	18.2
Median	90.4	2.3	9.6	2.2	0.00	0.00	220.0	1.6	49.5	6.8
Mode	86.0	0.0	4.0	0.0	0.00	0.00	0.0	0.0	50.0	0.0
Standard Deviation	687.0	21.6	205.8	69.9	0.85	6.05	485.0	46.6	1444.8	102.3
Minimum	0.0	0.0	0.0	0.0	0.00	0.00	0.0	0.0	0.0	0.0
Maximum	15419.7	586.5	6008.9	1617.3	15.50	185.00	8617.9	426.1	38143.8	2336.6

Figure 18h. Major ion hydrochemical signatures for the Hutton Sandstone in the Eromanga Basin, shown using Stiff diagrams and total dissolved solids (TDS). The Hutton water is mainly fresh and sodium-bicarbonate type (see table with descriptive statistics for 935 samples). The mineralogy is based on 60 samples analysed by X-ray diffraction by Carmichael (1989); chlorite, calcite and siderite occur as localised traces.

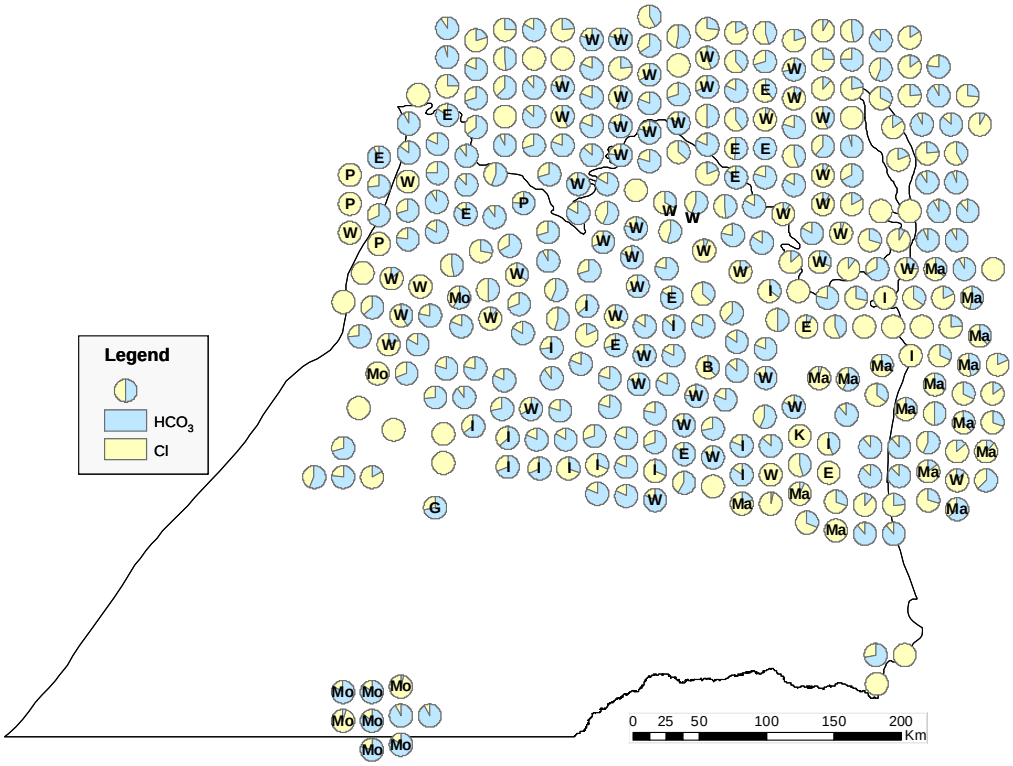

Figure 18i. Major anion distribution for the Hutton Sandstone in the Surat Basin (exploded view). Labels display known mixing between Hutton and Precipice (P), Evergreen (E), Walloon (W), Injune Creek (I), Gubberamunda (G), Mooga (Mo), Bungil (B), Marburg (Ma) and Kumbarilla (K) waters. The Hutton water is generally bicarbonate-rich, but it can become Cl-rich when mixed with some Walloon and Injune Creek waters. The Cl signature appears to be more prominent in the northern and western sections of the basin.

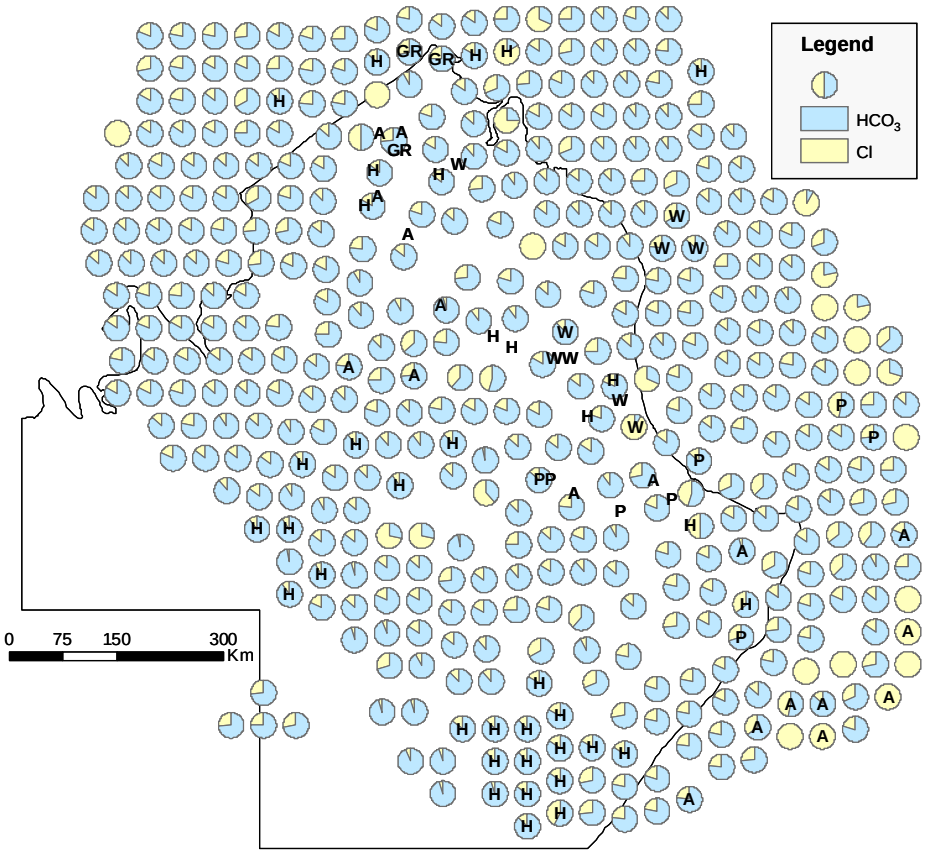

Figure 18j. Major anion distribution for the Hutton Sandstone in the Eromanga Basin (exploded view). Labels display known mixing between Hutton and Precipice (P), Adori (A), Hooray (H), Wallumbilla (W) and Griman Creek (GR) waters. The Hutton water is generally bicarbonate-rich, but it can become Cl-rich locally.

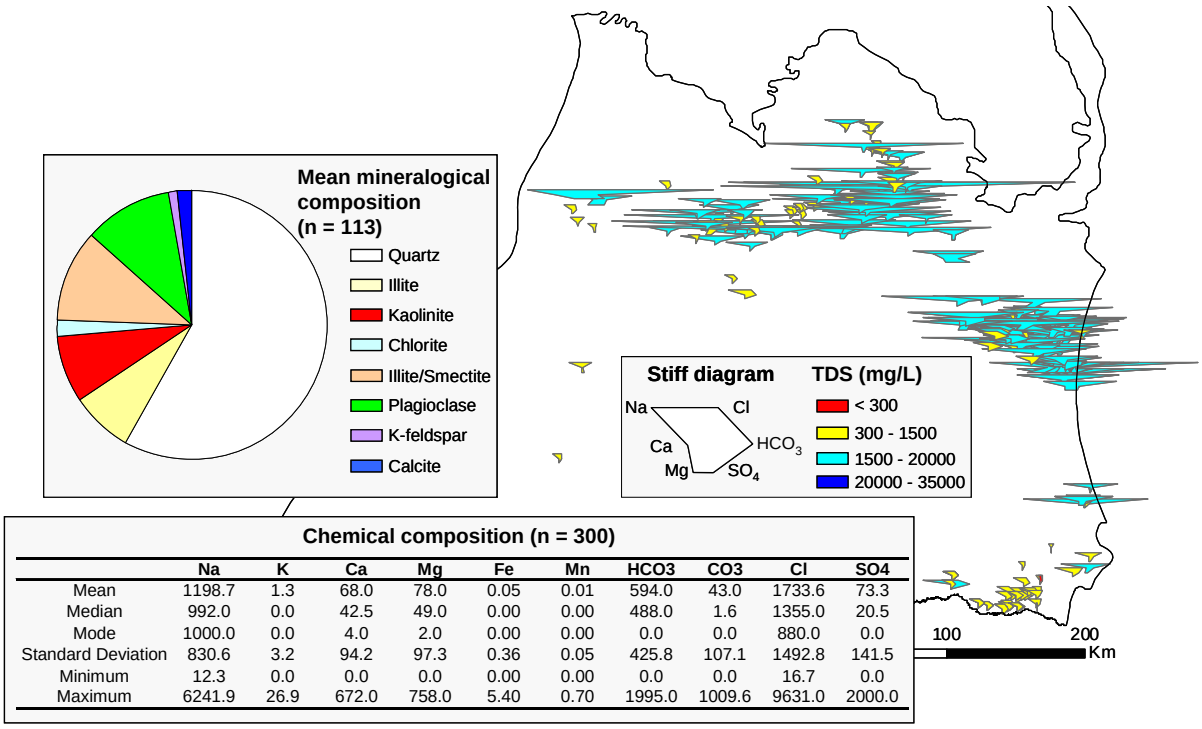

Chemical composition (n = 300)

	Na	K	Ca	Mg	Fe	Mn	HCO3	CO3	Cl	SO4
Mean	1198.7	1.3	68.0	78.0	0.05	0.01	594.0	43.0	1733.6	73.3
Median	992.0	0.0	42.5	49.0	0.00	0.00	488.0	1.6	1355.0	20.5
Mode	1000.0	0.0	4.0	2.0	0.00	0.00	0.0	0.0	880.0	0.0
Standard Deviation	830.6	3.2	94.2	97.3	0.36	0.05	425.8	107.1	1492.8	141.5
Minimum	12.3	0.0	0.0	0.0	0.00	0.00	0.0	0.0	16.7	0.0
Maximum	6241.9	26.9	672.0	758.0	5.40	0.70	1995.0	1009.6	9631.0	2000.0

Figure 18k. Major ion hydrochemical signatures for the Walloon Subgroup in the Surat Basin, shown using Stiff diagrams and total dissolved solids (TDS). The Walloon water is generally brackish and sodium-chloride type (see table with descriptive statistics for 300 samples). The mineralogy is based on 113 samples analysed by X-ray diffraction by Carmichael (1989); calcite, siderite, dolomite, pyrite and halite occur as localised traces. Limitations: the mineralogy is based on samples collected from the Eromanga Basin, from depths of 400 to 2200 m.

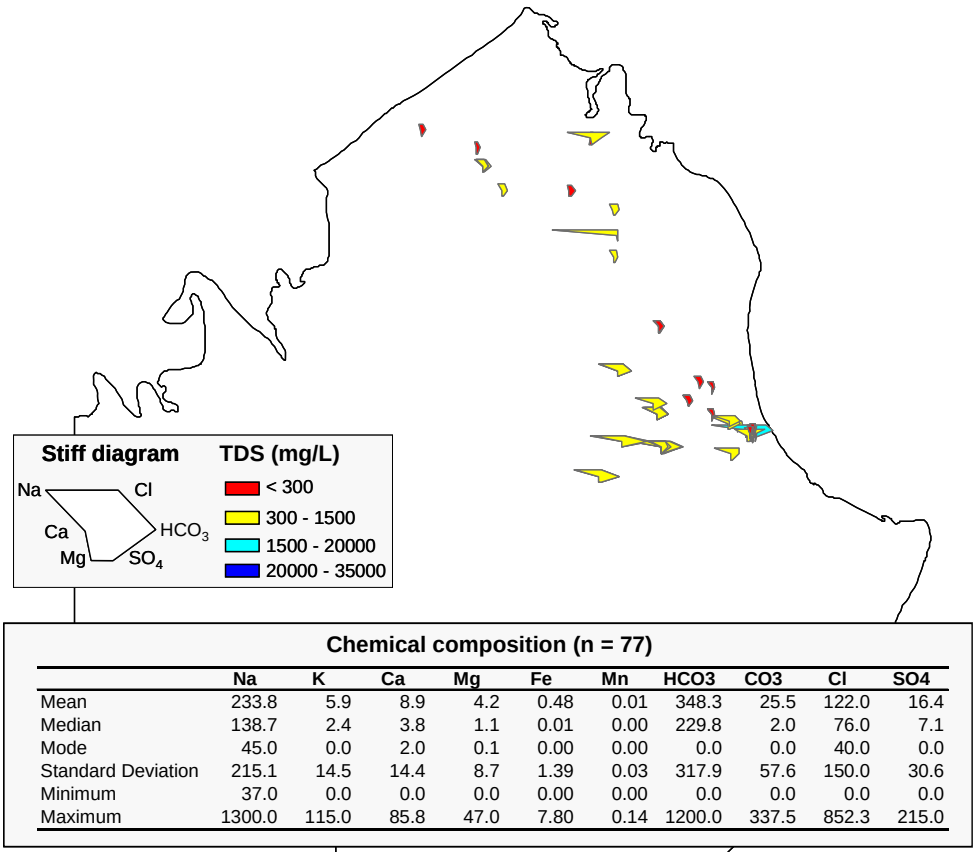

Chemical composition (n = 77)

	Na	K	Ca	Mg	Fe	Mn	HCO3	CO3	Cl	SO4
Mean	233.8	5.9	8.9	4.2	0.48	0.01	348.3	25.5	122.0	16.4
Median	138.7	2.4	3.8	1.1	0.01	0.00	229.8	2.0	76.0	7.1
Mode	45.0	0.0	2.0	0.1	0.00	0.00	0.0	0.0	40.0	0.0
Standard Deviation	215.1	14.5	14.4	8.7	1.39	0.03	317.9	57.6	150.0	30.6
Minimum	37.0	0.0	0.0	0.0	0.00	0.00	0.0	0.0	0.0	0.0
Maximum	1300.0	115.0	85.8	47.0	7.80	0.14	1200.0	337.5	852.3	215.0

Figure 18l. Major ion hydrochemical signatures for waters assigned to the Injune Creek Group in the Eromanga Basin (equivalent Birkhead, Adori and Westbourne), shown using Stiff diagrams and total dissolved solids (TDS). The Injune water is mainly fresh and sodium-bicarbonate type (see table with descriptive statistics for 77samples). No mineralogy is available.

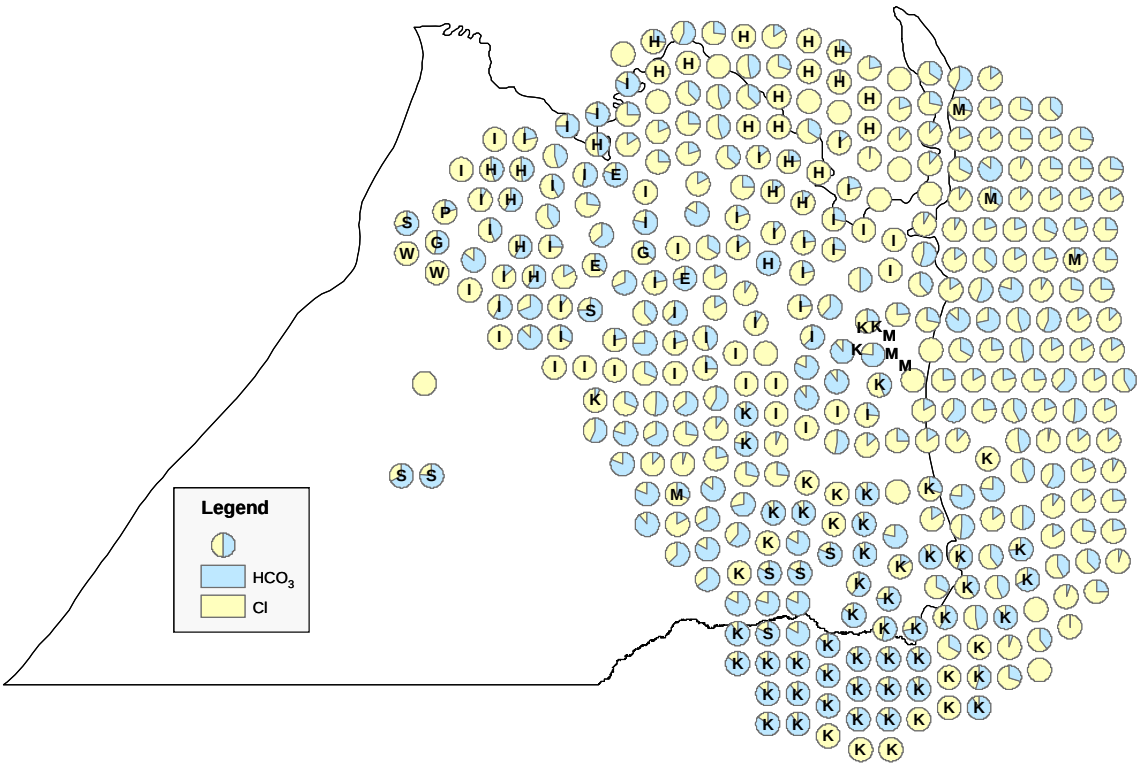

Figure 18m. Major anion distribution for the Walloon Subgroup in the Surat Basin (exploded view). Labels display known mixing between Walloon and Eurombah (E), Precipice (P), Hutton (H), Springbok (S), Injune Creek (I), Westbourne (W), Gubberamunda (G), Marburg (M) and Kumbarilla (K) waters. The Walloon water is generally chloride-rich, but it can become bicarbonate-rich when mixed with some Kumbarilla waters. Overall, the water becomes richer in bicarbonate southwards.

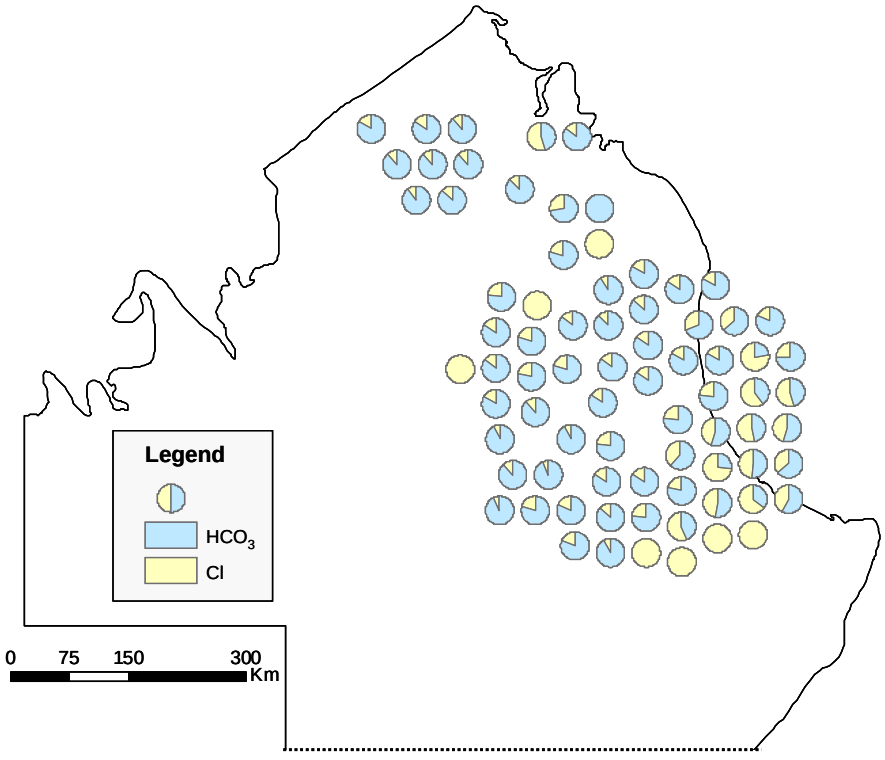

Figure18n. Major anion distribution for the Injune Creek Group in the Eromanga Basin (exploded view). The Injune water is generally bicarbonate-rich, with localised Cl enrichments. No water mixtures are reported.

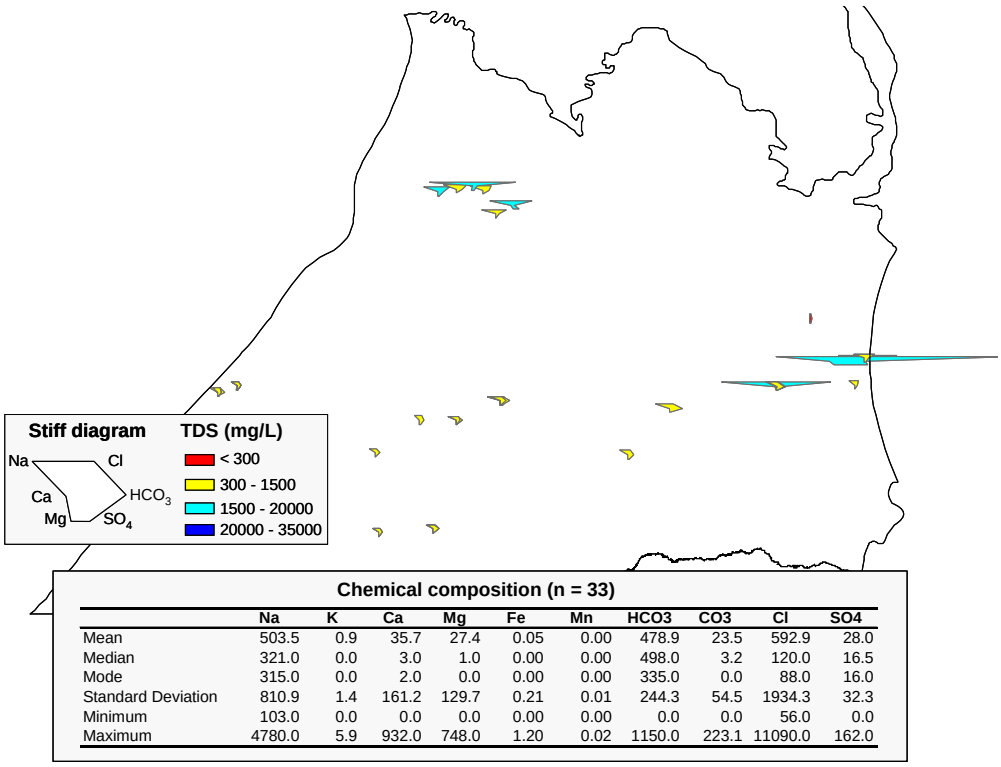

Chemical composition (n = 33)

	Na	K	Ca	Mg	Fe	Mn	HCO3	CO3	Cl	SO4
Mean	503.5	0.9	35.7	27.4	0.05	0.00	478.9	23.5	592.9	28.0
Median	321.0	0.0	3.0	1.0	0.00	0.00	498.0	3.2	120.0	16.5
Mode	315.0	0.0	2.0	0.0	0.00	0.00	335.0	0.0	88.0	16.0
Standard Deviation	810.9	1.4	161.2	129.7	0.21	0.01	244.3	54.5	1934.3	32.3
Minimum	103.0	0.0	0.0	0.0	0.00	0.00	0.0	0.0	56.0	0.0
Maximum	4780.0	5.9	932.0	748.0	1.20	0.02	1150.0	223.1	11090.0	162.0

Figure 18o. Major ion hydrochemical signatures for the Springbok Sandstone in the Surat Basin, shown using Stiff diagrams and total dissolved solids (TDS). The Springbok water is generally fresh and sodium-bicarbonate type (see table with descriptive statistics for 33 samples) with some chloride input in the east and north-east. Limitations: 1) no mineralogical data are available; 2) the number of water analyses is limited.

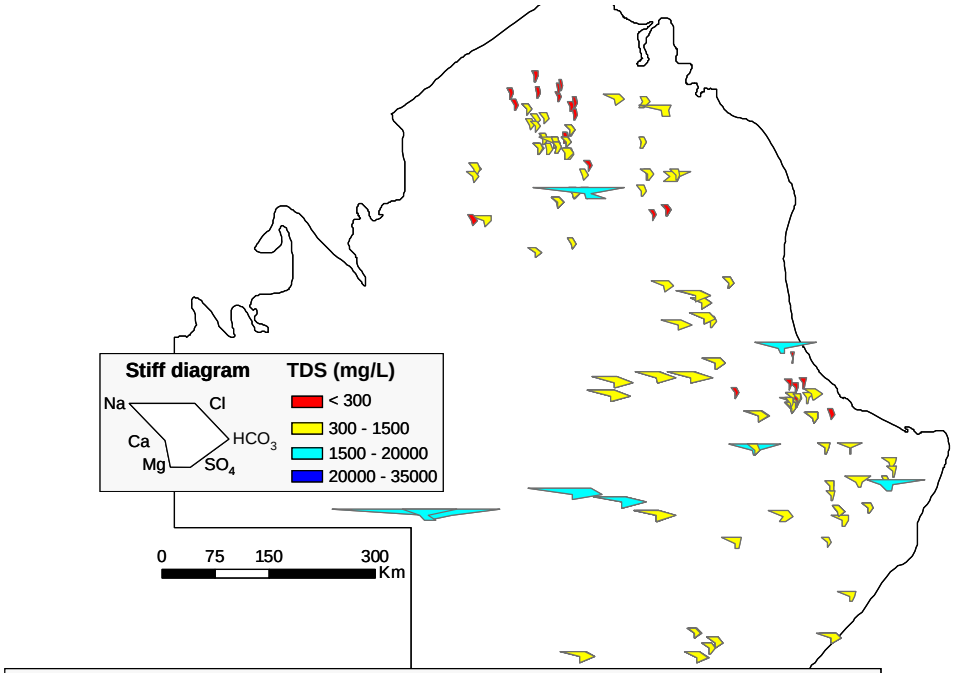

Chemical composition (n = 190)

	Na	K	Ca	Mg	Fe	Mn	HCO3	CO3	Cl	SO4
Mean	203.3	4.2	14.0	5.8	0.04	0.02	334.2	20.6	122.7	24.7
Median	133.0	1.0	11.3	2.0	0.00	0.00	253.8	1.8	66.0	10.0
Mode	110.0	0.0	12.0	0.0	0.00	0.00	0.0	0.0	60.0	0.0
Standard Deviation	215.3	5.6	16.9	11.2	0.13	0.04	287.0	61.1	238.2	74.8
Minimum	29.5	0.0	0.0	0.0	0.00	0.00	0.0	0.0	17.5	0.0
Maximum	2107.3	31.2	162.0	120.0	1.00	0.19	1700.0	527.7	2487.0	856.0

Figure 18p. Major ion hydrochemical signatures for the Adori Sandstone in the Eromanga Basin, shown using Stiff diagrams and total dissolved solids (TDS). The Adori water is mainly fresh and sodium-bicarbonate type (see table with descriptive statistics for 190 samples). No mineralogy is available.

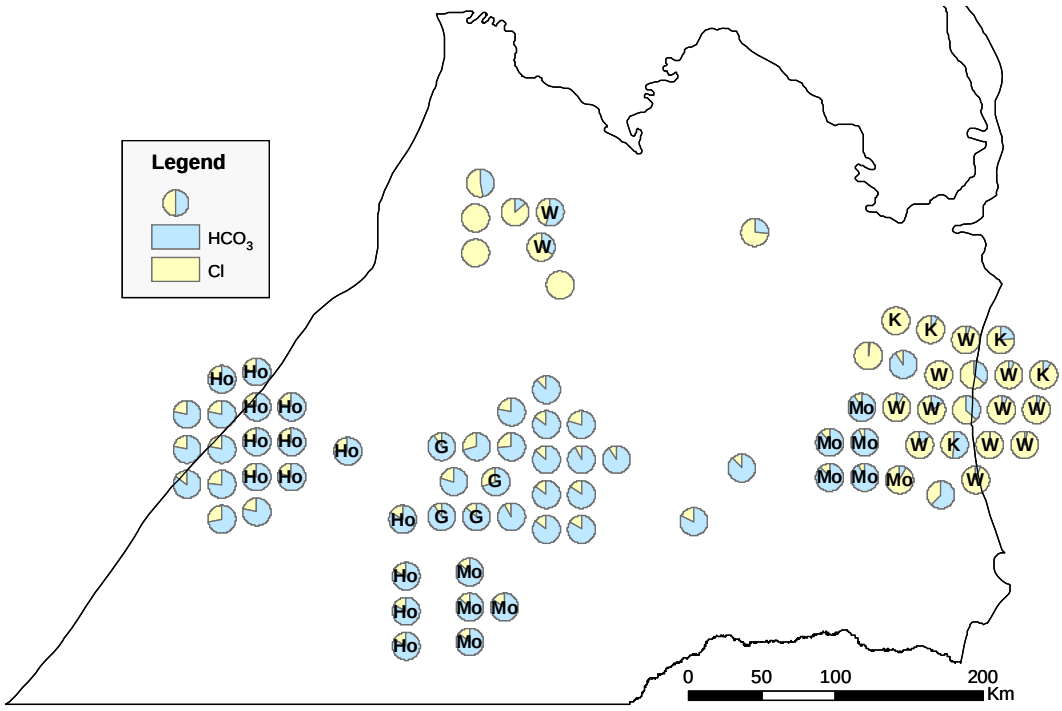

Figure 18q. Major anion distribution for the Springbok Sandstone in the Surat Basin (exploded view). Labels display known mixing between Springbok and Walloon (W), Gubberamunda (G), Mooga (Mo), Hooray (Ho), and Kumbarilla (K) waters. The Springbok water is generally bicarbonate-rich, but it can become Cl-rich when mixed with Walloon waters. The Cl signature appears to be more prominent in the north and east of the basin and caused by Walloon water.

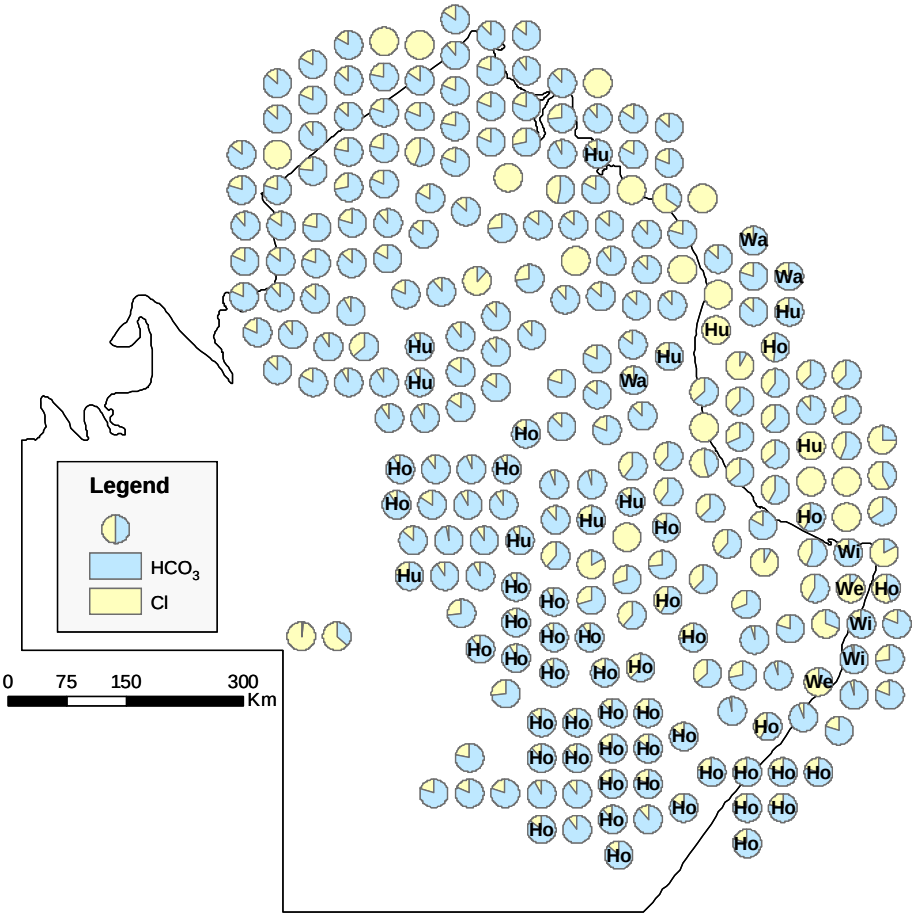

Figure 18r. Major anion distribution for the Adori Sandstone in the Eromanga Basin (exploded view). Labels display known mixing between Adori and Hutton (Hu), Westbourne (We), Hooray (Ho), Wallumbilla (Wa) and Winton (Wi) waters. The Adori water is generally bicarbonate-rich, with localised Cl enrichments.

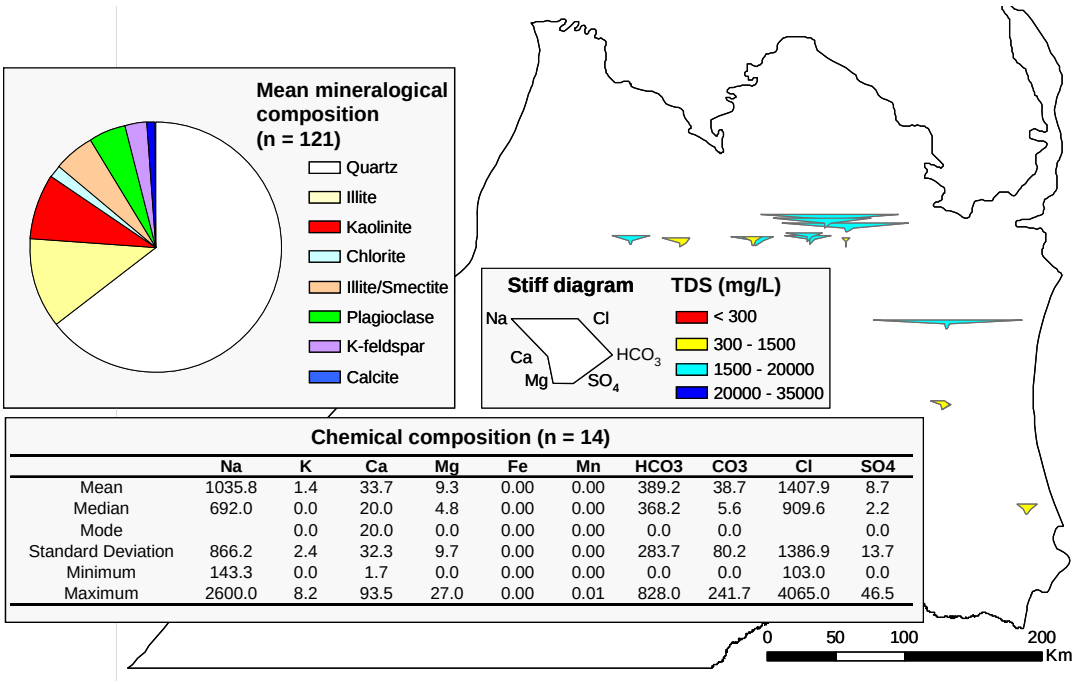

Chemical composition (n = 14)

	Na	K	Ca	Mg	Fe	Mn	HCO3	CO3	Cl	SO4
Mean	1035.8	1.4	33.7	9.3	0.00	0.00	389.2	38.7	1407.9	8.7
Median	692.0	0.0	20.0	4.8	0.00	0.00	368.2	5.6	909.6	2.2
Mode		0.0	20.0	0.0	0.00	0.00	0.0	0.0		0.0
Standard Deviation	866.2	2.4	32.3	9.7	0.00	0.00	283.7	80.2	1386.9	13.7
Minimum	143.3	0.0	1.7	0.0	0.00	0.00	0.0	0.0	103.0	0.0
Maximum	2600.0	8.2	93.5	27.0	0.00	0.01	828.0	241.7	4065.0	46.5

Figure 18s. Major ion hydrochemical signatures for the Westbourne Formation in the Surat Basin, shown using Stiff diagrams and total dissolved solids (TDS). The Westbourne water is highly variable in terms of salinity and type (see table with descriptive statistics for 14 samples). The mineralogy is based on 121 samples analysed by X-ray diffraction by Carmichael (1989); calcite, siderite, dolomite, pyrite and halite occur as localised traces. Limitations: 1) the number of water analyses is very limited and no mixtures are reported; 2) the mineralogy is based on samples collected from the Eromanga Basin, from depths of 200 to 2000 m.

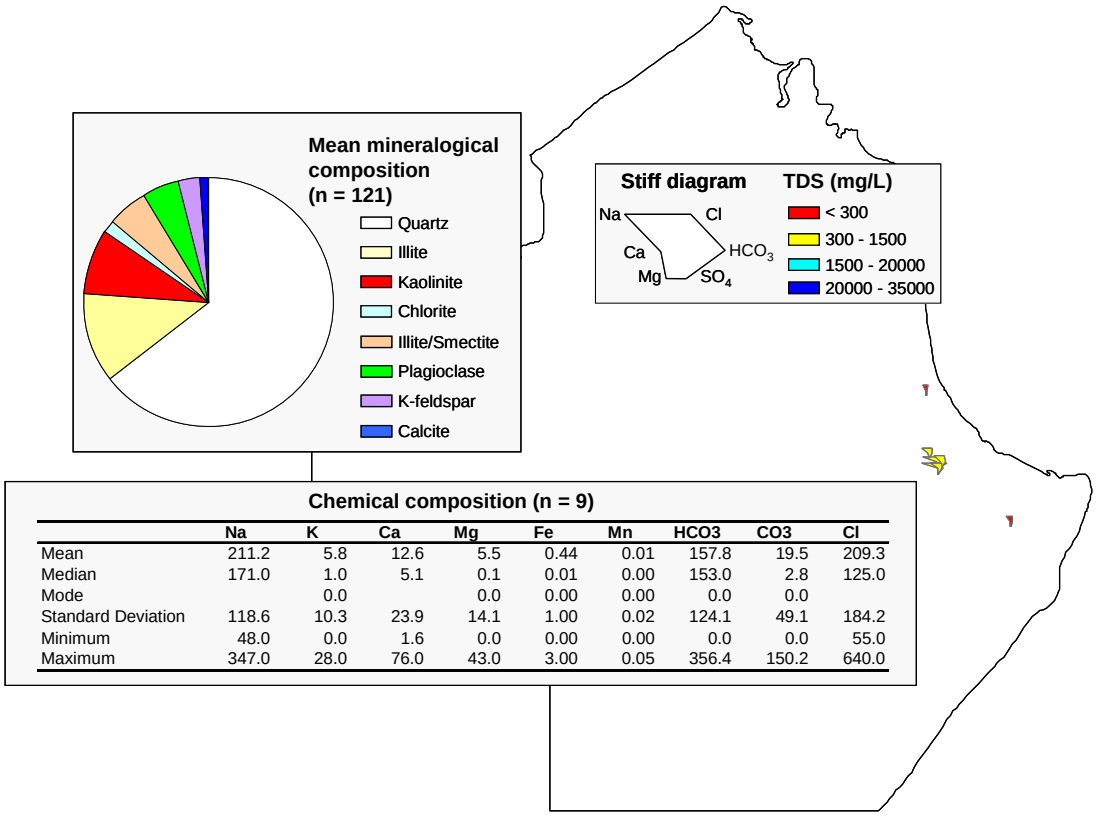

Chemical composition (n = 9)

	Na	K	Ca	Mg	Fe	Mn	HCO3	CO3	Cl
Mean	211.2	5.8	12.6	5.5	0.44	0.01	157.8	19.5	209.3
Median	171.0	1.0	5.1	0.1	0.01	0.00	153.0	2.8	125.0
Mode		0.0		0.0	0.00	0.00	0.0	0.0	
Standard Deviation	118.6	10.3	23.9	14.1	1.00	0.02	124.1	49.1	184.2
Minimum	48.0	0.0	1.6	0.0	0.00	0.00	0.0	0.0	55.0
Maximum	347.0	28.0	76.0	43.0	3.00	0.05	356.4	150.2	640.0

Figure 18t. Major ion hydrochemical signatures for the Westbourne Formation in the Eromanga Basin, shown using Stiff diagrams and total dissolved solids (TDS). The Westbourne water is fresh and largely sodium-chloride type (see table with descriptive statistics for 9 samples). The mineralogy is based on 121 samples analysed by X-ray diffraction by Carmichael (1989); calcite, siderite, dolomite, pyrite and halite occur as localised traces.

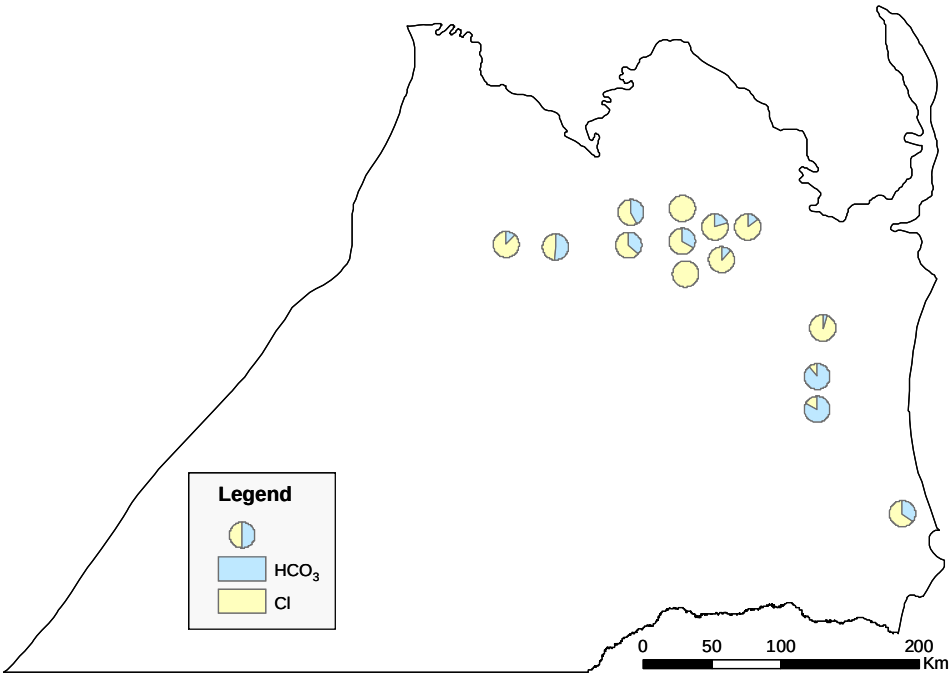

Figure 18u. Major anion distribution for the Westbourne Formation in the Surat Basin (exploded view). The Westbourne water is highly variable, but largely chloride type. Due to the limited number of samples, no definitive conclusions can be drawn; no water mixtures are reported.

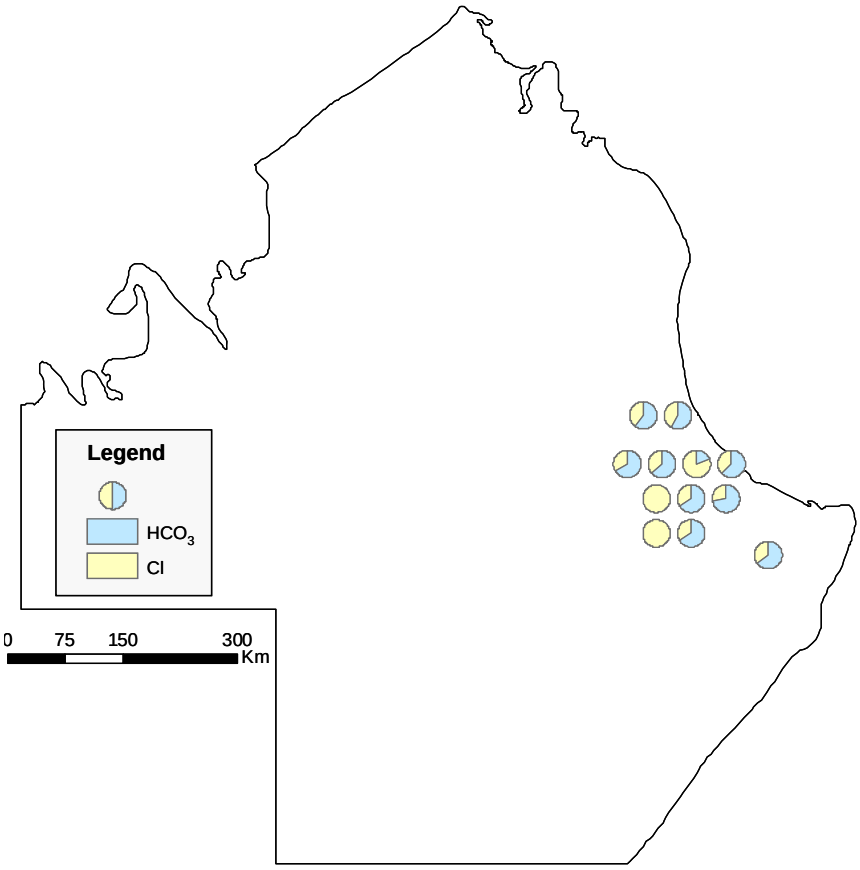

Figure 18v. Major anion distribution for the Westbourne Formation in the Eromanga Basin (exploded view). The Westbourne water is highly variable, but due to the limited number of samples, no definitive conclusions can be drawn; no water mixtures are reported.

Chemical composition (n = 260)

	Na	K	Ca	Mg	Fe	Mn	HCO3	CO3	Cl	SO4
Mean	483.6	1.3	25.7	8.4	0.50	0.02	580.4	34.9	403.9	45.6
Median	354.0	0.5	3.0	1.0	0.00	0.00	525.9	10.1	135.0	10.0
Mode	235.0	0.0	2.0	0.0	0.00	0.00	0.0	0.0	100.0	0.0
Standard Deviation	653.7	2.0	127.2	50.5	5.43	0.16	331.2	90.9	1275.2	141.8
Minimum	12.9	0.0	0.0	0.0	0.00	0.00	0.0	0.0	0.0	0.0
Maximum	7805.0	15.0	1488.0	748.0	79.00	2.00	1336.0	675.0	15700.0	1500.0

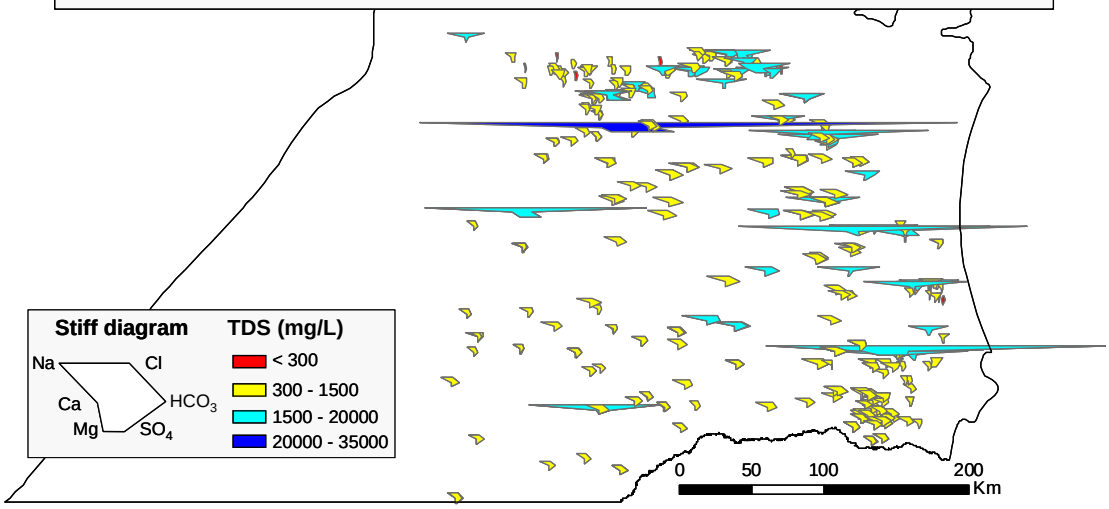

Figure 18w. Major ion hydrochemical signatures for the Gubberamunda Sandstone in the Surat Basin, shown using Stiff diagrams and total dissolved solids (TDS). The Gubberamunda water is generally fresh and sodium-bicarbonate type (see table with descriptive statistics for 260 samples) with some chloride input in the east. Limitations: no mineralogical data are available.

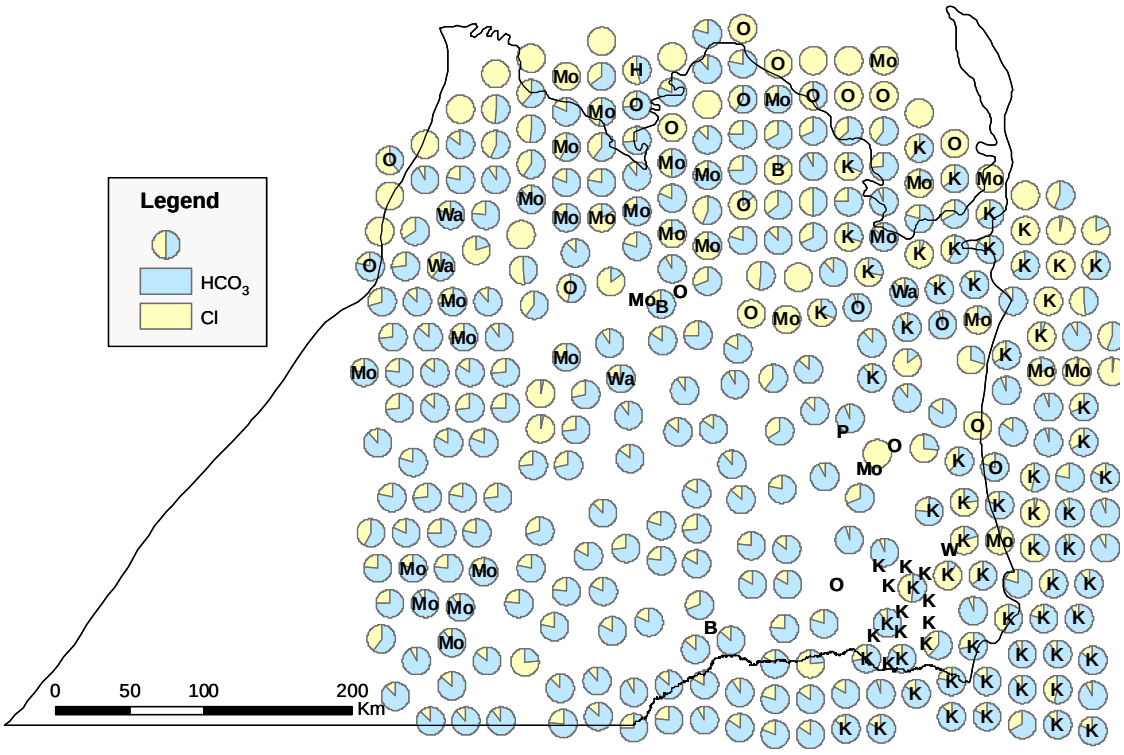

Figure 18x. Major anion distribution for the Gubberamunda Sandstone in the Surat Basin (exploded view). Labels display known mixing between Gubberamunda and Precipice (P), Hutton (H), Walloon (W), Mooga (Mo), Orallo (O), Wallumbilla (Wa), and Kumbarilla (K) waters. The Gubberamunda water is generally bicarbonate-rich, but it can become Cl-rich when mixed with younger brackish waters.

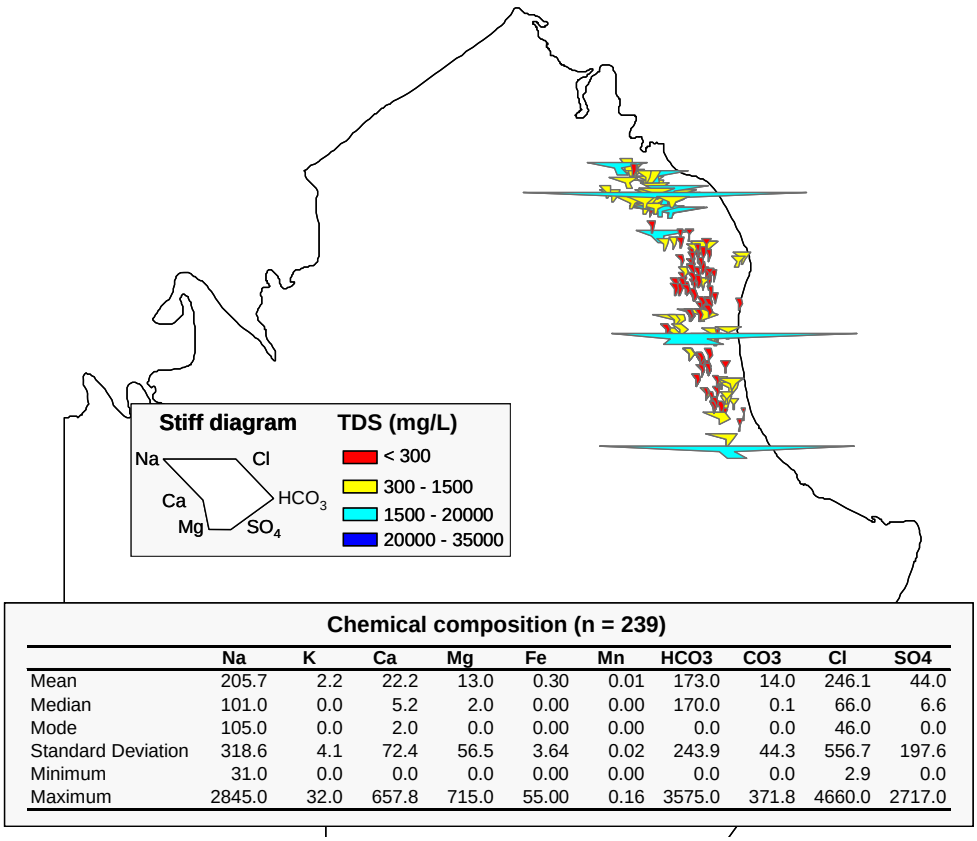

Chemical composition (n = 239)

	Na	K	Ca	Mg	Fe	Mn	HCO3	CO3	Cl	SO4
Mean	205.7	2.2	22.2	13.0	0.30	0.01	173.0	14.0	246.1	44.0
Median	101.0	0.0	5.2	2.0	0.00	0.00	170.0	0.1	66.0	6.6
Mode	105.0	0.0	2.0	0.0	0.00	0.00	0.0	0.0	46.0	0.0
Standard Deviation	318.6	4.1	72.4	56.5	3.64	0.02	243.9	44.3	556.7	197.6
Minimum	31.0	0.0	0.0	0.0	0.00	0.00	0.0	0.0	2.9	0.0
Maximum	2845.0	32.0	657.8	715.0	55.00	0.16	3575.0	371.8	4660.0	2717.0

Figure 18y. Major ion hydrochemical signatures for the Ronlow beds in the Eromanga Basin, shown using Stiff diagrams and total dissolved solids (TDS). The Ronlow water is mainly fresh and of mixed types (see table with descriptive statistics for 239 samples). No mineralogy is available.

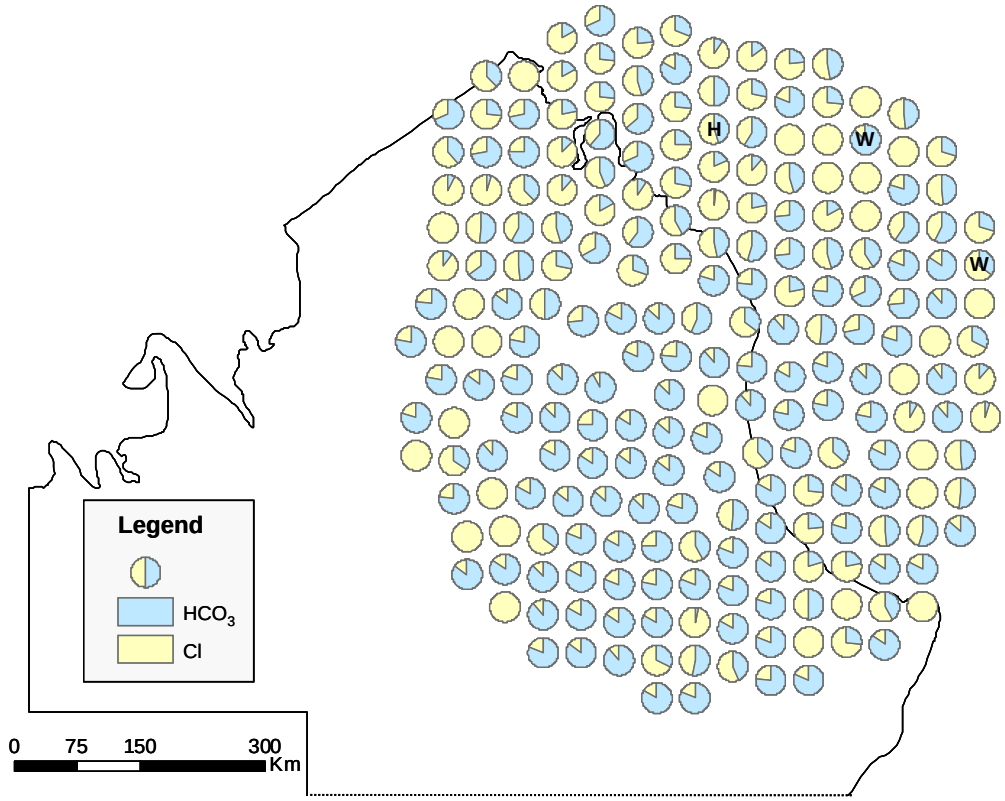

Figure 18z. Major anion distribution for the Ronlow beds in the Eromanga Basin (exploded view). Labels display known mixing between Ronlow and Hooray (H) and Wallumbilla (W) waters. The Ronlow water is highly variable and no clear spatial distribution of water types can be identified.

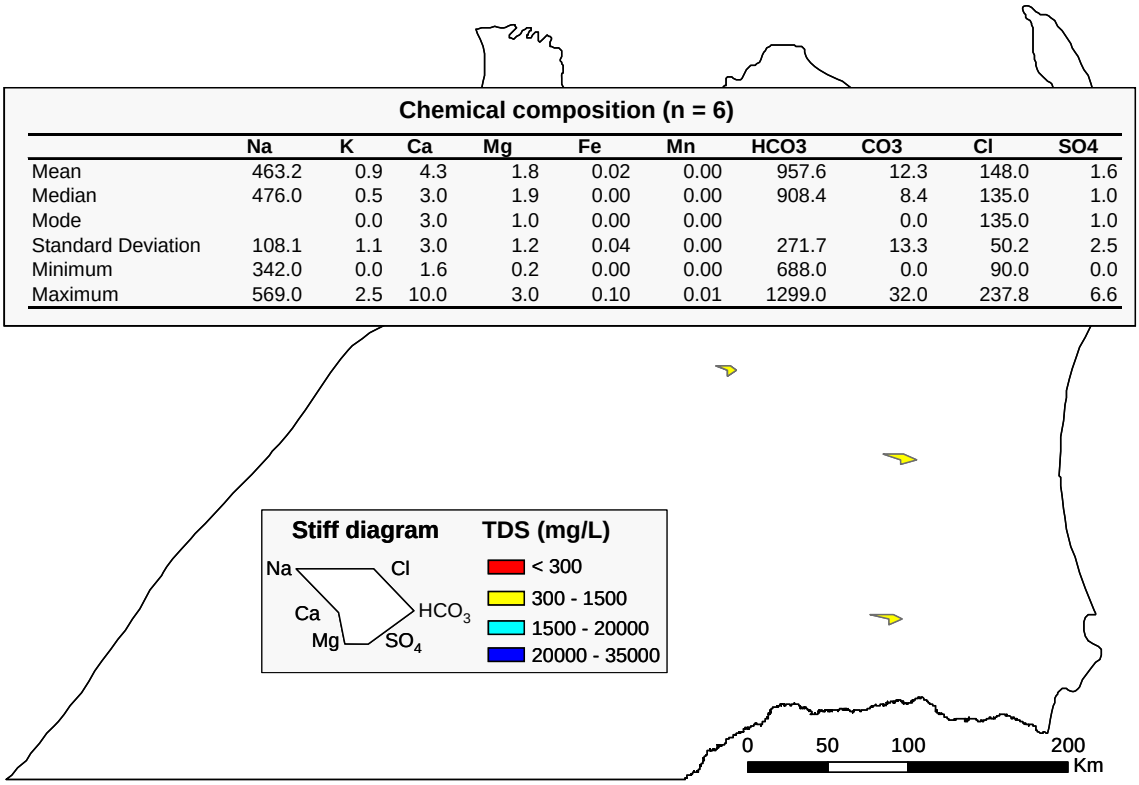

	Na	K	Ca	Mg	Fe	Mn	HCO3	CO3	Cl	SO4
Mean	463.2	0.9	4.3	1.8	0.02	0.00	957.6	12.3	148.0	1.6
Median	476.0	0.5	3.0	1.9	0.00	0.00	908.4	8.4	135.0	1.0
Mode		0.0	3.0	1.0	0.00	0.00		0.0	135.0	1.0
Standard Deviation	108.1	1.1	3.0	1.2	0.04	0.00	271.7	13.3	50.2	2.5
Minimum	342.0	0.0	1.6	0.2	0.00	0.00	688.0	0.0	90.0	0.0
Maximum	569.0	2.5	10.0	3.0	0.10	0.01	1299.0	32.0	237.8	6.6

Figure 18aa. Major ion hydrochemical signatures for the Orallo Formation in the Surat Basin, shown using Stiff diagrams and total dissolved solids (TDS). The Orallo water is fresh and sodium-bicarbonate type (see table with descriptive statistics for 6 samples). Limitations: very limited chemical data and no mineralogy.

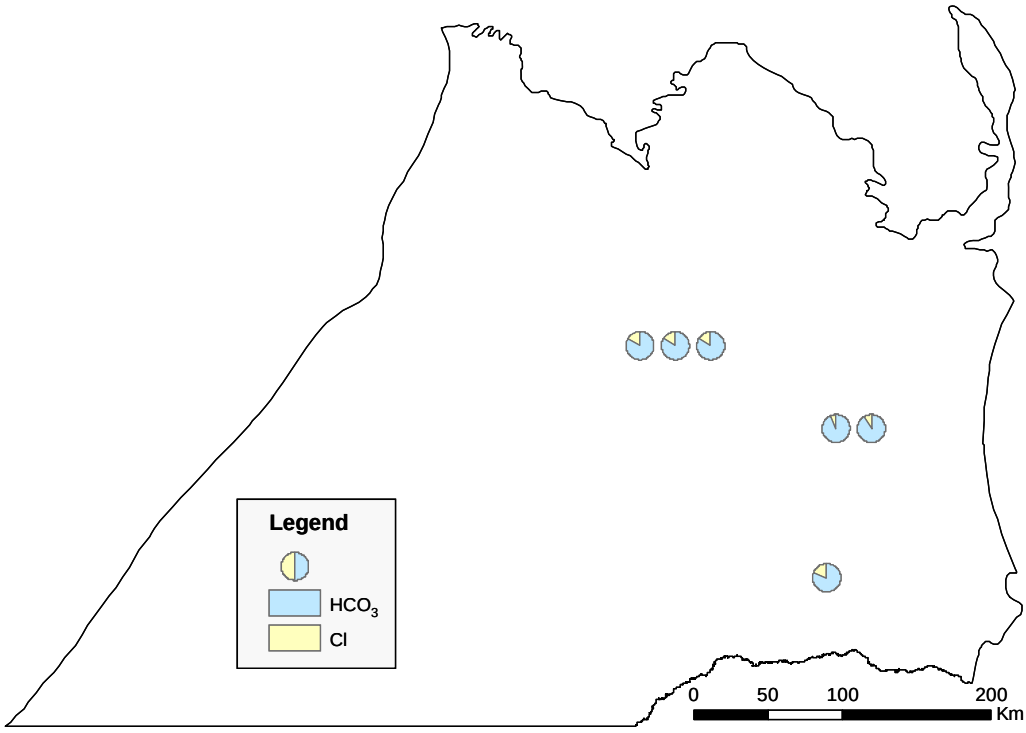

Figure 18bb. Major anion distribution for the Orallo Formation in the Surat Basin (exploded view). The Orallo water is bicarbonate-rich, but due to the limited number of samples, no definitive conclusions can be drawn; no water mixtures are reported.

Chemical composition (n = 486)

	Na	K	Ca	Mg	Fe	Mn	HCO3	CO3	Cl	SO4
Mean	553.9	1.1	23.7	9.7	0.067	0.011	607.2	61.4	454.2	64.4
Median	445.5	0.0	2.9	0.4	0.000	0.000	665.1	18.5	155.0	2.0
Mode	510.0	0.0	2.0	0.0	0.000	0.000	0.0	0.0	120.0	0.0
Standard Deviation	659.8	2.1	112.0	80.9	0.407	0.107	403.1	118.6	1393.4	202.5
Minimum	0.0	0.0	0.0	0.0	0.000	0.000	0.0	0.0	0.0	0.0
Maximum	11189.8	29.0	1707.4	1678.8	7.600	2.300	1371.0	634.9	24816.2	1997.7

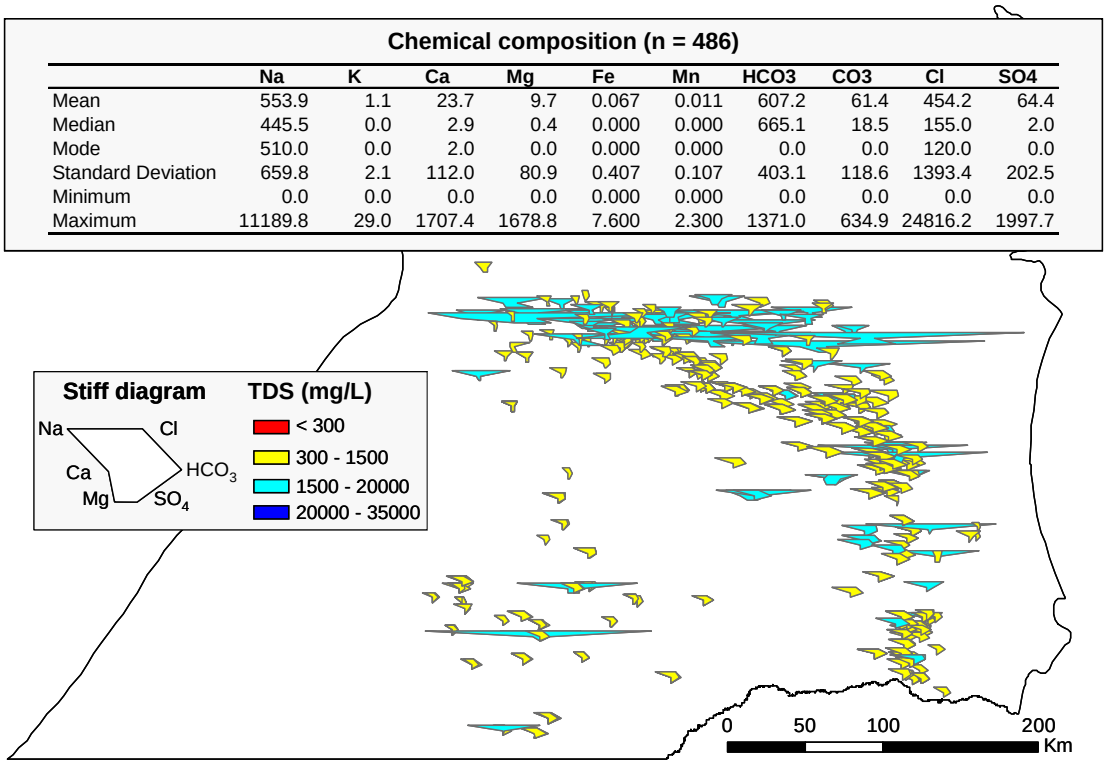

Figure 18cc. Major ion hydrochemical signatures for the Mooga Sandstone in the Surat Basin, shown using Stiff diagrams and total dissolved solids (TDS). The Mooga water is fresh to brackish and sodium-bicarbonate type (see table with descriptive statistics for 486 samples). Limitations: no mineralogical data.

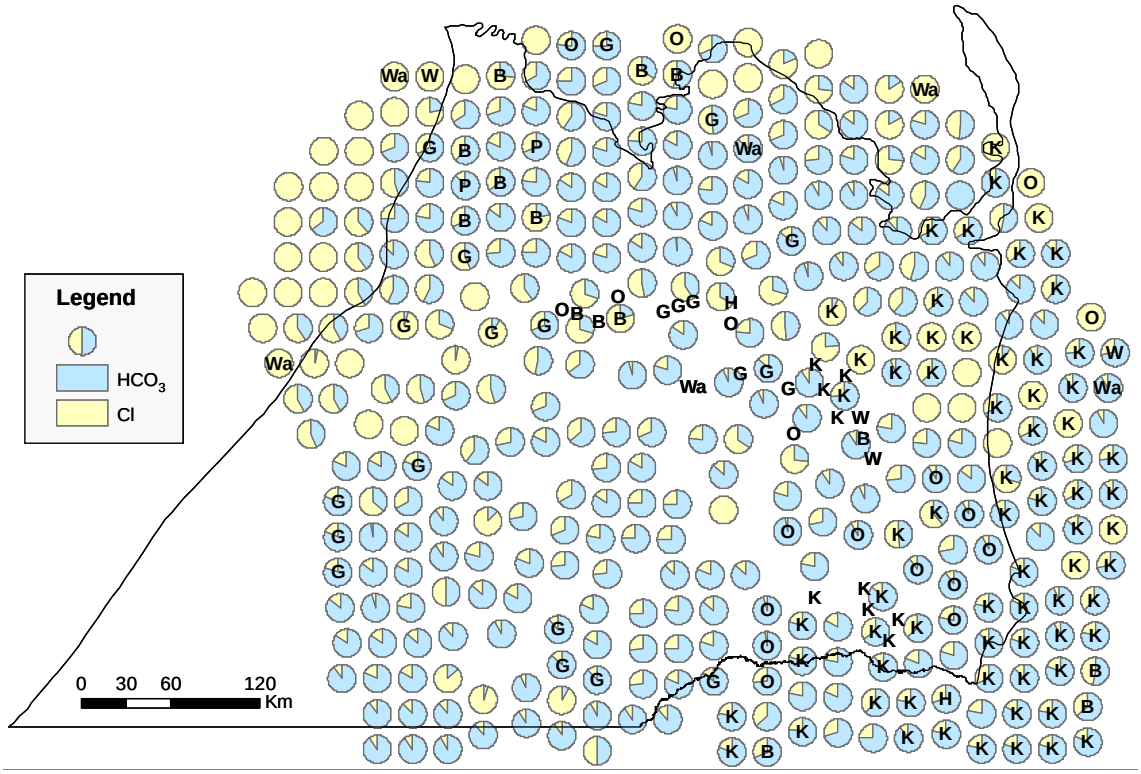

Figure 18dd. Major anion distribution for the Mooga Sandstone in the Surat Basin (exploded view). Labels display known mixing between Mooga and Precipice (P), Hutton (H), Walloon (W), Gubberamunda (G), Orallo (O), Bungil (B), Wallumbilla (Wa), and Kumbarilla (K) waters. The Mooga water is generally bicarbonate-rich, but it becomes chloride-rich in the north, presumably due to recharge.

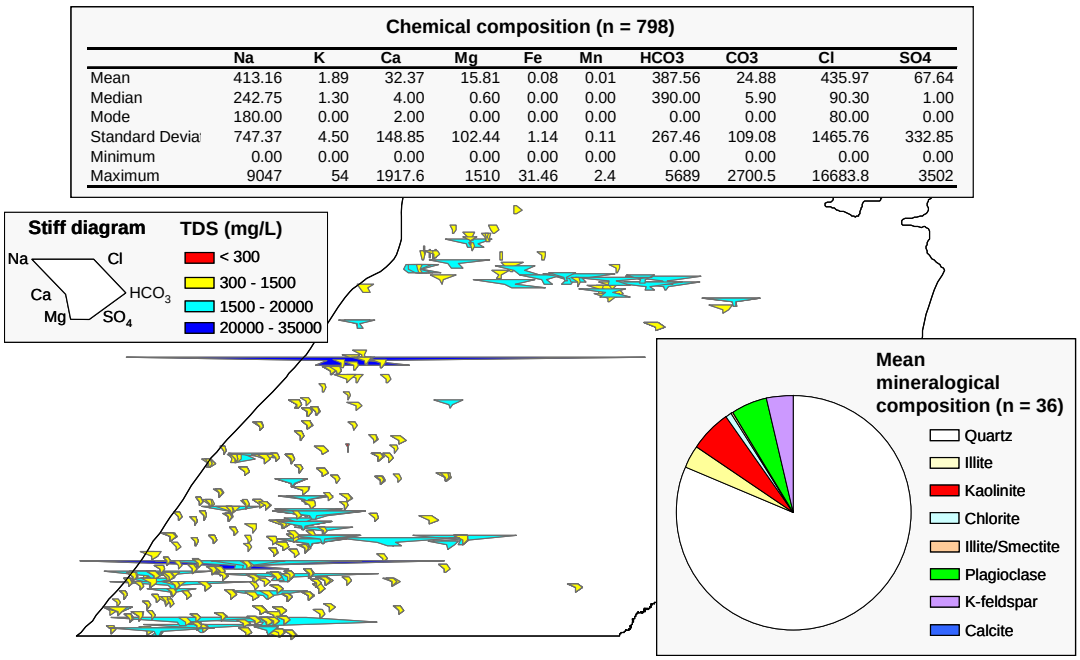

	Na	K	Ca	Mg	Fe	Mn	HCO3	CO3	Cl	SO4
Mean	413.16	1.89	32.37	15.81	0.08	0.01	387.56	24.88	435.97	67.64
Median	242.75	1.30	4.00	0.60	0.00	0.00	390.00	5.90	90.30	1.00
Mode	180.00	0.00	2.00	0.00	0.00	0.00	0.00	0.00	80.00	0.00
Standard Devia	747.37	4.50	148.85	102.44	1.14	0.11	267.46	109.08	1465.76	332.85
Minimum	0.00	0.00	0.00	0.00	0.00	0.00	0.00	0.00	0.00	0.00
Maximum	9047	54	1917.6	1510	31.46	2.4	5689	2700.5	16683.8	3502

Figure 18ee. Major ion hydrochemical signatures for the waters assigned to the Hooray Sandstone in the Surat Basin, shown using Stiff diagrams and total dissolved solids (TDS). The mineralogy is based on 36 samples analysed by X-ray diffraction by Carmichael (1989); chlorite, calcite and siderite occur as localised traces. This water is fresh to brackish and sodium-bicarbonate type (see table with descriptive statistics for 798 samples). Limitations: the mineralogy is based on samples collected from the true Hooray Sandstone in the Eromanga Basin, from depths of 700 to 1800 m.

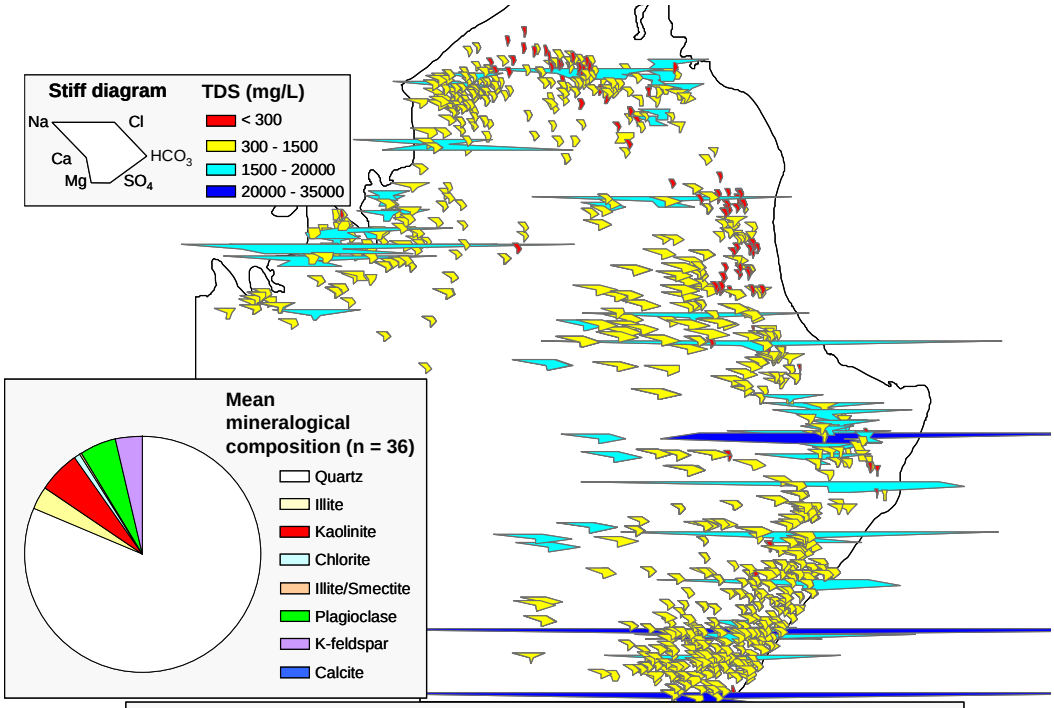

Chemical composition (n = 1979)

	Na	K	Ca	Mg	Fe	Mn	HCO3	CO3	Cl	SO4
Mean	303.3	2.3	17.0	7.8	0.12	0.01	404.4	17.0	221.8	41.3
Median	195.0	1.4	3.5	0.4	0.00	0.00	356.0	4.9	65.8	2.0
Mode	180.0	0.0	2.0	0.0	0.00	0.00	0.0	0.0	60.0	0.0
Standard Deviation	1044.6	5.4	107.5	61.6	3.43	0.10	335.2	47.0	1462.6	295.2
Minimum	0.0	0.0	0.0	0.0	0.00	0.00	0.0	0.0	0.0	0.0
Maximum	27927.9	125.0	2488.2	1373.0	152.00	4.00	8165.3	760.0	38000.0	7810.0

Figure 18ff. Major ion hydrochemical signatures for the Hooray Sandstone in the Eromanga Basin, shown using Stiff diagrams and total dissolved solids (TDS). The mineralogy is based on 36 samples analysed by X-ray diffraction by Carmichael (1989); chlorite, calcite and siderite occur as localised traces. This water is fresh to brackish and sodium-bicarbonate type (see table with descriptive statistics for 1979 samples).

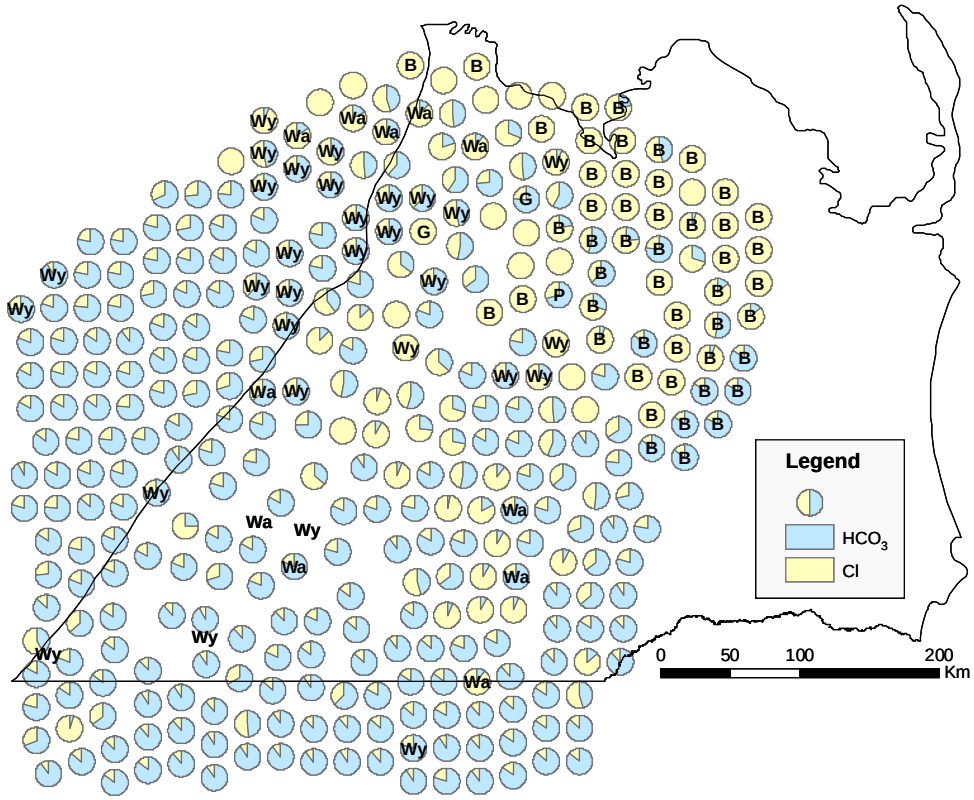

Figure 18gg. Major anion distribution for the Hooray Sandstone in the Surat Basin (exploded view). Labels display known mixing between Hooray and Precipice (P), Gubberamunda (G), Bungil (B), Wyandra (Wy) and Wallumbilla (Wa) waters. The Hooray water is generally bicarbonate-rich, but it becomes chloride-rich when mixed with Bungil and Wallumbilla waters.

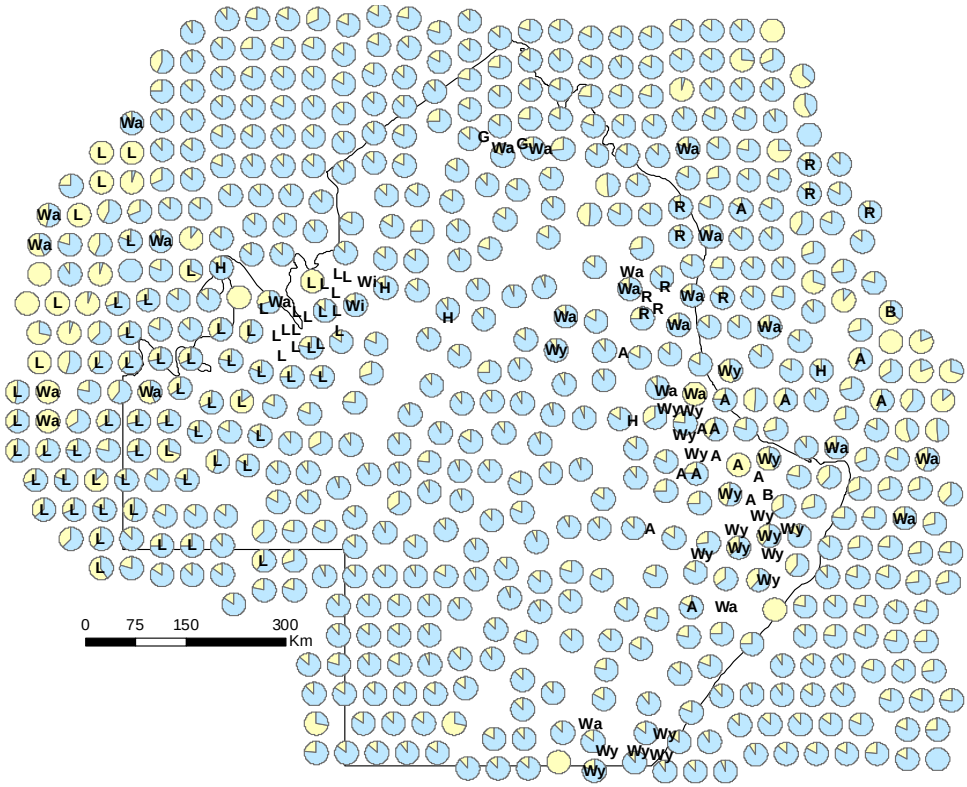

Figure 18hh. Major anion distribution for the Hooray Sandstone in the Eromanga Basin (exploded view). Labels display known mixing between Hooray and Hutton (H), Birkhead (B), Adori (A), Ronlow (R), Gilbert River (G), Longsight (L), Wyandra (Wy), Wallumbilla (Wa) and Winton (Wi) waters. The Hooray water is generally bicarbonate-rich, but it becomes chloride-rich when mixed with Longsight waters.

Chemical composition (n = 100)

	Na	K	Ca	Mg	Fe	Mn	HCO3	CO3	Cl	SO4
Mean	595.7	1.0	52.3	21.9	0.13	0.01	329.2	66.2	657.3	199.1
Median	445.0	0.0	6.0	1.5	0.00	0.00	200.0	18.3	300.0	10.3
Mode	455.0	0.0	5.7	0.0	0.00	0.00	0.0	0.0	530.0	0.0
Standard Deviation	601.9	2.4	144.0	57.7	0.75	0.02	350.1	98.2	1171.0	424.8
Minimum	0.0	0.0	0.0	0.0	0.00	0.00	0.0	0.0	0.0	0.0
Maximum	4837.7	18.0	1032.5	308.9	6.4	0.14	1150.0	421.9	9861.3	2299.0

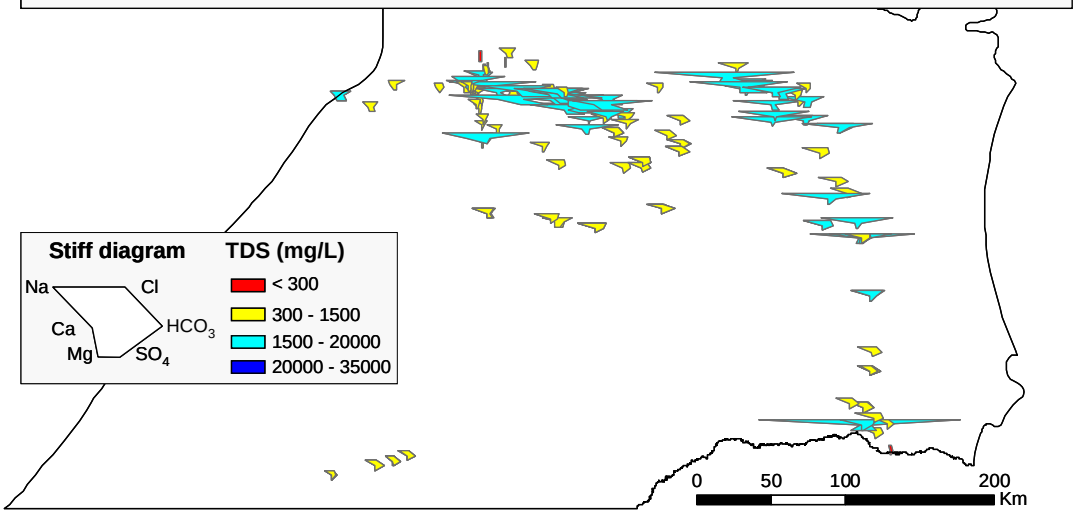

Figure 18ii. Major ion hydrochemical signatures for the Bungil Formation in the Surat Basin, shown using Stiff diagrams and total dissolved solids (TDS). The Bungil water is fresh to slightly brackish and mixed types (see table with descriptive statistics for 100 samples). Limitations: no mineralogical data.

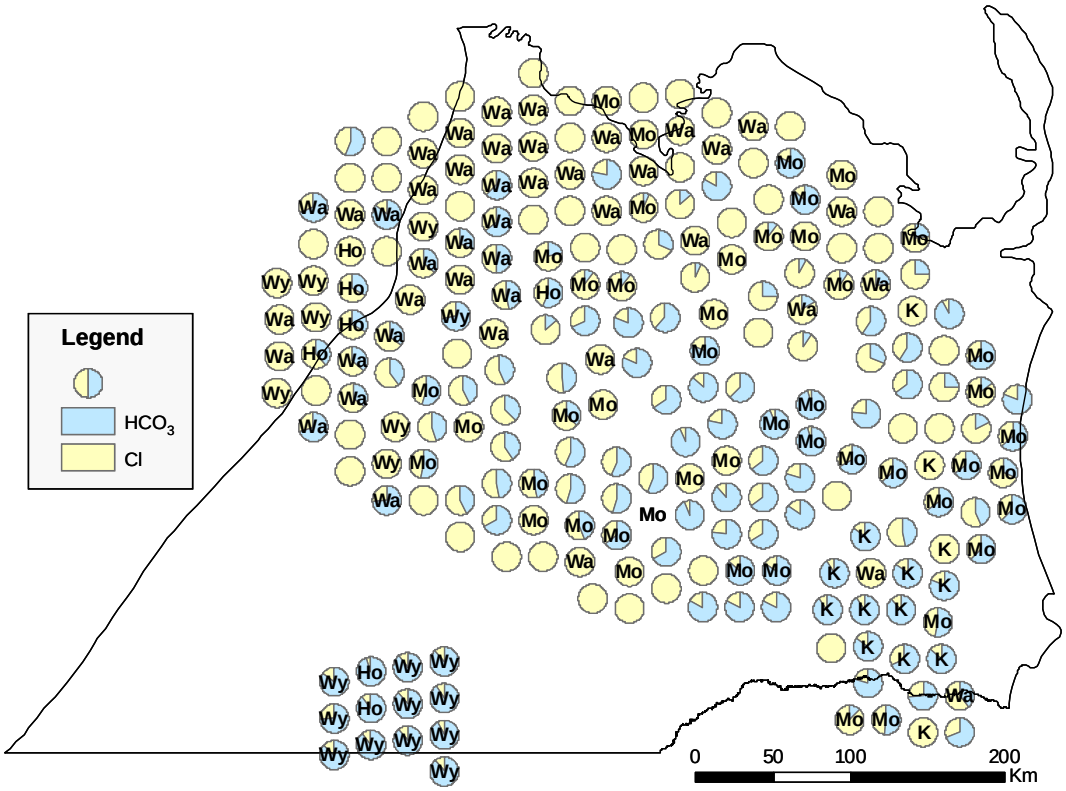

Figure 18jj. Major anion distribution for the Bungil Formation in the Surat Basin (exploded view). Labels display known mixing between Hooray and Mooga (Mo), Wyandra (Wy), Wallumbilla (Wa) and Kumbarilla (K) waters. The Bungil water can be both bicarbonate-rich or chloride-rich, with complex mixtures that do not match the known character of those waters. For example, Mooga is sodium-bicarbonate type but in this case it appears to change the character of Bungil waters towards chloride-dominated.

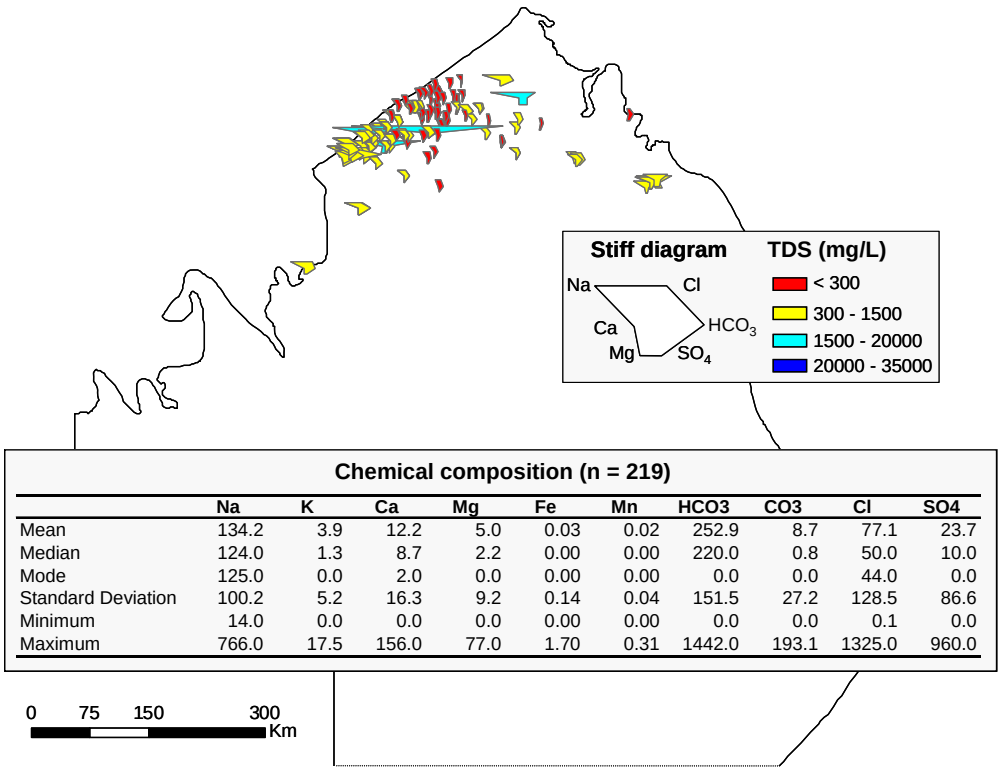

Chemical composition (n = 219)

	Na	K	Ca	Mg	Fe	Mn	HCO3	CO3	Cl	SO4
Mean	134.2	3.9	12.2	5.0	0.03	0.02	252.9	8.7	77.1	23.7
Median	124.0	1.3	8.7	2.2	0.00	0.00	220.0	0.8	50.0	10.0
Mode	125.0	0.0	2.0	0.0	0.00	0.00	0.0	0.0	44.0	0.0
Standard Deviation	100.2	5.2	16.3	9.2	0.14	0.04	151.5	27.2	128.5	86.6
Minimum	14.0	0.0	0.0	0.0	0.00	0.00	0.0	0.0	0.1	0.0
Maximum	766.0	17.5	156.0	77.0	1.70	0.31	1442.0	193.1	1325.0	960.0

Figure 18kk. Major ion hydrochemical signatures for the Gilbert River Formation in the Eromanga Basin, shown using Stiff diagrams and total dissolved solids (TDS). The Gilbert water is mainly fresh and sodium-bicarbonate type (see table with descriptive statistics for 219 samples). No mineralogy is available.

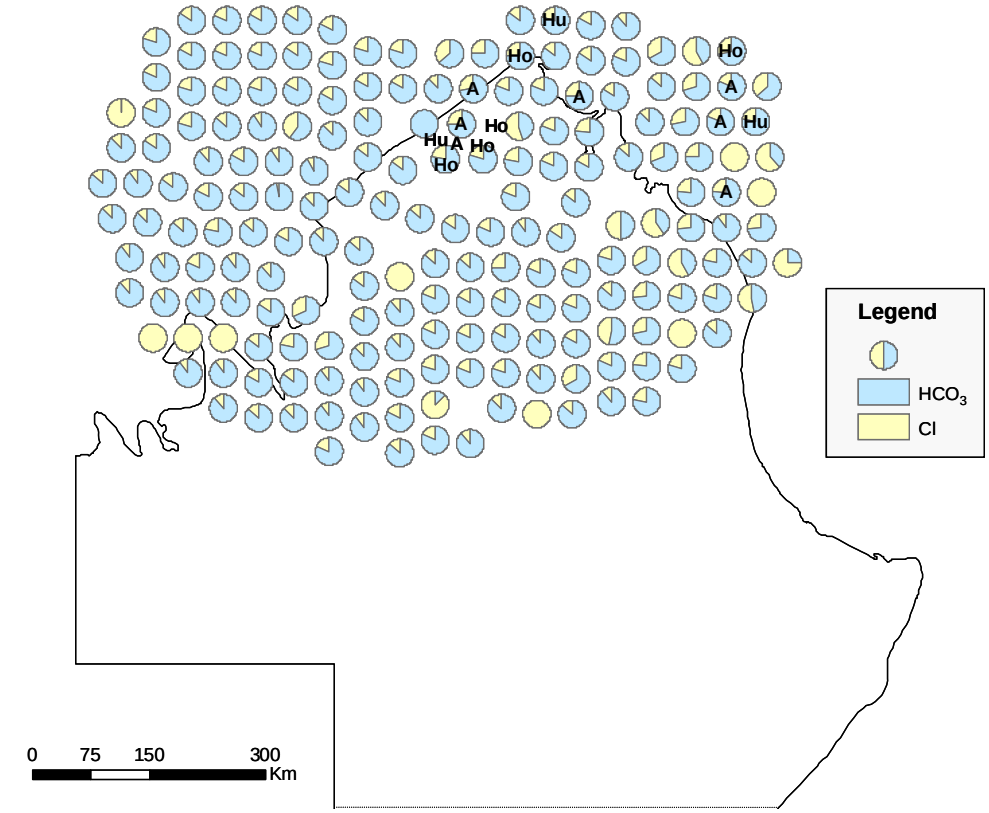

Figure 18ll. Major anion distribution for the Gilbert River Formation in the Eromanga Basin (exploded view). Labels display known mixing between Gilbert River and Hutton (Hu), Adori (A) and Hooray (Ho) waters. The Gilbert water is generally bicarbonate-rich, with localised Cl input.

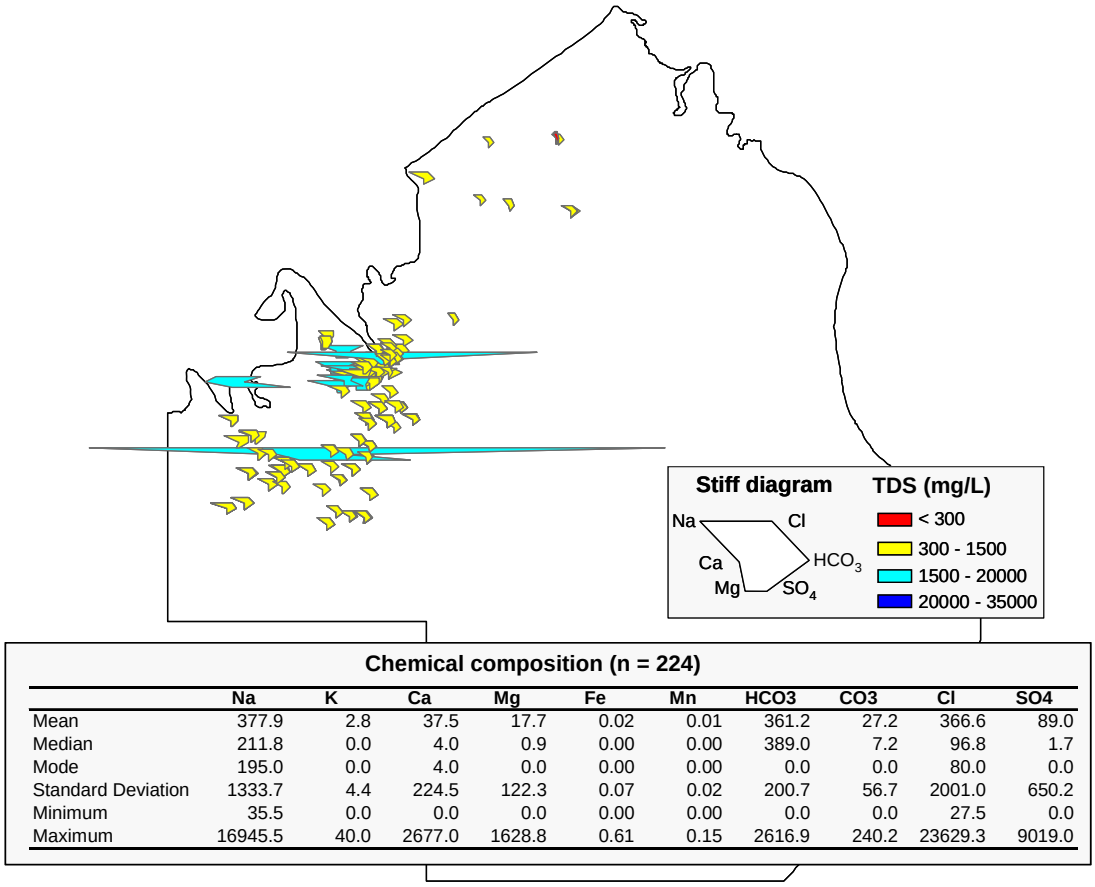

Chemical composition (n = 224)

	Na	K	Ca	Mg	Fe	Mn	HCO3	CO3	Cl	SO4
Mean	377.9	2.8	37.5	17.7	0.02	0.01	361.2	27.2	366.6	89.0
Median	211.8	0.0	4.0	0.9	0.00	0.00	389.0	7.2	96.8	1.7
Mode	195.0	0.0	4.0	0.0	0.00	0.00	0.0	0.0	80.0	0.0
Standard Deviation	1333.7	4.4	224.5	122.3	0.07	0.02	200.7	56.7	2001.0	650.2
Minimum	35.5	0.0	0.0	0.0	0.00	0.00	0.0	0.0	27.5	0.0
Maximum	16945.5	40.0	2677.0	1628.8	0.61	0.15	2616.9	240.2	23629.3	9019.0

Figure 18mm. Major ion hydrochemical signatures for the Longsight Sandstone in the Eromanga Basin, shown using Stiff diagrams and total dissolved solids (TDS). The Longsight water is mainly fresh and sodium-bicarbonate type (see table with descriptive statistics for 224 samples). No mineralogy is available.

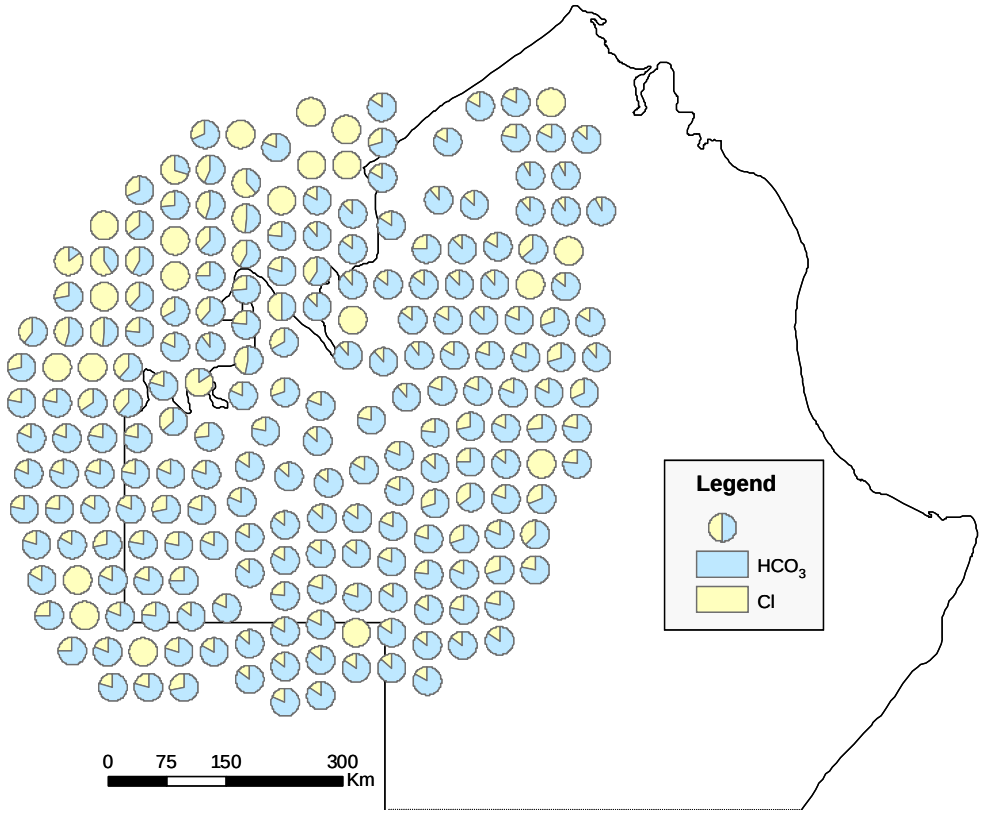

Figure 18nn. Major anion distribution for the Longsight Sandstone in the Eromanga Basin (exploded view). The water is generally bicarbonate-rich, with localised Cl input. No mixtures are reported.

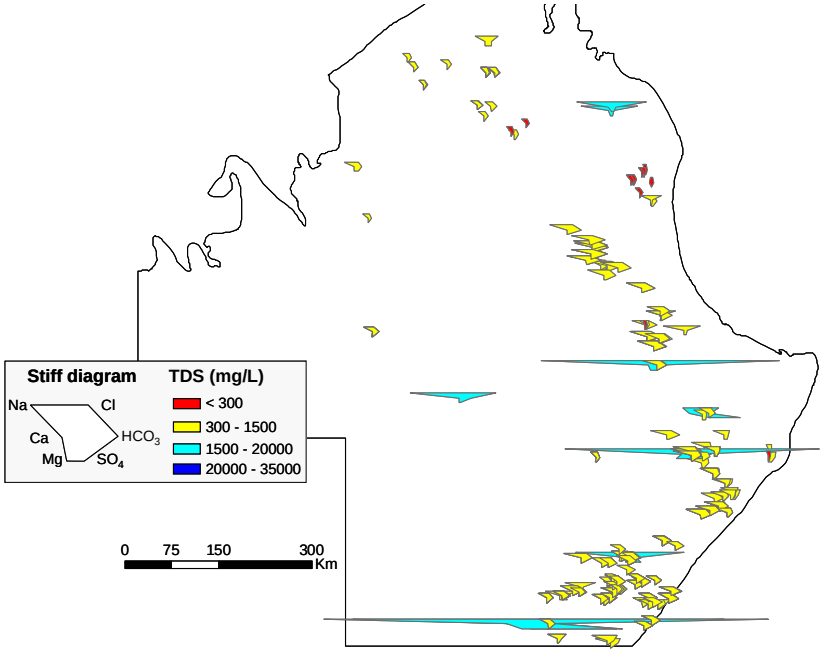

Chemical composition (n = 254)

	Na	K	Ca	Mg	Fe	Mn	HCO3	CO3	Cl	SO4
Mean	468.9	1.2	18.2	8.2	0.65	0.01	446.0	31.6	431.0	72.7
Median	268.7	1.2	3.7	0.4	0.00	0.00	514.2	8.5	83.0	3.2
Mode	270.0	0.0	4.0	0.0	0.00	0.00	0.0	0.0	160.0	0.0
Standard Deviation	1757.6	1.5	89.6	54.9	9.87	0.01	237.7	75.7	2741.8	404.3
Minimum	10.0	0.0	0.0	0.0	0.00	0.00	0.0	0.0	0.0	0.0
Maximum	26513.6	16.0	1145.4	767.9	157.30	0.12	1050.0	634.9	41245.5	4553.1

Figure 18oo. Major ion hydrochemical signatures for the Wyandra Sandstone Member in the Eromanga Basin, shown using Stiff diagrams and total dissolved solids (TDS). The Wyandra water is mainly fresh and sodium-bicarbonate type (see table with descriptive statistics for 254 samples). No mineralogy is available.

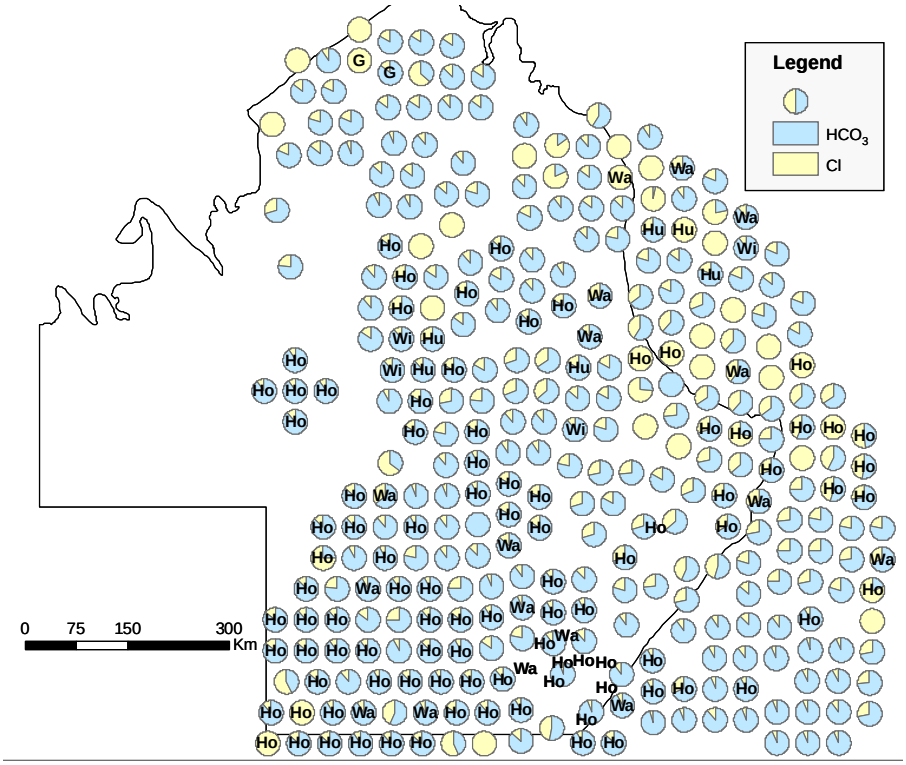

Figure 18pp. Major anion distribution for the Wyandra Sandstone Member in the Eromanga Basin (exploded view). Labels display known mixing between Wyandra and Hutton (Hu), Hooray (Ho), Gilbert River (G), Wallumbilla (Wa) and Winton (Wi) waters. The water is generally bicarbonate-rich, with localised Cl input.

Chemical composition (n = 255)

	Na	K	Ca	Mg	Fe	Mn	HCO3	CO3	Cl	SO4
Mean	993.91	4.15	89.02	39.91	0.02	0.09	285.74	23.10	1537.87	117.60
Median	673.00	2.30	26.00	9.30	0.00	0.00	261.50	2.80	934.00	1.00
Mode	1150.00	0.00	22.00	1.00	0.00	0.00	0.00	0.00	65.00	0.00
Standard Deviation	988.01	5.79	195.64	113.58	0.07	0.51	207.16	57.18	1949.52	404.44
Minimum	6.00	0.00	0.00	0.00	0.00	0.00	0.00	0.00	7.70	0.00
Maximum	5799.5	42	1349.9	1115.4	0.8	6	1250	408	11766	2841.4

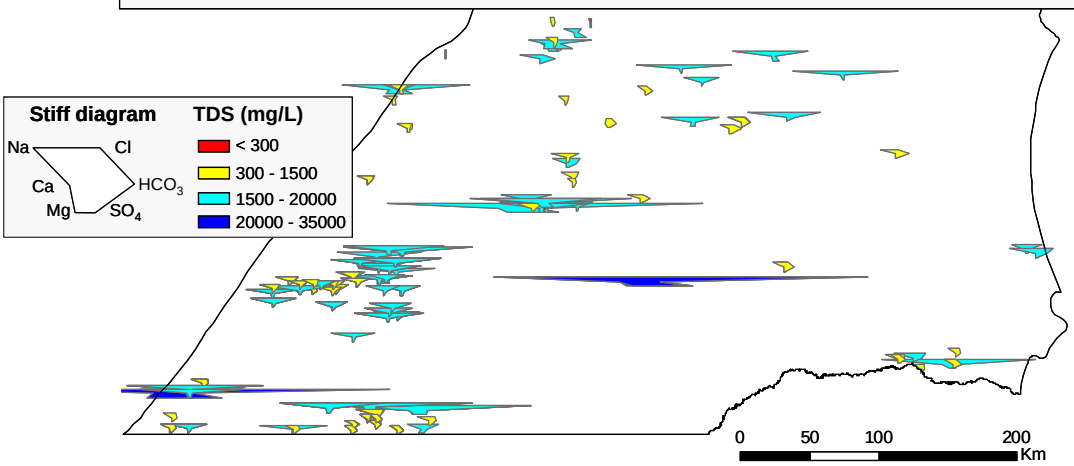

Figure 18qq. Major ion hydrochemical signatures for the Wallumbilla Formation in the Surat Basin, shown using Stiff diagrams and total dissolved solids (TDS). The Wallumbilla water is generally brackish and sodium-chloride type (see table with descriptive statistics for 255 samples). Limitations: no mineralogical data.

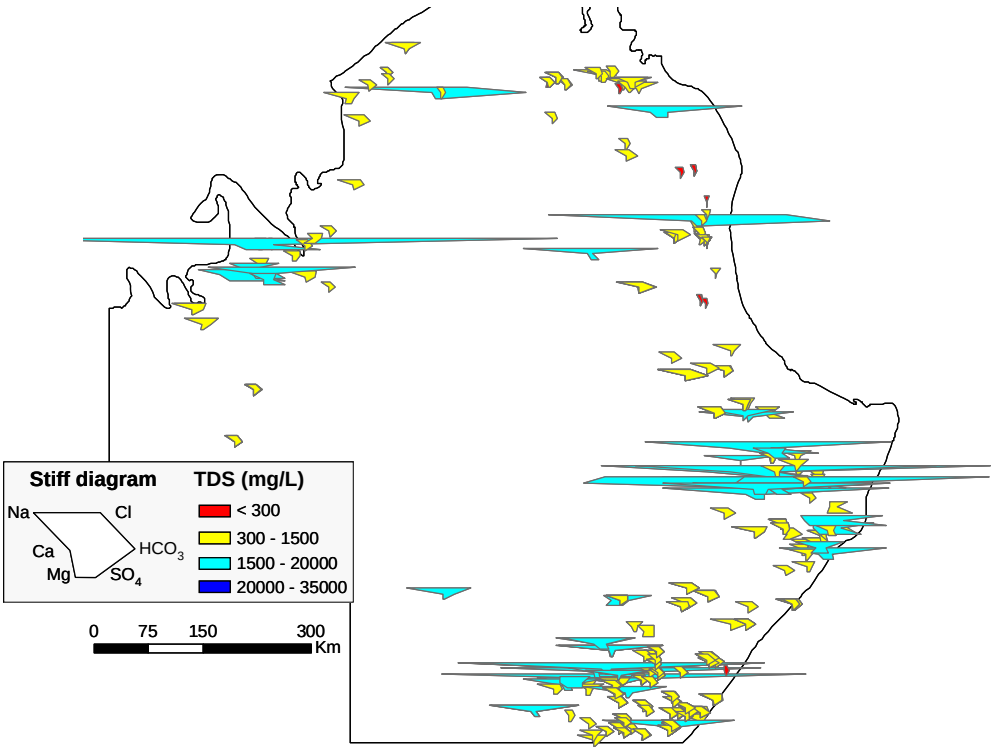

Chemical composition (n = 298)

	Na	K	Ca	Mg	Fe	Mn	HCO3	CO3	Cl	SO4
Mean	603.2	2.6	77.9	24.1	0.02	0.02	326.6	31.0	752.9	156.8
Median	295.0	0.0	8.9	2.9	0.00	0.00	248.5	4.0	195.0	11.0
Mode	305.0	0.0	4.0	0.0	0.00	0.00	0.0	0.0	160.0	0.0
Standard Deviation	746.8	12.2	297.2	65.3	0.06	0.08	665.9	65.7	1175.2	355.8
Minimum	0.0	0.0	0.0	0.0	0.00	0.00	0.0	0.0	0.0	0.0
Maximum	4700.0	203.3	4508.0	750.0	0.60	0.80	7679.1	600.6	6117.5	2513.9

Figure 18rr. Major ion hydrochemical signatures for the Wallumbilla Formation in the Eromanga Basin, shown using Stiff diagrams and total dissolved solids (TDS). The Wallumbilla water is fresh to brackish and sodium-chloride type (see table with descriptive statistics for 298 samples). No mineralogy is available.

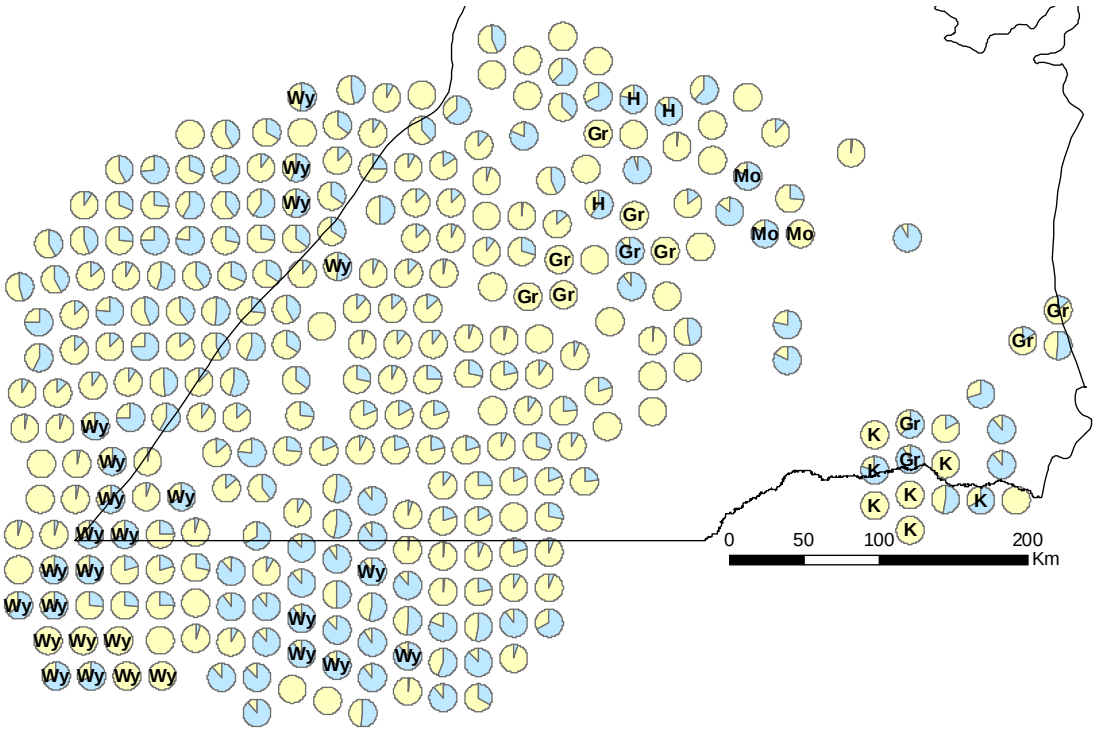

Figure 18ss. Major anion distribution for the Wallumbilla Formation in the Surat Basin (exploded view). Labels display known mixing between Wallumbilla and Hutton (H), Wyandra (Wy), Wallumbilla (Wa), and Kumbarilla (K) waters. The Wallumbilla water is generally chloride-rich, with localised enrichments in bicarbonate.

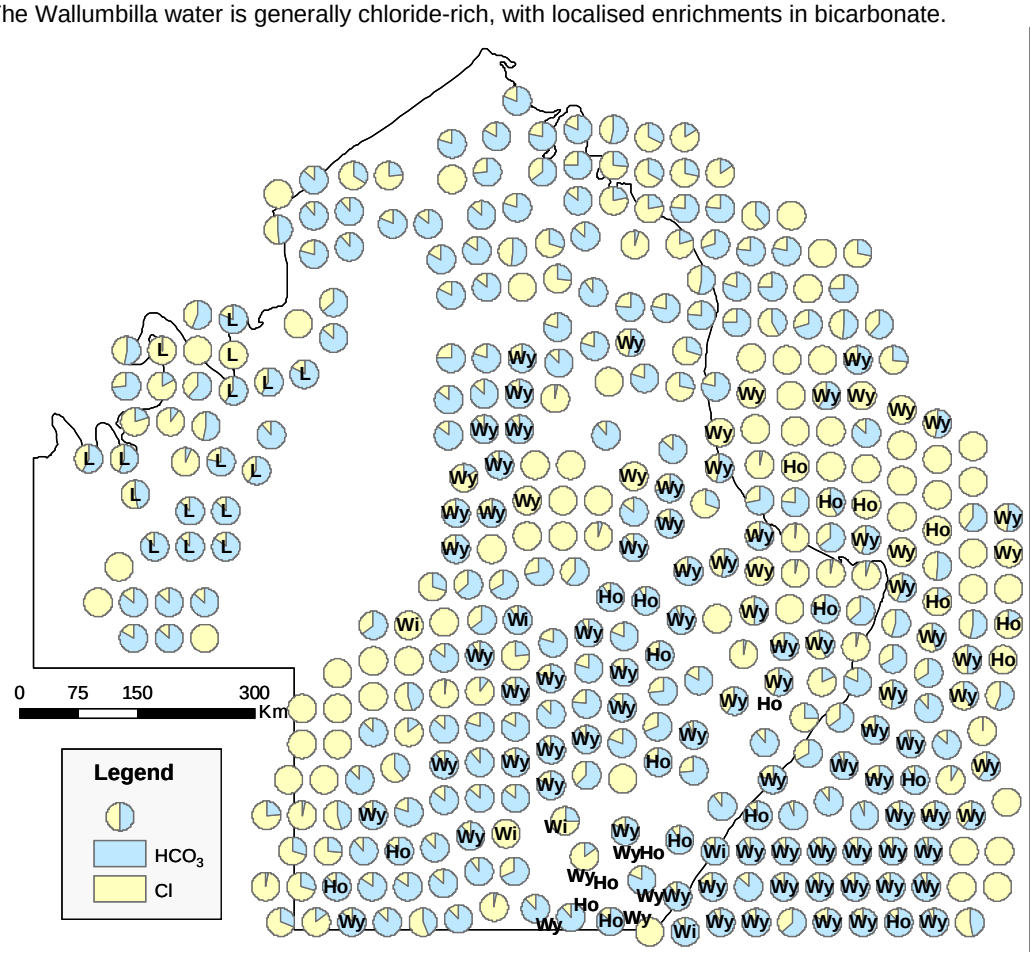

Figure 18tt. Major anion distribution for the Wallumbilla Formation in the Eromanga Basin (exploded view). Labels display known mixing between Wallumbilla and Hooray (Ho), Longsight (L), Wyandra (Wy), and Winton (Wi) waters. The water is generally chloride-rich, with localised HCO_3 input from Wyandra.

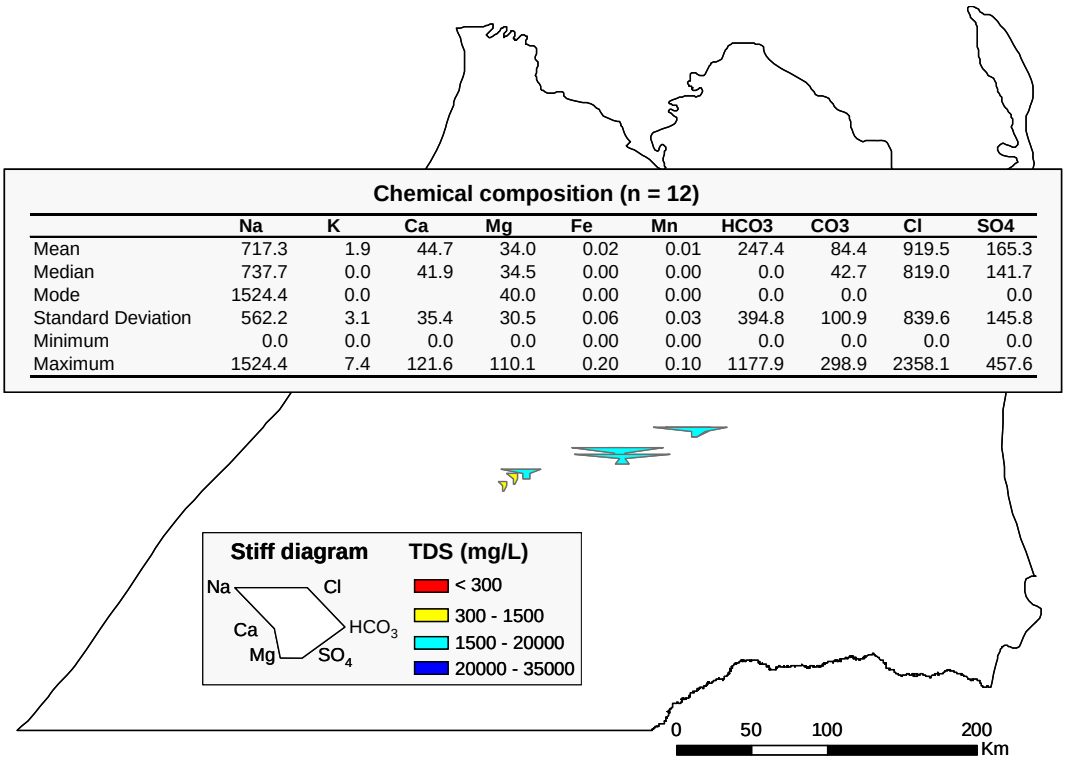

	Na	K	Ca	Mg	Fe	Mn	HCO3	CO3	Cl	SO4
Mean	717.3	1.9	44.7	34.0	0.02	0.01	247.4	84.4	919.5	165.3
Median	737.7	0.0	41.9	34.5	0.00	0.00	0.0	42.7	819.0	141.7
Mode	1524.4	0.0		40.0	0.00	0.00	0.0	0.0		0.0
Standard Deviation	562.2	3.1	35.4	30.5	0.06	0.03	394.8	100.9	839.6	145.8
Minimum	0.0	0.0	0.0	0.0	0.00	0.00	0.0	0.0	0.0	0.0
Maximum	1524.4	7.4	121.6	110.1	0.20	0.10	1177.9	298.9	2358.1	457.6

Figure 18uu. Major ion hydrochemical signatures for the Surat Siltstone in the Surat Basin, shown using Stiff diagrams and total dissolved solids (TDS). The Surat water is generally brackish and sodium-chloride type (see table with descriptive statistics for 12 samples). Limitations: limited chemical data and no mineralogy.

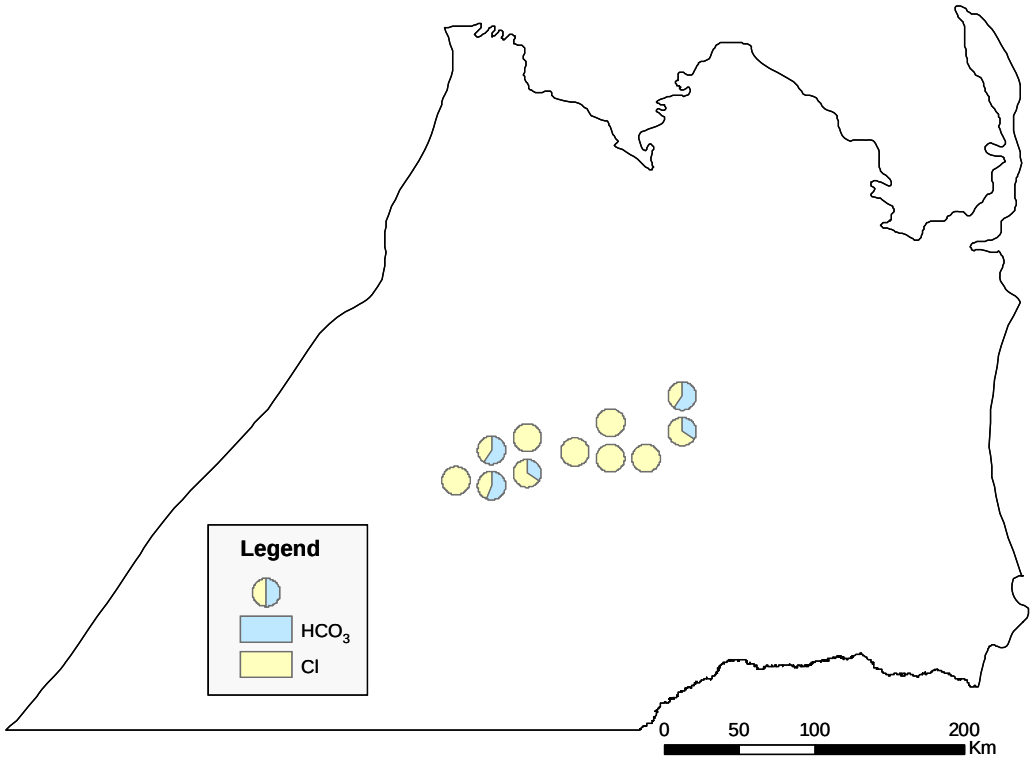

Figure 18vv. Major anion distribution for the Surat Siltstone in the Surat Basin (exploded view). The Wallumbilla water is generally chloride-rich, with localised enrichments in bicarbonate.

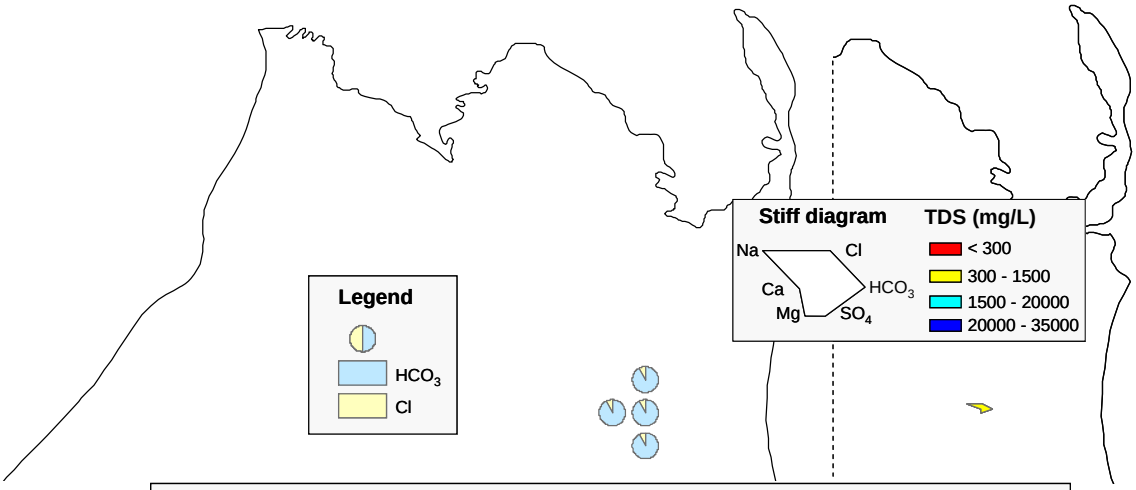

Chemical composition (n = 4)

	Na	K	Ca	Mg	Fe	Mn	HCO3	CO3	Cl	SO4
Mean	478.3	0.8	1.9	0.4	0.11	0.00	1052.3	26.4	94.4	0.7
Median	480.7	0.8	1.7	0.4	0.07	0.00	1041.1	31.2	94.4	0.5
Mode			1.6			0.00				
Standard Deviation	13.3	0.7	0.4	0.4	0.13	0.00	31.9	19.1	5.0	0.9
Minimum	460.0	0.0	1.6	0.0	0.00	0.00	1029.0	0.0	89.0	0.0
Maximum	492.0	1.4	2.4	1.0	0.29	0.00	1098.0	43.1	100.0	1.9

Figure 18www. Major ion hydrochemical signatures for the Griman Creek Formation in the Surat Basin, shown using Stiff diagrams, total dissolved solids (TDS) and pie diagrams. The water is fresh and sodium-bicarbonate type (see table with descriptive statistics for 4 samples, collected from one bore). Limitations: very limited chemical data and no mineralogy.

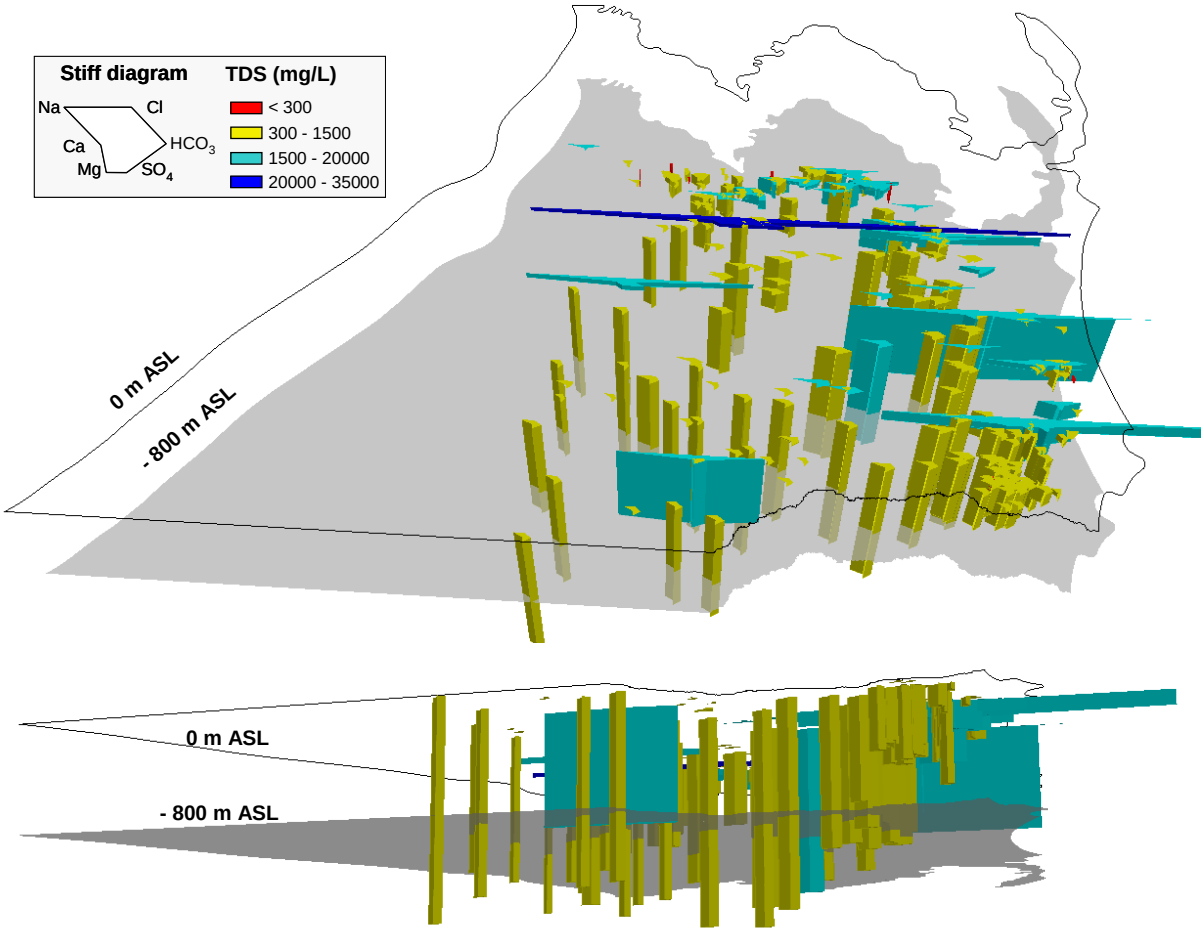

Figure 19. Water type variation with depth – an example for the Gubberamunda waters in the Surat Basin. Deep waters are fresh Na-HCO_3 waters, while the shallower waters can become chloride-rich and saltier. The very fresh waters that occur close to the recharge areas are mainly Na-Cl. The -800 m critical depth is shown for reference.

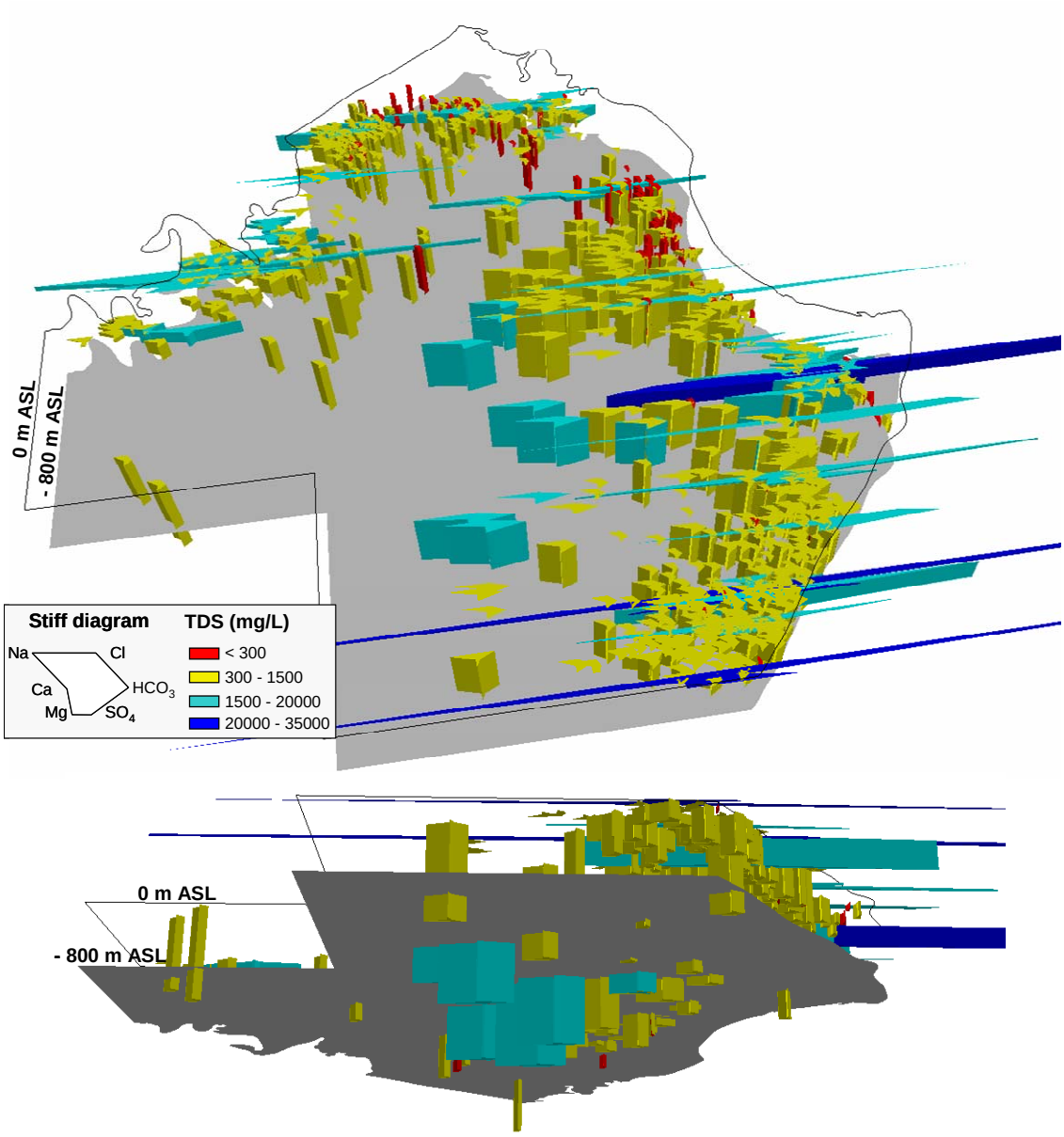

Figure 20. Water type variation with depth – an example for the Hooray waters in the Eromanga Basin. The Na-HCO_3 character does vary with the depth; the deeper waters from the central basin are saltier but preserve the Na-HCO_3 character. The -800 m critical depth is shown for reference.

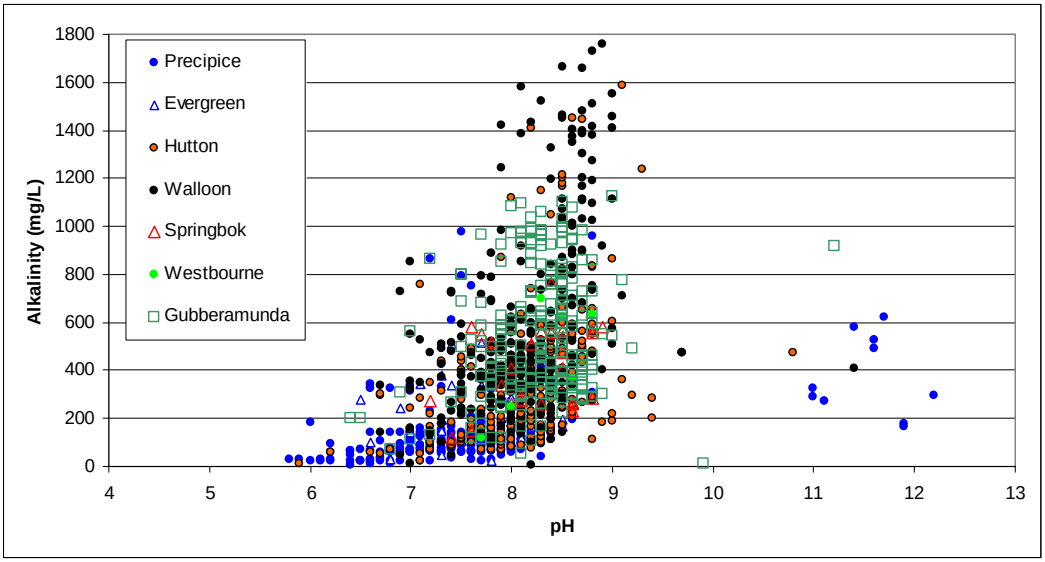

Figure 21a. pH – alkalinity relationship for the main Jurassic groundwaters of the Surat Basin. The pH largely varies between 6 and 9, while the alkalinity can reach 1800 mg/L. The Precipice waters are generally circumneutral, with low alkalinities, while the Walloon waters include some high pH and alkalinity samples. Other groundwaters such as the Hutton and Gubberamunda are highly variable. Note: interpretation is based only on non-mixed water analyses.

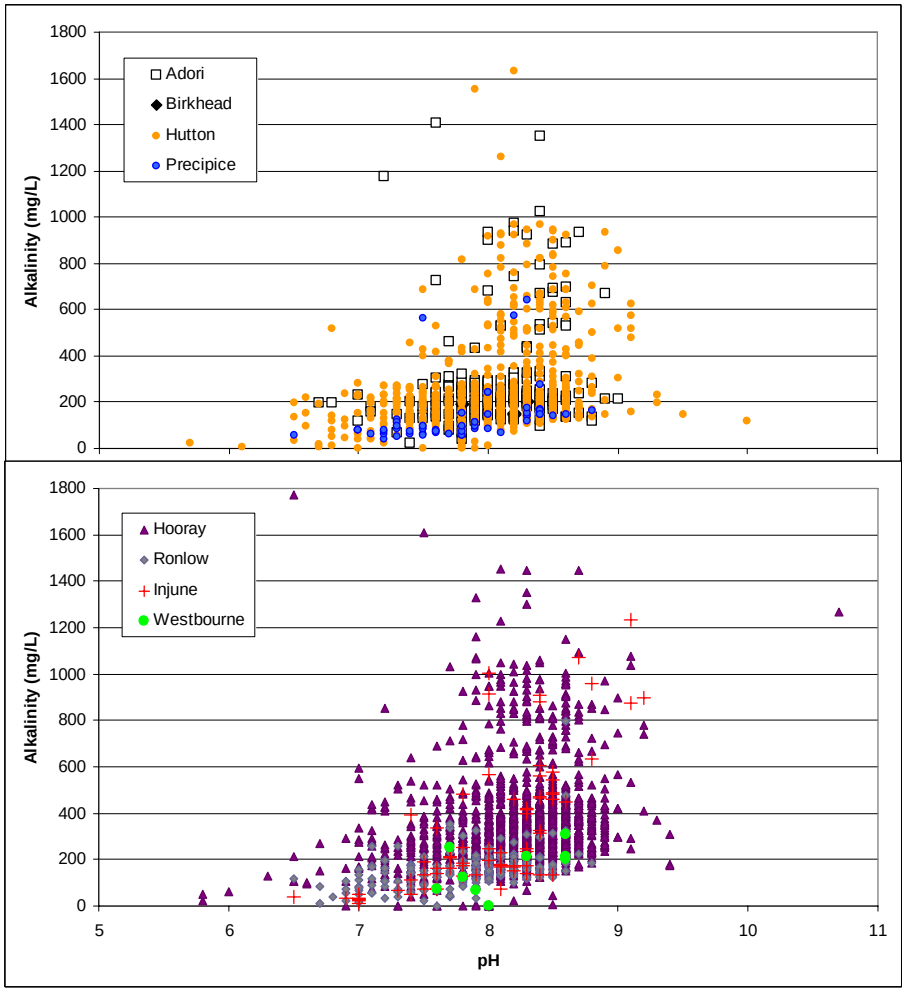

Figure 21b. pH – alkalinity relationship for the main Jurassic groundwaters of the Eromanga Basin. The pH largely varies between 6.5 and 9, while the alkalinity can reach 1800 mg/L. The Precipice and Ronlow waters are generally circumneutral, with low alkalinities, while the Adori and some Hooray waters include high pH and alkalinity samples. Other groundwaters such as the Hutton and Injune are highly variable. Note: interpretation is based only on non-mixed water analyses.

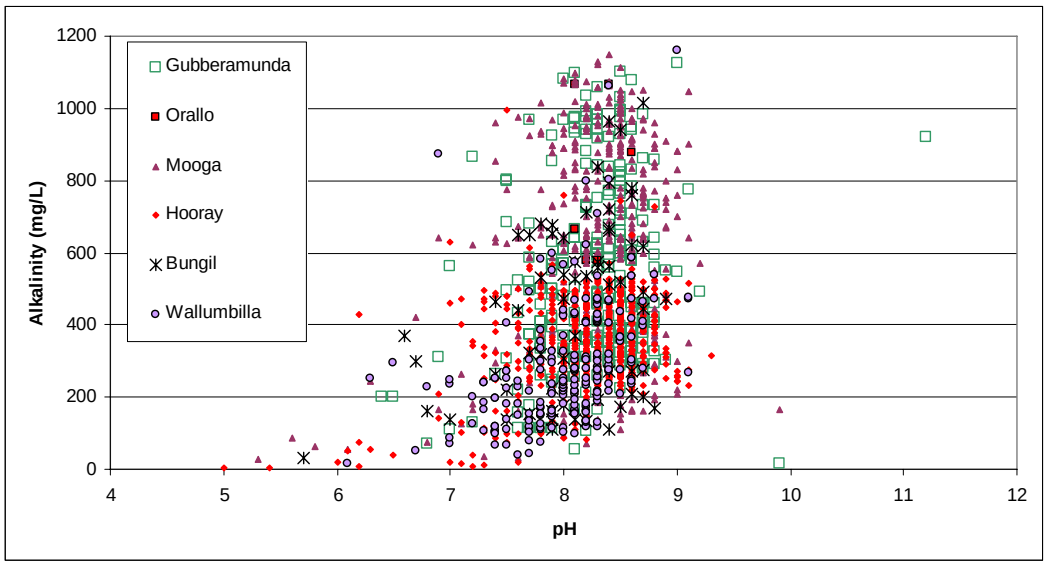

Figure 21c. pH – alkalinity relationship for the main Cretaceous groundwaters of the Surat Basin. The pH varies largely between 6 and 9, while the alkalinity can reach 1200 mg/L. The Mooga waters have pHs around 8 and high alkalinities, while the Wallumbilla waters tend to have a similar pH, but lower alkalinity. Note: interpretation is based only on non-mixed water analyses.

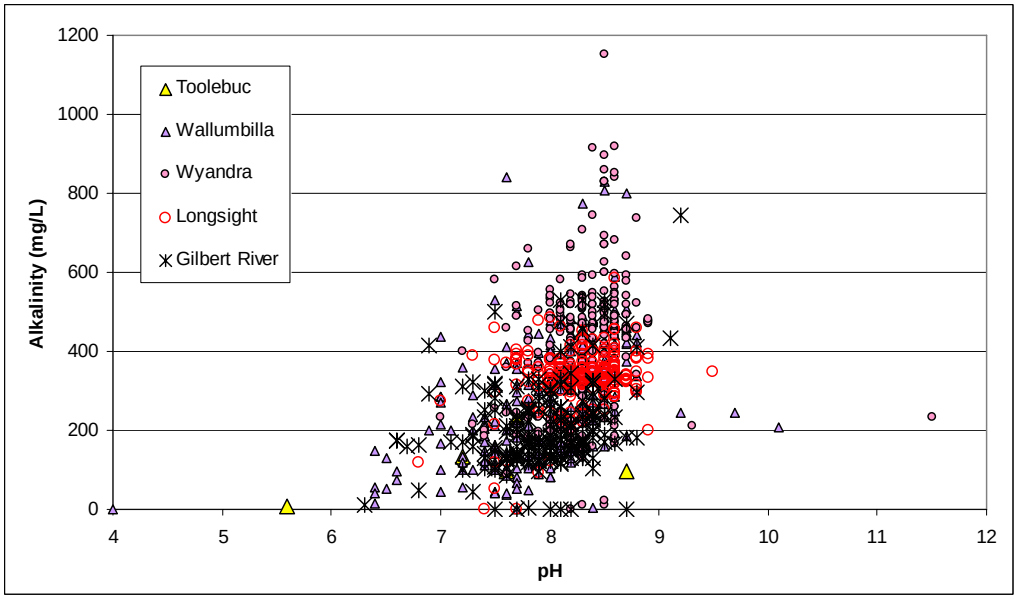

Figure 21d. pH – alkalinity relationship for the main Cretaceous groundwaters of the Eromanga Basin. The pH varies largely between 6 and 9, while the alkalinity can reach 1200 mg/L. The Wyandra waters have pHs around 8 and high alkalinities, while the Wallumbilla waters tend to have a similar pH, but lower alkalinity. The Longsight water has pHs from 7 to 9, but constant alkalinity, around 400; Gilbert River water is similar in terms of pH values, but has lower than 400 alkalinities. Note: interpretation is based only on non-mixed water analyses.

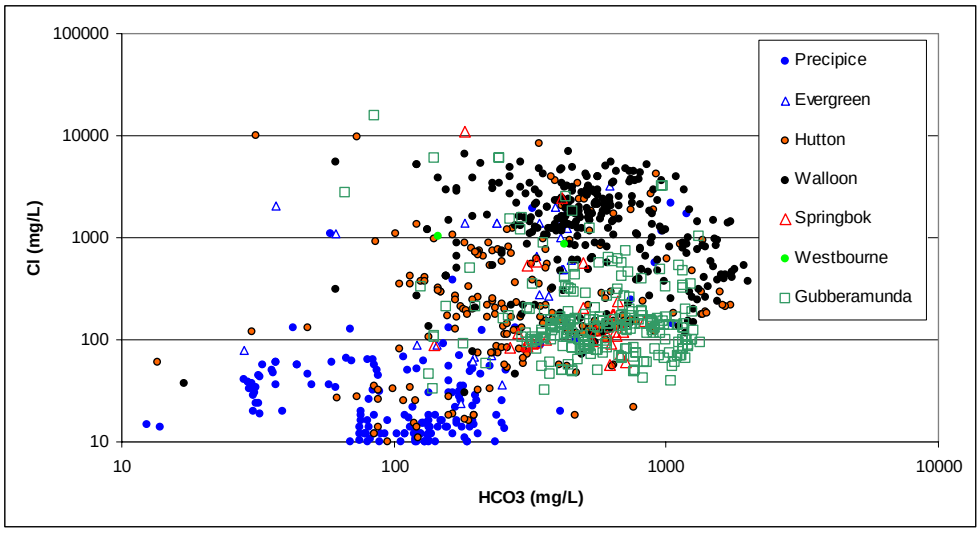

Figure 22a. Bicarbonate – chloride relationship for the main Jurassic groundwaters in the Surat Basin. The HCO_3 can reach concentrations of thousands of mg/L, while chloride has concentrations of up to 10,000 mg/L. The Precipice waters are very fresh with both anions present in the order of hundreds of mg/L. The Hutton water is highly variable, with a significant proportion of waters that have a similar concentration of HCO_3 and Cl. The Walloon has the saltiest water, with about 10 times more Cl than HCO_3; in addition, the two parameters display an inverse relationship, although the overall trend is of direct proportionality. The Gubberamunda water has an intermediate character, similar to the Hutton, but with about 10 times more HCO_3 than Cl. Note: interpretation is based only on non-mixed water analyses.

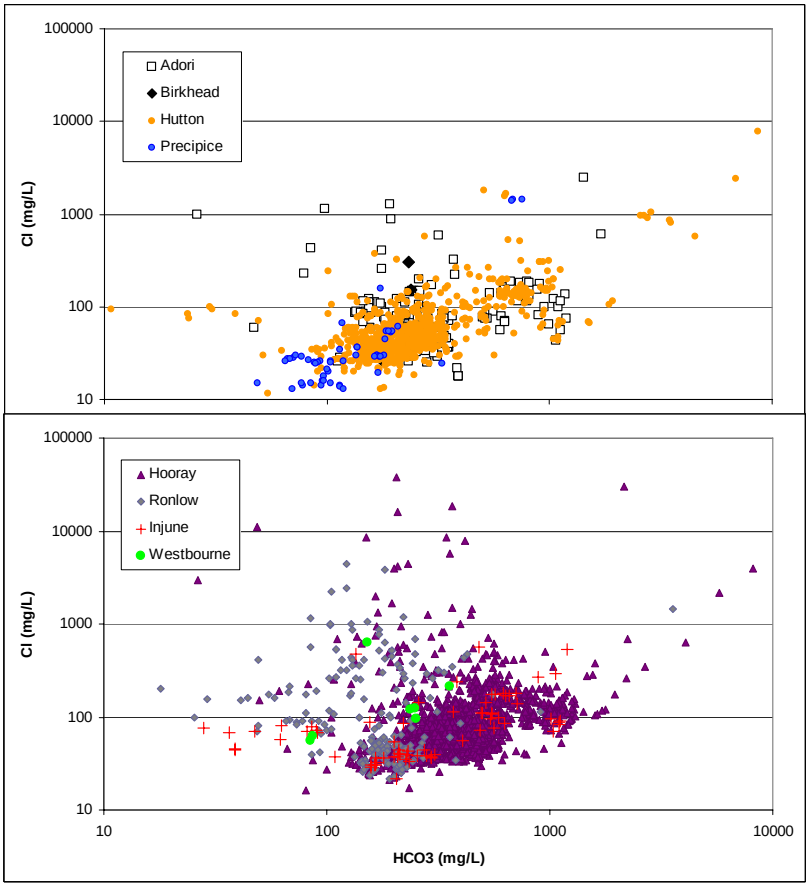

Figure 22b. Bicarbonate – chloride relationship for the main Jurassic groundwaters in the Eromanga Basins. The HCO_3 can reach concentrations of thousands of mg/L, while chloride has concentrations of up to 30,000 mg/L. The elements are directly proportional. The Precipice waters are very fresh with both anions present in the order of hundreds of mg/L. The Hutton and Adori waters are highly variable, but largely HCO_3-dominated, with 5 - 10 times more HCO_3 than Cl. The Hooray and Ronlow contain well-defined populations of HCO_3-rich samples, but they also have numerous outliers of Cl-dominated waters. Note: interpretation is based only on non-mixed water analyses.

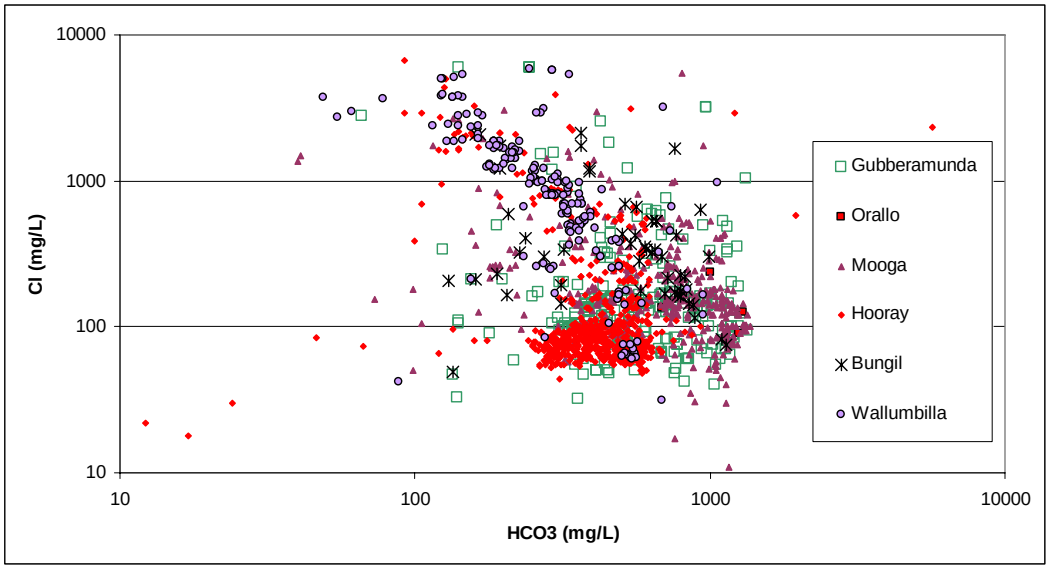

Figure 22c. Bicarbonate – chloride relationship for the main Cretaceous groundwaters in the Surat Basin. The HCO_3 can reach concentrations of up to 1000 mg/L, while chloride of up to 10,000 mg/L; the elements are inversely proportional. The Mooga waters have an intermediate character, similar to Gubberamunda, with about 10 times more HCO_3 than Cl. The Wallumbilla water is saltier, with about 10 times more Cl than HCO_3. The water assigned to the Hooray Sandstone consists of several populations: 1) bicarbonate-rich, similar in character to Mooga, but with less HCO_3; 2) salty, similar to Wallumbilla; and 3) very fresh. Note: interpretation is based only on non-mixed water analyses.

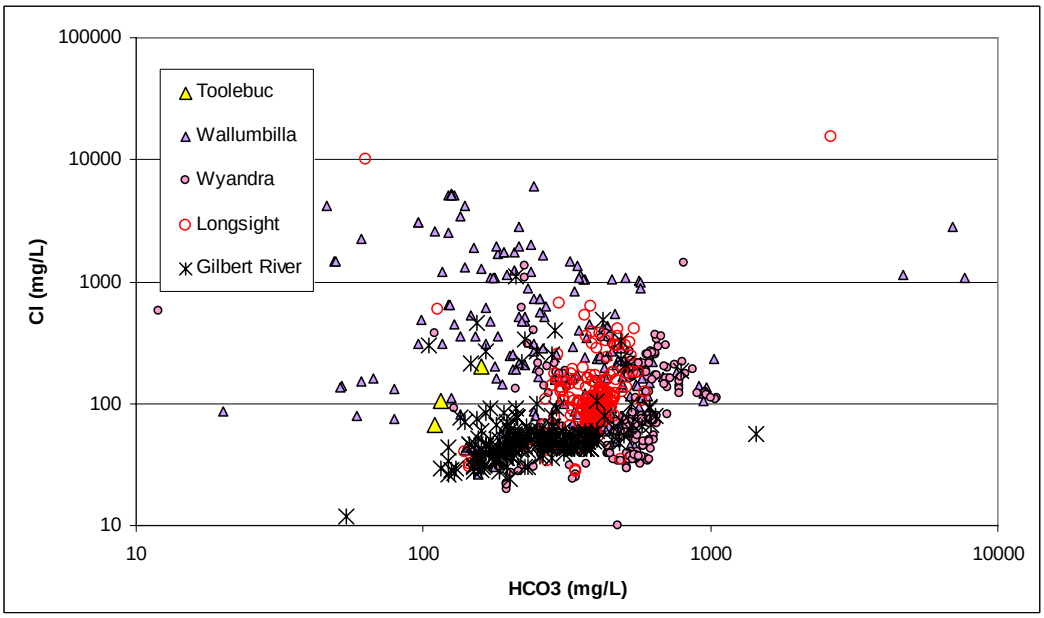

Figure 22d. Bicarbonate – chloride relationship for the main Cretaceous groundwaters in the Eromanga Basin. The HCO_3 can reach concentrations of up to 5000 mg/L, while chloride of up to 12,000 mg/L; the elements are inversely proportional. The Gilbert River waters are fresh with a slight dominance of HCO_3 over Cl. The Longsight waters are similar, but contain more HCO_3. The Wyandra waters contain the largest concentration of HCO_3 of all the Cretaceous groundwaters. The Wallumbilla water is saltier, with about 10 times more Cl than HCO_3. Note: interpretation is based only on non-mixed water analyses.

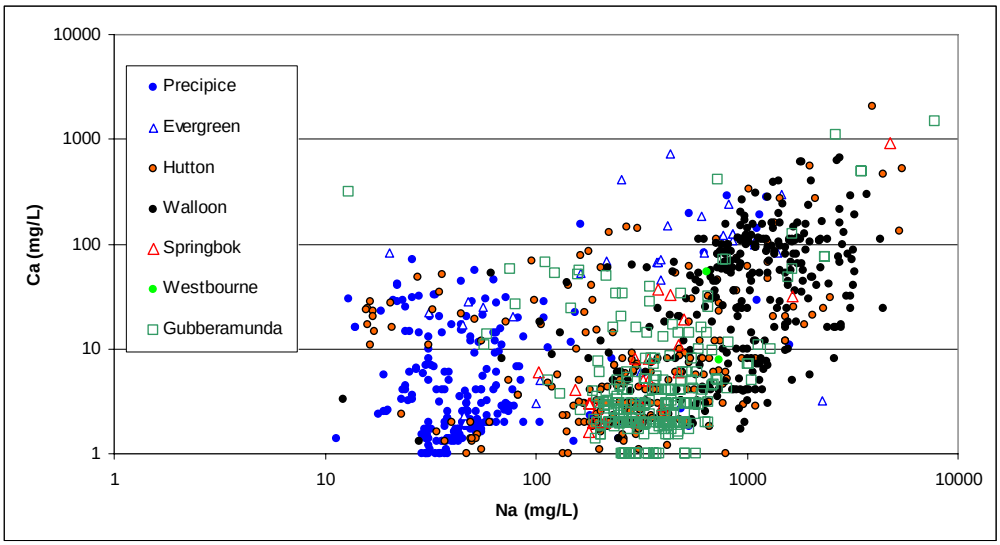

Figure 23a. Sodium – calcium relationship for the main Jurassic groundwaters in the Surat Basin. The Na can reach concentrations of thousands of mg/L, while Ca is up to 1000 mg/L; the elements are directly proportional. The Precipice waters are very fresh with more Na than Ca. The Hutton water is highly variable, with a significant proportion of waters that have 10 to 100 times more Na than Ca. The Walloon has the saltiest water, with about 10 times more Na than Ca. The Gubberamunda water has an intermediate character, similar to the Hutton, but with about 100 times more Na than Ca. Note: interpretation is based only on non-mixed water analyses.

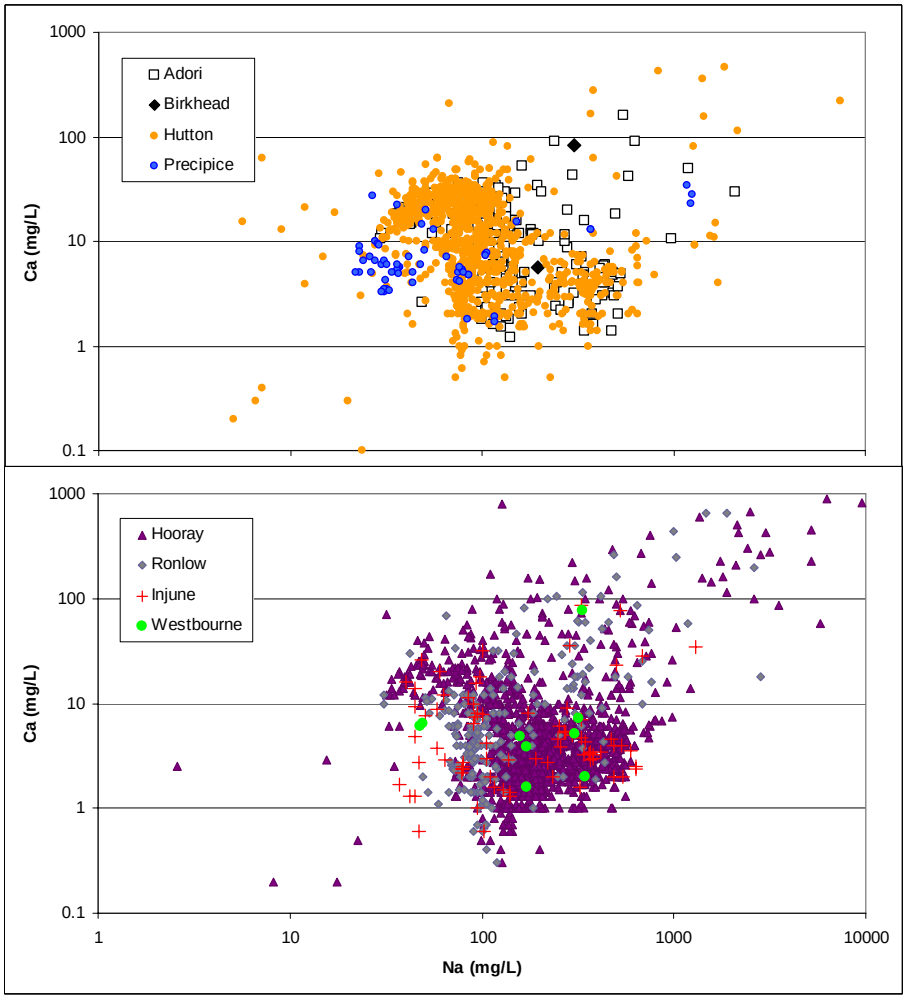

Figure 23b. Sodium – calcium relationship for the main Jurassic groundwaters in the Eromanga Basin. The Na can reach concentrations of thousands of mg/L, while Ca is up to 1000 mg/L; the elements are directly proportional. Overall, Na occurs in much larger concentrations than Ca, at least 10 times more. There also are salty outliers (e.g. Hutton and Hooray) with 100 times more Na than Ca. Note: interpretation is based only on non-mixed water analyses.

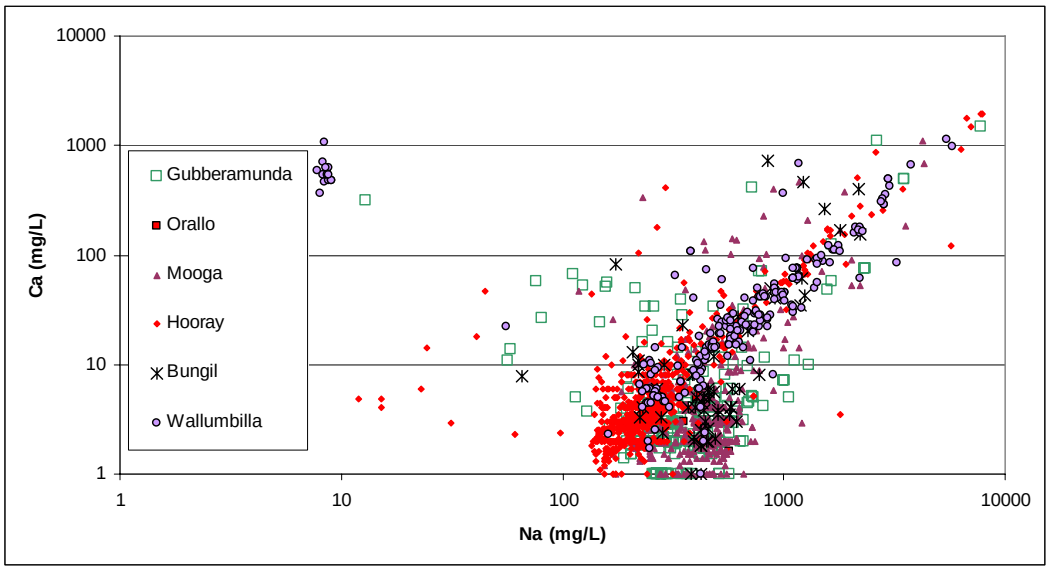

Figure 23c. Sodium – calcium relationship for the main Cretaceous groundwaters in the Surat Basin. The Na can reach concentrations of thousands of mg/L, while Ca is up to 1000 mg/L; the elements are directly proportional. The Mooga waters have an intermediate character, similar to Gubberamunda, with about 10 – 100 times more Na than Ca. The Wallumbilla water is saltier, with about 10 times more Cl than HCO_3. The water assigned to the Hooray Sandstone consists of several populations: 1) Na-rich, similar in character to Mooga, but with less Na; 2) salty, similar to Wallumbilla; and 3) very fresh with little Na and Ca. Note: interpretation is based only on non-mixed water analyses.

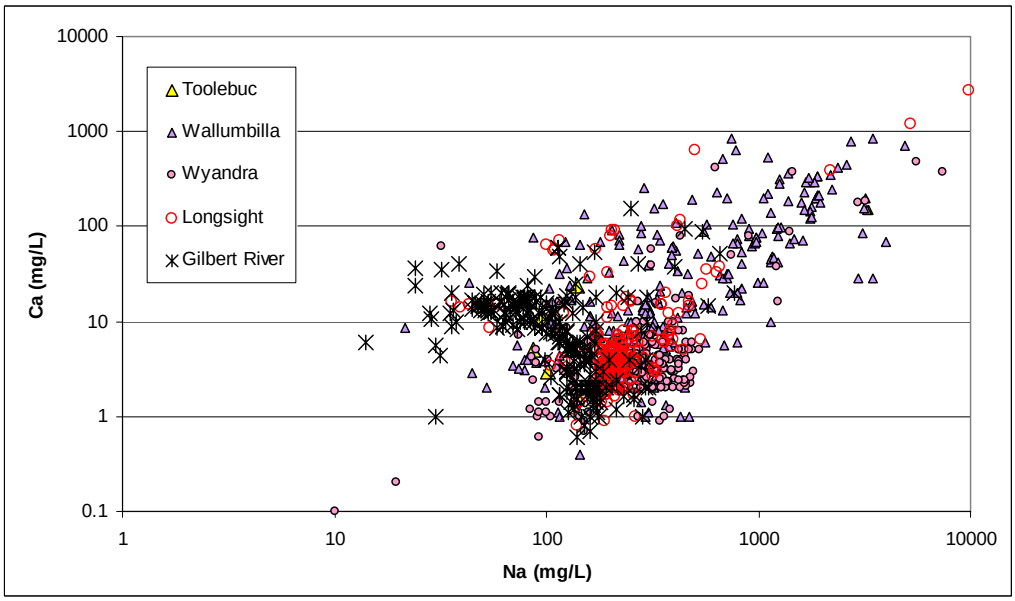

Figure 23d. Sodium – calcium relationship for the main Cretaceous groundwaters in the Eromanga Basin. The Na can reach concentrations of thousands of mg/L, while Ca is up to 1000 mg/L; the elements are directly proportional. Overall, Na occurs in much larger concentrations than Ca, at least 10 times more. There also are salty outliers (e.g. Wallumbilla) with 100 times more Na than Ca. Note: interpretation is based only on non-mixed water analyses.

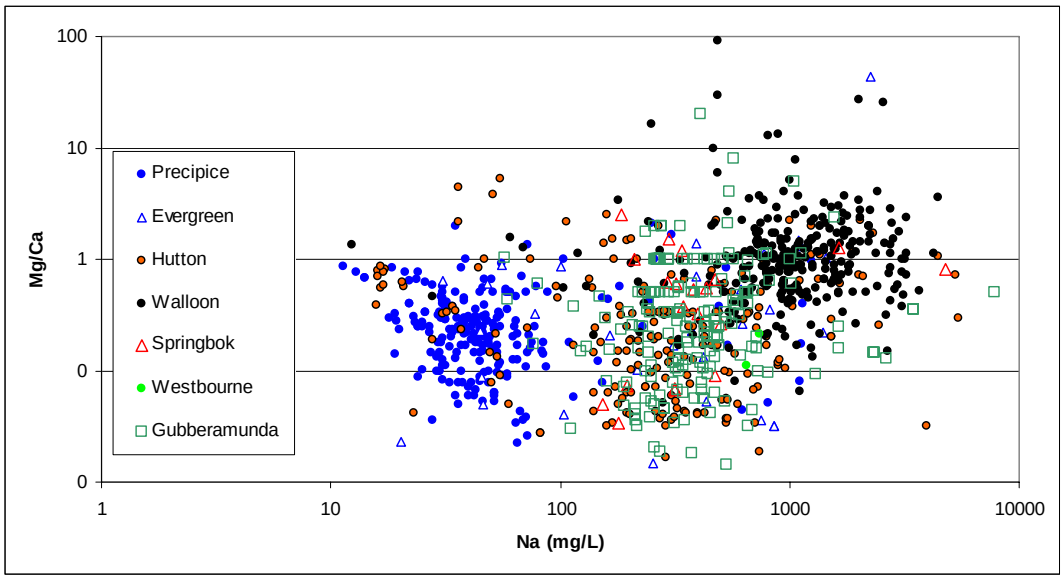

Figure 24a. Sodium – magnesium/calcium relationship for the main Jurassic groundwaters in the Surat Basin. The Na can reach concentrations of thousands of mg/L, while Mg/Ca is up to 100. The vast majority of samples are dominated by Ca, with a few outliers (mainly Walloon) where Mg is up to 10 times greater than Ca. Note: interpretation is based only on non-mixed water analyses.

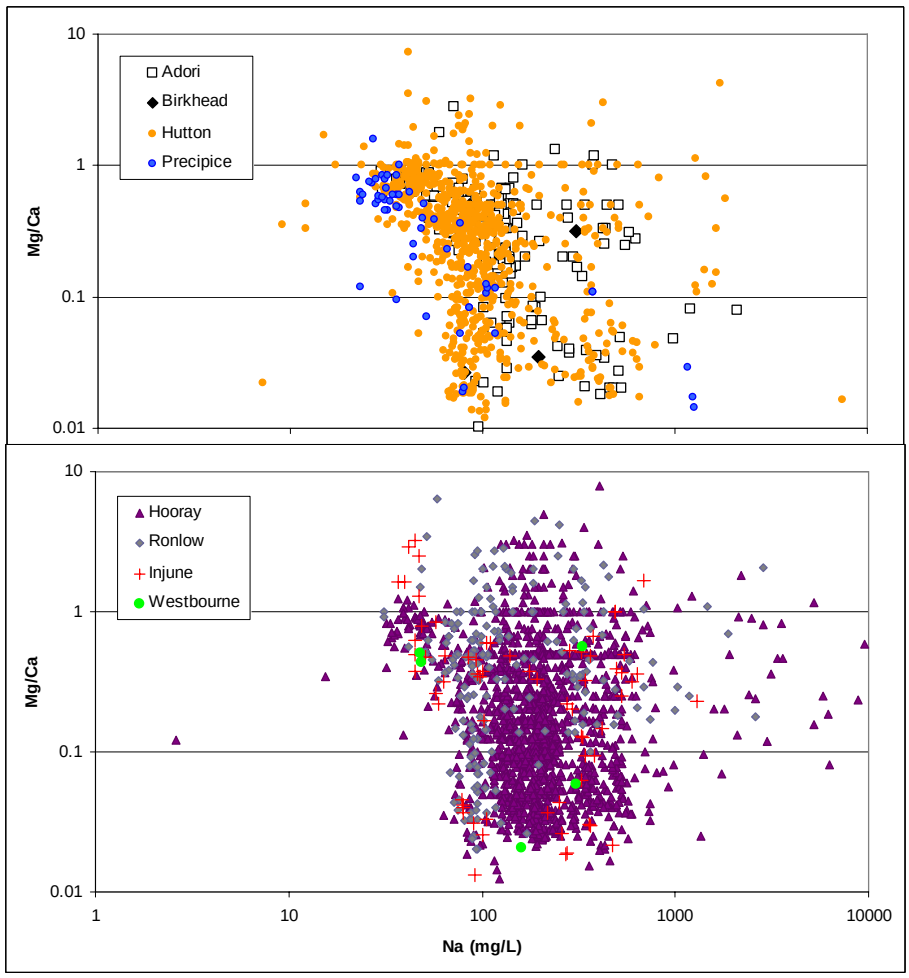

Figure 24b. Sodium – magnesium/calcium relationship for the main Jurassic groundwaters in the Eromanga Basin. The Na can reach concentrations of thousands of mg/L, while Mg/Ca is up to 10. The vast majority of samples are dominated by Ca, with a few outliers where Mg is up to 10 times greater than Ca. Note: interpretation is based only on non-mixed water analyses.

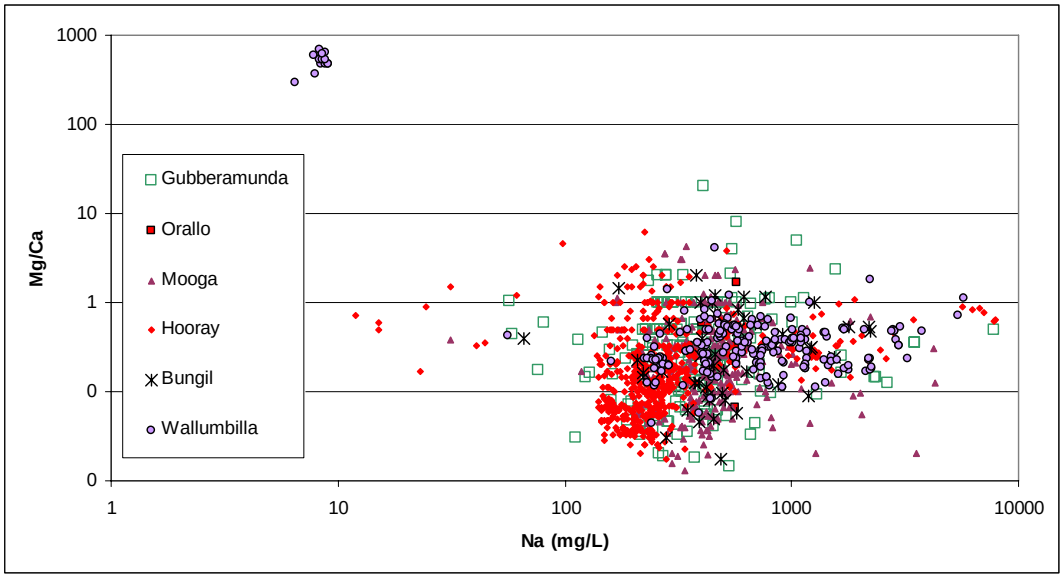

Figure 24c. Sodium – magnesium/calcium relationship for the main Cretaceous groundwaters in the Surat Basin. The Na can reach concentrations of thousands of mg/L, while Mg/Ca is up to 1000, in a few Wallumbilla waters. The vast majority of samples are dominated by Ca, with a few outliers where Mg is up to 10 times greater than Ca. Note: interpretation is based only on non-mixed water analyses.

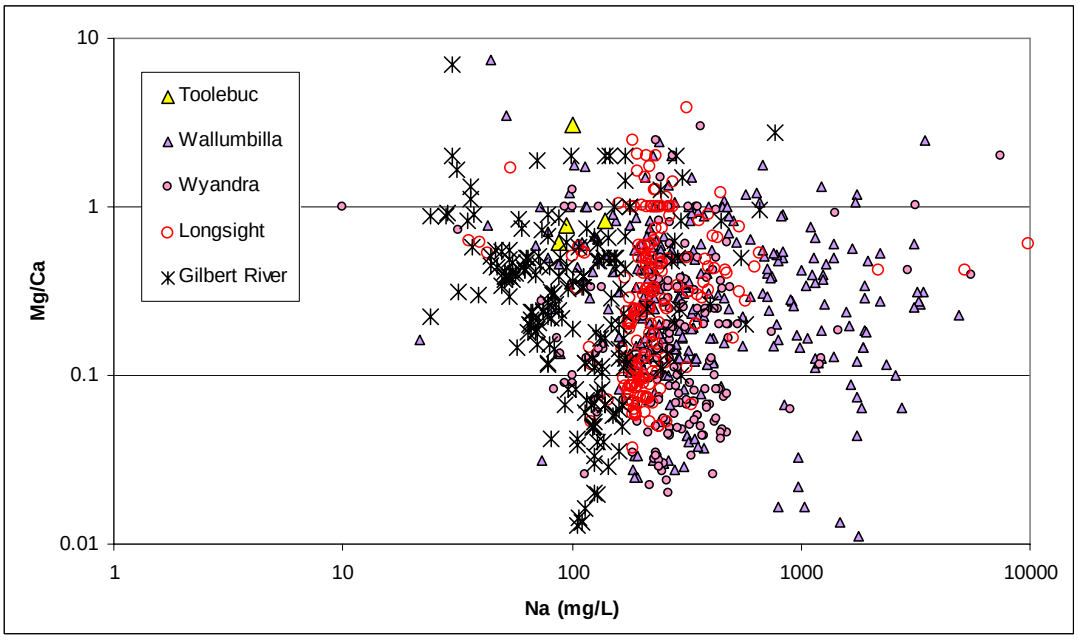

Figure 24d. Sodium – magnesium/calcium relationship for the main Cretaceous groundwaters in the Eromanga Basin. The Na can reach concentrations of thousands of mg/L, while Mg/Ca is up to 10. The vast majority of samples are dominated by Ca, with a few outliers where Mg is up to 10 times greater than Ca. Note: interpretation is based only on non-mixed water analyses.

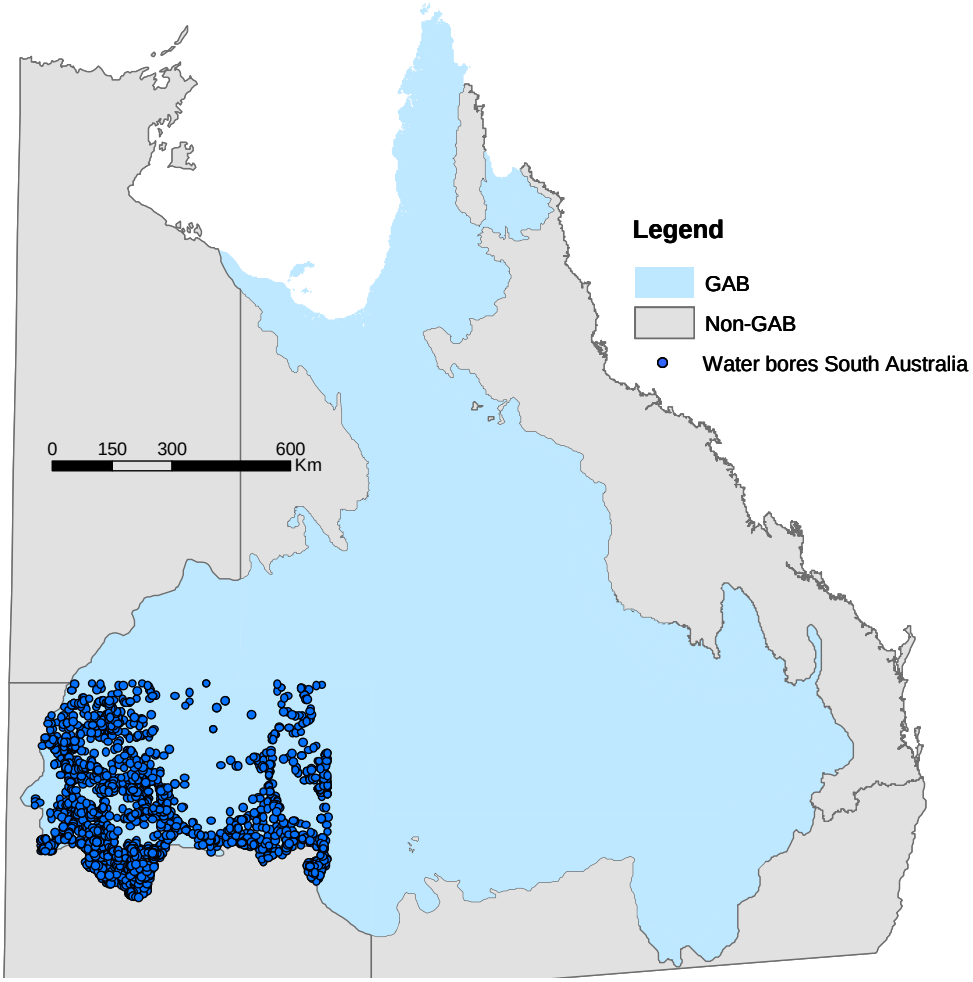

Figure 25. Location of groundwater bores in the South Australian section of the Great Artesian Basin (n = 2600 bores).

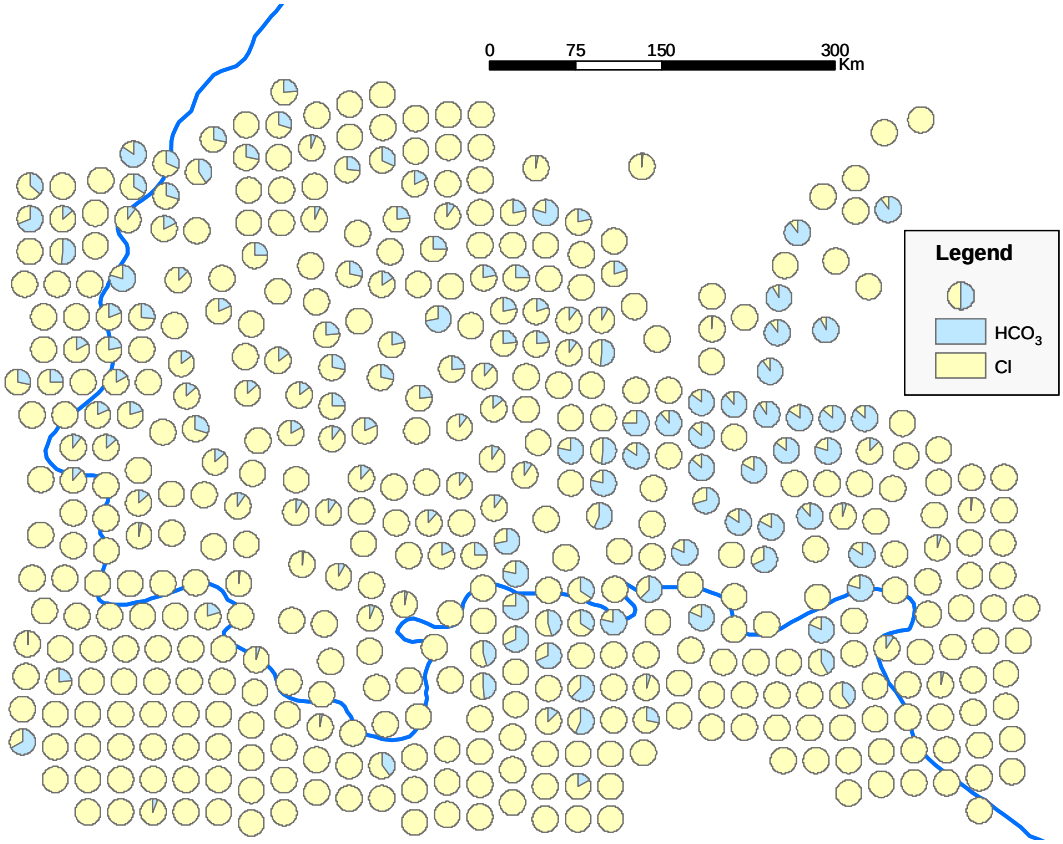

Figure 26a. Major anions in the South Australian section of the Great Artesian Basin. Out of the 2600 bores, about 600 have chemical analyses. The water is generally chloride-rich, with the exception of some deep bores (400 - 1200 m), which have a bicarbonate character.

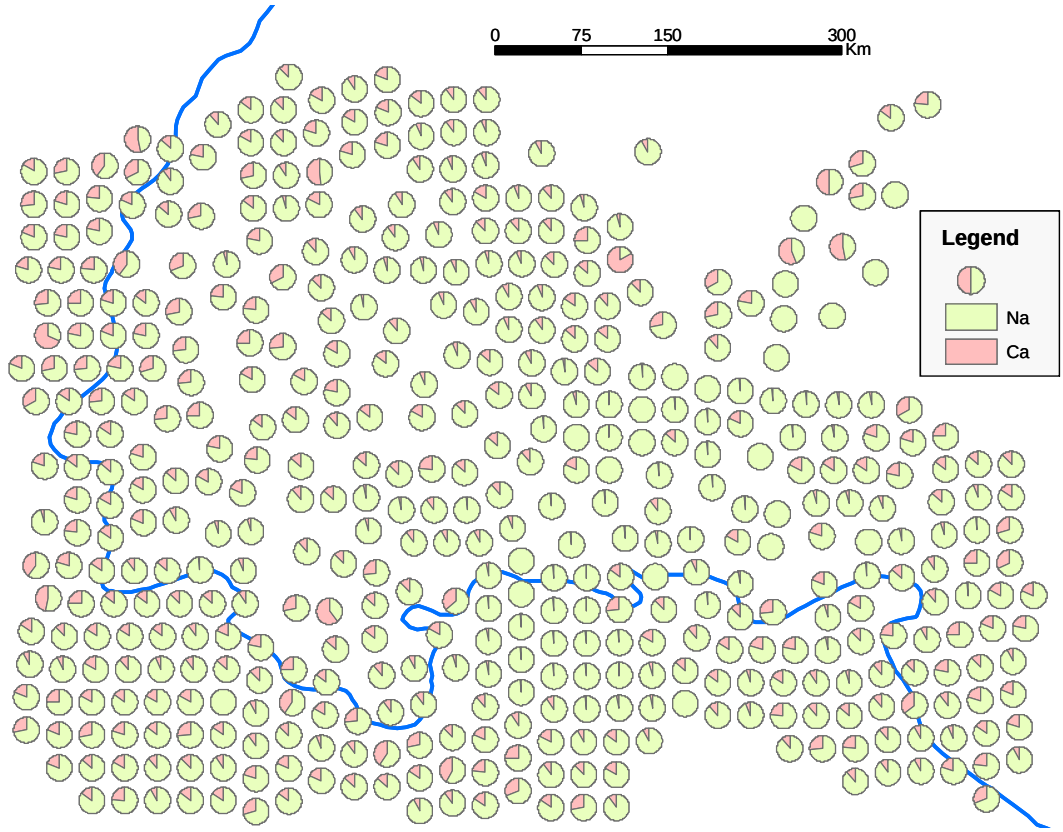

Figure 26b. Major cations in the South Australian section of the Great Artesian Basin. Out of the 2600 bores, about 600 have chemical analyses. The water is generally sodium-rich.

Aquifer Media Mineral Compositions

The mineralogy of the earliest Jurassic formations (Precipice Sandstone and Poolowanna Formation) is distinct from the overlying Jurassic and Cretaceous units (Fig. 27). The rock type is dominated by quartz arenite modal compositions. No feldspars were identified in any of the samples. The clay assemblage is dominated by the kaolinite group, with significant amounts of illite/mica and subordinate chlorite. Calcite was identified in one sample. Although highly variable, the samples from the basal Jurassic unit have the lowest average clay content.

The overlying Hutton Sandstone framework compositions are dominated by a mixture of quartz arenite and subarkose with subordinate arkose (Fig. 27). Maximum and average clay contents are higher than the basal Jurassic with a similar heterogeneous distribution. The clay mineral assemblage is similar to that in the basal Jurassic, dominated by kaolinite and illite/mica but with subordinate amounts of mixed layer illite/smectite and lower chlorite values. K-feldspar is dominant over other feldspars.

Clay content is much higher in the Birkhead Formation (equivalent to the Walloon Subgroup in the Surat Basin), overlying the Hutton Sandstone. Framework compositions in the Birkhead Formation are dominantly subarkose and arkose with minor quartz arenite (Fig. 27). Average bulk clay content is almost twice that of the Hutton Sandstone and the assemblage is dominated by mixed layer illite/smectite. Feldspathic content is mainly plagioclase, which is also the opposite to the Hutton Sandstone samples which generally have higher concentrations of K-feldspars.

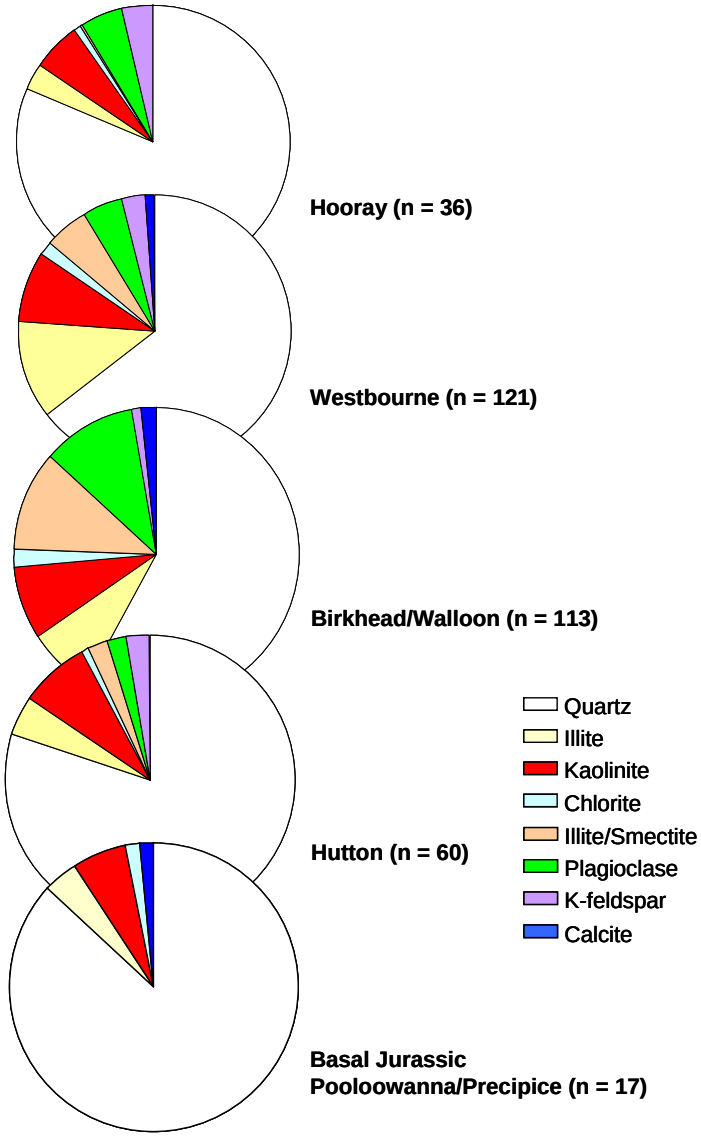

Figure 27. Average mineral composition of Mesozoic formations based on Carmichael (1989). See also Fig. 11 for site locations and Fig. 18 for details.

The Westbourne Formation mineral content is similar to the Birkhead Formation (Fig. 27), but with a primarily subarkose framework and quartz arenite dominant over arkose. Average bulk clay content is similar but illite/mica is dominant. Mixed layer illite/smectite is subordinate to the kaolinite group clays, the average value of the former being approximately half that in the Birkhead Formation. Average kaolinite content is the same for both the Westbourne Formation and the Birkhead Formation.

The lowest average bulk clay content was exhibited by the Hooray Sandstone samples (Fig. 27). Framework compositions are predominantly subarkose with subordinate quartz arenite, similar to the Westbourne Formation. Average feldspathic content is also similar to the Westbourne Formation, plagioclase being dominant over K-feldspars as in the Birkhead Formation. The kaolinite group minerals dominate the clay assemblage with subordinate illite/mica and chlorite, and very low concentrations of mixed layer illite/smectite.

In the context of water-rock interactions, the basal Jurassic unit has the most stable mineralogy under acidic conditions. The Hutton Sandstone has a greater propensity for mineral alteration due to the higher feldspathic content. Both these units, however, are resistant to significant induced diagenetic alteration under acidic conditions, because of the dominance of quartz in the framework compositions and kaolinite in the clay assemblages. The Hooray Sandstone has a similar kaolinite-dominated clay assemblage and also has a quartz dominated framework composition. The marginally higher feldspathic content in the framework composition of the Hooray Sandstone, dominated by plagioclase is less stable than both the basal Jurassic and the Hutton Sandstone. Framework compositions in the Westbourne are similar to the Hooray Sandstone and it is the clay assemblage that has the greater potential for alteration under acidic conditions. The Birkhead Formation has the greatest alteration potential in an acidic environment, having the highest average feldspathic content which is overwhelmingly plagioclase-rich, and also a mixed layer illite/smectite-dominated clay assemblage.

Geochemical Modelling

Aqueous equilibrium speciation simulation results show that groundwater in the Precipice Sandstone is close to thermodynamic equilibrium with the aquifer media. Silica polymorphs are almost at saturation and the carbonate minerals are at saturation or slightly undersaturated. K-feldspars and clay minerals are slightly supersaturated.

Groundwater in the Evergreen Formation shows much greater supersaturation for the feldspar mineral series and clays. It is also supersaturated with respect to the main carbonate minerals and slightly supersaturated with respect to quartz. The lack of data for the mineralogy of the Evergreen Formation precludes an assessment of the relationship between the aquifer media and the groundwater. The aqueous speciation results do suggest, however, that the groundwater is not in equilibrium with the aquifer mineralogy.

Results for the Hutton Sandstone show a similar state of thermodynamic equilibrium between the groundwater and the aquifer media to the Precipice Sandstone. Hutton Sandstone groundwater is at saturation with respect to the silica polymorphs, part of the feldspar series and calcite. It is also at saturation with respect to most of the clay minerals. Dolomite and some of the less common phylosilicates are slightly supersaturated. The simulation does show, however, that the groundwater is slightly undersaturated with respect to some of the plagioclase and K-feldspars and the more complex smectitic clay minerals.

The Walloon Subgroup groundwater shows variable relationships which are largely dependent on pH. Low pH groundwater is at saturation with respect to the complex smectitic clays, slightly supersaturated with respect to quartz and kaolinite and undersaturated with respect to the feldspar series, calcite and illite. The high pH groundwater samples show similar saturation relationships for the feldspars, but are undersaturated with respect to kaolinite and quartz, and supersaturated with respect to the complex clays and calcite. The average Walloon aquifer media composition reflects this, containing a mixture of the complex clays and kaolinite and the presence of calcite (Fig. 27).

Equilibration of the average Precipice Sandstone groundwater composition with a representative volume of the average aquifer media mineralogy shows some changes in mineral composition (Fig. 28a). Equilibrating the new aquifer media composition with a 1 molar CO_2 aqueous solution makes little difference to the framework composition (Fig. 28b). Displacement flushing of the aquifer with a 1 molar CO_2 charged fluid removes most minerals (Fig. 28c). The framework composition is unchanged, but the groundwater salinity increases to hypersaline concentrations; pH is reduced to less than 5 and CO_2 fugacity is close to maximum gas saturation.

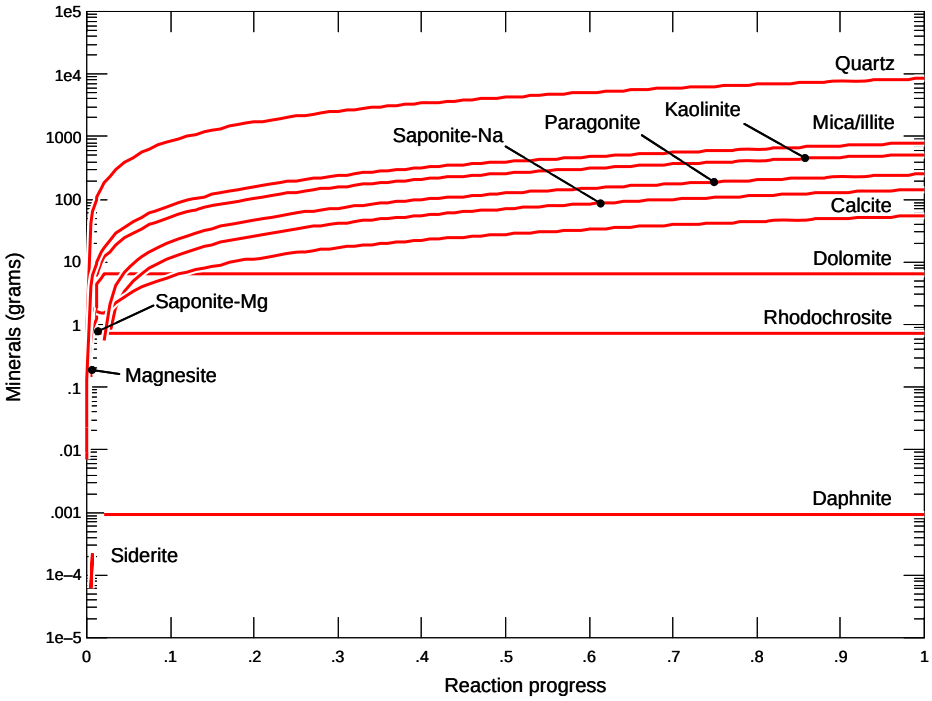

Figure 28a. Equilibration of mean Precipice Sandstone groundwater with mean aquifer mineral composition. The reaction paths show the increase in the quantity of minerals precipitated during the reaction to the end point of equilibrium between the groundwater and the aquifer media. The overall change in mineral composition is minor: quartz content is unchanged; calcite is reduced by 12%; illite/mica is reduced by 40%; kaolinite is increased by 19%; dolomite, daphnite and saponite precipitate in small quantities and chlorite dissolves. Overall the aquifer media remains dominated by quartz arenites. Groundwater type remains as Na-HCO_3 but with a reduction of 41% in HCO_3, concomitant with reductions in dissolved silica and potassium and an increase in dissolved calcium due to carbonate dissolution.

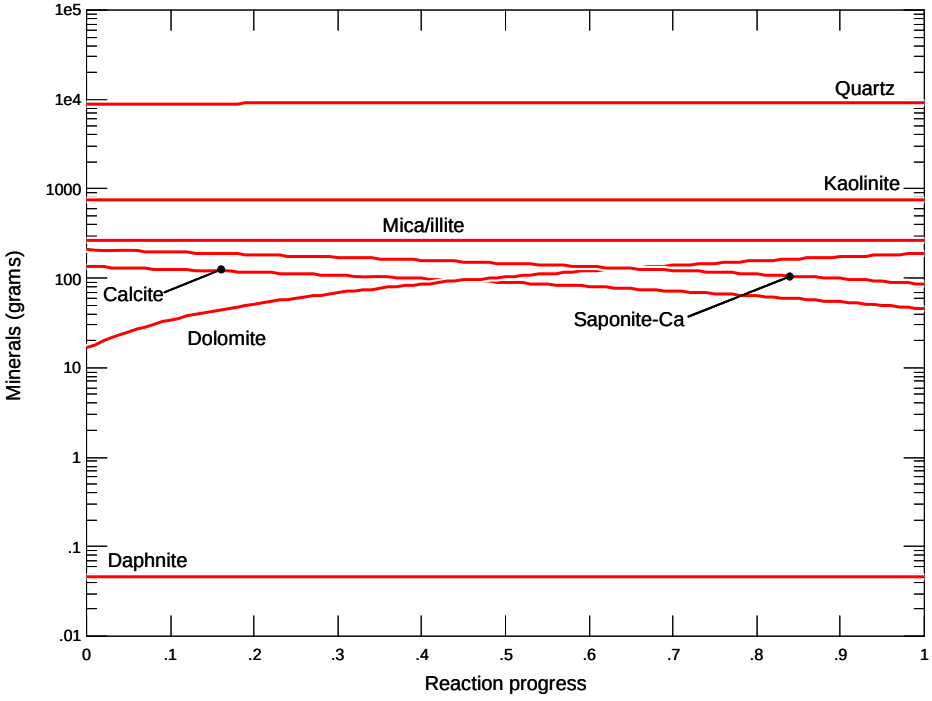

Figure 28b. Changes in aquifer media mineral composition in the Precipice Sandstone after equilibration with 1 mole of CO_2 (this equates to the approximate maximum solubility of CO_2 in fresh water under the conditions of interest). The starting solution composition and the aquifer mineralogy are taken from the equilibrated mean groundwater composition and the equilibrated mean aquifer media mineral composition. Solution pH remains constant throughout the simulation, buffered by the dissolution of calcite. There is a substantial increase in dolomite at the expense of calcite and saponite. The silicate minerals show little change due to the buffered circum-neutral pH of the groundwater. Fluid composition remains largely unchanged.

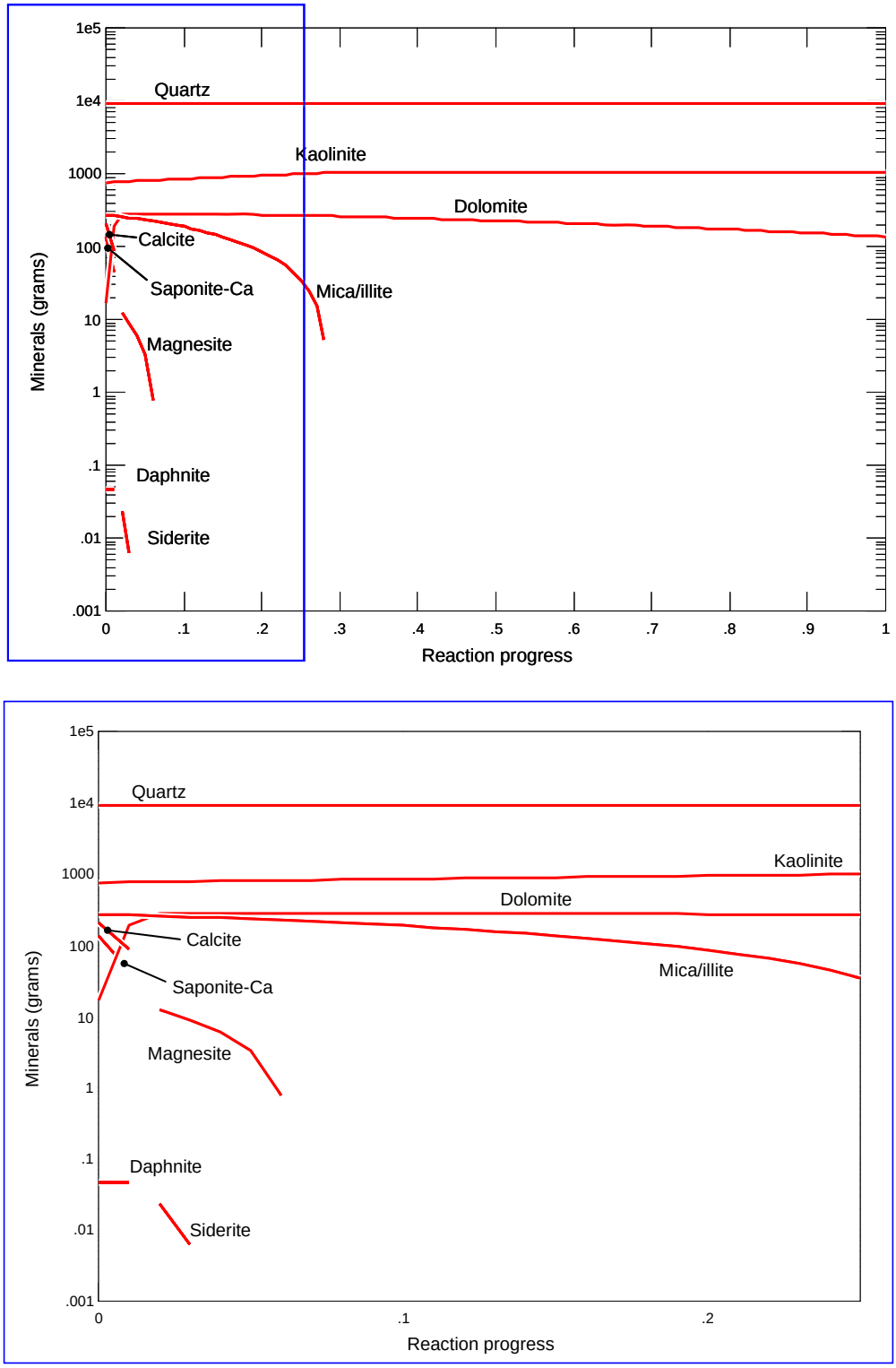

Figure 28c. Mineral transformations resulting from flushing of Precipice Sandstone aquifer media with 100 kg of 1 molar CO_2 aqueous solution. Constant flushing of the rock mass with CO_2 saturated fluid induces a rapid drop in pH, rapidly consuming carbonates, daphnite and saponite. Dolomite precipitates as calcite and saponite are consumed and magnesite and siderite precipitate, but are re-dissolved early in the flushing event. Kaolinite precipitates at the expense of mica/illite and there is minor precipitation of quartz, some dolomite is consumed in the latter stages of flushing. There are significant mineralogical changes within the aquifer media, but the overall framework composition remains highly quartzose. Fluid composition is radically changed with a very large increase in salinity and pH of less than 5. Dissolved potassium, magnesium and calcium concentrations are orders of magnitude greater than the initial solution and CO_2 fugacity is close to saturation.

The same sequence of simulations for the Hutton Sandstone aquifer shows a marked change in average framework composition after the initial equilibration with average groundwater (Fig. 29a). Groundwater pH and salinity increase slightly, although still remaining in the very low brackish category (~2000 mg/L TDS). The solution also becomes charged with Al. Equilibrating with a 1 molar CO_2 solution produces some significant mineralogical changes but the new quartz arenite framework composition remains constant (Fig. 29b). The solution pH remains alkaline and salinity doubles, but still remains in the low brackish range and charged with bicarbonate. Flushing of the system with 1 molar CO_2 solution shows much the same evolution in aquifer mineralogy to the Precipice Sandstone simulation (Fig. 29c). Most phases are dissolved and the solution chemistry is affected similarly, with a massive increase in salinity, high CO_2 fugacity and reduced pH. A comparative summary of simulations, including initial conditions, and modelling results is presented in Figure 30a,b.

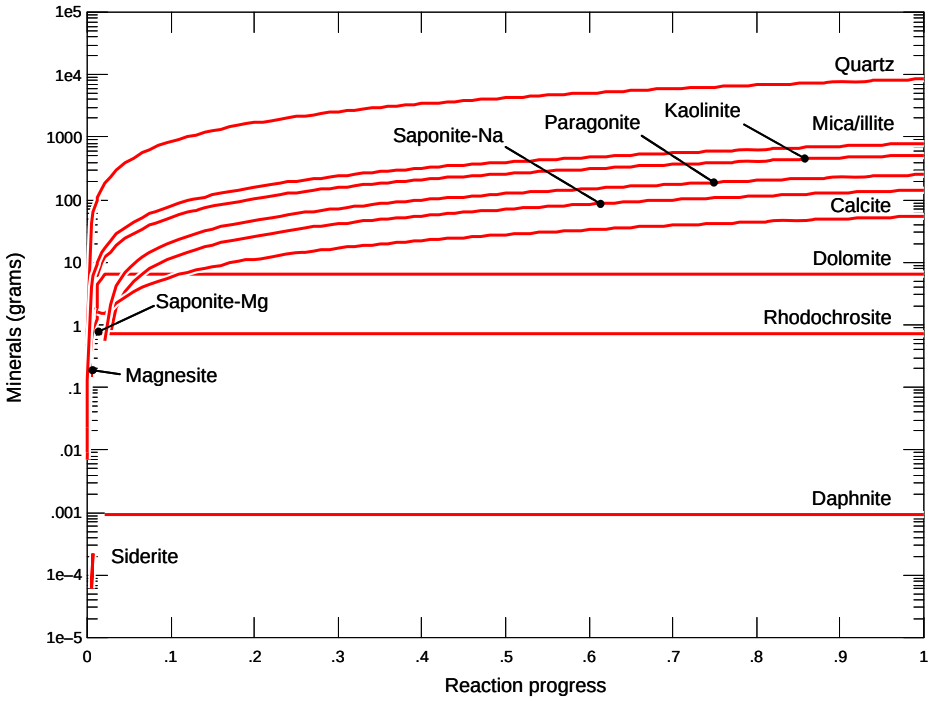

Figure 29a. Equilibration of mean Hutton Sandstone groundwater with mean aquifer mineral composition. The reaction paths show the increase in the quantity of minerals precipitated during the reaction to the end point of equilibrium between the groundwater and the aquifer media. The change in aquifer media mineral composition is quite significant, suggesting that groundwater in the Hutton Sandstone is not in equilibrium with the aquifer media. There is a slight increase in groundwater salinity, pH is 0.2 higher, combined with the complete dissolution of albite, K-feldspar and chlorite. Additional quartz and kaolinite precipitate, along with some micaceous minerals and dolomite. The new fluid composition is enriched in dissolved aluminium and sodium from the dissolution of albite and severely depleted in magnesium and calcium, due to calcite and dolomite precipitation.

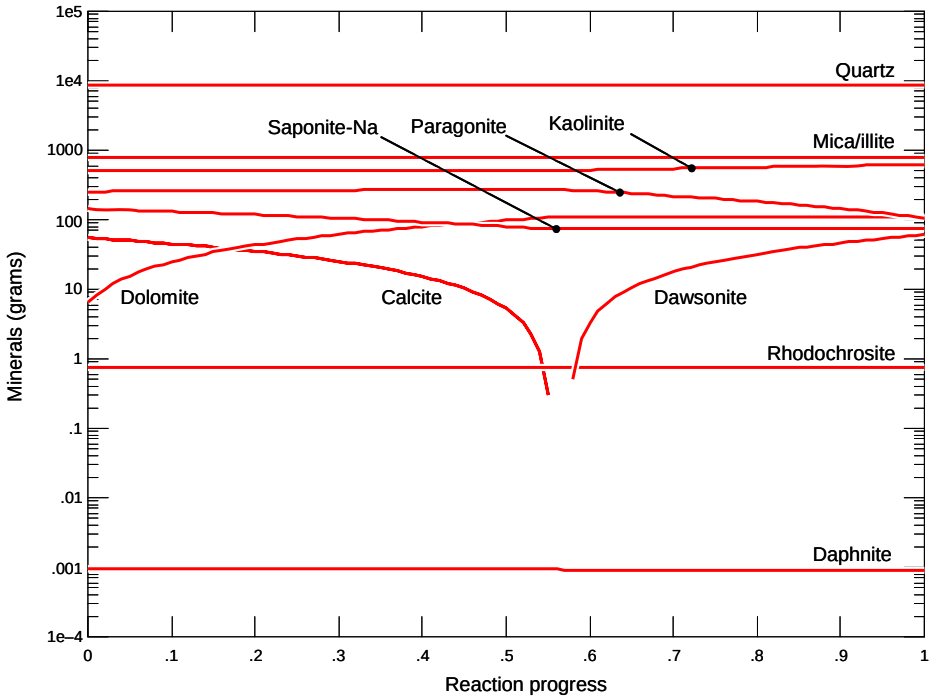

Figure 29b. Changes in aquifer media mineral composition in the Hutton Sandstone after equilibration with 1 mole of CO_2 (this equates to the approximate maximum solubility of CO_2 in fresh water under the conditions of interest). The starting solution composition and the aquifer mineralogy are taken from the equilibrated mean groundwater composition and the equilibrated mean aquifer media mineral composition. Solution pH remains generally constant throughout the simulation, buffered by the dissolution of calcite. There is a substantial increase in dolomite at the expense of calcite and saponite. Dawsonite also precipitates due to the release of aluminium and sodium from the dissolution of albite. The silicate minerals show little change due the buffered alkaline pH of the groundwater. There is an 87% increase in fluid salinity; however, the groundwater remains in the low brackish range (4120 mg/L). There is a substantial increase in bicarbonate concentration and a significant reduction in calcium.

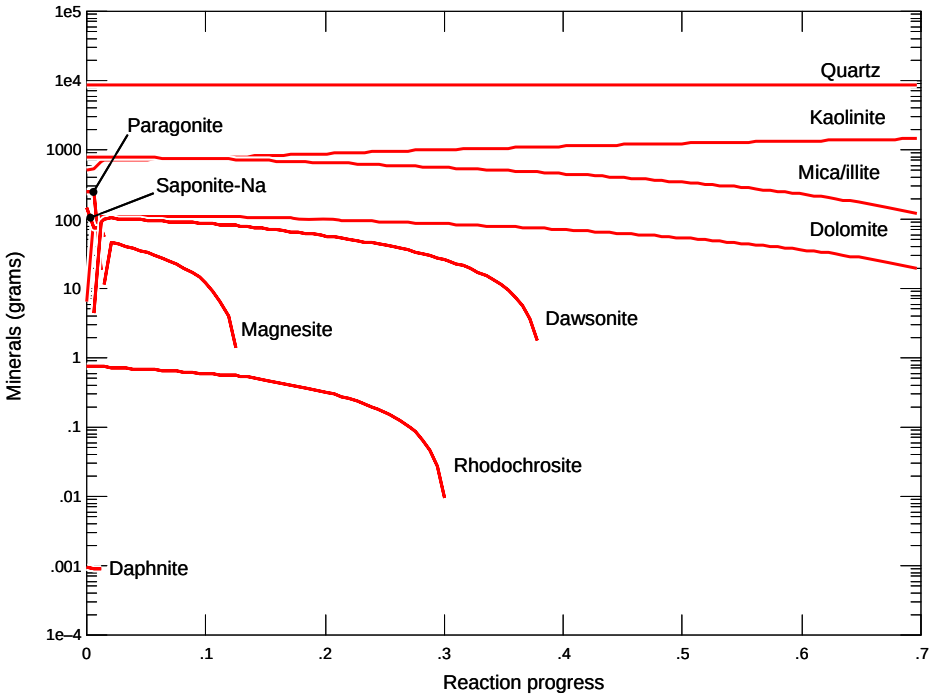

Figure 29c. Mineral transformations resulting from flushing of Hutton Sandstone aquifer media with 100 kg of 1 molar CO_2 aqueous solution. Constant flushing of the rock mass with CO_2 saturated fluid induces a rapid drop in pH, rapidly consuming carbonates, daphnite, saponite and paragonite. Dolomite precipitates as calcite and saponite are consumed and magnesite precipitates, but is re-dissolved early in the flushing event. Kaolinite precipitates at the expense of mica/illite and there is minor precipitation of quartz, some dolomite is consumed in the latter stages of flushing. There are significant mineralogical changes within the aquifer media and the framework composition becomes dominated by quartz arenite. Fluid composition is radically changed with a very large increase in salinity and pH of 5.1. Dissolved potassium, magnesium and calcium concentrations are orders of magnitude greater than the initial solution and CO_2 fugacity is greatly increased.

Initial concentrations (mg/L)										
Sandstone/element	**Na**	**K**	**Ca**	**Mg**	**Fe**	**Mn**	**HCO_3**	**CO_3**	**Cl**	**SO_4**
Precipice	88.5	2.2	12.4	4.7	0.16	0.02	149.2	9.6	64.6	9.3
Hutton	487.2	2	33.5	16.2	0.37	0.13	364.8	27.4	602.7	24.7

Initial conditions - Precipice
silica and dolomite at equilibrium
calcite dissolution
K-feldspars, clays precipitation

Initial conditions - Hutton
silica, feldspar, calcite, clays at equilibrium
dolomite precipitation

Equilibration with aquifer mineralogy – 25ºC/1 bar
constant quartz content
calcite, illite, chlorite dissolution
kaolinite, dolomite precipitation
constant pH and salinity

Equilibration with aquifer mineralogy – 25ºC/1 bar
quartz and kaolinite precipitation
feldspars, chlorite dissolution
calcite, dolomite and clay precipitation
pH and salinity increase

Equilibration with 1 molar CO_2 – 50ºC/100 bars
dolomite and calcite precipitation
dolomite increase at the expense of calcite
constant alkaline pH and salinity

Equilibration with 1 molar CO_2 – 50ºC/100 bars
calcite dissolution
dolomite and dawsonite precipitation
constant alkaline pH
salinity doubles

Flushing with 1 molar CO_2 – 50ºC/100 bars
dissolution of most minerals
dolomite precipitates as calcite dissolves
kaolinite precipitates as illite dissolves
salinity reaches hypersaline conditions
precipitated dolomite, magnesite, siderite dissolve in latter stages
pH < 5
increased CO_2 fugacity

Flushing with 1 molar CO_2 – 50ºC/100 bars
dissolution of most minerals
dolomite precipitates as calcite dissolves
kaolinite precipitates as illite dissolves
salinity reaches hypersaline conditions
precipitated dolomite dissolves in latter stages
minor quartz precipitation
pH = 5.1
increased CO_2 fugacity

Figure 30a. Comparative simulation results for the target aquifers, the Precipice and Hutton sandstones. The results of the simulations are similar for both aquifer materials. The main difference relates to the salinity changes that can occur when the system is equilibrated with 1 molar CO_2. The mineralogical composition of the Hutton Sandstone is more prone to dissolution than the Precipice and, under acidic conditions, the dissolution of minerals can produce saltier water that can lead to carbonate precipitation (mainly dolomite). Flushing with 1 molar CO_2 produces similar results with most minerals being initially removed; dolomite may precipitate but it would be redissolved under the persistent acidic conditions.

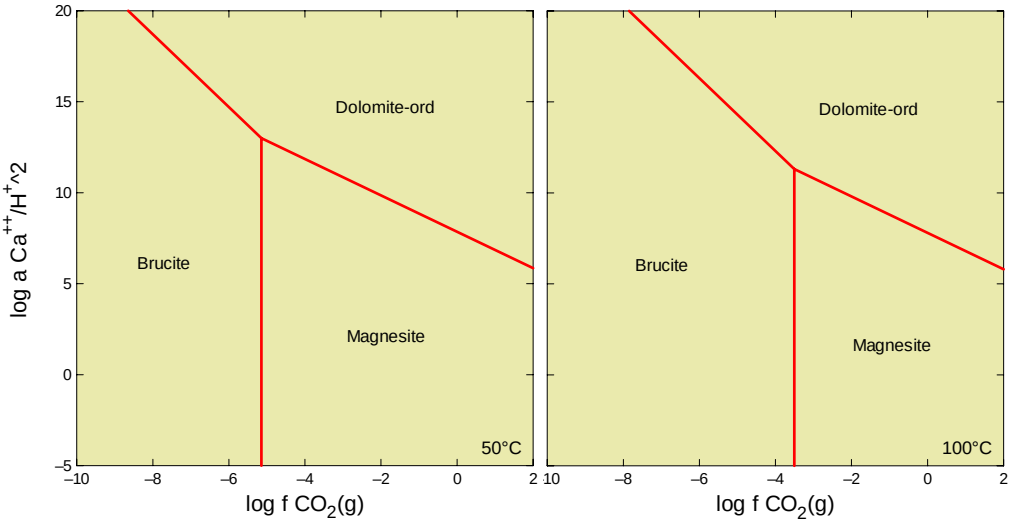

Figure 30b. Mineral stability diagrams for dolomite at different temperatures, in the presence of Precipice average major ions. Temperature affects the domains of brucite and magnesite, but it does not affect the stability of dolomite, which persists even at low pH, providing that there is enough Ca in the system.

These simulations are in agreement with mineral stability relationships; Figures 31 and 32 show two temperature-based examples for K-feldspar and albite: 50°C is typical of the Surat Basin and 100°C is more representative of the hotter conditions in the Eromanga Basin. Most of the water samples analysed in this project plot within the domain of stability for kaolinite.

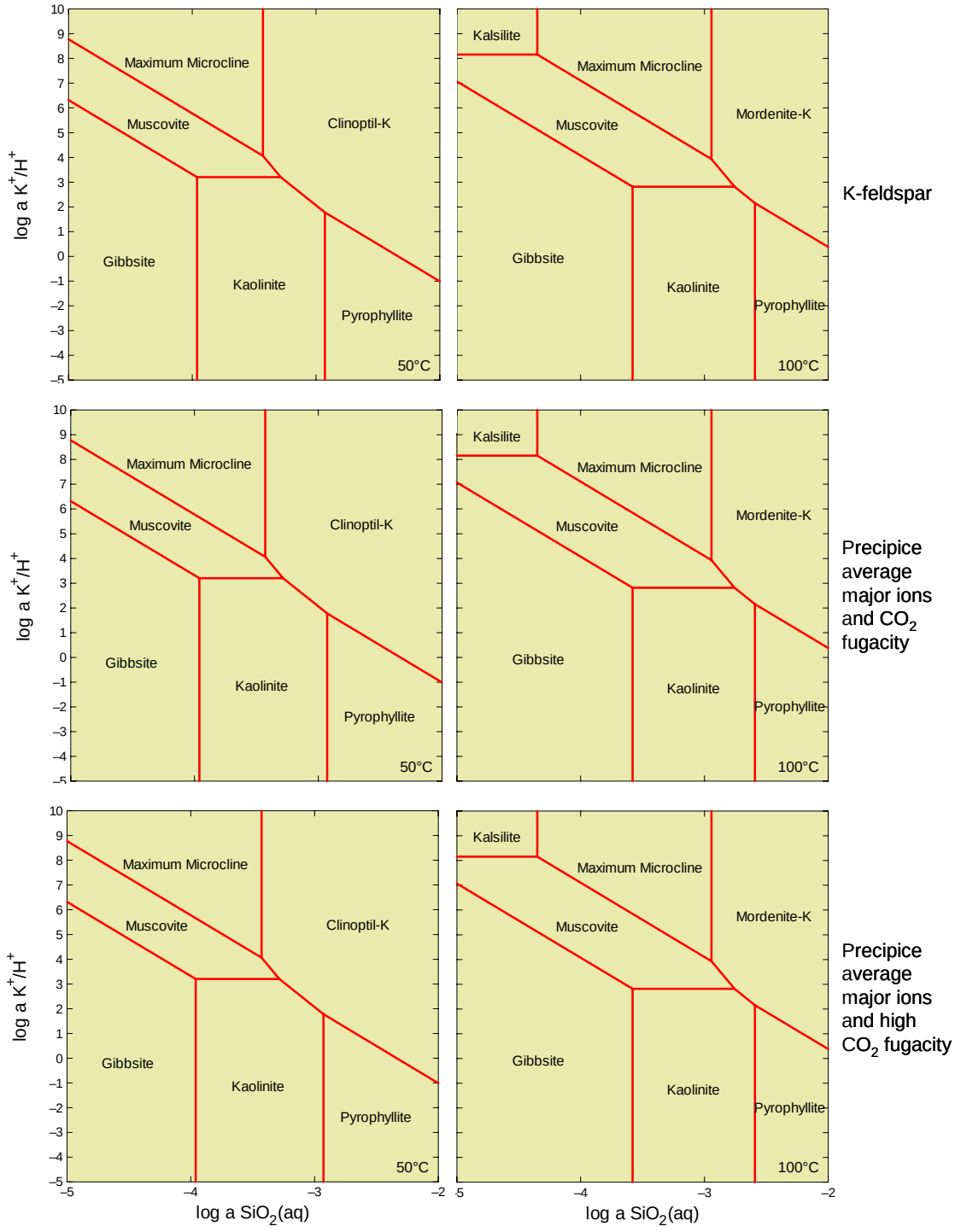

Figure 31. Stability diagrams for K-feldspar under various conditions of temperature and CO_2 fugacity. Pressure is 100 bars in all cases. The domain of kaolinite stability shifts towards higher silica activity, with increased temperature, while CO_2 fugacity has little effect.

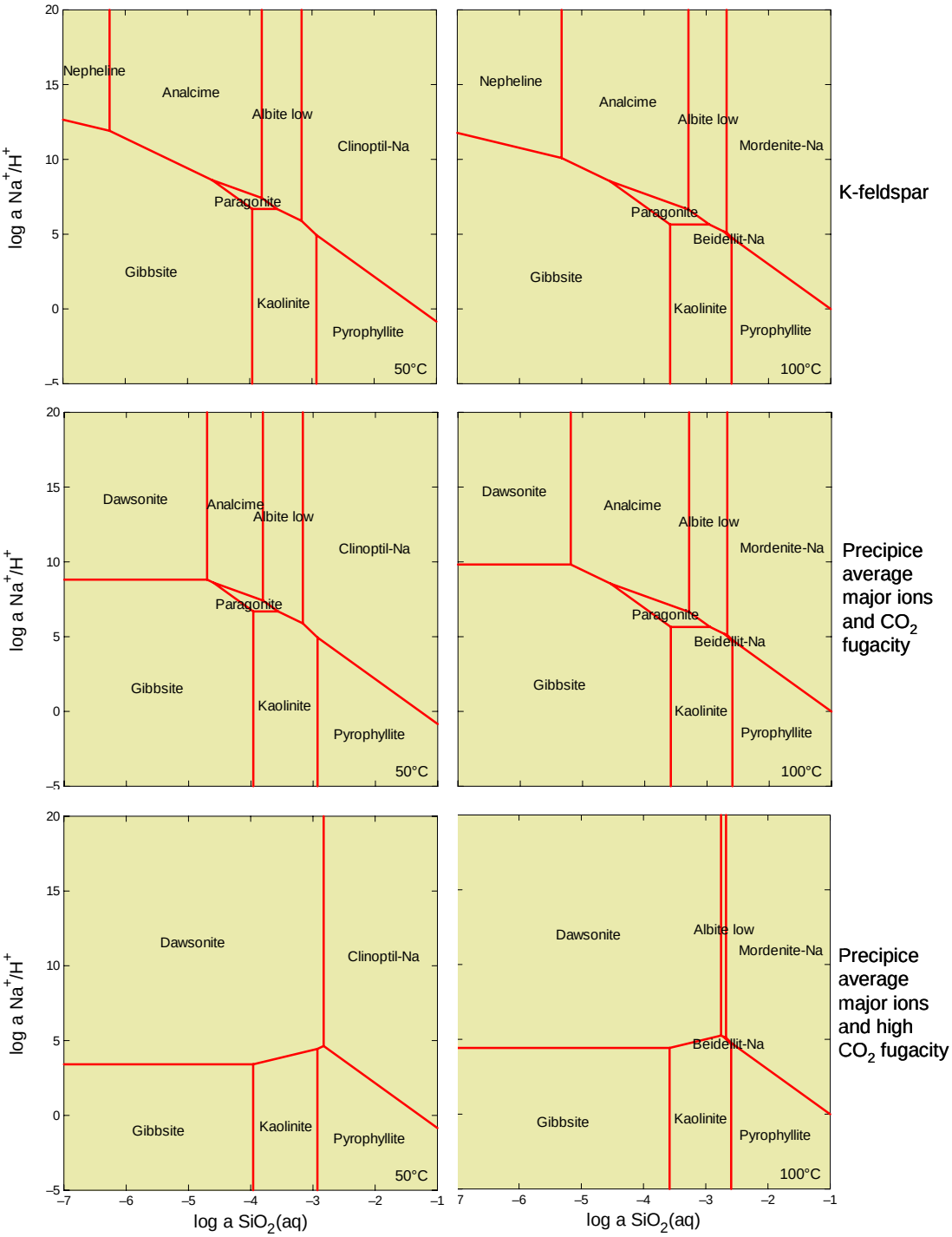

Figure 32. Stability diagrams for albite under various conditions of temperature and CO_2 fugacity. Pressure is 100 bars in all cases. The domain of kaolinite stability shifts towards higher silica activity, with increased temperature, while CO_2 fugacity controls the stability of dawsonite.

Hydrodynamic Analysis

The hydrodynamic analysis is focused on the Precipice Sandstone and the Hutton Sandstone as primary injection targets, and the Evergreen Formation as a regional seal to the Precipice Sandstone. Most of the data points for these units that have been assessed to date are located in the east-central region of the Surat Basin (Fig. 33).

Wells that have pressure data and formation water analyses for two or more units show hydraulic separation between the Precipice Sandstone and Hutton Sandstone (Fig. 34) with pressure data from the Precipice Sandstone generally lying below the hydrostatic gradient. Results for the Evergreen Formation illustrate the heterogeneous distribution of permeability characteristics (Figs. 34c,d). Very low pressure recordings (Fig. 35) suggest 'tight' low permeability areas of the formation. However, in some wells pressure measurements in the Evergreen Formation fall on the same gradient as measurements from the Hutton Sandstone (Fig. 34c,d), implying local hydraulic connectivity between the two units. This relationship is clearly shown in the petroleum exploration well PPC Yarrala-1 (Fig. 34d), where 5 out of 6 DSTs are classified as reliable using the PressureQC™ methodology. The formation pressure results from this well suggest that a low permeability horizon exists at the top of the Precipice Sandstone or at the base of the overlying Evergreen Formation limiting hydraulic communication between the two units. The second test in the Precipice Sandstone in this well is of low reliability but is only marginally off-gradient with respect to the shallower DST result (Fig. 34d).

Figure 35 shows the formation pressure data from two wells, PPC Yarrala-1 and PPC Waggaba-1 converted to freshwater equivalent hydraulic heads and plotted against depth to illustrate the hydraulic head difference between the two units and their relationship with the intervening aquitard, the Evergreen Formation. The data from PPC Yarrala-1 show that the Evergreen Formation is in hydraulic communication with the Hutton Sandstone, but that both units are separated from the underlying Precipice Sandstone. The data from the PPC Waggaba-1 well show that at this well, the Evergreen Formation has low permeability (insufficient permeability to produce a reliable pressure measurement). Again the Hutton Sandstone and the Precipice Sandstone are hydraulically separated with a difference ~100m of hydraulic head shown in both wells. The hydraulic head values in each unit for both wells are similar suggesting that there is regional lateral communication. This data suggests that although the Evergreen Formation can be considered a regional seal to the Precipice Sandstone, in some places it is in local communication with the overlying Hutton Sandstone.

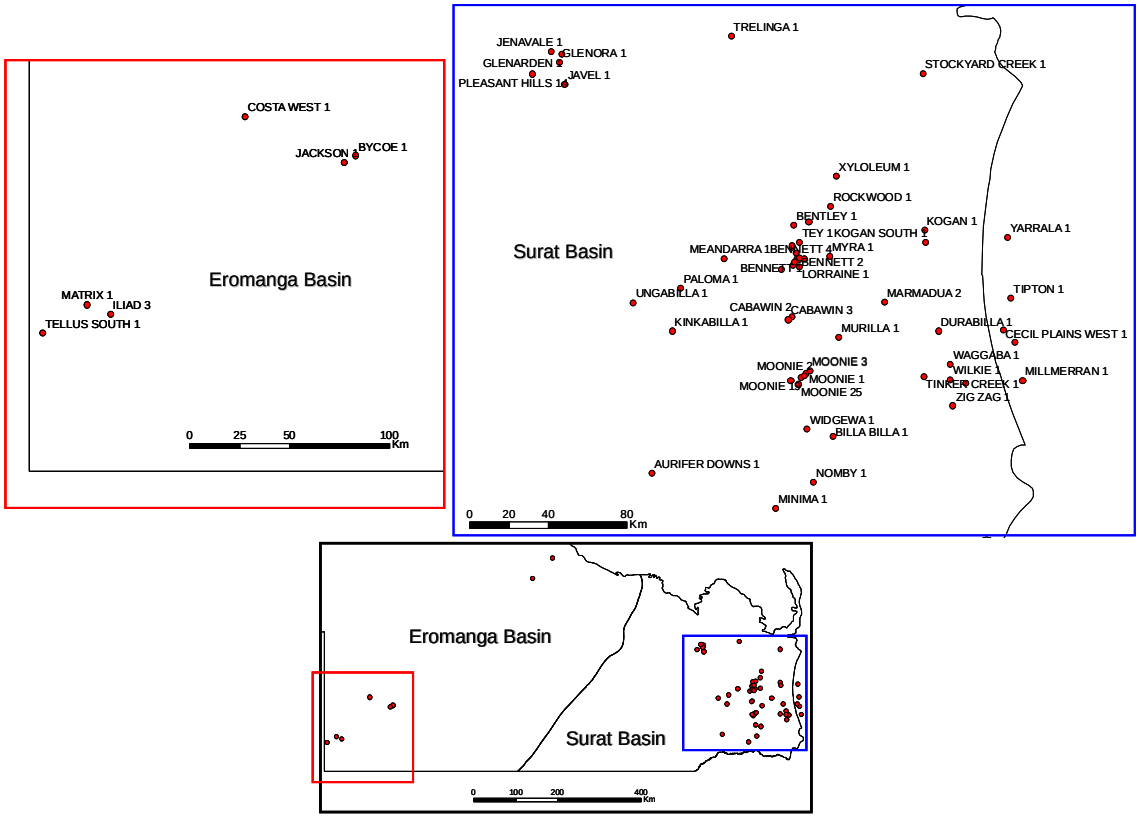

Figure 33. Locations of formation pressure data points from petroleum wells that have been assessed using the CSIRO PressureQC methodology.

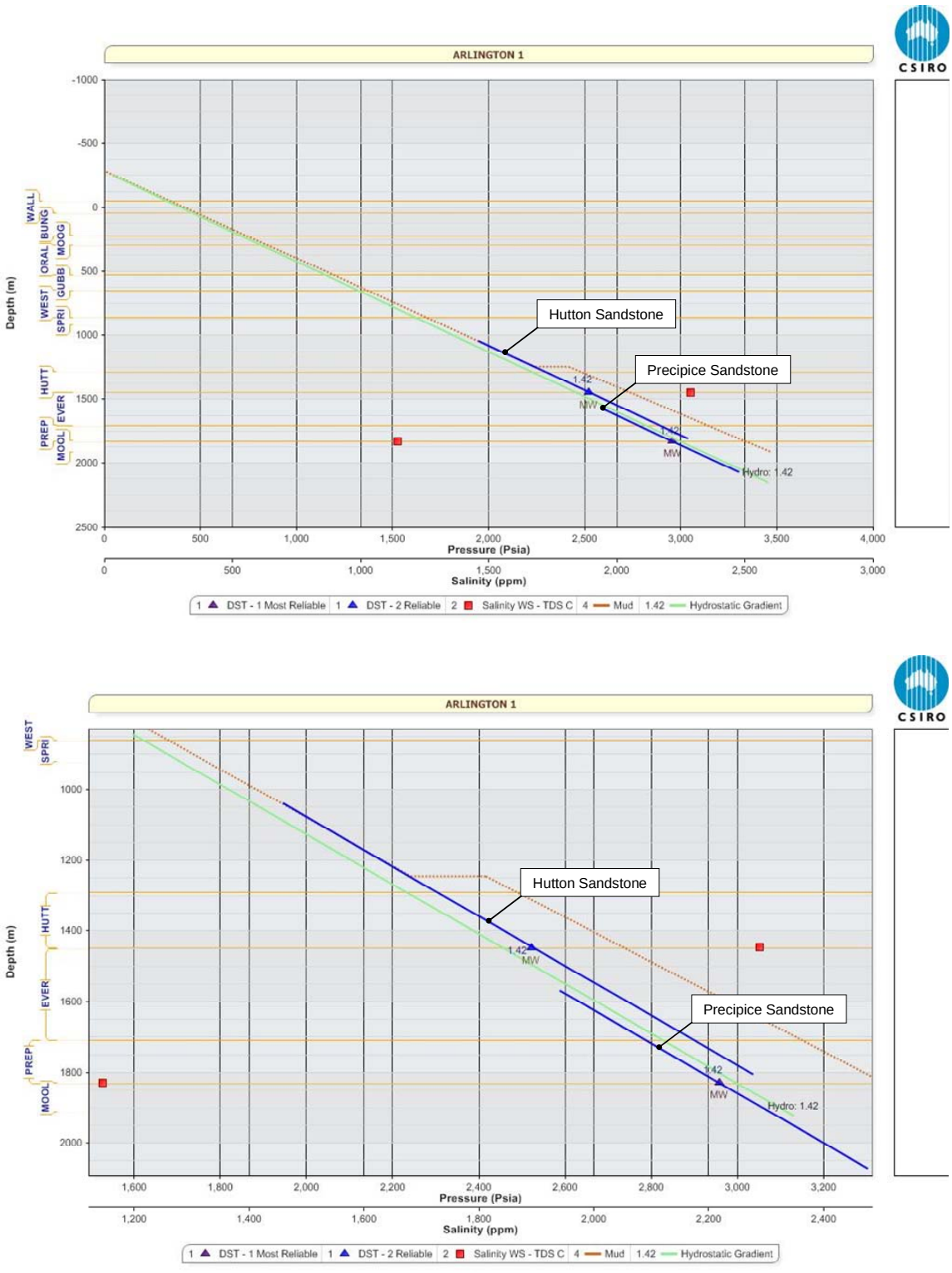

Figure 34a. Pressure/depth relationship between the Precipice Sandstone and the Hutton Sandstone in the eastern Surat Basin, north of the Moonie oil field. The pressure measurements show good reliability and the separation between values is much greater than the accepted 30 psia error margin. The pressure values in this well show that the Precipice Sandstone is slightly underpressured relative to the Hutton Sandstone. The relationship implies that the Evergreen Formation may be acting as a seal inhibiting flow between the two sandstone dominated units. MW – mud/water fluid recovery, hydrostatic drilling mud pressure is shown by the brown dotted line.

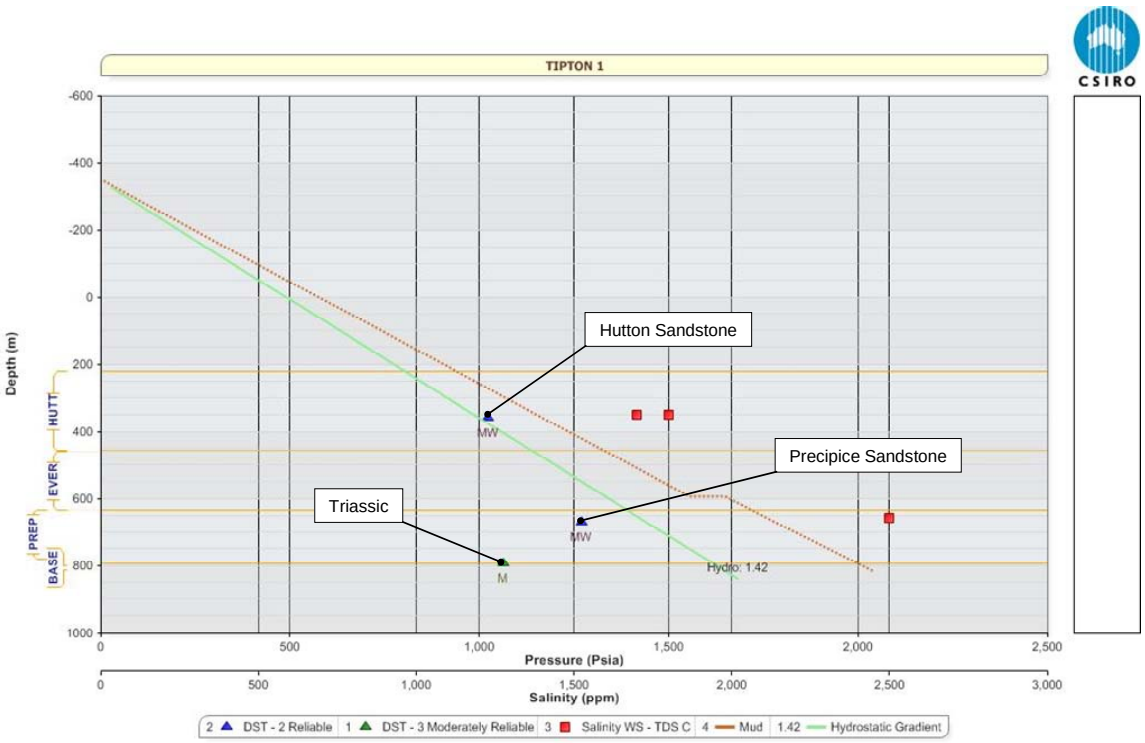

Figure 34b. Pressure/depth relationship between the Precipice Sandstone and the Hutton Sandstone on the Kumbarilla Ridge, southwest of Dalby. The pressure measurements in both the formations of interest show good reliability and the separation between values is much greater than the accepted 30 psia error margin. The relationship is similar to that in Arlington 1, northwest of Moonie. MW – mud/water fluid recovery, M – mud fluid recovery, hydrostatic drilling mud pressure is shown by the brown dotted line.

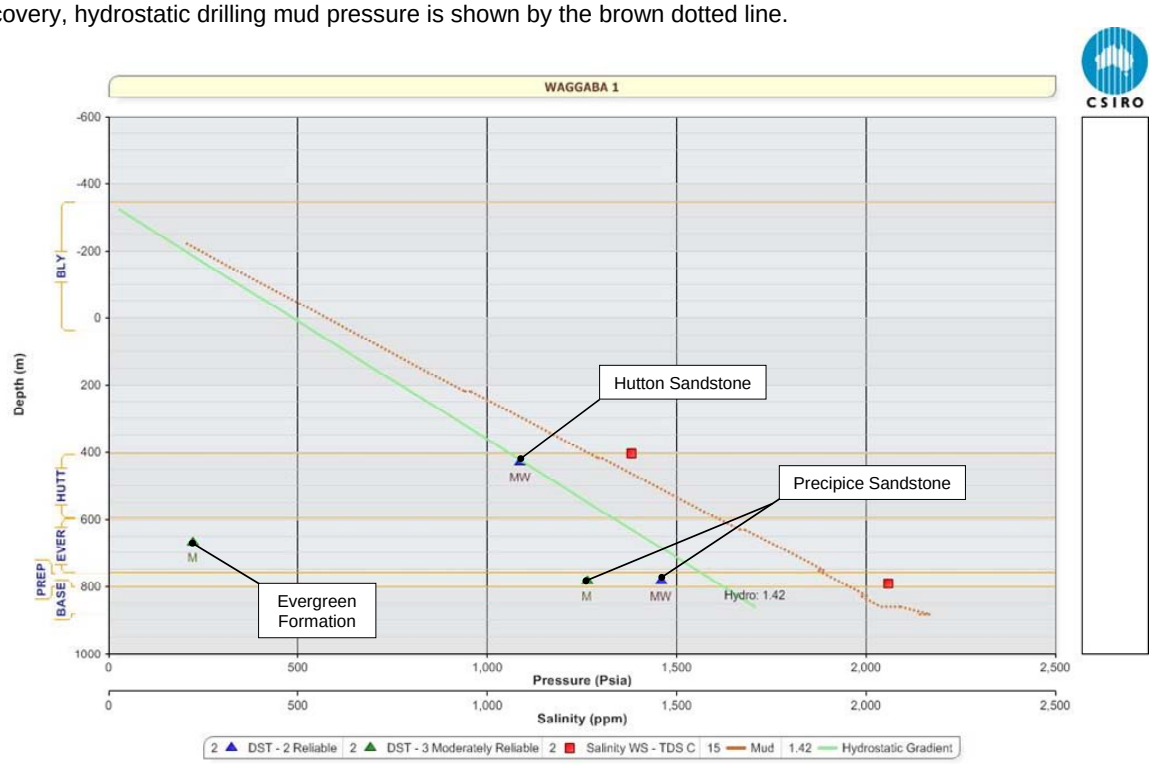

Figure 34c. Pressure/depth relationship between the Precipice Sandstone and the Hutton Sandstone near the eastern margin of the Surat Basin, east of Moonie. The relationship between the two units is similar to that in the wells Arlington 1 and Tipton 1, whereby the Precipice Sandstone is slightly underpressured relative to the Hutton Sandstone. A drill stem test in the Evergreen Formation shows the low permeability characteristic of this unit in many areas. Although the Evergreen Formation test is less reliable that those in the more permeable formations, it suggests that this unit has low permeability, hydraulically separating the Precipice Sandstone and the Hutton Sandstone.

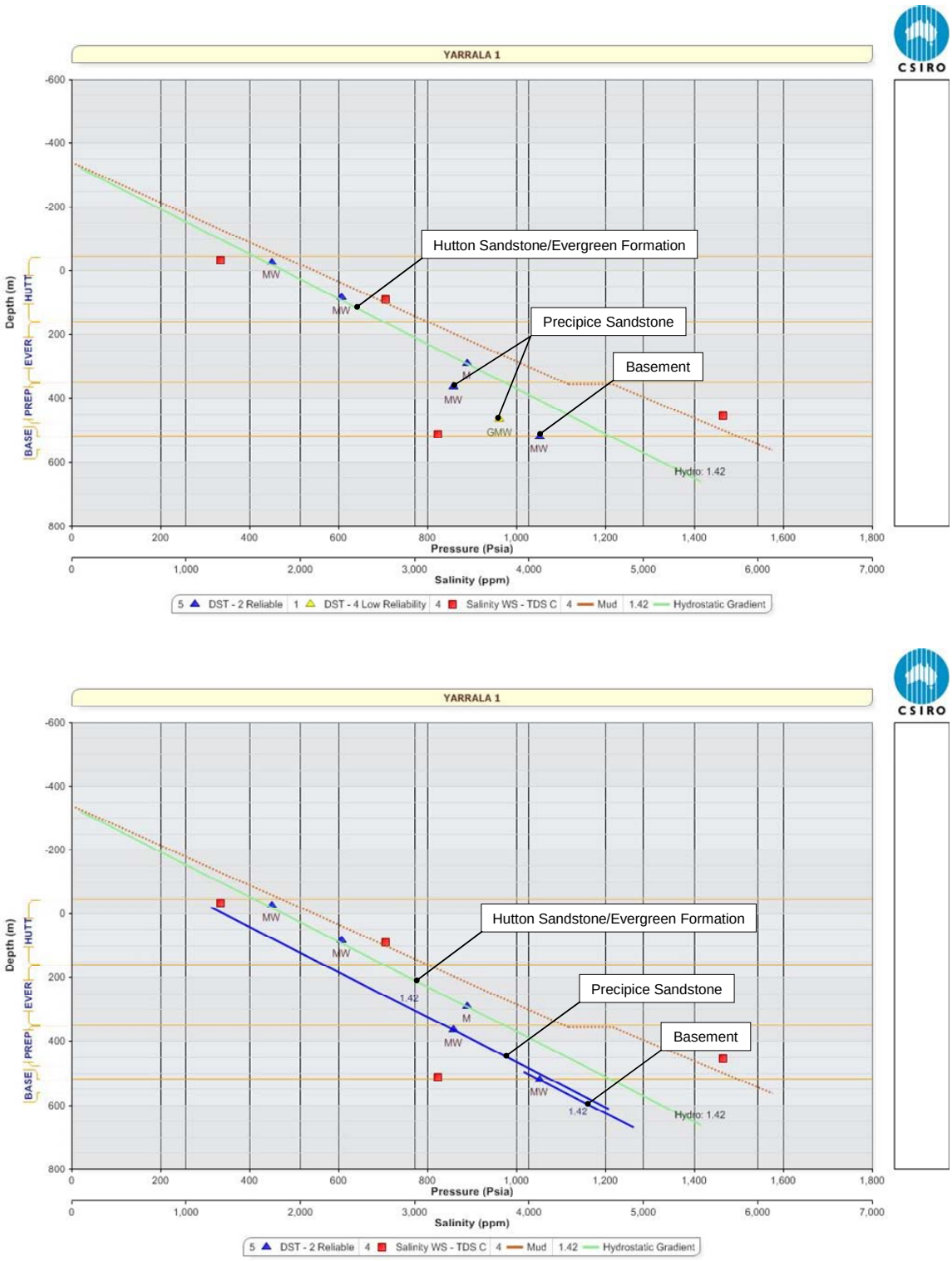

Figure 34d. Drill stem tests in PPC Yarrala 1 also show the Precipice Sandstone as having a lower pressure than both the Evergreen Formation and Hutton Sandstone, implying the presence of a seal between the upper Precipice Sandstone and the Evergreen Formation. The formation pressure in the Evergreen Formation is on-gradient with the overlying Hutton Sandstone, so the Evergreen Formation has sufficient permeability to produce a reliable pressure measurement in this well. The drill stem test in the deeper section of the Precipice Sandstone has slightly lower pressure compared to the shallower test; however, the test has a low reliability score and the fluid recovery contained gas. It is likely that the pressure measurement here does not represent the actual formation pressure. MW – mud/water fluid recovery, M – mud fluid recovery, GMW – gas/mud/water fluid recovery, hydrostatic drilling mud pressure is shown by the brown dotted line.

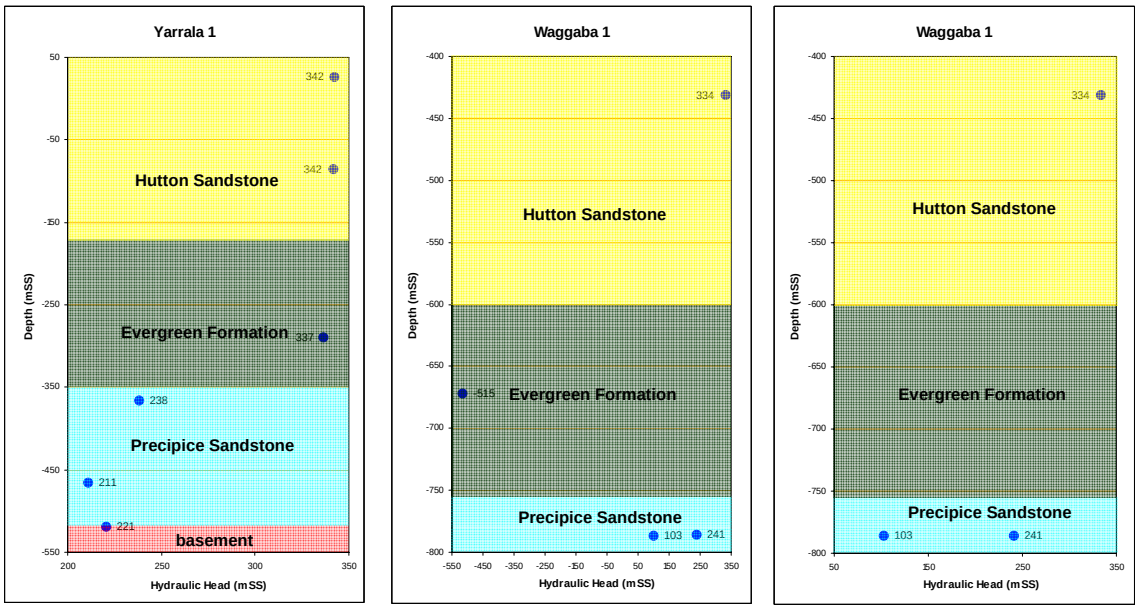

Figure 35. Equivalent freshwater hydraulic heads derived from formation pressure data for two wells. The data from PPC Yarrala-1 show that the Evergreen Formation is in hydraulic communication with the Hutton Sandstone, but that both units are separated from the underlying Precipice Sandstone. The data from the PPC Waggaba-1 well show that at this well, the Evergreen Formation has low permeability (insufficient permeability to produce a reliable pressure measurement). Again the Hutton Sandstone and the Precipice Sandstone are hydraulically separated with a difference of ~100m of hydraulic head shown in both wells. The hydraulic head values in each unit for both wells are similar suggesting that there is regional lateral communication. The measurement in the Evergreen Formation from PPC Waggaba-1 has been omitted for clarity in the third diagram.

To further examine the distribution of the pressure/depth relationship, two groups of wells were clustered for comparative analysis (Fig. 36). Data from both clusters show that the Precipice Sandstone is hydraulically separated from the Hutton Sandstone by the low permeability Evergreen Formation, confirming that the Evergreen Formation is an effective seal for the Precipice Sandstone. There is the suggestion of intra-formational compartmentalisation in the Hutton Sandstone in one well from Cluster 1. The formations of interest in cluster 2 (blue circle) are at subcritical CO_2 depths but illustrate the spatial extent of the hydraulic separation between the Precipice Sandstone and the Hutton Sandstone

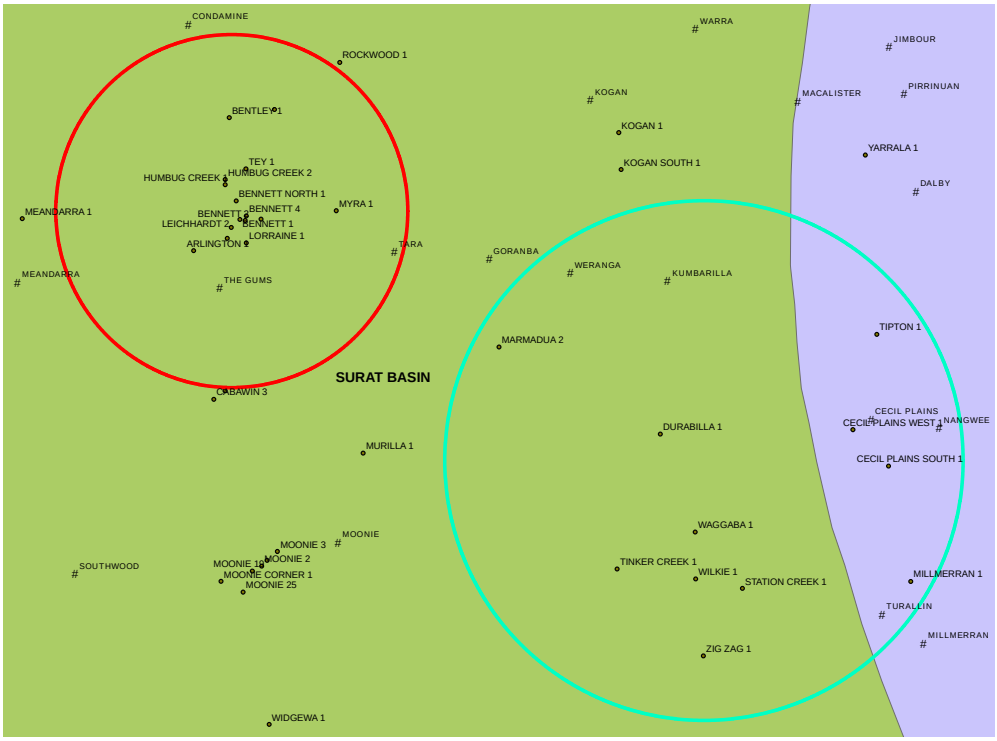

Figure 36a. Location of two well clusters used for comparative pressure/depth analysis in following figures.

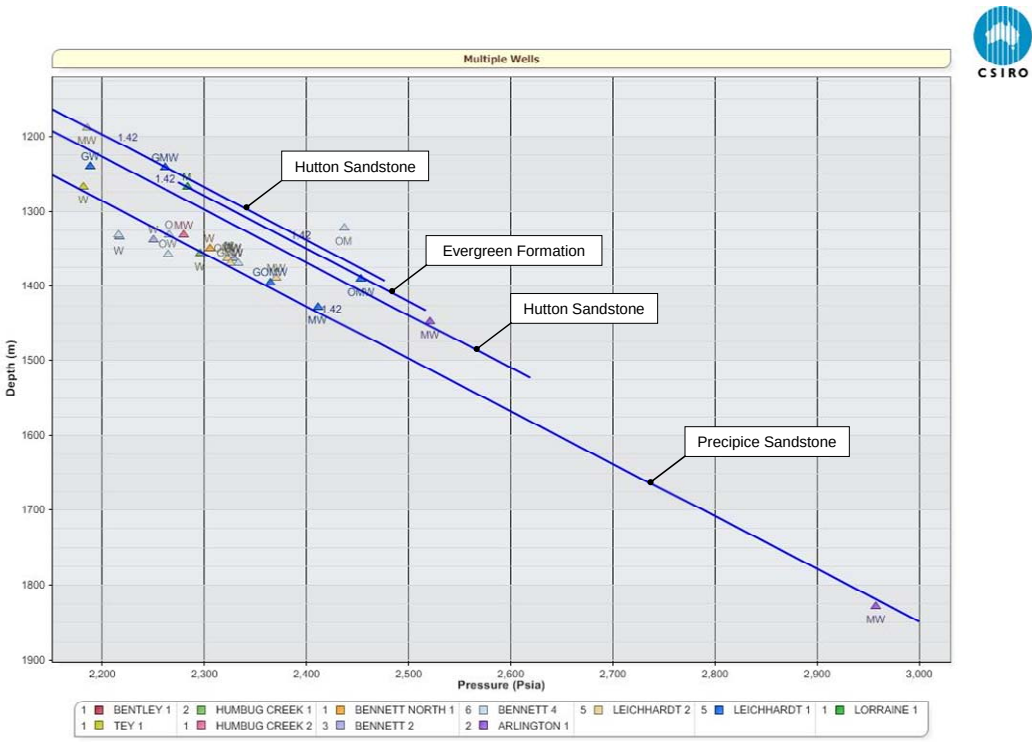

Figure 36b. Drill stem tests from a group of wells located in the Leichhardt oil field, in the Surat Basin (red circle, Figure 36a). Formation water samples recovered from these wells were in the low brackish salinity range. An equivalent freshwater hydrostatic gradient has been applied for both the Hutton Sandstone and the Precipice Sandstone. Almost all of the data from the Precipice Sandstone lie on the same gradient, suggesting it is in hydraulic communication across this area. Data from the Hutton Sandstone lie on two different gradients, suggesting some degree of internal compartmentalisation within this unit. This data also clearly shows that the two units are not in hydraulic communication in this area. Fluid recovery codes: M – mud, MW – mud/water, W – water, GMW – gas/mud/water, GOM – gas/oil/mud, GOW – gas/oil/water.

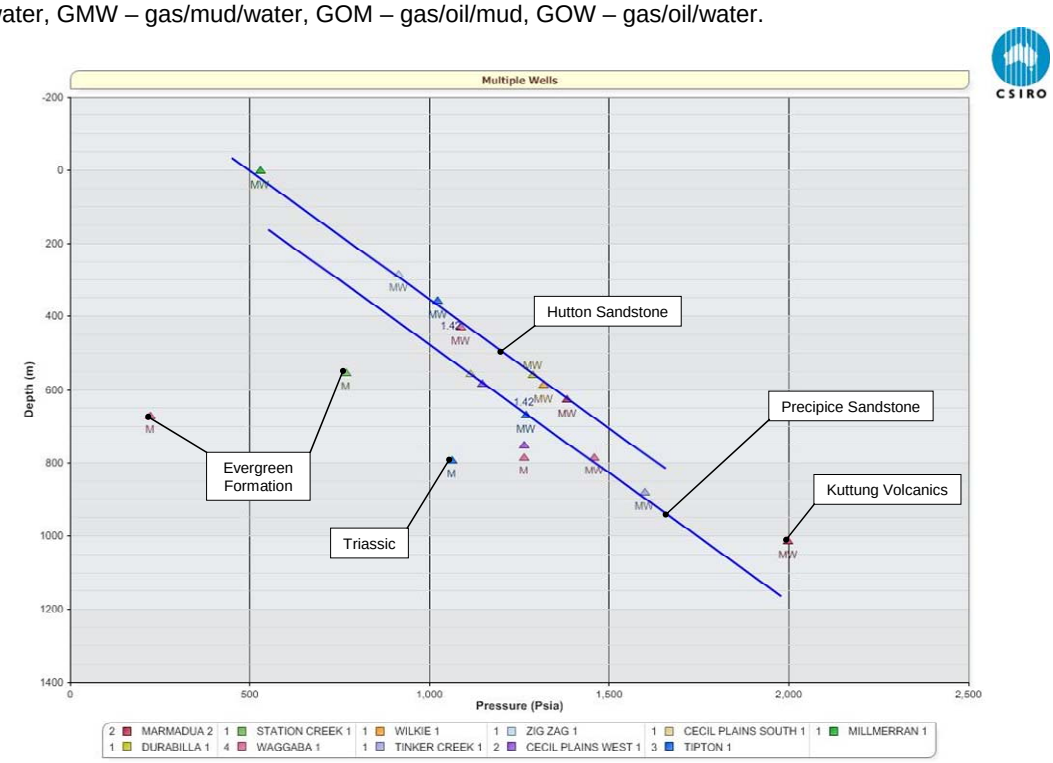

Figure 36c. Drill stem tests from a group of wells located near to the eastern margin of the Surat Basin and across the Kumbarilla Ridge (blue circle, Figure 36a). Formation water samples recovered from these wells were in the low brackish salinity range. An equivalent freshwater hydrostatic gradient has been applied for both the Hutton Sandstone and the Precipice Sandstone, Once again, the data for the Precipice Sandstone lie along a single gradient. However, in this area the Hutton Sandstone data also lie along a single gradient suggesting the unit can be considered as a single aquifer in this area. Data from the Evergreen Formation is also shown and suggests low permeability, effectively separating the two units and acting as a seal for the Precipice Sandstone.

Manual 2D and interpolated 3D vector models for the units of interest are shown in figures 37-39. The manual interpretations are gross estimates of flow only and do not show local detail nor the impact of faults. The interpolated 3D vector models for the Evergreen Formation and the Precipice Sandstone show close agreement with manual interpretations (Figs. 37 and 38). The Hutton Sandstone shows some discrepancies between the two models and does not resolve the northward flow component in the Surat Basin identified in the manual interpretation (Figs. 39b). More data are available for the Hutton Sandstone and there is significant variation in head values in small data clusters. The interpolation algorithms cannot resolve the small scale variability and, therefore, do not show the northward component correctly.

The post 1960 interpolations (Fig. 39c) show reasonable agreement with the pre 1960 models (Fig. 39b), with only minor variations. The post 1960 Hutton model does, however, show a northward flow component in the Surat Basin, due to less variability in closely clustered data points. The post 1960 models are based on potentiometric head measurements only and do not include data from petroleum wells. The impact of oil production from the eastern Surat oil fields on the northern region of the groundwater system is not currently known.

Flow vector interpretations for the Precipice Sandstone are shown in Figure 37. The Precipice Sandstone aquifer system is complicated by localised flow regimes in the east, with several apparent groundwater confluence areas (Fig. 37). Regional flow is predominantly south-southwest; however, there are significant flow components to the east into the Clarence-Moreton Basin and to the northeast of the Surat Basin. A possible hydrostatic area in the central region of the Surat Basin may also exist. A 3D interpolated flow vector model shows a similar regime (Fig. 37b) and a further interpolation using post 1960 groundwater bore data only, exhibits little change in the flow patterns (Fig. 37c).

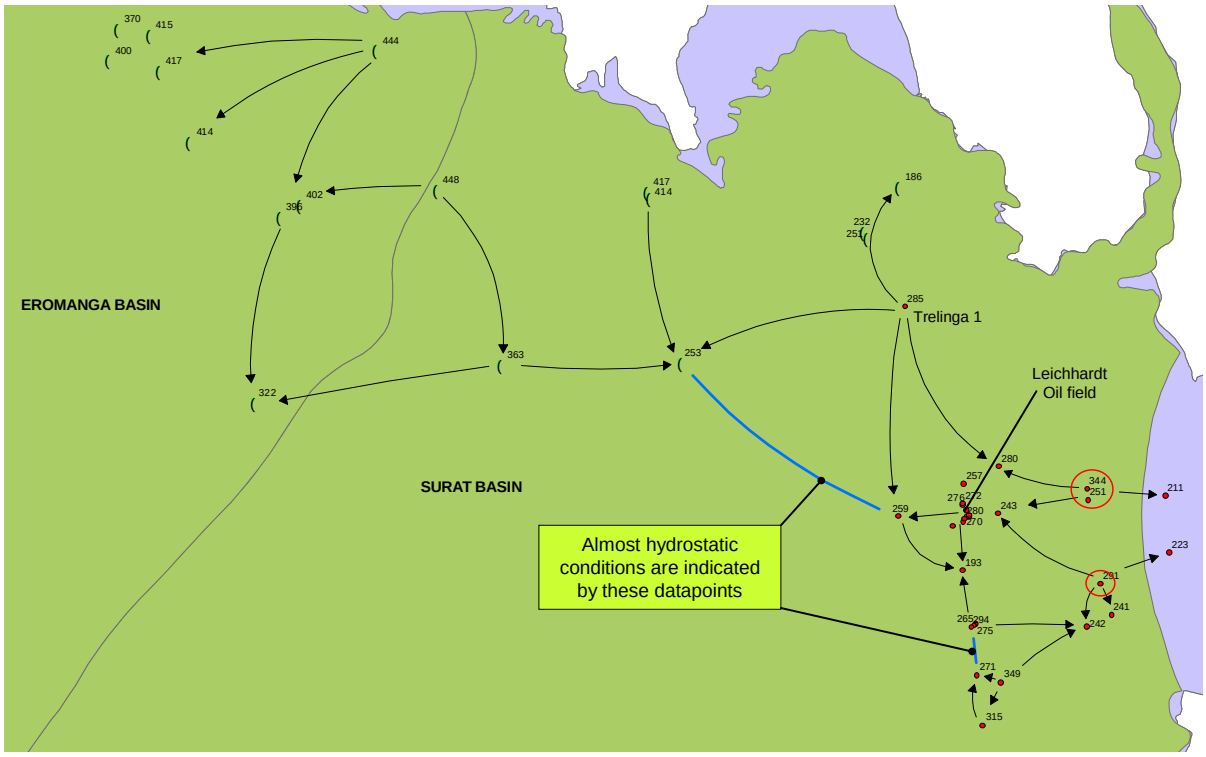

Figure 37a. Interpreted regional flow vectors for the Precipice Sandstone in the northeastern Surat and Eromanga basins. Filled green circles are datapoints for pre 1960 groundwater levels from the DERM GWDB and red dots are hydraulic heads calculated from formation pressure measurements in petroleum wells. The general pattern of groundwater flow is from northeast to southwest, but there are important deviations from this trend in the northeast and east. Most significantly, there is evidence for deep groundwater flow to the east and updip flow to the northeast.

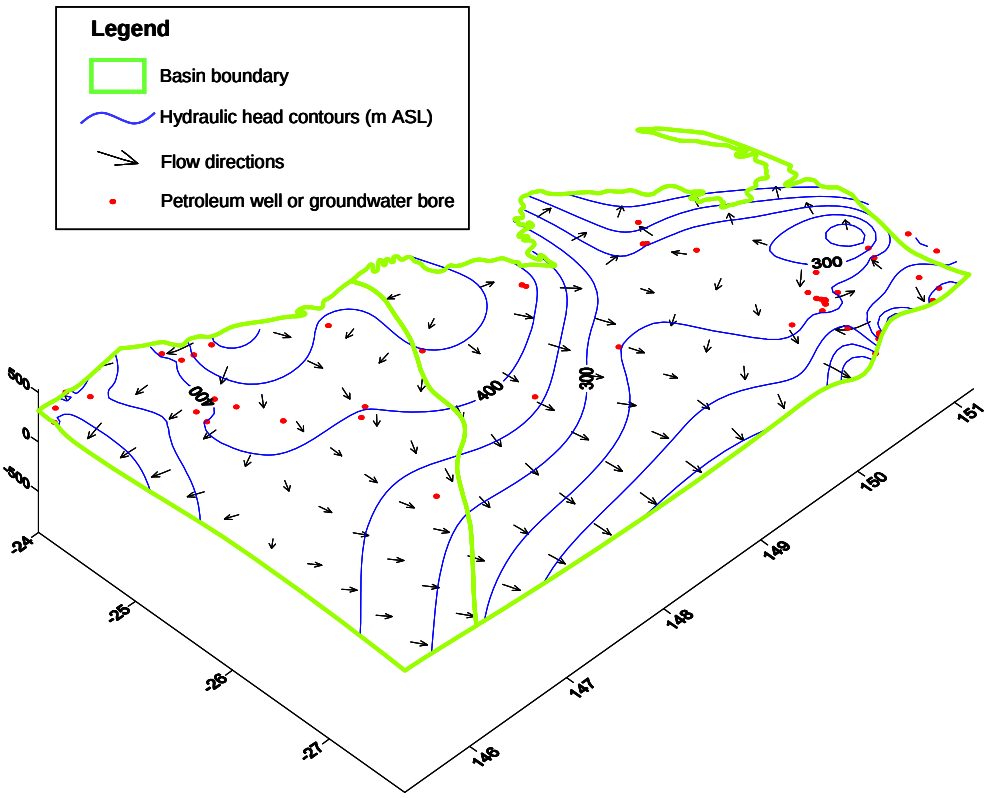

Figure 37b. 3D flow vector plot for the Precipice Sandstone incorporating the results of early/pre-production formation pressure tests (1960-65) and groundwater potentiometric heads prior to 1960.

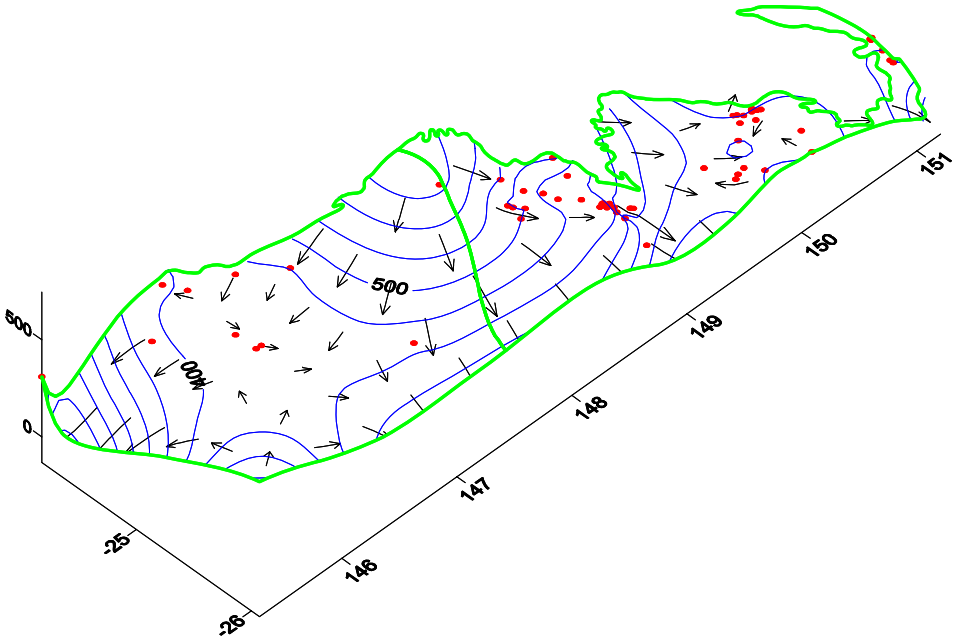

Figure 37c. 3D flow vector plot for the Precipice Sandstone incorporating groundwater potentiometric heads only post 1960.

Flow vector interpretations for the Evergreen Formation and the Hutton Sandstone are shown in Figures 38 and 39. Although there are less data for the Evergreen Formation due to its low permeability, where there is sufficient permeability for flow, the hydraulic head values in the Evergreen Formation and the Hutton Sandstone aquifers are generally similar and significantly higher than those in the underlying Precipice Sandstone aquifer. This suggests that these units may be in regional hydraulic communication. Overall, the flow dynamics are similar in both the Evergreen Formation and the Hutton Sandstone, having a strong northward directed component in the north Surat Basin. A large apparent hydrostatic area is present in the Evergreen Formation in the central and east-central region of the Surat Basin. This is also present to lesser extent in the Hutton Sandstone (Fig. 39). The lack of groundwater motion implied by these results is most likely to be an artefact of sparse data distribution and cannot be quantified. The eastward flow component in the Precipice Sandstone is reversed in both the Evergreen Formation and the Hutton Sandstone, with flow from the Clarence-Moreton Basin into the Surat Basin (Figs. 38 and 39).

Flow vectors in the Eromanga Basin are similar for all three stratigraphic units, predominantly showing flow to the southwest. Petroleum well data are currently being assessed for the Eromanga Basin and have not been included in interpretations in this study. The current models have been constructed using groundwater potentiometric head measurements and will be augmented with petroleum well data when available.

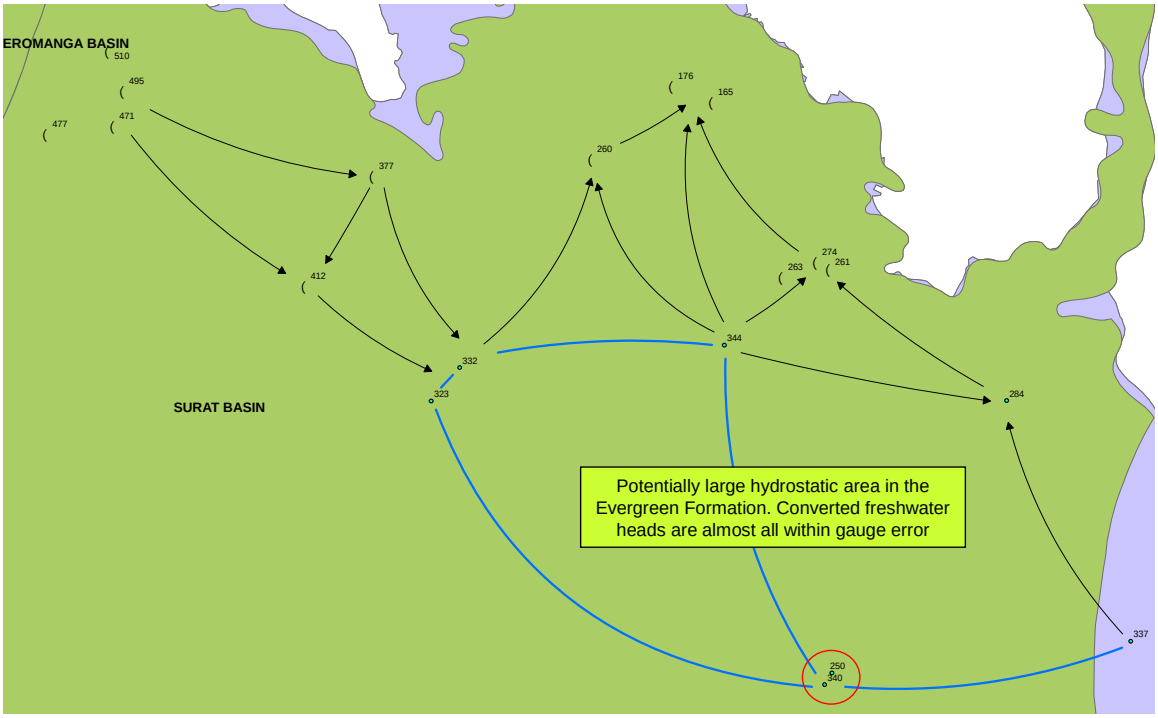

Figure 38a. Interpreted regional flow vectors for the Evergreen Formation in the northeastern Surat and Eromanga basins. Filled yellow circles are datapoints for pre 1960 groundwater levels from the DERM GWDB and blue dots are hydraulic heads calculated from formation pressure measurements in petroleum wells. The groundwater flow patterns differ quite significantly from the underlying Precipice Sandstone. Flow in the northwest of the Surat Basin is towards the southeast and there is a dominant northward flow trend in the north and east of the basin. Data from petroleum wells are very limited for the Evergreen Formation and there are some discrepancies in pressure values for closely spaced wells (points with the red circle).

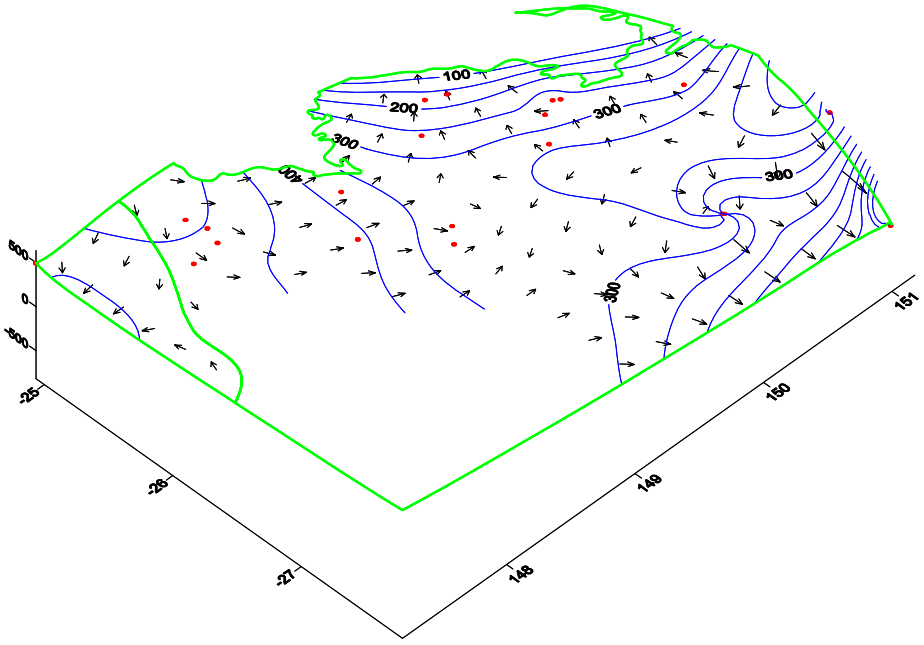

Figure 38b. 3D flow vector plot for the Evergreen Formation incorporating the results of early/pre-production formation pressure tests (1960-65) and groundwater potentiometric heads prior to 1960.

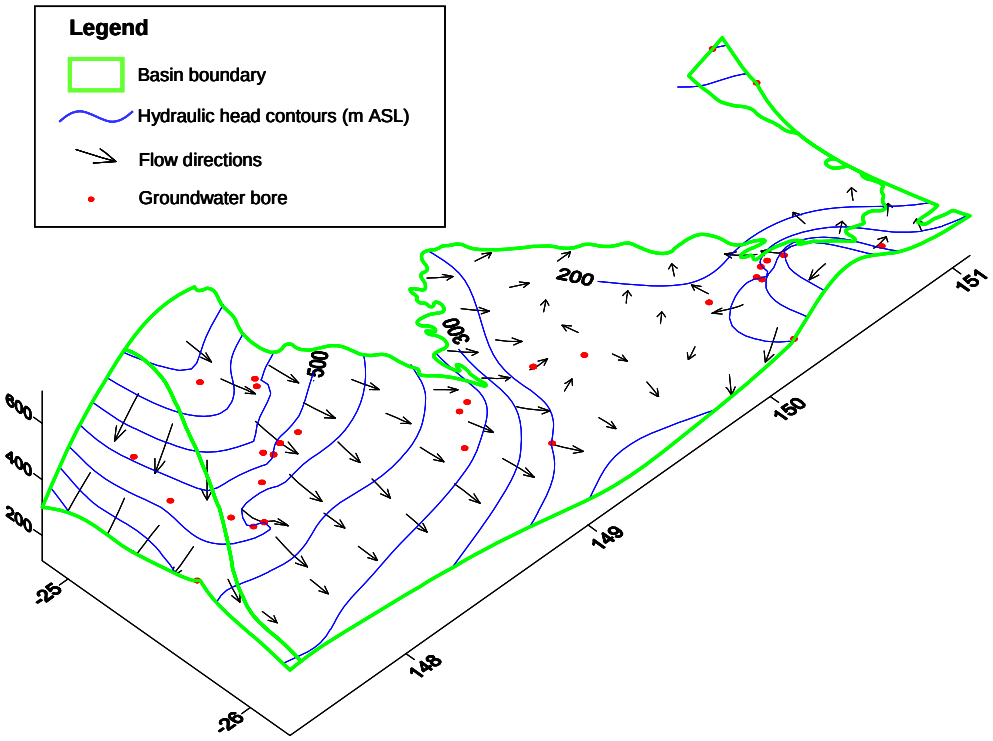

Figure 38c. 3D flow vector plot for the Evergreen Formation incorporating groundwater potentiometric heads only post 1960.

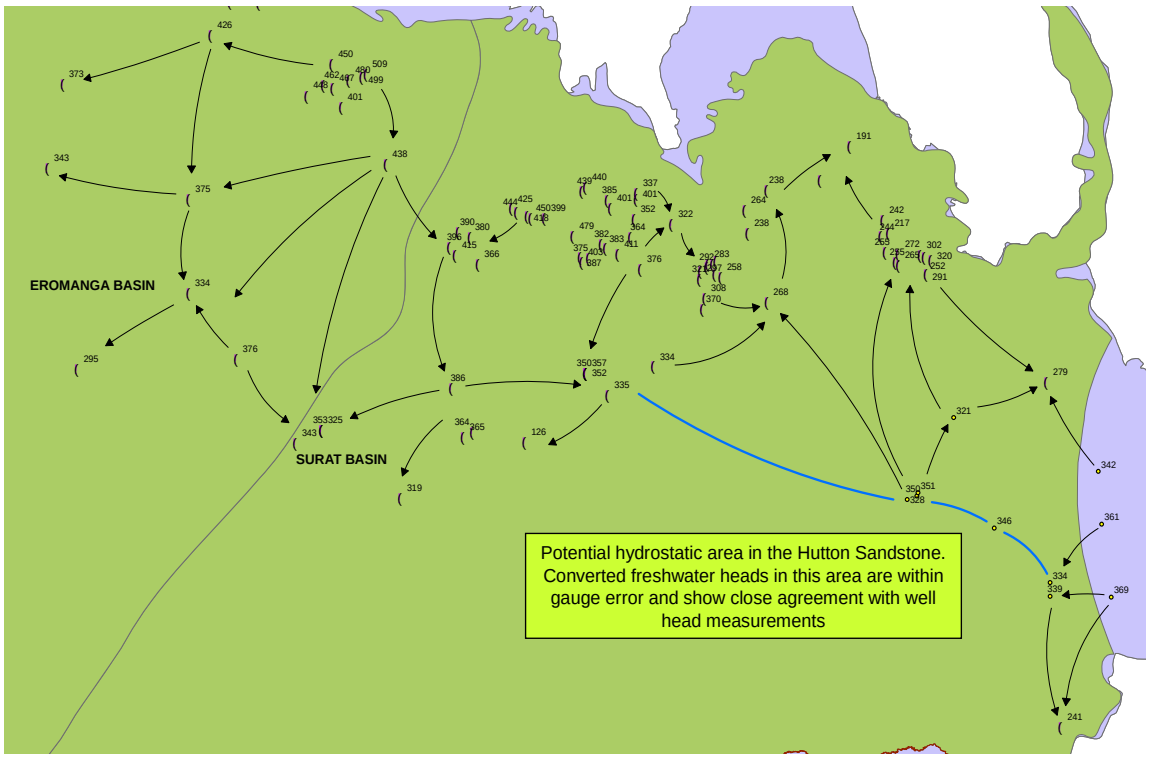

Figure 39a. Interpreted regional flow vectors for the Hutton Sandstone in the northeastern Surat and Eromanga basins. Filled pink circles are datapoints for pre 1960 groundwater levels from the DERM GWDB and yellow dots are hydraulic heads calculated from formation pressure measurements in petroleum wells. Groundwater flow vectors in the Eromanga are based on similar data to the model of Habermehl (1980) and, therefore, show agreement with the earlier hypothesis. The flow regime in the northern Surat Basin was largely excluded from the earlier model and shows a strong northward flow component similar to that in the Evergreen Formation. There is also some evidence for the presence of a groundwater divide in the central region of the basin, which concurs with Hitchon and Hays' (1971) interpretation.

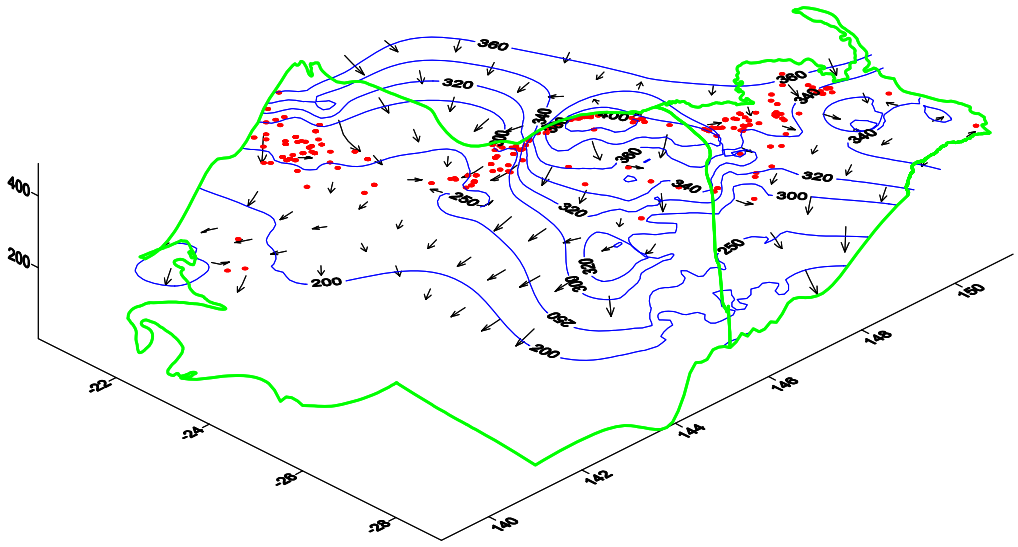

Figure 39b. 3D flow vector plot for the Hutton Sandstone incorporating the results of early/pre-production formation pressure tests (1960-65) and groundwater potentiometric heads prior to 1960.

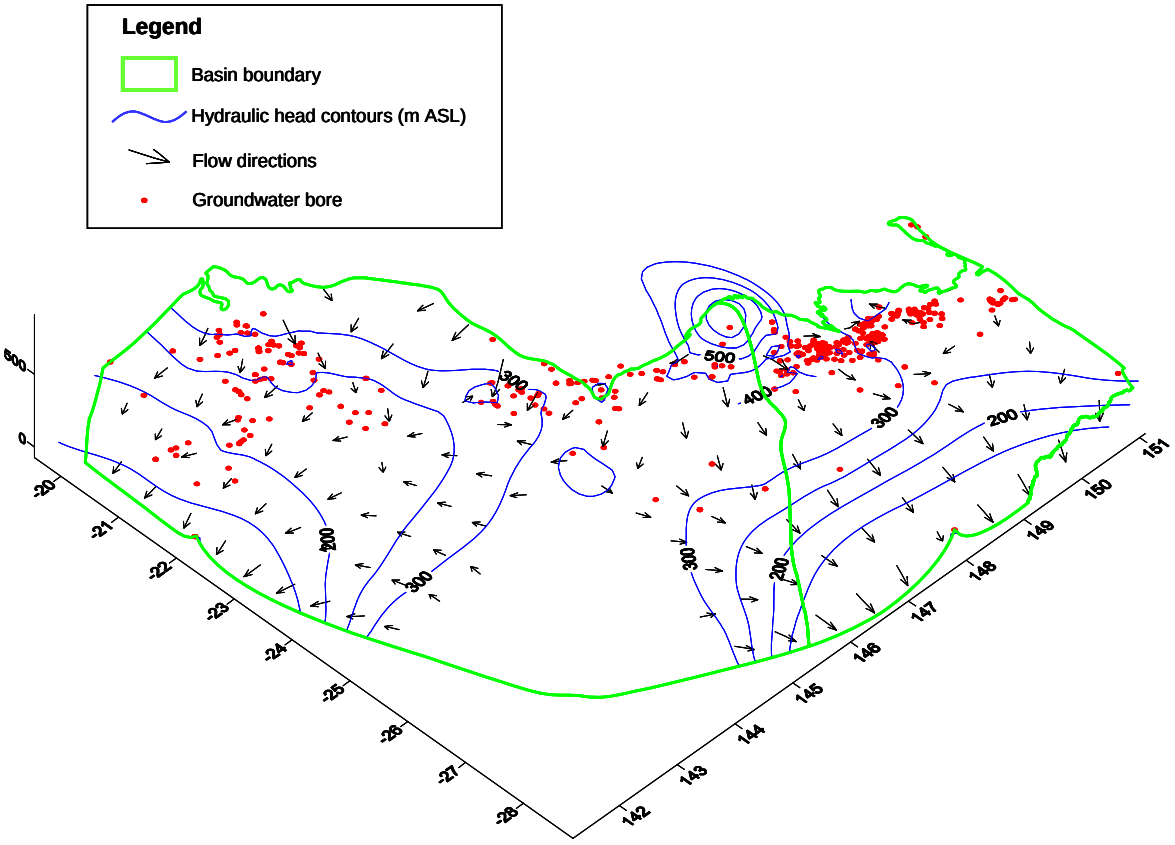

Figure 39c. 3D flow vector plot for the Hutton Sandstone incorporating groundwater potentiometric heads only post 1960.

Models for Gubberamunda Sandstone and Hooray Sandstone are included for completeness, but no petroleum well data are available (Figs. 40 and 41). Both units are well represented by thousands of chemical analyses and water level measurements. The Gubberamunda Sandstone data give an indication of flow in the southern most section of the Surat Basin, close to the NSW border, while the

Hooray Sandstone data provide a regional view of shallow flow directions, covering most of the study area. These two formations are not considered suitable targets for carbon geostorage but are included in order to compare flow regimes with the deeper sandstone units. Hydraulic separation of these units from the injection target formations must be quantified because of their importance as major exploited aquifers.

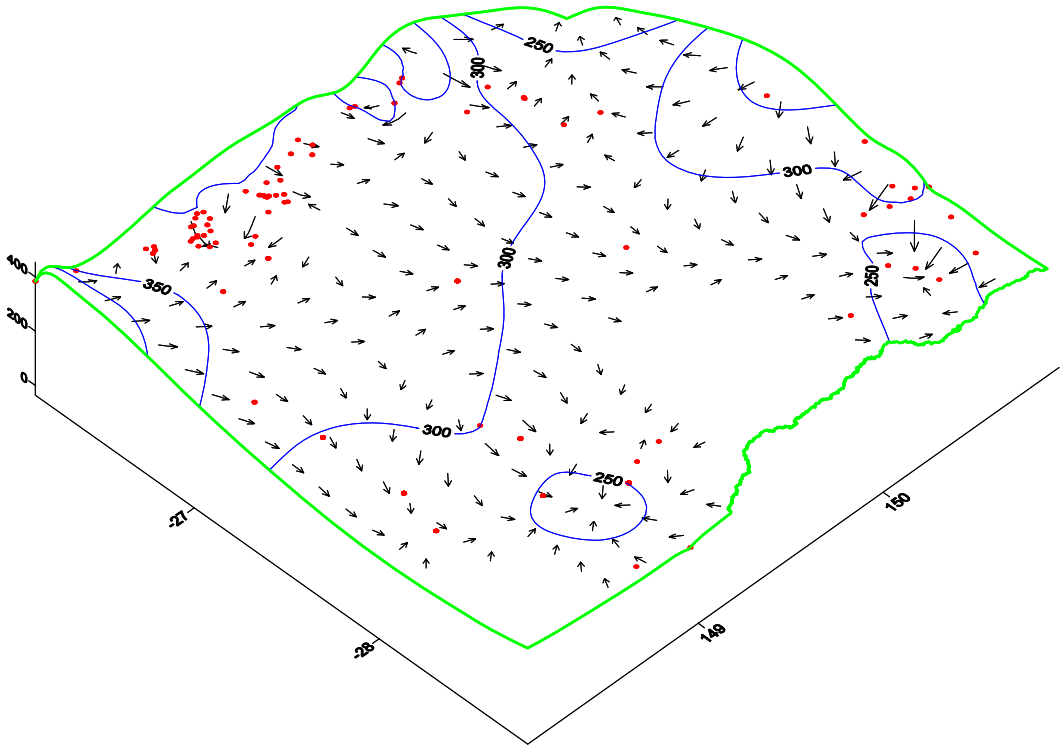

Figure 40a. 3D flow vector plot for the Gubberamunda Sandstone incorporating the results of early/pre-production formation pressure tests (1960-65) and groundwater potentiometric heads prior to 1960.

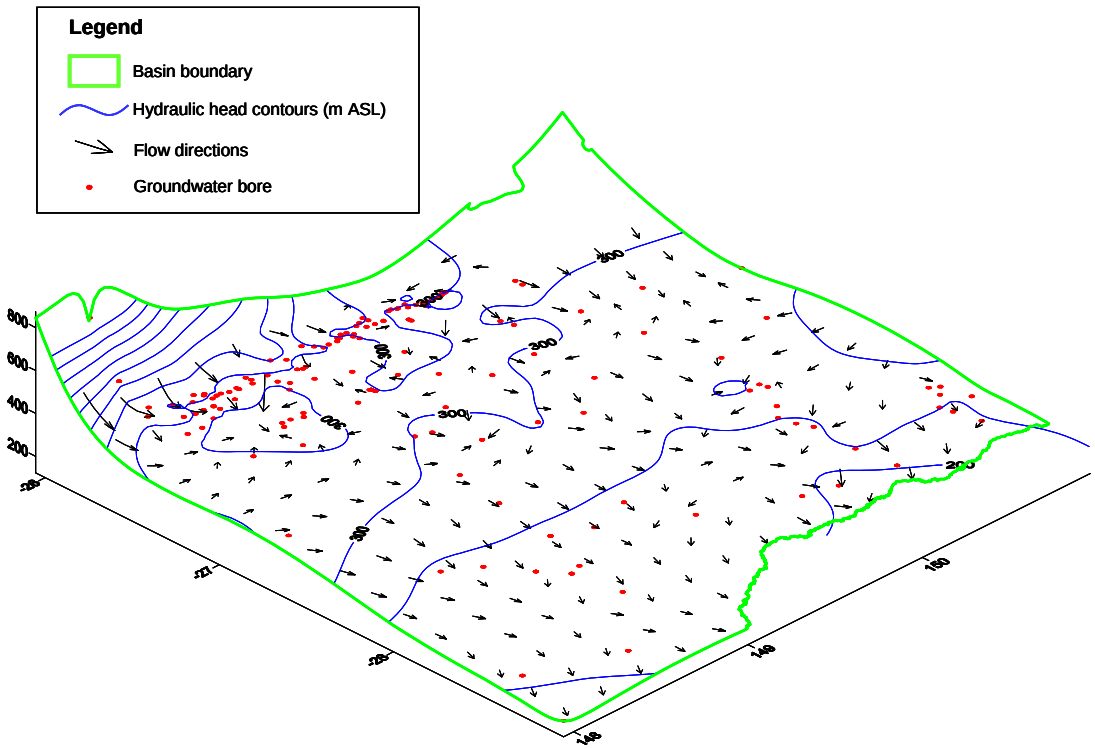

Figure 40b. 3D flow vector plot for the Gubberamunda Sandstone incorporating groundwater potentiometric heads only post 1960.

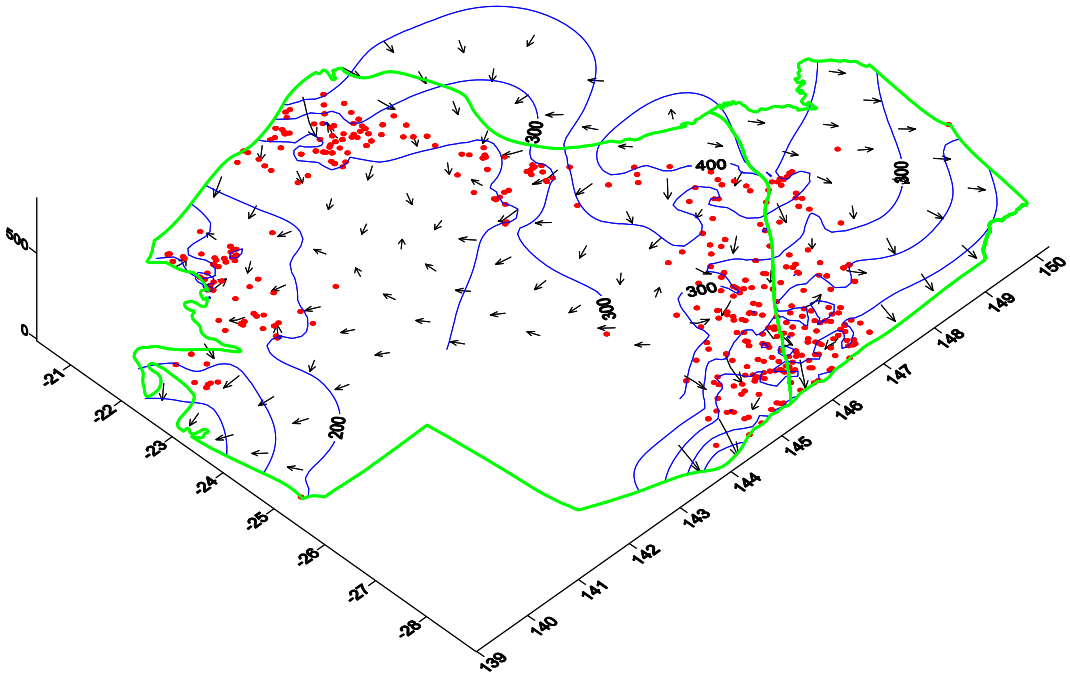

Figure 41a. 3D flow vector plot for the Hooray Sandstone incorporating the results of early/pre-production formation pressure tests (1960-65) and groundwater potentiometric heads prior to 1960.

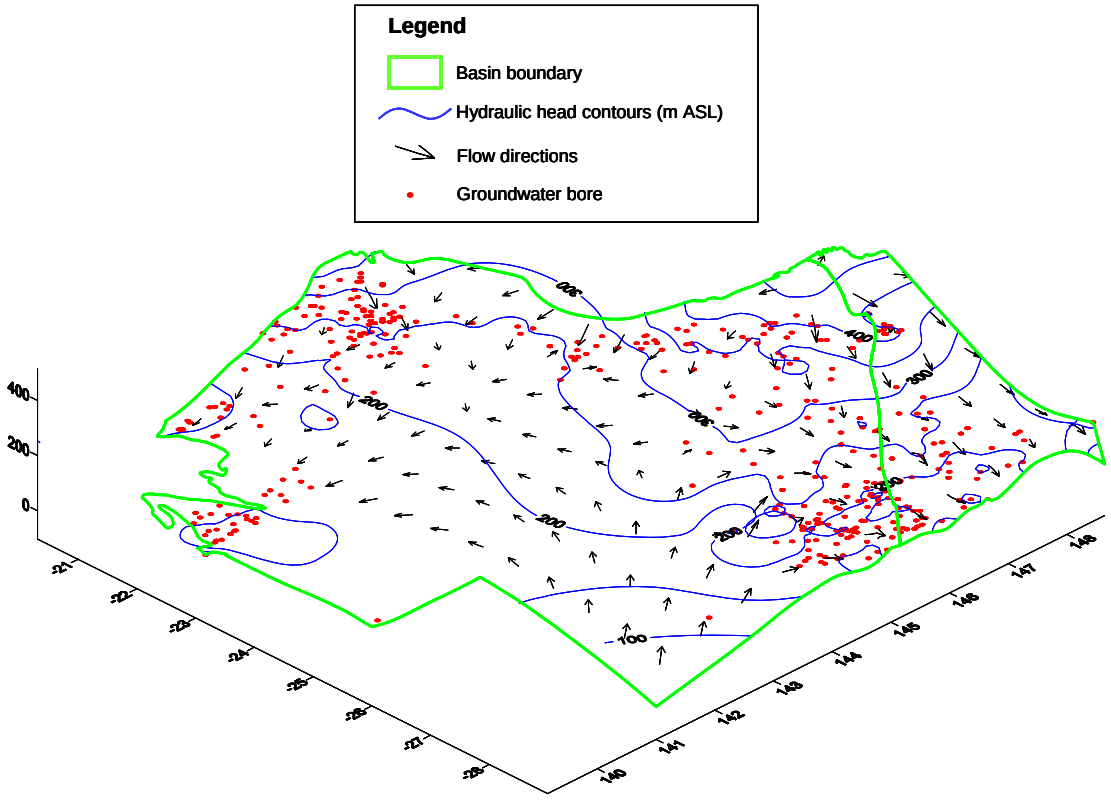

Figure 41b. 3D flow vector plot for the Hooray Sandstone incorporating groundwater potentiometric heads only post 1960. The implied northward regional flow is based on limited data and should be considered with caution.

Discussion

Geological Framework

The subsurface behaviour of injected CO_2 is influenced by many variables. These include reservoir and seal structure, heterogeneity, stratigraphic architecture, absolute and relative permeability, faults/fractures, in-situ pressure and temperature conditions, mineralogical composition of the rock framework, fluid properties and geochemistry and hydrodynamic flow conditions. Therefore, accurate appraisal of a potential CO_2 storage site requires detailed reservoir and seal characterisation, 3D geological modelling and numerical flow simulation (Gibson-Poole et al., 2005). After injection ceases, the buoyancy of the supercritical CO_2 will result in it migrating to the highest point in the reservoir. Stratigraphic heterogeneities will influence the rate of this migration. Once the CO_2 has reached the top of the reservoir the structural geometry at the base of the overlying seal will have a strong influence on the subsequent migration direction. The Surat and Eromanga basins are attractive targets for the long term storage of CO_2 because of the presence of large aquifer volumes and long migration pathways beneath a competent regional seal.

Both the Surat and Eromanga basins have experienced only minor deformation over geological time. Due to a late stage contractional event, the Eromanga Basin acquired a series of low amplitude, long wave-length antiform/synform pairs, which form a number of stacked hydrocarbon reservoir/seal pairs. The Surat Basin has one major axial synform and deformation associated with fault reactivation along the east and west flanks. The style of deformation in both basins is largely controlled by structural elements in the underlying Permo-Triassic basins.

In general terms, the Eromanga Basin contains more conventional fluid trapping structures, which is one of the potential reasons that significant oil reserves are present, unlike the Surat Basin (Fig. 4a). The sedimentary units of interest with respect to carbon geostorage are located at greater depths in the Eromanga Basin, although the maximum depths are similar in both basins (Fig. 6). The gross geometry is of predominantly low gradient flat-lying sedimentary units that are largely undeformed (Figs. 5 and 6). Heterogeneity and anisotropy increase upward in a cyclic pattern and the discrete cycles can arguably be grouped into a mega-cycle. The younger units were deposited by terrestrial stream networks that increased in sinuosity over time, with a concomitant increase in finer grained sediment fractions. Heterogeneity and anisotropy increases with each depositional cycle and late stage units contain abundant fine grained marine sediments (Draper et al., 2002; Green et al., 1997).

The Hutton Sandstone and the lower sections of the Precipice Sandstone and Poolowanna Formation offer the greatest potential for carbon geostorage. These units contain a large proportion of braided stream deposits which are dominated by medium to coarse-grained sandstones. This imparts good permeability and porosity characteristics and less heterogeneity and anisotropy. It is expected that injectability characteristics would be favourable and the low sinuosity stream deposits potentially provide a greater CO_2 sweep efficiency than the greater heterogeneity and anisotropy exhibited by high sinuosity meandering stream deposits. The more quartzose nature of the Precipice Sandstone and Lower Poolowanna Formation deposits also exhibit lower reactivity potential under CO_2 injection conditions than the Hutton Sandstone, which is more arkosic (Figs. 27). Shallower units in the Eromanga Basin, such as the Adori Sandstone and Hooray Sandstone have greater potential for storage than their equivalents in the Surat Basin. This is primarily because they are located at greater depths and are overlain by more extensive fine-grained sealing units (Fig. 6). These sandstone formations do, however, have similar arkosic compositions to the Hutton Sandstone (Figs. 27) and will be less stable in the presence of CO_2 charged fluids. These units also host heavily exploited fresh groundwater resources and are unfavourable geostorage targets for this reason.

The principle sealing lithology above the Precipice Sandstone in the Surat Basin and the eastern Eromanga Basin is the Evergreen Formation (Fig. 6). The Upper Poolowanna Formation in the Eromanga Basin is equivalent to the Evergreen Formation and has similar characteristics (Fig. 6, Table 1). The Evergreen Formation and equivalents qualify as regional seals, but contain high permeability compartments, as evidenced by oil production in the Surat Basin and by formation pressure measurements (Fig. 35). The Hutton Sandstone in the Eromanga Basin is overlain by multiple unconventional and conventional regional seals (Fig. 6). The very thick conventional seals of the Wallumbilla Formation and the Allaru Mudstone are below CO_2 supercritical depths in most areas of the Eromanga Basin. This also provides potential for storage in the younger sandstone units below the Wallumbilla Formation in the Eromanga Basin. The distribution of regional seals above the Hutton Sandstone in the Surat Basin is not as favourable (Fig. 6). The overlying Walloon Subgroup can only

be considered an unconventional seal, due to its extensive heterogeneity. The Westbourne Formation falls into the same category as the Walloon Subgroup and the base of the Wallumbilla Formation in the Surat Basin is too shallow for supercritical CO_2 storage (Fig. 6). The definition of unconventional seals is subjective; the formational unit can be heterogeneous with high and low permeability regions, but must consist predominantly of fine grained lithology with low permeability and be of adequate thickness to prevent the vertical migration of CO_2. The concept of unconventional seals and their effectiveness as fluid/gas barriers is currently unproven.

Fault distributions in both basins need to be considered because of the potential for seal breaching and also the presence of hydraulic barriers. The influence of faulting in the Surat Basin is generally restricted to the east and west flanks (Fig. 7a-e), where conventional hydrostatic petroleum systems analogues are the dominant CO_2 traps (e.g. Moonie, Cabawin and the Roma Shelf). This type of trap is more prevalent in the Eromanga Basin and localised faulting associated with stratal folding is significant in the central regions (Fig. 7f). Fault geometry and displacements are the foundations for analysis; although faults can be sealing with regard to fluid flow (Otto et al., 2001), in which case a highly faulted area may not necessarily provide unfavourable characteristics for geostorage. Groundwater from a deep bore in the town of Miles shows variable water quality and it has been suggested that this could be the result of mixing between aquifers along a fault boundary. It is, therefore, vital to understand the hydraulic significance of faults for carbon geostorage.

Reservoir/Aquifer Geochemistry/Hydrochemistry

The approach to geochemical/hydrochemical characterisation adopted in this study provides a qualitative understanding of the regional trends in composition of both the storage media and the host fluids. The disparate nature of the datasets and the datapoint distributions necessitate the application of certain assumptions and the use of mean compositional values. The results provide a basis for regional characterisation and should not be used for detailed site assessment and characterisation. The reaction simulation results do, however, provide an accurate representation of the potential impacts of CO_2 injection on both the composition of the storage media and the fluid hydrochemistry.

Probably the most striking characteristic of the GAB groundwater is that the salinity is low even in the deepest areas of the component sedimentary basins. Although not as reliable as groundwater bore samples, formation water analyses from petroleum wells show major ion hydrochemical signatures that are consistent with trends mapped from the former. There are small 'compartments' within the aquifers that show high salinity groundwater spikes, but these are generally localised (Fig. 13a,b). Hydrochemical evolution is the reverse of that seen in many deep aquifers, which typically exhibit a shift from fresh Na-HCO_3 compositions to more saline Na-Cl character. Although groundwater is of low salinity in the very shallow regions of the GAB aquifers, the dominant pattern is of higher salinity Na-Cl groundwater near to recharge and discharge zones (e.g. Fig. 19). This is most likely linked to mobilisation of salts in soil horizons by the influx of meteoric water and the discharge of fresh groundwater.

The composition of the recharge waters is not accurately known, but the pH buffering capacity of the groundwater is very large. Mildly acidic recharge waters would rapidly be neutralised along the flow paths to deeper regions of the aquifers. The low groundwater flow velocities and long residence times result in concentration of Na^+ and HCO_3^- ions leading to a low brackish salinity alkaline composition with remarkably consistent pH levels across broad areas of the basins (Figs. 14). Alkalinity distributions show similar trends, with increasing concentration with increasing depth (Figs. 15). Using major ion hydrochemistry for aquifer distinction is only effective when there is a deviation from the dominant Na-HCO_3 signature. Certain units, such as the Walloon Subgroup and the Wallumbilla Formation are dominated by Na-Cl groundwater and mixing lines associated with underlying and overlying aquifers/aquitards can be established (e.g. Figs. 18m,ww,xx). Many formations, however, have mixed distributions between these two main water types and a combination of spatial analysis and hydrochemistry is necessary to identify mixing between aquifers (Fig. 18, Table 2).

Studies such as that of Radke et al. (2000) show an integrated approach combining major ion hydrochemistry and isotope geochemistry. This could be effective in establishing the relationships between the stacked aquifers in the GAB, but would require significant investment in data acquisition. There is also the possibility that lateral isotopic trends may be similar between aquifers and not offer any useful information with regard to vertical relationships. Minor and trace element contents often yield important information, due to ion exchange processes associated with the clay fraction in aquitards. This information is very sparse and potentially unreliable in the currently available datasets. Tracer injection tests and minor/trace element geochemical analysis are likely to be the only reliable

methods to quantify vertical hydraulic relationships between the aquifers and aquitards, and also to estimate the flux magnitude if hydraulic communication is apparent. A nested observation well/bore network is required to accurately establish vertical mixing relationships in stacked aquifer/aquitard systems.

The extensive mapping and stratigraphic drilling programs conducted by the state Geological Surveys provide enough supporting information to correlate mineralogical trends across the two basins. Regional correlations based on these data combined with the mineralogical analyses conducted in the Eromanga Basin provide constraints for the application of mineral stability modelling. The long residence times and low flow velocities in the GAB should allow natural equilibration between the groundwater and the aquifer media. Although redox equilibrium is unlikely, the fluid-rock system is potentially very close to thermodynamic equilibrium. This hypothesis is supported by aqueous speciation simulations using groundwater hydrochemical data from the DERM GWDB and formation water analyses from petroleum wells. Simulations run using average groundwater samples show reasonable agreement with those conducted on individual samples. Initial water-rock reaction simulations were carried out to equilibrate the average rock compositions with the average groundwater compositions for the Hutton Sandstone and the Precipice Sandstone. This is to reduce the state of disequilibrium between the average aquifer media/groundwater compositions to more closely represent the postulated equilibrium state derived from speciation simulation runs for individual groundwater samples. This approach also contributes to reducing the bias introduced by comparing groundwater samples collected large distances from mineral analysis sample sites.

Two types of simulation are subsequently conducted on the equilibrated water-rock compositions to examine the potential near well and distal effects of CO_2 injection. The results of equilibration of a 1 molar CO_2 aqueous solution with the aquifer media show that the natural buffering capacity can accommodate the change in solution composition without a radical change in solution salinity or pH (Figs. 28b, 29b, 30a). The sandstone compositions of the Precipice Sandstone and the Hutton Sandstone, however, respond quite differently (Fig. 30a). This is primarily due to the difference in framework compositions between the two formations (Fig. 27). The equilibrated average groundwater composition from the Hutton Sandstone is charged with Na^+, K^+ and Al^{3+} from the dissolution of feldspars. Equilibration of the CO_2-rich fluid with the Precipice Sandstone has a minor effect on mineral distribution, whereas the Hutton Sandstone shows significant changes. There are possible detrimental effects on both rock types that are related to pore throat plugging by mineral precipitation. The dissolution of carbonate would increase secondary porosity, but the precipitation of dolomite in both cases and also dawsonite in the Hutton Sandstone could reduce both porosity and permeability. The impact of this process would depend on the rate at which dissolution and precipitation took place. The equilibrium modelling approach cannot account for the time-distance factor and the relationship must be examined further by applying kinetic rate laws and reactive transport modelling.

Further insights into the effects of CO_2 injection are given by simulating flushing of the aquifer media with a CO_2-charged fluid. The difference between this simulation and the static approach above is that an approximation of reactive transport effects can be achieved with an equilibrium model. Time and distance effects are still not quantified, but the longer term impact of injection can be assessed. Flushing of the system with a 1 molar CO_2-charged aqueous fluid causes substantial changes to both the groundwater and aquifer media compositions in both formations (Figs. 28c, 29c, 30a). The most severe changes in groundwater salinity and pH would occur proximal to the injection well. The radius of influence cannot be estimated from an equilibrium model and would be governed by plume migration and groundwater velocity, diffusion and hydrodynamic dispersion. The hypersaline conditions predicted by the model results are not indicative of the true groundwater salinity, because of the limitations of the approach. The resultant solution has very large electro-neutrality charge balance errors because of excessive HCO_3^- ion. This is indicative of a two phase system, whereby the high HCO_3^- concentration represents a mixture of dissolved CO_2 and free-phase CO_2. The phase division cannot be quantified with the current model, but is still indicative of near-well conditions in a qualitative sense.

The resultant mineralogy of both the Hutton Sandstone and Precipice Sandstone aquifer media is a quartz/kaolinite dominated assemblage with lesser amounts of mica/illite and dolomite. The groundwater pH in both systems is close to 5, which would be corrosive. These changes would be of primary interest for injection well design and construction. The possible impact on existing infrastructure, groundwater resources and the environment cannot be examined without the addition of kinetic simulations and a hydrodynamic model. The results must be put into context with regard to the potential for contamination of groundwater resources away from the injection site. The geological framework and derived hydrostratigraphy, including the location of structural and stratigraphic traps,

combined with reactive transport modelling is required to correctly estimate the spatial influence of the near well fluid compositions. The work of Zhang et al. (2009) using the TOUGHREACT simulator code, shows that the concentration of dissolved CO_2 and the induced mineralogical changes extend to between 500 and 1000 m in the first 100 years. Even after several thousand years the modelled radius of influence extends only to 10-15 km from the injection well (Zhang et al., 2009).

Hydrodynamics

The required output resolution must be considered prior to the construction of a hydrodynamic model; from a groundwater resource assessment perspective, a long-term change in hydraulic head of 1-3 metres is significant. The gauge error in formation pressure measurements from older wells commonly equates to ~21 m of hydraulic head. Taking this factor into consideration, it is overambitious to expect to achieve a resolution finer than 21 m in a model derived from data of this quality. Modern temperature compensated quartz gauges are, however, very accurate (Brown, 2003) providing a much finer resolution than mechanical strain gauges.

Initial focus on data assessment for hydrodynamic analysis has been in the Surat Basin (Fig. 33). Work has started in the Eromanga Basin, but more of the data require quality control assessment prior to incorporation into a hydrodynamic model. The interpretations and examples in this study are, therefore, primarily based on the work carried out in the Surat Basin. Data quality is predominantly reliable, although there are some tests that show very low reliability. The possible problems with using unreliable measurements in the analysis have mostly been overcome where wells are clustered and the more reliable data point can be compared with those of a lower confidence level. In cases where data points are isolated, such as the PPC Kogan 1 and PPC Durabilla 1 wells (red circled areas in Fig. 37a), the formation pressure measurements are compared to a freshwater hydrostatic gradient. In these cases, the reported values are underpressured relative to the gradient and should be higher. This provides more confidence in the interpretation because these areas represent groundwater highs using the underpressured values (Figs 37a).

The formation pressures used to illustrate the hydraulic relationships between the Precipice Sandstone and the Hutton Sandstone fall into the reliable and very reliable categories, apart from one data point (Figs. 34d). This level of data quality provides robust constraints on the interpretations. Analysis of pressure data from the Trelinga 1 petroleum well by Patchett (2006) implied hydraulic connection between the Precipice Sandstone, the underlying Triassic Showgrounds Sandstone and the overlying Evergreen Formation. The analysis of all the areas south of Trelinga 1 in the east of the Surat Basin show that vertical hydraulic communication between the Precipice and the overlying units is unlikely (Figs. 36b,c).

Formation water analyses from drill stem tests are of limited use for geochemical modelling, but provide important salinity information for fluid density calculations. All of the samples analysed from the eastern Surat Basin wells are fresh to low brackish and, therefore, permit the use of freshwater hydrostatic gradients for comparison. Formation pressures have been converted to equivalent freshwater hydraulic heads in wells that have pressure measurements in multiple formations (Fig. 35). These interpretations show similar relationships to the traditional pressure/depth plots (Fig. 34). A significant finding is that, in the event that hydraulic communication between the units was apparent, flow would be down from the Hutton Sandstone and Evergreen Formation into the underlying Precipice Sandstone. This disagrees with previous interpretations of vertical flow, which suggest upward movement of groundwater (e.g. Habermehl, 1980).

Spatial flow patterns show that upward flow may take place in deep regions of the basin as suggested by Hitchon and Hays (1971). The regional model proposed by these authors implies vertical communication with the underlying Triassic units of the Bowen Basin. This hypothesis is a generalisation, but it is clearly evident that vertical hydraulic communication is apparent in some area and not others. Regions of the basins that show a lack of vertical communication are extensive and form large sub-regional areas within the overall flow domain of the GAB. Detailed work in the Wunger Ridge area of the Roma shelf beneath the Surat Basin has shown that there is little if any hydraulic communication between the Triassic and overlying Jurassic units (Hennig et al., 2006). In this area the Snake Creek Mudstone at the base of the Moolayember Formation provides a laterally extensive conventional seal above the permeable Showgrounds Sandstone. The Snake Creek Mudstone does not persist across the whole extent of the Surat Basin and, although the Moolayember Formation is also dominated by low permeability, there may be areas where low magnitude flow between the Triassic and Jurassic units occurs.

Most previous studies have considered the stacked aquifer/aquitard systems in the Eromanga and Surat basins as a regional continuum for groundwater flow assessment (e.g. Habermehl, 1980; Hitchon and Hays, 1971). For the purposes of assessing the suitability of an aquifer for CO_2 geostorage, the sub-regional scale systems and their interrelationships must be taken into consideration. The south directed flow component in the Precipice Sandstone aquifer (Figs. 37a,b) needs to be further constrained with additional data and flow velocities estimated. The hydrostatic conditions postulated for the central region also need to be clarified. If the hydrodynamics are favourable for these regions, there is the possibility of exploiting southward verging 'nose' structures for geostorage. Further assessment of the topographic flow components leading to 'quasi-stagnant' pools in the groundwater systems suggested by Hitchon and Hays (1971) also need to be verified.

The flow interpretations provided in this study are static models based on data gathered in the 1960s and, although additional information can be collected from groundwater bores, additional data cannot be obtained for the petroleum wells. Elements of these interpretations are, however, valid for the groundwater systems in their current state. The vertical hydraulic relationships will not have changed and effort needs to be focused on establishing the rate of movement across identified boundaries, which may be 'leaky' over long time periods. The effective sealing capacity also needs to be quantified on the basis of CO_2/water relative permeability and capillary pressure characteristics. The hydraulic significance of faults also needs to be established. The post-production state of the system will be assessed in the future using additional formation test data; the study in the Wunger Ridge area (Hennig et al., 2006) will be used as a benchmark for this work.

Oil production from the Eromanga Basin presents greater complications for post-production characterisation than in the Surat Basin. Hydrocarbon exploitation from the Surat Basin is restricted to small fields on the eastern flanks and the radius of influence is likely to be small. This allows the combination of pre-production data with new measurement from wells in areas that are not affected by production effects. Constraining hydrodynamics in the Eromanga Basin is more complex; many of the formation tests provide data for oleostatic gradients and radii of influence from oil production will be much larger than in the Surat Basin.

Potential Targets and Associated Impacts

General

This section discusses the potential carbon geostorage targets in the Surat and Eromanga Basins, and the possible impacts of carbon geostorage in the deep regions of freshwater aquifers. The suggested impacts include some speculative arguments, being based on preliminary interpretations of limited datasets. Far more data are required and a considerable modelling effort is needed to determine the potential perturbation of the systems subject to large-scale CO_2 injection.

The most appealing targets for carbon geostorage are the aquifers of the Precipice Sandstone in the Surat Basin and the Precipice Sandstone, Poolowanna Formation and Hutton Sandstone in the Eromanga Basin. The Hutton Sandstone in the Surat Basin is a less favourable injection target, because it would predominantly rely on the overlying Walloon Subgroup as an unconventional seal. Although the Walloon Subgroup provides additional security, in the event that CO_2 injected into the Precipice Sandstone leaks through the Evergreen Formation, its capacity to inhibit the vertical migration of free-phase CO_2 is not currently proven. In addition, the extensive dewatering programs associated with coal seam gas operations and the impact of underground coal gasification exploiting the Walloon Subgroup coals will have to be considered in any assessment for carbon geostorage.

Resource conflicts in the Surat Basin are predominantly with groundwater used for municipal supply and agriculture. The extensive hydrocarbon exploitation in the Eromanga Basin presents an added resource conflict. The substantial exploration efforts made in the Eromanga Basin provide tighter constraints on the distribution of reservoir quality and the extent of sealing lithology. The large number of wells does, however, equate to greater remediation costs to prevent leakage through breached seals and degraded cement plugs. There are substantial areas of the deep Surat Basin which remain unexplored and interpretations of reservoir/seal and aquifer/aquitard properties are highly subjective and purely model-driven in these regions.

There is enough evidence to indicate that a regional seal exists above the Precipice Sandstone, over a large area in the east of the Surat Basin. Data from the Trelinga 1 petroleum exploration well suggests that this regional seal pinches out to the north (Patchett, 2006). Interpreted flow patterns in

the Precipice Sandstone, in this region, show southward directed flow towards the Leichhardt oil field (Fig. 37a). Evidence from petroleum wells in this area indicates adequate sealing potential in the upper Precipice Sandstone and lower Evergreen Formation. Groundwater force potential from the north is low, due to the low hydraulic gradients. This has two potential effects: hydrodynamic forcing may not be of great enough magnitude to contain a large CO_2 plume migrating north under buoyancy forces; injection pumping stress has the potential to reverse the hydraulic gradient and induce up-dip groundwater flow (Nicot, 2008).

Small isolated petroleum and conventional gas style traps have the potential to store small volumes of CO_2 without influencing the regional groundwater flow patterns, as long as pumping stress is not excessive. It is important to understand, however, that these low aspect ratio structural closures are still part of the regional groundwater system and are not isolated traps. Injection of CO_2 will displace groundwater into the surrounding aquifers and, unlike hydrocarbons, a significant proportion of dissolved CO_2 could be transported with the displaced groundwater. It should be noted, however, that the dissipation of dissolved CO_2 across the dual fluid phase boundary would likely be dominated by chemical diffusion, which is a very slow transport mechanism. The much larger traps in the Eromanga Basin should provide a much lower risk of discharge of CO_2 charged groundwater, but this would depend on the magnitude of injection activity and storage availability is dependent on hydrocarbon depletion.

The area in the central Surat Basin that may be hydrostatic could offer the opportunity for very large scale carbon geostorage. Limited well control in this region precludes anything more than a poorly constrained hypothesis regarding the hydrogeology. Reversal of the groundwater flow vectors would not necessarily result in resource contamination. The induced pressure gradients would probably cause an increase in hydraulic head in many groundwater bores over 100 km from the injection site, and advective migration of both free and dissolved CO_2 could take place towards groundwater abstraction areas. The rate of migration and the effects of reactive transport in this scenario are crucial to understanding the potential risks of contamination. The low velocity of groundwater flow and the dilution effects of the surrounding groundwater, coupled with water-rock reaction are key factors in controlling the effects of CO_2 migration. The current level of knowledge, however, does not allow for definitive conclusions on these fundamental issues.

Abstraction pumping stress must also be considered as an influence on localised hydraulic gradients. Significant draw-down in a groundwater bore field could induce an artificial gradient enhancing the force potential towards the bores. Vertical hydraulic gradients could also be reversed under injection stress. The downward vertical flow gradients identified in the eastern Surat Basin could be reversed in the vicinity of a CO_2 injection field. This may not present a problem if the overlying seal capacity is adequate and able to physically and chemically contain the CO_2 column. The preferred option for the location of an injection well field would be in the deeper regions of the aquifer, in a concentrated zone, with a proven regional seal of adequate lateral extent. In the case where the vector of plume migration corresponds with the direction of groundwater advection, the low flow velocities would assist in retarding free-phase and dissolved CO_2. The principle CO_2 immobilisation mechanism would most likely be dissolution trapping (Gilfillan et al., 2009), relying on groundwater alkalinity to buffer pH. The injection methodology could also be designed to maximise capillary and relative permeability hysteresis trapping, by adapting water alternating gas injection techniques (e.g. Spiteri and Juanes, 2006) to immobilise CO_2 as a residual non-wetting phase.

The trends in groundwater composition and the results of the basic geochemical simulations carried out in this study show that the acid neutralising capacity in most areas of the GAB is large. The extreme near-well compositional changes to both the groundwater and the aquifer media are, therefore, unlikely to persist beyond a short distance from the injection point. The 1 molar CO_2 concentrations used in the static simulations are also at maximum solubility, which would not be the case across a large area including distal regions from an injection well field. The experimental data for the solubility of CO_2 in Na-HCO_3 solutions is lacking. The results of published simulations in chloride-rich waters must, therefore, only be used as approximations of CO_2 behaviour in the Surat and Eromanga basins (e.g. Gunter et al., 2000; Portier and Rochelle, 2005; Zhang et al., 2009). The potential dual/multi-phase fluid flow pathways need to be constrained on a site-specific basis, to asses the migration patterns of a free CO_2 phase.

Case Scenarios

Case 1 (best case scenario) assumptions:
Effective regional seal
Favourable hydrodynamics
High acid neutralising capacity
Injection field location remote from groundwater and hydrocarbon production operations

This scenario provides for good vertical containment, high sweep efficiency, slow lateral migration of free-phase CO_2 and CO_2-charged groundwater and effective buffering of acidity. In the case where the overlying seal capacity is exceeded and vertical CO_2 migration takes place, the high alkalinity of the groundwater in the overlying aquifers would mitigate any detrimental effects on water quality, due to low volume contamination. In the case where pressure effects enhanced or reversed fluid flow towards groundwater production bores, a remote injection location at depth would allow for effective dissolution trapping and buffering, and residual trapping prior to reaching the bore-field. The impacts on natural discharge springs and agricultural activities would be very low to negligible under these conditions. Hydrocarbon resources are also unlikely to be affected detrimentally under these conditions, due to the small volumes of escaping CO_2.

Case 2 (worst case scenario) assumptions:
Leaky regional seal
Unfavourable hydrodynamics
High acid neutralising capacity
Injection field proximal to existing groundwater and hydrocarbon production operations

Scenario 2 takes into account the uncertainty regarding regional seal continuity and less favourable hydrodynamics, but still incorporating the high acid neutralising capacity apparent over most of the basin area. Rapid vertical migration of free-phase CO_2 and CO_2-charged fluids through discontinuities in the sealing lithology presents significant problems. If the volume of released fluid is of low density (e.g. free CO_2) and rises rapidly under buoyancy forces, overlying resources will be contaminated. Groundwater that contains a high dissolved CO_2 load, however, has a greater density than uncontaminated groundwater, which would negate the buoyancy effects and inhibit vertical migration. The high buffering capacity of the groundwater in most areas of the GAB is likely to be able to naturally remediate significant volumes of contaminated groundwater, if the distance between injection and abstraction sites is great enough, both vertically and horizontally. Close proximity to at risk resources dramatically reduces the trapping potential prior to the contamination threshold.

If the hydrodynamic conditions are reversed, enhancing the lateral migration of both free CO_2 and CO_2-charged groundwater towards abstraction areas, the distance factor still largely controls the impacts. The low hydraulic gradients in both the Surat and Eromanga Basins would still be the principle control on groundwater flow velocity, unless injection pumping rates were excessively high in close proximity to the basin margins. The situation would be potentially very damaging for natural environments and agriculture. Large areas of forest have been destroyed in the United States because of excessive soil CO_2 concentrations resulting from degassing magma bodies at depth. Groundwater dependent ecosystems associated with discharge areas would also be at high risk and it is likely that remediation measures would not be effective in dealing with widespread groundwater contamination. In the case of CO_2 leaking into an existing oil or gas field, the economic impact is dependent on the existing operation. In situations where existing infrastructure has not been designed to cope with CO_2 charged fluids, the impacts could be prohibitively costly to remediate. Where CO_2 stripping operations are already in place, additional CO_2 could be dealt with without significant impact, as long as the hydrocarbon to CO_2 production ratio remained manageable.

Rapid vertical migration of low density CO_2-rich fluid presents the highest risk to overlying hydrocarbon reservoirs and aquifers exploited for irrigation and municipal supply. Rapid lateral migration would potentially provide the greatest risk to natural discharge springs and shallow groundwater dependent ecosystems. Underground and open pit mining operations and groundwater bore fields located on the margins of the basins could also be at risk from lateral migration of CO_2 into shallow regions of the aquifers. The key factor controlling the potential detrimental impacts of carbon geostorage is distance, both vertically and horizontally. After initial primary trapping, the effectiveness of secondary trapping mechanisms in aquifers is predominantly time-dependent. The low lateral groundwater flow velocities in the Surat and Eromanga basins provide an environment where timescales are great enough for secondary CO_2 trapping to take place on a large scale, if vertical migration can be sufficiently inhibited.

Economic implications

Any CO_2 storage and injection strategy must include a detailed risk analysis, including economic impacts of loss of containment. However, without detailed economic analysis, it is not possible to provide anything more than general approximations regarding the financial impacts associated with CO_2 contamination. Naturally occurring, slightly acidic, CO_2-laden groundwater is currently used in some areas of the GAB for irrigation and stock watering. The passage of naturally carbonated water in the shallow sub-surface is not necessarily detrimental to agricultural practices; however, excessive buildup of CO_2 in the soil horizon is very damaging and potentially irreversible. The latter situation would render crop production untenable and effectively sterilise grazing land. Damage to groundwater dependent ecosystems is dependent on the current environmental conditions (presence of CO_2 or not) and the ability of a system to naturally mitigate change.

In the event that groundwater becomes corrosive but remains useable, a groundwater bore completed with standard casing has to be plugged and abandoned and a new well drilled. The cost of a new groundwater bore of 500 m depth, with inert casing (fibre-glass or stainless steel) in a remote area is approximately $500,000 at current prices (pers. comm. J. Dingley and I. Hair, 2009). The cost of drilling rig mobilisation is up to $100,000 for remote areas, although this can be substantially reduced if multiple groundwater bores are required in the same area. The costs of remediating hydrocarbon production infrastructure are orders of magnitude greater than for groundwater abstraction. Unless a producing field is highly profitable, an oil or gas production facility could be shut down because of CO_2 contamination.

Appropriate early warning monitoring systems would need to be put in place to protect the agricultural industry, the natural environment, groundwater resources, mining operations and hydrocarbon resources. Groundwater observation bore networks are currently the most effective method of monitoring subsurface fluid flow and contamination. The configuration of such a network would be dependant on high quality geological and hydrological modelling to predict the rate and direction of movement of the CO_2 plume and the identification of key aquifers to monitor. This would enable optimisation of the number and type of bores required. Areas of high risk (such as faults or old wells) may require extra monitoring. Post-injection the behaviour of the CO_2 plume would need to be calibrated seismically, however, the high cost of seismic surveys are likely to limit its usefulness as a long term sentinel monitoring system. Although the cost of such networks can be high because of the number of bores required, they represent the most cost effective form of long term sentinel monitoring for injected CO_2, either trapped or migrating slowly under buoyancy.

A large monitoring bore network may consist of 50 to 100 sample points of 100 to 200 m depth. Inert casing is currently priced at approximately $400/m and drilling costs range between $200/m and $400/m, depending on depth required and rig size. The estimated cost of completing a network of this scale is $700,000 to $1 million including drilling rig mobilisation. Installation of a wireless telemetry network for remote monitoring purposes is estimated at $300-500,000. This estimate could increase substantially, if deeper wells and/or a higher density network are required.

Recent research shows that injection has far reaching effects on the pressure regime in a groundwater flow system (Birkholzer et al., 2009; Nicot, 2008). If a monitoring well network (or other observation method such as seismic surveys) identifies unexpected migration of CO_2, the injection well field could be shut down and the pressure conditions would re-equilibrate. The main force driving the plume migration would be removed, with the potential to slow down or halt the injected CO_2. Over time, this static plume would dissolve into the surrounding groundwater and the natural system hydrodynamics would prevail. A similar hypothesis can be postulated for the use of pressure-release bores, but there is currently a lack of published research to substantiate this as an effective mitigation strategy for carbon geostorage. Many natural systems take extensive time periods to revert back to a pre-disturbed state and the effects of an induced change may persist for longer than expected. This factor should not be underestimated in the design of large scale contamination mitigation strategies.

Conclusions

The Surat and Eromanga basins show promising characteristics for both short-term (small to medium volume) and long-term (very large volume) carbon geostorage. Some parts of the basin can be excluded as unsuitable, for example, near the basin margins where the target aquifers are too shallow to contain supercritical CO_2. However, there are large parts of the basin where the geochemistry, the hydrogeology and the geology may be suitable to store large volumes of CO_2. This report illustrates what can be achieved with the currently available open file datasets and discusses the limitations as a consequence of data gaps. A conceptual model is presented in Figure 42 and a summary of findings in Table 3.

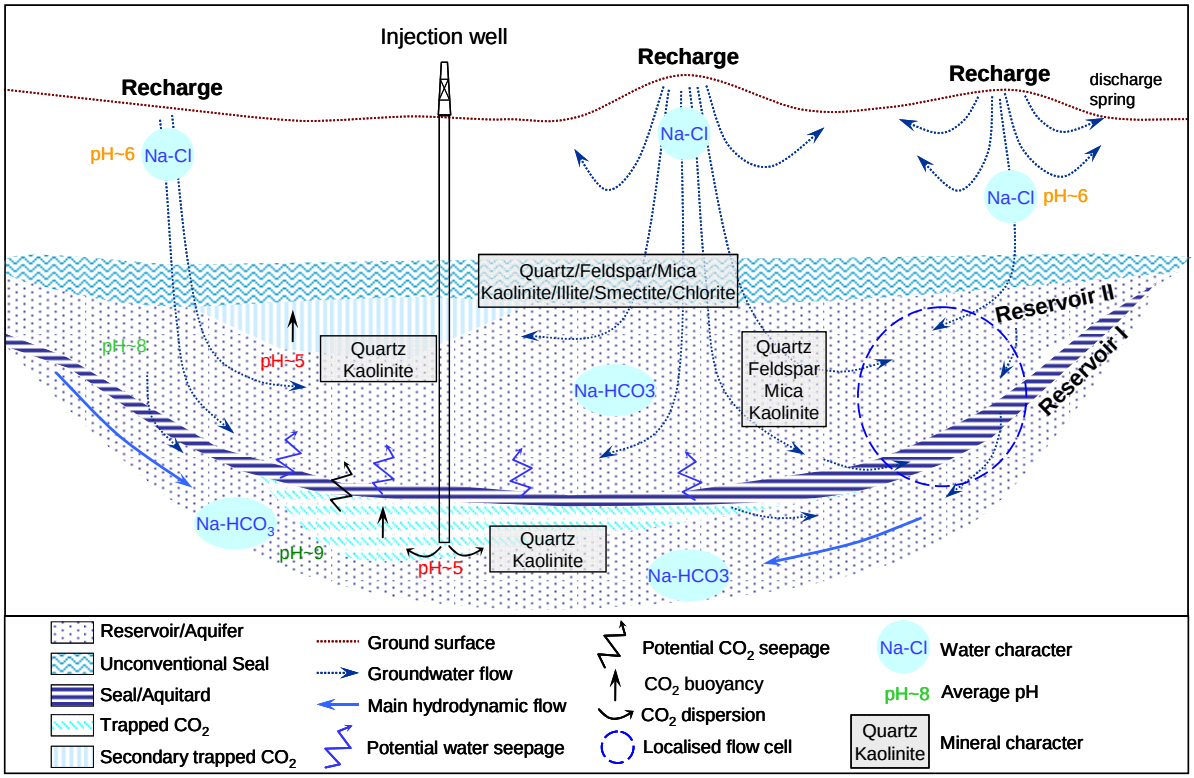

Figure 42. Conceptual model of a multi-reservoir – conventional/unconventional seal system, similar to the Precipice-Evergreen (conventional regional seal) / Hutton-Walloon (unconventional regional seal) reservoir/seal pairs. The recharge water is slightly acidic and of Na-Cl type, while the deeper groundwater is alkaline and of Na-HCO_3 type. The reservoirs/aquifers are largely quartz-rich ± feldspar ± mica, while the seals/aquitards are clay-rich. Opposite flow patterns due to topographic highs can create localised flow cells. Injection of CO_2 will dissolve most mineral phases and lower the pH; the mineral matrix will be dominated by quartz and kaolinite, with short-lived carbonate phases (e.g. dolomite). Favourable hydrodynamics assist in limiting vertical and horizontal migration of the CO_2 plume; however, injection pressure induced reversal of the hydraulic gradient could reduce the effectiveness of the retardation mechanism.

Table 3. Comparative summary

Basin	Eromanga	Surat
Basin structure	long wave-length antiform/synform pairs	one major axial synform, plus large wavelength open faults on flanks
Major fault distribution	central area	generally restricted to flanks
Potential carbon storage units	**Lower Poolowanna Formation, Precipice Sandstone and Hutton Sandstone**	**Precipice Sandstone and Hutton Sandstone**
Potential regional seals	Upper Poolowanna Formation and Birkhead Formation	Evergreen Formation and Walloon Subgroup
Number of bores	> **11,000** bores recorded	> **11,000** bores recorded
Available information	~ **4400** bores (40%) have reliable information on aquifer formation, depth and flow regime	~ **5300** bores (48%) have reliable information on aquifer formation, depth and flow regime
Bore status	~ **2100 artesian bores** (49%) ~ 2300 sub-artesian bores (51%)	~ **1200 artesian bores** (23%) ~ 4100 sub-artesian bores (77%)
Main Jurassic aquifers	**Hutton Sandstone** with more than 700 bores, followed by the Ronlow beds and Adori Sandstone	**Gubberamunda Sandstone** with almost 700 bores, followed by Walloon Subgroup, Evergreen Formation and Precipice Sandstone
Main Cretaceous aquifers	**Hooray Sandstone** with almost 1400 bores, followed by Wallumbilla and Gilbert River formations	**Mooga Sandstone** with almost 1200 bores, followed by Bungil Formation
Other aquifers	~ 150 bores in older and younger units (e.g. Quaternary alluvium)	~ 600 bores in older (e.g. Clematis Group and Moolayember Formation) or younger units (e.g. Quaternary alluvium and Tertiary basalt)
Number of chemical analyses	~ 5700 available water analyses ~ **3800** samples from the units of interest - **Hooray Sandstone** ~ 2300 analyses - Hutton Sandstone ~ 1000 analyses - Wallumbilla and Wyandra formations ~ 600 to 400 analyses, respectively - Gilbert River, Adori and Longsight formations ~ 200-300 analyses each - Precipice, Birkhead, Westbourne, Toolebuc and Winton formations are poorly represented	~ 4500 available water analyses ~ **3700** sample the units of interest - **Mooga Sandstone** ~ 1500 analyses - Gubberamunda Sandstone and the Walloon Subgroup ~ 500 analyses each - Precipice Sandstone ~ 300 - Bungil Formation ~ 230 - other formations of interest ~ 100 analyses or less - Orallo Sandstone - 6 analyses
pH	**8 - 8.6** (66% of samples); circumneutral waters occur in the north, close to recharge areas. A small proportion is either very acid or very alkaline (Table 2)	**8 - 8.6** (62% of samples); circumneutral waters occur in the north, close to recharge areas. A small proportion is either very acid or very alkaline (Table 2)
Alkalinity	~ **500 mg/L** (64% of samples), with a small number of outliers in the order of thousands of mg/L; the Hutton and Hooray waters tend to have the highest neutralising capacity (Table 2)	~ **500 mg/L** (44% of samples), with a small number of outliers in the order of thousands of mg/L; the Walloon and Hooray waters tend to have the highest neutralising capacity (Table 2)
Mineralogical samples (X-ray diffraction)	basal Jurassic (equiv. Precipice), Hutton, Birkhead, Westbourne and Hooray	no data
Mineralogical composition	major constituent is **quartz**, which is around 80% in the basal Jurassic, Hutton and Hooray, and decreases to 50-60% in the Birkhead and Westbourne; minor **mica** is present in all units, while chlorite, calcite, dolomite, pyrite and salt occur as occasional traces. The dominant clay mineral is **kaolinite**, followed by **illite-dominated mixed layers illite/smectite**. Feldspars (largely plagioclase) are sparsely found in the Hutton and Hooray, but increase in concentration (around 10%) in the Birkhead and Westbourne	major constituent is **quartz**, which is around 80% in the basal Jurassic and Hutton, and decreases to 50-60% in the Birkhead and Westbourne; minor **mica** is present in all units, while chlorite, calcite, dolomite, pyrite and salt occur as occasional traces. The dominant clay mineral is **kaolinite**, followed by **illite-dominated mixed layers illite/smectite**. Feldspars (largely plagioclase) are sparsely found in the Precipice and Hutton, but increase in concentration (around 10%) in the Birkhead and Westbourne
Water character	largely **Na-HCO_3** (Table 2), with the exception of Westbourne and Wallumbilla, which are Na-Cl. Ronlow has a mixed character (neither type is dominant)	largely **Na-HCO_3** (Table 2), with the exception of Walloon and Wallumbilla, which are Na-Cl. Westbourne and Bungil have a mixed character
Major cations	**Na** (often present in concentrations much larger than any other cation), followed by Ca, Mg, with very little K. Other cations such as Fe, Mn, Zn and Al are occasional; no particular pattern of distribution has been observed	
Major anions	**HCO_3**, followed by Cl; SO_4 is always minor	
Water character *vs* depth	shallower water tends to be Na-Cl type, with the HCO_3 character becoming prominent with depth	
Hydrodynamic flow (preliminary findings)	generally towards the centre of the basin, but with localised cells of opposite flow (based on groundwater data for the Hutton Sandstone and Hooray Sandstone at shallow depths)	potential divide separating northward and southward flows (based on groundwater and petroleum data from the deeper regions of the basin for the Precipice Sandstone, Evergreen Formation and Hutton Sandstone)

At the regional scale, a number of simplifying assumptions can be made with regard to the expected behaviour of the groundwater system, in response to stress induced by the injection of CO_2. Major ion hydrochemical signatures are predominantly of uniform Na-HCO_3 type throughout the basin, with the exception of the shallow regions proximal to the basin margins. Groundwater in the Walloon Subgroup, Westbourne Formation, Bungil Formation and Wallumbilla Formation is of Na-Cl type and vertical mixing between the overlying and underlying units appears nominal. The preliminary results of equilibrium speciation modelling and geochemical reaction path modelling indicate that the acid buffering capacity of the groundwater is large. This concurs with the mainly high pH and alkalinity measurements collected across the GAB. Simulation results also suggest that the groundwater systems have the capacity to naturally remediate the induced low pH conditions resulting from CO_2 injection.

Extrapolation of mineralogical data across the basins shows favourable mineral stability characteristics in the sandstones of the principle storage targets. Mineral stability modelling and water-rock reaction simulations suggest that the compositions of the Precipice Sandstone and the Lower Poolowanna Formation would be the least affected by carbon storage activities. The Hutton Sandstone and some of the shallower prospective geostorage units in the Eromanga Basin have a less stable mineral composition. The aquifer media in these units is predicted to evolve to a mineralogical composition similar that of the Precipice Sandstone in close proximity to the injection wells.

The interpretations of hydrodynamic data show that the aquifers of the Precipice Sandstone in the Surat Basin operate independently of the underlying and overlying groundwater systems over a large area. Combination of formation pressure data from petroleum wells with potentiometric head data from groundwater bores suggests that a number of groundwater divides and subsurface confluence areas exist within the Precipice Sandstone. Further data assessment is required prior to the construction of a similar model for the Eromanga Basin. The preliminary results of this study show that the continuum model of Hitchon and Hays (Hitchon and Hays, 1971) is not likely to be appropriate for the assessment of carbon geostorage in the Surat Basin. The resolution of published regional flow models for the GAB (Habermehl, 1980; Radke et al., 2000) is too coarse for carbon geostorage assessment purposes and also assumes a high level of vertical connectivity between aquifers. In addition only the Hooray Sandstone and equivalent aquifers are explicitly modelled in these groundwater flow studies. Additional data and further interpretations are required to put tighter constraints on the interrelationships between the stacked aquifers and aquitards in both basins.

The location of carbon geostorage injection well fields relative to existing resource and environmentally sensitive areas is critical to the mitigation of detrimental contamination effects. In the short-term the seal capacity of aquitards overlying the target aquifers needs to be great enough to inhibit the vertical migration of free-phase CO_2. The long-term effects of injection-induced pressure wave propagation need to be modelled to predict the potential changes in the hydrodynamic regime and the consequent effects on CO_2 plume migration. The prevailing hydrodynamic regime will dictate the volume of CO_2 that can be safely stored in the long-term, without negative impacts on groundwater resources, hydrocarbon production, mining operations and groundwater-dependent ecosystems.

The cost of remediation strategies for damage to existing infrastructure resulting from CO_2 contamination could be prohibitive. Environmental impacts could be severe but remain speculative and cannot be quantified with currently available information. It should be considered, however, that the severe near-well changes to the groundwater system are most likely to be restricted to a limited radius from the injection well. A combination of high acid buffering capacity, low fluid flow velocities and high groundwater residence times would contribute to a high level of confidence in an adequate safety margin, if injection well fields are sited correctly.

Future work

This study shows that significant efforts need to be made in gathering new data, assessment and quality control of existing datasets and in modelling the potential behaviour of systems perturbed by the injection of CO_2. The current and future QCGI program includes the following:

Drilling and new data collection program

A proposal has been submitted for the drilling of several deep fully cored wells in the Surat, Eromanga, Bowen and Galilee basins. Selected sites will also have a number of shallower wells drilled to form a 'nested' bore network for subsequent groundwater monitoring. Extensive formation pressure testing is to be included in the program, in addition to comprehensive wireline logging of the intersected formations. Sampling techniques will be adapted to recover uncontaminated formation water samples during the drilling program and the wells will subsequently be completed as deep peizometers for the collection of time-series data.

Regional basin modelling

A 3D regional geological model of the Surat Basin is in the early stages of development. Interpolated seismic horizons tied to petroleum and groundwater bore data have been used as the basis of the model. Seismic profiles and well data are being integrated to interpret the fault systems in the basin, the aim being to produce a coarse scale regional block model for the interpretation of aquifer/aquitard and reservoir/seal geological relationships.

Hydrodynamic analysis

Quality control of formation pressure data from petroleum wells using the CSIRO PressureQC™ methodology will continue to focus on the Surat Basin and will subsequently be extended to the Eromanga Basin. This information will be used to improve the initial hydrodynamic models to further constrain the regional groundwater flow regimes. New information to be collected as part of the CGI data collection program will also be incorporated into the models. The 2D flow vector interpretations will be integrated with the 3D regional geological model to produce a 3D hydrodynamic model of the Surat Basin. This work is to be carried out in collaboration with CSIRO Petroleum.

Mineralogical and geochemical analysis

Core retrieved from the Geological Survey stratigraphic drilling program will be slabbed and samples taken for mineralogical and geochemical analysis using: X-ray diffraction, X-ray fluorescence and scanning electron microscopy techniques. This will provide accurate mineral compositions for the units of interest in the Surat Basin and will be used to model water-rock reactions and mineral stability for specific sites. Laboratory experiments are planned to establish the reaction rates of minerals for kinetic geochemical modelling studies. It is also necessary to assess the solubility characteristics of CO_2 in Na-HCO_3 fresh groundwater.

Groundwater sampling and analysis

A groundwater sampling and analysis plan will be conducted in collaboration with the Department of the Environment and Resource Management and Geoscience Australia. The controlled sampling program will target a broad range of dissolved ions and elemental isotopes to provide a dataset for hydrochemical and geochemical modelling. Sample sites will be selected in close proximity to previously drilled stratigraphic bores, to provide groundwater samples that are representative of the regions for which aquifer/aquitard media samples are available. This will provide the basis for well constrained models of the potential water-rock interaction resulting from carbon geostorage.

Geochemical modelling

The basic modelling carried out as part of this study forms the basis for future advanced simulations, which will be used to explore the limits of applying equilibrium approaches. Subsequent modelling work will also incorporate chemical reaction rate laws to illustrate the timescales associated with water-rock interaction. Reactive transport modelling is also planned to examine the spatial impact of near-well effects on the aquifer/aquitard media and associated groundwater.

Acknowledgements

We would like to acknowledge the contribution made by Ross Lane, Paula Deacon and Gina Nuttall of the Geological Survey Graphical Services Unit, for their assistance with the illustrative content. We would also like to express our thanks to John Dingley of JD Drilling Services and Iain Hair of Douglas Partners for their guidance on groundwater bore remediation strategies and the associated costs of specialist completions needed in corrosive environments.

References

Ainsworth, B., Allinson, G., Berly, T., Causebrook, R., Chirinos, A., Cinar, Y., Cook, P.J., Dance, T., Daniel, R., Dodds, K., Esterle, J., Faiz, M., Funnell, R., Gibson-Poole, C., Golab, A., Gurba, L., Hennig, A., Kaldi, J.G., Kirste, D., Paterson, L., Sherlock, D., Tingate, P., Underschultz, J., Vakarelov, B., van Ruth, P., Watson, M. and Werner, M., 2008. Storage capacity estimation, site selection and characterisation for CO_2 storage projects. RPT08-1001, CO2CRC, Canberra, 1-51 pp.

Anderson, G., 2005. Thermodynamics of natural systems second edition. Cambridge University Press, Cambridge, U.K.

Bachu, S., 1995a. Flow of variable-density formation water in deep sloping aquifers: review of methods of representation with case studies. Journal of Hydrology, 164(1-4): 19-38.

Bachu, S., 1995b. Synthesis and model of formation-water flow, Alberta Basin, Canada. AAPG Bulletin, 79(8): 1159-1178.

Bachu, S., 2000. Sequestration of CO_2 in geological media: criteria and approach for site selection in response to climate change. Energy Conversion and Management, 41(9): 953-970.

Bachu, S., 2002. Sequestration of CO_2 in geological media in response to climate change: road map for site selection using the transform of the geological space into the CO2 phase space. Energy Conversion and Management, 43(1): 87-102.

Bachu, S. and Adams, J.J., 2003. Sequestration of CO_2 in geological media in response to climate change: capacity of deep saline aquifers to sequester CO_2 in solution. Energy Conversion and Management, 44(20): 3151-3175.

Bachu, S. and Bennion, B., 2008. Effects of in-situ conditions on relative permeability characteristics of CO_2-brine systems. Environmental Geology, 54(8): 1707-1722.

Bachu, S., Bonijoly, D., Bradshaw, J., Burruss, R., Holloway, S., Christensen, N.P. and Mathiassen, O.M., 2007. CO_2 storage capacity estimation: Methodology and gaps. International Journal of Greenhouse Gas Control, 1(4): 430-443.

Bachu, S., Gunter, W.D. and Perkins, E.H., 1994. Aquifer disposal of CO_2: Hydrodynamic and mineral trapping. Energy Conversion and Management, 35(4): 269-279.

Bachu, S. and Michael, K., 2002. Flow of variable-density formation water in deep sloping aquifers: minimizing the error in representation and analysis when using hydraulic-head distributions. Journal of Hydrology, 259(1-4): 49-65.

Baker, J.C., Kassan, J.P. and Hamilton, J., 1995. Early diagenetic siderite as an indicator of depositional environment in the Triassic Rewan Group, southern Bowen Basin, eastern Australia. Sedimentology, 43(1): 77-88.

Beaucaire, C., Michelot, J.L., Savoye, S. and Cabrera, J., 2008. Groundwater characterisation and modelling of water-rock interaction in an argillaceous formation (Tournemire, France). Applied Geochemistry, 23(8): 2182-2197.

Bénézeth, P., Palmer, D.A., Anovitz, L.M. and Horita, J., 2007. Dawsonite synthesis and reevaluation of its thermodynamic properties from solubility measurements: implications for mineral trapping of CO_2. Geochimica et Cosmochimica Acta, 71(18): 4438-4455.

Bermejo, M.D., Martín, A., Florusse, L.J., Peters, C.J. and Cocero, M.J., 2005. The influence of Na_2SO_4 on the CO_2 solubility in water at high pressure. Fluid Phase Equilibria, 238(2): 220-228.

Bethke, C.M. and Yeakel, S., 2007. The Geochemist's Workbench release 7.0 collection of manuals. Rockware Inc., Golden, CO.

Birkholzer, J.T., Zhou, Q. and Tsang, C.-F., 2009. Large-scale impact of CO_2 storage in deep saline aquifers: A sensitivity study on pressure response in stratified systems. International Journal of Greenhouse Gas Control, 3(2): 181-194.

Brown, A., 2003. Improved interpretation of wireline pressure data. AAPG Bulletin, 87(2): 295-311.

Carmichael, D.C., 1989. The mineralogy of the Hooray Sandstone, Westbourne Formation, Birkhead Formation, Hutton Sandstone and the 'basal Jurassic' unit in the southern Eromanga Basin, Queensland. Record 1989/7, Geological Survey of Queensland, Brisbane, 102 pp.

Chebotarev, I.I., 1955. Metamorphism of natural waters in the crust of weathering. Geochimica et Cosmochimica Acta, 8: 22-48.
Chiquet, P., Broseta, D. and Thibeau, S., 2007. Wettability alteration of caprock minerals by carbon dioxide. Geofluids, 7(2): 112-122.
Cinar, Y., 2006. Reservoir simulation of CO_2 in Wunger Ridge Fields, SE Queensland. RPT06-0124, Cooperative Research Centre for Greenhouse Gas Technologies - CO2CRC, Canberra, RPT05-0225, 22 pp.
CSLF, 2007. Estimation of CO_2 storage capacity in geological media - phase II [online]. Prepared by the Task Force on CO_2 Storage Capacity Estimation for the Technical Group (RG) fo the Carbon Sequestraiotn leadership Forum (CSLF) [Bachu, S., Bonijoly, D., Bradshaw, J., Burruss, R., Christensen, N. P., Holloway, S. and Mathiassen, O. M.]. http://www.cslforum.org/documents/PhaseIIReportStorageCapacityMeasurementTaskForce.pdf.
Dahlberg, E.C., 1995. Applied hydrodynamics in petroleum exploration. Springer-Verlag, New York, 295 pp.
Daniel, R.F., 2008. Carbon dioxide seal capacity study, Wunger Ridge, Bowen-Surat Basin, southern Queensland, Australian School of Petroleum and Cooperative Research Centre for Greenhouse Gas Technologies - CO2CRC, Adelaide, 1-17 pp.
Davies, P.B., 1987. Modeling areal, variable-density, ground-water flow using equivalent freshwater head -- analysis of potentially significant errors, Proceedings of the NWWA-IGWMC conference - Solving groundwater problems with models. National Water Well Association Dublin, Denver, Colorado, pp. 888-903.
Debye, P.J., 1954. The collected papers of P. J. Debye. Interscience, New York.
Dhima, A., de Hemetime, J.C. and Moracchini, G., 1998. Solubility of light hydrocarbons and their mixtures in pure water under high pressure. Fluid Phase Equilibria, 145: 129-150.
Diamond, L.W. and Akinfiev, N.N., 2003. Solubility of CO_2 in water from -1.5 to 100 °C and from 0.1 to 100 MPa: evaluation of literature data and thermodynamic modelling. Fluid Phase Equilibria, 208(1-2): 265-290.
DOE, 2006. Carbon sequestration atlas of the United Staes and Canada: Appendix A - methodology for development of carbon sequestration capacity estimates [online]. National Energy Technology Laboratory, Department of Energy, http://www.netl.doe.gov/publications/carbon_seq/atlas.
Doughty, C., 2008. Estimating Plume Volume for Geologic Storage of CO_2 in Saline Aquifers. Ground Water, 46(6): 810-813.
Doughty, C., Benson, S.M., Pruess, K., Gale, J. and Kaya, Y., 2003. Capacity investigation of brine-bearing sands for geologic sequestration of CO_2, Greenhouse Gas Control Technologies - 6th International Conference. Pergamon, Oxford: 1645-1648.
Doughty, C., Freifeld, B. and Trautz, R., 2008. Site characterization for CO_2 geologic storage and vice versa: the Frio brine pilot, Texas, USA as a case study. Environmental Geology, 54(8): 1635-1656.
Draper, J.J., (Editor), Davies, C., Dingwell, J.A., Dixon, O., Gray, A.R.G., Green, P., Heim, A.L., Hoffmann, K.L., McKellar, J.L. and McKillop, M., 2002. Geology of the Cooper and Eromanga Basins, Queensland. ISBN 0 7345 2411 0, Geological Survey of Queensland, Queensland Department of Natural Resources and Mines, Brisbane, 85 pp.
Ennis-King, J. and Paterson, L., 2007. Coupling of geochemical reactions and convective mixing in the long-term geological storage of carbon dioxide. International Journal of Greenhouse Gas Control, 1(1): 86-93.
Ennis-King, J., Paterson, L., Gale, J. and Kaya, Y., 2003. Rate of dissolution due to convective mixing in the underground storage of carbon dioxide, Greenhouse Gas Control Technologies - 6th International Conference. Pergamon, Oxford: 507-510.
Exon, N.F., 1976. Geology of the Surat basin in Queensland, Bulletin 166. Australian Government Publishing Service, Canberra.
Exon, N.F. and Senior, B.R., 1976. The Cretaceous of the Eromanga and Surat Basins. Bureau of Mineral Resources Journal of Australian Geology and Geophysics, 1: 33-50.
Ezzy, T.R., Cox, M.E., O'Rourke, A.J. and Huftile, G.J., 2006. Groundwater flow modelling within a coastal alluvial plain setting using a high-resolution hydrofacies approach; Bells Creek plain, Australia. Hydrogeology Journal, 14(5): 675-688.
GABCC, 1998. Great Artesian Basin Resource Study, Great Artesian Basin Consultative Council, Brisbane, 236 pp.
GABCC, 2008. A research prospectus for the Great Artesian Basin, Great Artesian Basin Coordinating Committee, Brisbane, 15 pp.

Gallagher, K., 1990. Permian to Cretaceous subsidence history along the Eromanga-Brisbane geoscience transect: a guide to basin development across Phanerozoic Australia in southern Queensland. Bureau of Mineral Resources Bulletin(232): 133-151.
Gaus, I., Audigane, P., André, L., Lions, J., Jacquemet, N., Durst, P., Czernichowski-Lauriol, I. and Azaroual, M., 2008. Geochemical and solute transport modelling for CO2 storage, what to expect from it? International Journal of Greenhouse Gas Control, 2(4): 605-625.
Gaus, I., Azaroual, M. and Czernichowski-Lauriol, I., 2005a. Reactive transport modelling of the impact of CO_2 injection on the clayey cap rock at Sleipner (North Sea). Chemical Geology, 217(3-4): 319-337.
Gaus, I., Le Guern, C., Pearce, J., Pauwels, H., Shepherd, T., Hatziynnis, G., Metaxas, A., Rubin, E.S., Keith, D.W., Gilboy, C.F., Wilson, M., Morris, T., Gale, J. and Thambimuthu, K., 2005b. Comparison of long-term geochemical interactions at two natural CO_2-analogues: Montmiral (Southeast Basin, France) and Messokampos (Florina Basin, Greece) case studies, Greenhouse Gas Control Technologies 7. Elsevier Science Ltd, Oxford: 561-569.
Ghomian, Y., Pope, G.A. and Sepehrnoori, K., 2008. Reservoir simulation of CO_2 sequestration pilot in Frio brine formation, USA Gulf Coast. Energy, 33(7): 1055-1067.
Gibson-Poole, C.M., Root, R.S., Lang, S.C., Streit, J.E., Hennig, A.L., Otto, C.J., Underschultz, J., Rubin, E.S., Keith, D.W., Gilboy, C.F., Wilson, M., Morris, T., Gale, J. and Thambimuthu, K., 2005. Conducting comprehensive analyses of potential sites for geological CO_2 storage, Greenhouse Gas Control Technologies 7. Elsevier Science Ltd, Oxford: 673-681.
Gilfillan, S., Lollar, B.S., Holland, G., Blagburn, D., Stevens, S., Schoell, M., Cassidy, M., Ding, Z., Zhou, Z., Lacrampe-Couloume, G. and Ballentine, C., 2009. Solubility trapping in formation water as dominant CO_2 sink in natural gas fields. Nature, 458: 614-618.
Gray, A.R.G., McKillop, M. and McKellar, J.L., 2002. Eromanga Basin stratigraphy. In: J.J. Draper (Editor), Geology of the Cooper and Eromanga Basins, Queensland. Geological Survey of Queensland, Brisbane: 30-56.
Green, P.M., (Editor), Hoffmann, K.L., Brain, T.J., Gray, A.R.G., Murray, C.G., Carmichael, D.C., McKellar, J.L., Beeston, J.W., Price, P.L., Smith, M.D., McKillop, M., Craig, C.H., Newsome, R.W. and Boreham, C., 1997. The Surat and Bowen Basins South-East Queensland, Geological Survey of Queensland, Brisbane, 238 pp.
Green, P.M., Eadington, P.J., Hamilton, P.J. and Carmichael, D.C., 1989. Regional diagenesis - an important influence in porosity development and hydrocarbon accumulations within the Hutton Sandstone, Eromanga Basin. In: B.J. O'Neil (Editor), Proceedings of The Cooper and Eromanga Basins Conference. Petroleum Exploraitn Society of Australia, Society of Petroleum Engineers, Australian Society of Exploration Geophysicists, Adelaide, pp. 619-627.
Gunter, W.D., Bachu, S., Law, D.H.S., Marwaha, V., Drysdale, D.L., Macdonald, D.E. and McCann, T.J., 1996. Technical and economic feasibility of CO_2 disposal in aquifers within the Alberta sedimentary basin, Canada. Energy Conversion and Management, 37(6-8): 1135-1142.
Gunter, W.D., Perkins, E.H. and Hutcheon, I., 2000. Aquifer disposal of acid gases: modelling of water-rock reactions for trapping of acid wastes. Applied Geochemistry, 15(8): 1085-1095.
Gunter, W.D., Perkins, E.H. and McCann, T.J., 1993. Aquifer disposal of CO_2-rich gases: Reaction design for added capacity. Energy Conversion and Management, 34(9-11): 941-948.
Gunter, W.D., Wiwehar, B. and Perkins, E.H., 1997. Aquifer disposal of CO_2-rich greenhouse gases: Extension of the time scale of experiment for CO_2-sequestering reactions by geochemical modelling. Mineralogy and Petrology, 59(1): 121-140.
Habermehl, M.A., 1980. The Great Artesian Basin, Australia. Bureau of Mineral Resources Journal of Australian Geology and Geophysics, 5: 9-38.
Habermehl, M.A., 1986. Regional groundwater movement, hydrochemisty and hydrocarbon migration in the Eromanga Basin. In: D.I. Gravestock, P.S. Moore and G.M. Pitt (Editors), Contributions to the geology and hydrocarbon potential of the Eromanga Basin: Geological Society of Australia Special Publication, 12: 353-376.
Harbaugh, A.W. and McDonald, M.G., 1996. User's documentation for MODFLOW an update to the U.S. Geological Survey modular finite-difference groundwater flow model. Open file report 96-485, United States Geological Survey, Denver, CO, U.S.A., 56 pp.
Hellevang, H., Aagaard, P., Oelkers, E.H. and Kvamme, B., 2005. Can dawsonite permanently trap CO_2? Environ. Sci. Technol., 39(21): 8281-8287.
Hennig, A., 2005. A summary of the hydrogeology of the southern Eromanga and Surat Basins of the Great Artesian Basin. RPT05-0024, CO2CRC/CSIRO Petroleum, Perth, 11 pp.
Hennig, A., 2007. Hydrodynamic interpretation of the formation pressures in CRC-1: Vertical and horizontal hydraulic communication. RPT07-0626, CO2CRC, Canberra, 7 pp.
Hennig, A., Underschultz, J., Johnson, L., Otto, C. and Trefry, C., 2006. Hydrodynamic characterisation of the Triassic Showgrounds aquifer at the Wunger Ridge site in Queensland:

Assessing suitability for CO_2 sequestration. RPT06-0036, CO2CRC, Canberra, RPT05-0225, 1-25 pp.
Hennig, A., Underschultz, J. and Otto, C., 2003. Confidential report - A hydrodynamic analysis of hydraulic continuity and production effects of the Flag Formation of theBarrow Sub-basin for the storage of CO_2. Report No 03-03, APCRC, Canberra
Hitchon, B., 1969a. Fluid flow in the Western Canada Sedimentary Basin, 1. Effect of topography. Water Resources Research, 5(1): 186-195.
Hitchon, B., 1969b. Fluid flow in the Western Canada Sedimentary Basin, 2. Effect of geology. Water Resources Research, 5(2): 460-469.
Hitchon, B., Bachu, S. and Underschultz, J.R., 1990. Regional subsurface hydrogeology, Peace River Arch area, Alberta and British Columbia. Bulletin of Canadian Petroleum Geology, 38(A): 196-217.
Hitchon, B. and Hays, J., 1971. Hydrodynamics and hydrocarbon occurrences Surat Basin, Queensland, Australia. Water Resources Research, 7(3): 658-676.
Hodgkinson, J., Cox, M.E. and McLoughlin, S., 2007. Groundwater mixing in a sand-island freshwater lens: density-dependent flow and stratigraphic controls. Australian Journal of Earth Sciences, 54(7): 927-946.
Hoffmann, K.L., Totterdell, J.M., Dixon, O., Simpson, G.A., Brakel, A.T., Wells, A.T. and Mckellar, J.L., 2009. Sequence stratigraphy of Jurassic strata in the lower Surat Basin succession, Queensland. Australian Journal of Earth Sciences, 56(3): 461 - 476.
Hortle (Hennig), A., Underschultz, J. and Otto, C., 2002. PressureQC^{TM}: A quality control method for formation pressure measurements. Confidential Report No. 02-075, CSIRO Petroleum, Perth, 25 pp.
Hortle (Hennig), A., Xu, J. and Dance, T., 2008. Hydrodynamic interpretation of the Waarre Fm aquifer in the onshore Otway Basin: Implications for the CO2CRC Otway project, GHGT9 - 9th International conference on greenhouse gas control technologies - Energy Procedia. Elsevier, Washington DC, U.S.A.
Johnson, J.W., Oelkers, E.H. and Helgeson, H.C., 1992. SUPCRT92: A software package for calculating the standard molal thermodynamic properties of minerals, gases, aqueous species, and reactions from 1 to 500 bar and 0 to 1000 ^{o}C. Computers @ Geosciences, 18(7): 899-947.
Kalinowski, A.A., 2006. CO_2 storage potential in the southeast Bowen Basin. RPT06-0042, CO2CRC, Canberra, RPT06-0042, 1-23 pp.
Kaszuba, J.P., Janecky, D.R. and Snow, M.G., 2003. Carbon dioxide reaction processes in a model brine aquifer at 200°C and 200 bars: implications for geologic sequestration of carbon. Applied Geochemistry, 18(7): 1065-1080.
Kaszuba, J.P., Janecky, D.R. and Snow, M.G., 2005. Experimental evaluation of mixed fluid reactions between supercritical carbon dioxide and NaCl brine: Relevance to the integrity of a geologic carbon repository. Chemical Geology, 217(3-4): 277-293.
Knauss, K.G., Johnson, J.W. and Steefel, C.I., 2005. Evaluation of the impact of CO_2, co-contaminant gas, aqueous fluid and reservoir rock interactions on the geologic sequestration of CO_2. Chemical Geology, 217(3-4): 339-350.
Korsch, R.J., O'Brien, P.E., Sexton, M.J., Wake-Dyster, K.D. and Wells, A.T., 1989. Development of Mesozoic transtensional basins in easternmost Australia. Australian Journal of Earth Sciences, 36: 13-28.
Korsch, R.J. and Totterdell, J.M., 2009. Subsidence history and basin phases of the Bowen, Gunnedah and Surat Basins, eastern Australia. Australian Journal of Earth Sciences, 56(3): 335 - 353.
Koschel, D., Coxam, J.-Y., Rodier, L. and Majer, V., 2006. Enthalpy and solubility data of CO_2 in water and NaCl(aq) at conditions of interest for geological sequestration. Fluid Phase Equilibria, 247(1-2): 107-120.
Lusczynski, N.J., 1961. Head and flow of ground water of variable density. Journal of Geophysical Research, 66(12): 4247-4256.
Marsh, C., Rawsthorn, K., Causebrook, R., Kalinowski, A.A. and Newlands, I., 2008. A geological review of the Galilee basin, Queensland for possible storage of carbon dioxide, Geoscience Australia, Canberra, 36 pp.
Marsh, C. and Scott, A., 2005. Confidential review of the carbon dioxide injection and storage potential of the Denison Trough, Queensland. RPT05-0015, CO2CRC, Canberra, 23 pp.
Michael, K., Allinson, G., Golab, A., Sharma, S. and Shulakova, V., 2008a. CO_2 storage in saline aquifers II - experience from existing storage operations, GHGT0 - 9th International conference on greenhouse gas control technologies - Energy Procedia. Elsevier, Washington DC, U.S.A.

Michael, K., Arnot, M., Cook, P.J., Ennis-King, J., Funnell, R., Kaldi, J.G., Kirste, D. and Paterson, L., 2008b. CO_2 storage in saline aquifers I - current state of scientific knowledge, GHGT9 - 9th International conference on greenhosue gas control technologies - Energy Procedia, Washington DC, U.S.A.
Michael, K. and Bachu, S., 2001. Fluids and pressure distributions in the foreland-basin succession in the west-central part of hte Alberta basin, Canada: Evidence for permeability barriers and hydrocarbon generation and migration. AAPG Bulletin, 85(7): 1231-1252.
Middleton, M.F., 1980. A model of intracratonic basin formation entailing deep crustal metamorphism. Geophysical Journal of the Royal Astronomical Society, 62: 1-14.
Moore, J., Adams, M., Allis, R., Lutz, S. and Rauzi, S., 2003. CO_2 mobility in natural reservoirs benearth the Colorado Plateau and southern Rocky Mountains: An example from the Springerville-St. Johns field, Arizona and New Mexico, Second Annual Conference on Carbon Sequestration, NETL Proceedings, Alexandria, Virginia, U.S.A, pp. 1-22.
Naresh, D.J. and Singh, J.K., 2009. Virial coefficients and inversion curve of simple and associating fluids. Fluid Phase Equilibria, 279(1): 47-55.
Nicot, J.-P., 2008. Evaluation of large-scale CO_2 storage on fresh-water sections of aquifers: An example from the Texas Gulf Coast Basin. International Journal of Greenhouse Gas Control, 2(4): 582-593.
Nordbotten, J.M., Celia, M.A. and Bachu, S., 2005. Injection and storage of CO_2 in deep saline aquifers: Analytical solution for CO_2 plume evolution during injection. Transport in Porous Media, 58(3): 339-360.
Otto, C.J., Underschultz, J., Hennig, A. and Roy, V.J., 2001. Hydrodynamic analysis of flow systems and fault seal integrity in the north west shelf of Australia. APPEA Journal 2001: 347-364.
Patchett, A.M., 2006. CO_2 storage potential of environmentally sustainable sites for carbon dioxide injection (UEI 37 & 39) eastern Bowen Basin, Queensland. RPT06-0037, CO2CRC, RPT05-0225, 1-17 pp.
Pauwels, H., Gaus, I., le Nindre, Y.M., Pearce, J. and Czernichowski-Lauriol, I., 2007. Chemistry of fluids from a natural analogue for a geological CO_2 storage site (Montmiral, France): Lessons for CO_2-water-rock interaction assessment and monitoring. Applied Geochemistry, 22(12): 2817-2833.
Pitzer, K.S., 1973. Thermodynamics of electrolytes,1, theoretical basis and general equations. Journal of Physical Chemistry, 77: 268-277.
Pitzer, K.S., 1991. Ion interaction approach: theory and data correlation. In: K.S. Pitzer (Editor), Activity coefficients in electrolyte solutions second edition. CRC Press: 75-155.
Portier, S. and Rochelle, C., 2005. Modelling CO_2 solubility in pure water and NaCl-type waters from 0 to 300 °C and from 1 to 300 bar: Application to the Utsira Formation at Sleipner. Chemical Geology, 217(3-4): 187-199.
Pruess, K., 2005. ECO2N: A TOUGH2 Fluid property module for mixtures of water, NaCl and CO_2. Lawrence Berkeley National Laboratory, Berkeley, CA, U.S.A.
Pruess, K., Oldenburg, C. and Moridis, G., 1999. TOUGH2 User's Guide, version 2.0. Lawrence Berkeley National laboratory, Berkely, CA, USA.
QCGI, 2009. Potential for carbon geostorage in the Taroom Trough, Roma Shelf and the Surat, Eromanga and Galilee Basins - Preliminary Report, Geological Survey of Queensland Carbon Geostorage Initiative, Brisbane, 311 pp.
Qi, R., LaForce, T.C. and Blunt, M.J., 2009. Design of carbon dioxide storage in aquifers. International Journal of Greenhouse Gas Control, 3(2): 195-205.
Quarantotto, P., 1989. Hydrogeology of the Surat basin, Queensland. 1989/26, Geological Survey of Queensland, Brisbane, 34 pp.
Radke, B.M., Ferguson, J., Creswell, R.G., Ransley, T.R. and Habermehl, M.A., 2000. Hydrochemistry and implied hydrodynamics of the Cadna-owie-Hooray aquifer Great Artesian Basin, Bureau of Rual Science, Canberra, 229 pp.
Rawsthorn, K., Marsh, C. and Causebrook, R., 2009. Building of a geological model of the Triassic Clematis Sandstone of the Aramac Trough in the Galilee Basin, Queensland. RPT08-0999, CO2CRC, Canberra, 38 pp.
Rosenbauer, R.J., Koksalan, T. and Palandri, J.L., 2005. Experimental investigation of CO_2-brine-rock interactions at elevated temperature and pressure: Implications for CO_2 sequestration in deep-saline aquifers. Fuel Processing Technology, 86(14-15): 1581-1597.
Rumpf, B. and Maurer, G., 1993. An experimental and theoretical investigation on the solubility of carbon dioxide in aqueous solutions of strong electrolytes. Berichte der Bunsengesellschaft für Physikalische Chemie, 1: 85-97.
Sayers, J., Marsh, C., A., S., Cinar, Y., Bradshaw, J., Hennig, A., Kalinowski, A.A. and Pachett, A., 2005. Site specific studies for geological storage of carbon dioxide. Southeast Queensland

CO_2 storage sites - Geological basins desk-top study. . RPT05-0225, Cooperative Research Centre for Greenhouse Gas Technologies - CO2CRC Canberra
Schacht, U., 2008. Latrobe Group Sandstones in Tuna Field, Gippsland Basin. RPT08-0990, Cooperative Research Centre for Greenhouse Gas Technologies - CO2CRC, Canberra, 44 pp.
Seidel, G.E., 1980. Applicaton of the GABHYD groundwater model of the Great Artesian Basin, Australia. Bureau of Mineral Resources Journal of Australian Geology and Geophysics, 5: 39-45.
Senior, B.R., Mond, A. and Harrison, P.L., 1978. Geology of the Eromanga Basin, Bureau of Mineral Resources, Geology and Geophysics, Canberra, 167, 102 pp.
Spiteri, E.J. and Juanes, R., 2006. Impact of relative permeability hysteresis on the numerical simulation of WAG injection. Journal of Petroleum Science and Engineering, 50(2): 115-139.
Spycher, N. and Pruess, K., 2005. CO_2-H_2O mixtures in the geological sequestration of CO_2. II. Partitioning in chloride brines at 12-100°C and up to 600 bar. Geochimica et Cosmochimica Acta, 69(13): 3309-3320.
Spycher, N., Pruess, K. and Ennis-King, J., 2003. CO_2-H_2O mixtures in the geological sequestration of CO_2. I. Assessment and calculation of mutual solubilities from 12 to 100°C and up to 600 bar. Geochimica et Cosmochimica Acta, 67(16): 3015-3031.
Takenouchi, S. and Kennedy, G.C., 1964. The binary system H_2O-CO_2 at high temperatures and pressures. American Journal of Science, 262: 1055-1074.
Takenouchi, S. and Kennedy, G.C., 1965. The solubility of carbon dioxide in NaCl solutions at high temperatures and pressures. American Journal of Science, 263: 445-454.
U.S.G.S., 2005. MODFLOW - Three dimensional finite difference groundwater model. United States Geological Survey.
Underschultz, J., Otto, C. and Roy, V., 2003. Confidential report - Regional hydrodynamic analysis on the Gippsland Basin. Report No 03-04, APCRC, Canberra, 28 pp.
Veevers, J.J., Jones, J.G. and Powell, C.M., 1982. Tectonic framework of Australia's sedimentary basins. APPEA Journal, 22: 283-300.
Waschbusch, P., Korsch, R.J. and Beaumont, C., 2009. Geodynamic modelling of aspects of the Bowen, Gunnedah, Surat and Eromanga Basins from the perspective of convergent margin processes. Australian Journal of Earth Sciences, 56(3): 309 - 334.
Welsh, W.D., 2000. GABFLOW: A steady state groundwater flow model of the Great Artesian Basin. Bureau of Rural Sciences, Canberra.
Welsh, W.D., 2006. Great Artesian Basin transient groundwater model. Bureau of Rural Sciences, Canberra.
White, S.P., Allis, R.G., Moore, J., Chidsey, T., Morgan, C., Gwynn, W. and Adams, M., 2005. Simulation of reactive transport of injected CO_2 on the Colorado Plateau, Utah, USA. Chemical Geology, 217(3-4): 387-405.
Wigand, M., Carey, J.W., Schütt, H., Spangenberg, E. and Erzinger, J., 2008. Geochemical effects of CO_2 sequestration in sandstones under simulated in situ conditions of deep saline aquifers. Applied Geochemistry, 23(9): 2735-2745.
Worden, R.H., 2006. Dawsonite cement in the Triassic Lam Formation, Shabwa Basin, Yemen: A natural analogue for a potential mineral product of subsurface CO_2 storage for greenhouse gas reduction. Marine and Petroleum Geology, 23(1): 61-77.
Xu, T., Apps, J.A. and Pruess, K., 2005. Mineral sequestration of carbon dioxide in a sandstone-shale system. Chemical Geology, 217(3-4): 295-318.
Xu, T., Apps, J.A., Pruess, K. and Yamamoto, H., 2007. Numerical modeling of injection and mineral trapping of CO_2 with H_2S and SO_4 in a sandstone formation. Chemical Geology, 242(3-4): 319-346.
Yasanushi, Y. and Yoshida, F., 1979. Solubility of carbon dioxide in aqueous electrolyte solutions. Journal of Chemical and Engineering Data, 24: 11-14.
Zhang, W., Li, Y., Xu, T., Cheng, H., Zheng, Y. and Xiong, P., 2009. Long-term variations of CO_2 trapped in different mechanisms in deep saline formations: A case study of the Songliao Basin, China. International Journal of Greenhouse Gas Control, 3(2): 161-180.
Zhou, S., 1993. A 3-D backstripping method and its application to the Eromanga Basin in central and eastern Australia. Geophysical Journal International, 112: 225-243.